MAGNETO-THERMO-MECHANICAL COUPLING, STABILITY ANALYSIS AND PHENOMENOLOGICAL CONSTITUTIVE MODELING OF MAGNETIC SHAPE MEMORY ALLOYS

A Dissertation

by

KRISHNENDU HALDAR

Submitted to the Office of Graduate Studies of
Texas A&M University
in partial fulfillment of the requirements for the degree of

DOCTOR OF PHILOSOPHY

Approved by:

Chair of Committee,	Dimitris C. Lagoudas
Committee Members,	Ibrahim Karaman
	Christopher Pope
	Jay R. Walton
Head of Department,	Rodney Bowersox

December 2012

Major Subject: Aerospace Engineering

ABSTRACT

Magnetic shape memory alloys (MSMAs) are a class of active materials that deform under magnetic and mechanical loading conditions. This work is concerned with the modeling of MSMAs constitutive responses. The hysteretic magneto-mechanical responses of such materials are governed by two major mechanisms which are variant reorientation and field induced phase transformation (FIPT). The most widely used material for variant reorientation is Ni_2MnGa which can produce up to 6% magnetic field induced strain (MFIS) under 5 MPa actuation stress. The major drawback of this material is a low blocking stress, which is overcome in the NiMnCoIn material system through FIPT. This magnetic alloy can exhibit 5% MFIS under 125 MPa actuation stress. The focus of this work is to capture the key magneto-thermo-mechanical responses of such mechanisms through phenomenological modeling. In this work a detailed thermodynamic framework for the electromagnetic interaction within a continuum solid is presented. A Gibbs free energy function is postulated after identifying the external and internal state variables. Material symmetry restrictions are imposed on the Gibbs free energy and on the evolution equations of the internal state variables. Discrete symmetry is considered for single crystals whereas continuous symmetry is considered for polycrystalline materials. The constitutive equations are derived in a thermodynamically consistent way. A specific form of Gibbs free energy for FIPT is proposed and the explicit form of the constitutive equations is derived from the generalized formulation. The model is calibrated from experimental data and different predictions of magneto-thermo-mechanical loading conditions are presented. The generalized constitutive equations are then reduced to capture variant reorientation.

A coupled magneto-mechanical boundary value problem (BVP) is solved that accounts for variant reorientation to investigate the influence of the demagnetization

effect on the magnetic field and the effect of Maxwell stress on the Cauchy stress. The BVP, which mimics a real experiment, provides a methodology to correlate the difference between the externally measured magnetic data and internal magnetic field of the specimen due to the demagnetization effect. The numerical results show that localization zones appear inside the material between a certain ranges of applied magnetic field. Stability analysis is performed for variant reorientation to analyze these numerical observations. Detailed numerical and analytical analysis is presented to investigate these localization zones. Magnetostatic stability analysis reveals that the MSMA material system becomes unstable when localizations appear due to non-linear magnetization response. Coupled magneto-mechanical stability analysis shows that magnetically induced localization creates stress-localizations in the unstable zones. A parametric study is performed to show the constraints on material parameters for stable and unstable material responses.

DEDICATION

To my grandfather, Late *Nirode Baran Chowdhury*, who dedicated his life for the students

ACKNOWLEDGMENTS

I am immensely grateful to Dr. Dimitris Lagoudas, my advisor and chair of the Ph.D. advisory committee, for his guidance and support, investing his time to encourage my learning and teaching me to look beyond my original problem. I am also grateful to him for the opportunity to participate in many national and international conferences as well as other professional meetings. I am certain these experiences will prove to be extremely important for my future professional career.

Special thanks are also due to the members of my graduate advisory committee: Dr. Ibrahim Karaman, Dr. Christopher Pope, and Dr. Jay Walton. All of them, as my advisor, have been and will continue to be role models for me, as researchers, teachers and on a personal level. Their support throughout my studies has greatly contributed to the final form of this dissertation. Dr. Karaman, and his student Burak Basaran, have greatly aided my research with their experimental work on magnetic shape memory alloys.

I am also grateful for the administrative support provided by Ms. Pam McConal and Ms. Bonnie Reid, who many times made my life much easier. Finally, I gratefully acknowledge the support of the National Science Foundation (NSF) and the Army Research Office (ARO) and International Institute for Multifunctional Materials for Energy Conversion (NSF-IIMEC) for the financial support of this research.

I wish to acknowledge the affection, encouragement and sacrifices of my parents. Without their constant moral support, I'll never be able to continue my study. A very special thanks to Dr. Darren Hartl, who brought me to the Shape Memory Alloy and Research Technology (SMART) group. I am very grateful to Dr. Bjoern Kiefer for his friendly guidance to me whenever I needed. I was unfortunate as he graduated and left TAMU right when I joined the SMART group. But he was very kind to keep

in touch with me in spite of his busy schedule. He was the pioneer in the modeling of MSMAs in our research group and I was introduced to this field through his work. The introduction and the magneto-static boundary value problem of this dissertation is heavily influenced by him.

Also a very special thanks to George Chatzigeorgiou, who was a Post-doc in our group. I have never met such an overall enthusiastic person in my life. We spent many many hours discussing different technical topics. I am still surprised that one person can spend such an enormous amount of time just to help others. His influence is seen in the magneto-static stability problem.

I want to thank Dr. Amnaya P Awasthy for his friendship and the numerous scientific, philosophical and personal discussions that have been very valuable to me. I thank Dr. Piyush Thakre and Abidha for their friendship and the very warm interactions that we have enjoyed. I am also very grateful for the various professional and personal interactions with my colleagues and friends Dr. Peter Popov, Dr. Luciano Machado, Dr. Gary-Don Seidel, Dr. Olivier W. Bertacchini, Dr. Parikshith Kumar, Dr. Yves Chemisky, Dr. Theocharis Baxavanis, Nick Bruno and other members of the SMART group: Brent Volk, Brian Lester, Majid Tabesh, Antonino Parrinello, Babatunde O. Agboola, Austin Cox, Sameer Jape, Abhay Mohan, Stephen Cornell, Ken Cundiff, William Jinkins, Edwin Peraza Hernandez, John Rohmer, Brookelynn Russey, William Whitten and many more who made my life much more pleasant.

TABLE OF CONTENTS

LIST OF TABLES

LIST OF FIGURES

CHAPTER I

INTRODUCTION

A. General aspects of magnetic shape memory alloys

Shape memory alloys (SMAs) have been an important member of the class of active materials for at least two decades now. They have successfully been used in actuator and sensor design as well as biomedical and numerous other technological applications [4–6]. The large strains of 6–10% these materials exhibit when being subjected to thermal or mechanical loads, are caused by the change in crystallography associated with a reversible austenite to martensite phase transformation. *Magnetic shape memory alloys* (MSMAs), also referred to as ferromagnetic shape memory alloys (FSMAs) [7–9], have more recently emerged as an interesting extension of this class of materials. In addition to the strains originating from temperature- or stress-activated conventional shape memory behavior [10–13], large strains can be produced in these alloys under the application of magnetic fields. The macroscopically observable *field-induced strains* in MSMA are caused either by the microstructural *reorientation of martensitic variants* or by *phase transformation* from austenitic phase to martensitic phase.

Magnetic shape memory alloys exhibit one or even two orders of magnitude higher recoverable *magnetic field-induced strains* (MFIS) [14] than ordinary magnetostrictive materials, such as Terfenol-D [15] and Galfenol [16], and these strains are also much larger than the electric field-induced strains in piezoelectrics [6]. At comparable recoverable strains they also have an advantage over conventional shape memory alloys due to the much higher, up to 1kHz, frequency range at which they can be operated for some applications [17]. This is because their actuation is driven by

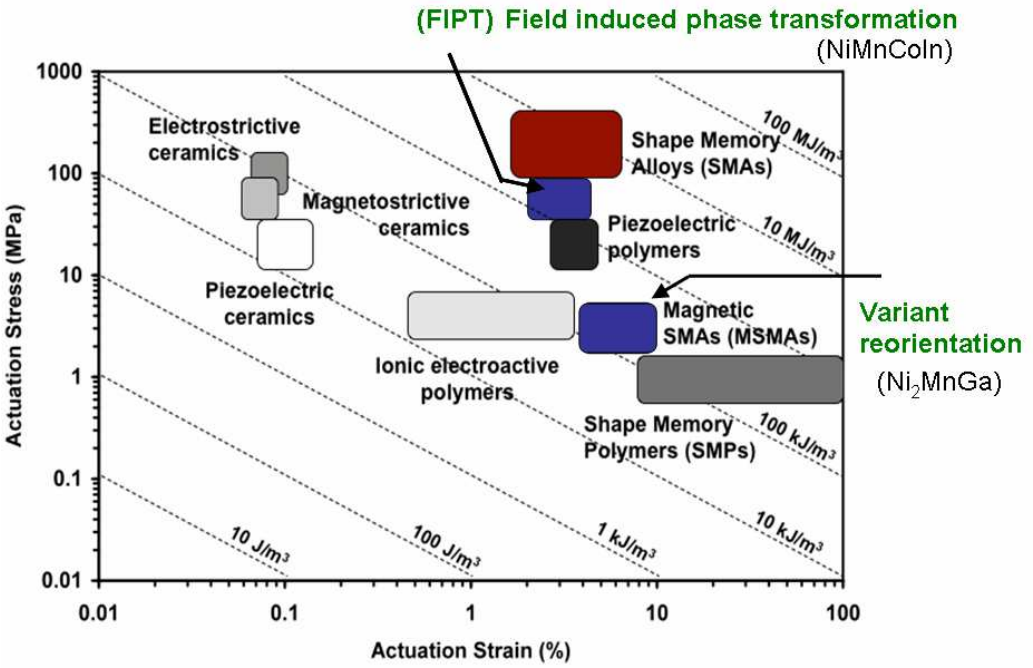

Fig. 1. Comparison of actuation energy density of different classes of active materials

.

the magnetic-field and not limited by heat transfer [18]. The main limitation of the variant reorientation is the relatively low blocking stress of typically 6-10 MPa, above which magnetic field-induced strains are completely suppressed. This difficulty, however, is overcome by *field induced phase transformation* or FIPT. A comparison of actuation energy density is presented in Fig. 1. The field-induced strain response of MSMAs is nonlinear, hysteretic, stress-dependent and intrinsically coupled to the magnetization response of the material. The coupled macroscopic response is driven by four mechanisms, the motion of magnetic domain walls, the local rotation of magnetization vectors (both of which also occur in regular ferromagnetic materials [19–21]), field induced variant reorientation and field induced phase transformation.

This unique coupling of mechanical and magnetic properties makes MSMAs interesting materials for smart structures, actuator and sensor applications [17, 22]. A

different class of applications aims to take advantage of the unique and adjustable magnetic properties of MSMAs in solenoid transducers [8] or voltage generators [23].

The most widely investigated magnetic shape memory materials is Ni-Mn-X (X=Sn, Ga, In) alloys [24]. Martensitic transformations in Ni_2MnGa alloys were first conclusively reported by Webster et al. [25]. Zasimchuk et al. [26] and Martynov and Kokorin [12] performed detailed studies on the crystal structure of martensite in the Ni_2MnGa alloy. Ullakko et al. [15] are credited with first suggesting the possibility of a magnetic field-controlled shape memory effect in these materials. They observed magnetic field-induced strains of nearly 0.2% in stress-free experiments on martensitic Ni_2MnGa single crystals. Further work on off-stoichiometric intermetallic compounds near the composition Ni_2MnGa, in combination with thermo-mechanical treatments and the utilization of a better understanding of the crystallographic structure of theses alloys, have yielded larger field-induced strains of 6% [7] and up to 10% [14, 27] in single crystals. Other magnetic shape memory alloys have been studied including Fe-Pd [28–31], Fe-Ni-Co-Ti, Fe-Pt, Co-Ni-Ga, Ni-Mn-Al [27, 32–36] and Co-Ni-Al [13, 37]. These alloys exhibit lower field-induced strains, but can have other advantages. The largest field-induced strains that have been observed in Fe-Pd, for example are 3.1% [31, 38], but this material is much more ductile than Ni-Mn-Ga [28].

The magnetic field-induced strains that can be generated in polycrystalline magnetic shape memory alloys are smaller than those observed for single crystals [39–43]. One effort aimed towards increasing the strain output of polycrystals is based on creating favorable texture in these materials. Marioni et al. [44] calculated the upper bound for the achievable field-induced strain in untextured NiMnGa polycrystals to be 21% of the single-crystal value and at most 50% for textured crystals.

The phenomenon of magnetic field-induced austenite-martensite phase transfor-

mations has also been investigated. Such transformations have been observed in Fe-Pt [45], Ni-Mn-Ga [46] and Ni-Mn-Fe-Ga [39] alloys. Magnetic fields have also been shown to influence the temperature- or stress-induced austenite-martensite phase transformation in MSMAs [39]. Furthermore, it has been observed that Ni-Mn-Ga alloys exhibit several different martensite morphologies and thus intermartensitic phase transformations [11, 47, 48]. Ni-Mn-Ga system can exhibit FIPT under stress levels on the order of 20 MPa with MFIS 0.5% [49]. In Ni-Mn-Co-In system, Kainuma et al. [50] found that 4 Tesla magnetic field can recover 3% pre applied strain in martensite at room temperature. Wang et al. [51] also reported reversible FIPT under 50 MPa with the application of 5 Tesla magnetic field with unknown MFIS values using in-situ high energy XRD measurement. In the present work the effect of simultenious application of high magnetic field (16 Tesla) and high stress (110 MPa) on the transformation is investigated.

B. Influence of the crystallographic and magnetic microstructure on the macroscopic response of MSMAs

In this section a more detailed description of the connection between the evolving crystallographic and magnetic microstructure of MSMAs and the observed macroscopic response is provided. This knowledge will then be used to motivate the formulation of the constitutive model.

Since the ternary intermetallic compound Ni-Mn-Ga is the most widely investigated magnetic shape memory alloy, it shall be the focus of the following discussion, which does not imply that the basic concepts or the modeling approach presented in this work are restricted in any way to this particular alloy.

The high temperature austenite phase of Ni-Mn-Ga alloys near the composition

Ni_2MnGa exhibits a $L2_1$ Heusler type structure, in which all of the atoms are located on the sites of a body centered cubic lattice [25]. The austenite phase is paramagnetic above the Curie temperature, which for the stoichiometric composition of Ni_2MnGa is 376 K [52], and ferromagnetic below it. The Curie temperature only shows a slight variation with changes in the composition [52, 53]. A strong compositional dependence, however, is observed for the austenite-martensite phase transformation start temperature [53–55], which is 202 K in stoichiometric Ni_2MnGa [52]. The martensite in these alloys can be of five-layered tetragonal (5M), seven-layered orthorhombic (7M), and non-modulated tetragonal martensite (NM) morphology [11, 47, 48]. Here only the most commonly observed tetragonal martensite of Ni_2MnGa is considered. In 2006, Kainuma etal. [50] reported that the parent and martensite phases have the $L2_1$ Heusler-type ordered structure where a = 0.5978 nm and the 14M modulated structure where a = 0.4349 nm, b = 0.2811 nm, c = 2.9892 nm and β= 93.24, respectively [56].

A simplified representation of the crystal structure, which is usually adopted for convenience [57, 58], is shown in Fig. 2. The undeformed austenite has cube edges of length a_0, whereas the undeformed tetragonal martensite unit cell has short and long edges of lengths a and c, respectively. Typical lattice parameters for Ni_2MnGa have been reported in the literature [25, 26, 59–61].

Since this transition temperature is well below Curie temperature the martensitic phase is ferromagnetic such that, even in the absence of an external magnetic field, the martensitic variants are *spontaneously magnetized* [19, 21]. The local magnetization vector in each ferromagnetic variant is oriented along one preferred crystallographic direction named the *magnetic easy axis*, which in this case is aligned with the short edge c of the tetragonal unit cell. The magnetization vectors can be oriented in either the positive or negative easy axis direction.

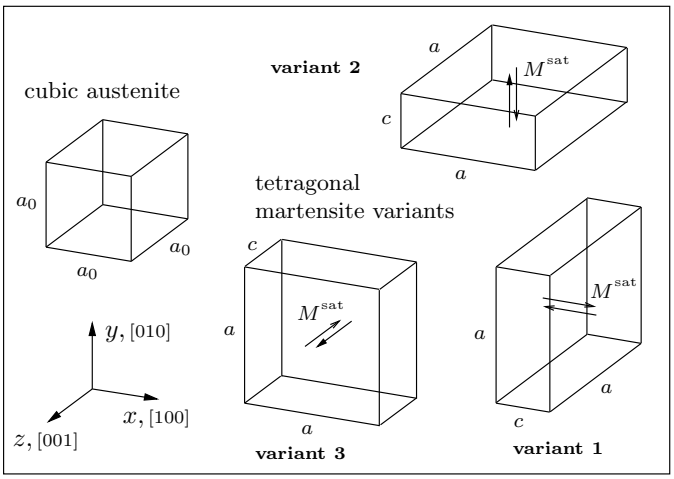

Fig. 2. Crystal structure of the austenitic and the tetragonal martensite phases in Ni_2MnGa. Arrows indicate possible magnetization vector orientations along the magnetic easy axis of each variant.

The austenitic phase is ferromagnetic and the spontaneous magnetization is oriented along the magnetic easy axis in NiMnCoIn. Since, the austenitic phase is cubic, all the three crystallographic directions are the direction of the easy axis. The martensitic phase is paramagnetic and so the magnitude of the saturation magnetization is very low compared to the ferromagnetic phase. The large difference of saturation magnetization between the parent phase and the martensitic phase is the key source of available magnetic energy for FIPT.

C. The magnetization response of MSMAs

If the reorientation of martensitic variants in a MSMA single crystal is completely suppressed by the application of a stress above the blocking stress, then the magnetization of the crystal can only change by means of the domain wall motion or magnetization rotation, or combinations thereof. The magnetization process of the

MSMA in this case is the same as that of a regular ferromagnetic material.

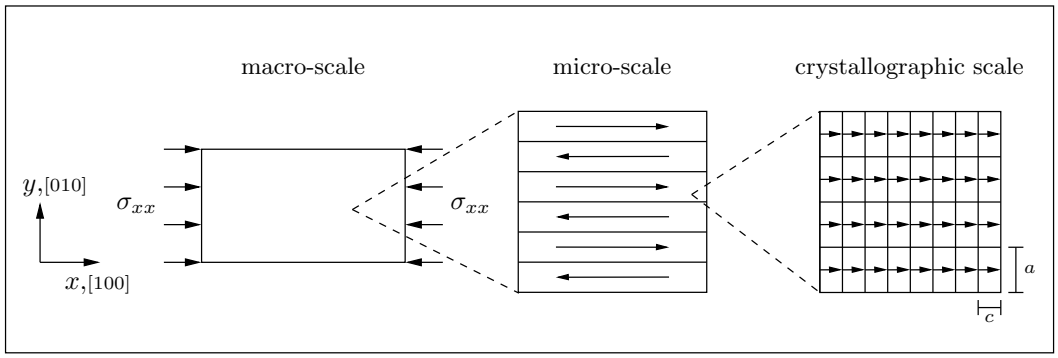

Fig. 3. A schematic of the initial single variant 1 martensite state. The variant reorientation is suppressed by an axial compressive stress higher than the blocking stress. Also shown, schematics of the corresponding microscopic scale and the crystallographic scale.

Fig. 3 shows a sketch of the initial single variant 1 configuration, except here a stress level above the blocking stress is considered to analyze the magnetization process without variant reorientation. Next to the macroscopic view of the specimen, Fig. 3 also depicts schematics of magnetic domains on the micro-scale. The crystallographic scale is shown simply to indicate the fact that magnetic domains generally span many unit cells. As discussed in the previous section, magnetic domains form to reduce the macroscopic magnetization of the material and thereby the magnetostatic energy [19–21, 62]. They are separated by magnetic domain walls. In these walls the magnetization vectors (magnetic dipole moments) are rotated over short distances to accommodate the magnetization directions of neighboring domains. The formation of many small domains leads to an increase in the amount of domain walls, whose formation also costs energy. This competition of energy terms determines the size of the domains and also the thickness of the domain walls. Depending on the material the domain wall thickness can range from 10 nm to 1μm [20].

If the constrained single crystal of is magnetized along different crystallographic directions, one observes an anisotropy of the magnetization response. The direction along which the least amount of energy is required to magnetize the crystal is termed the magnetic *easy axis*, and, correspondingly, the *hard axis* is the direction for which the most energy needs to be expended. This anisotropic behavior can be explained by the mechanism of magnetic domain wall motion and magnetization rotation as shown in the following sections.

1. Magnetization by magnetic domain wall motion

Fig. 4 schematically shows the evolution of the magnetic domain distribution at different applied field levels for the magnetization of the MSMA specimen along the [100]-direction. The starting configuration (left box) is the same microstructural view of the compressed single variant specimen that was presented in Fig. 3 (middle box).

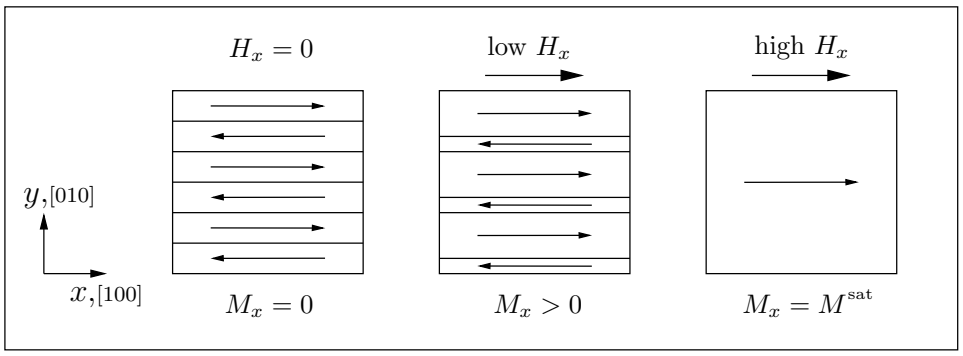

Fig. 4. Magnetization of the single variant specimen along the easy axis.

The applied field promotes the growth of these domains with favorably oriented magnetization vectors at the expense of the other domains. Since the external field

is applied in the [100]-direction, which coincides with the magnetic easy axis of the compressive stress-favored variant 1, the magnetization to saturation can completely be achieved by 180° domain wall motion.

2. Magnetization by rotation of magnetization vectors

Fig. 5 schematically illustrates the magnetization of the same single variant 1 sample perpendicular to the compression axis.

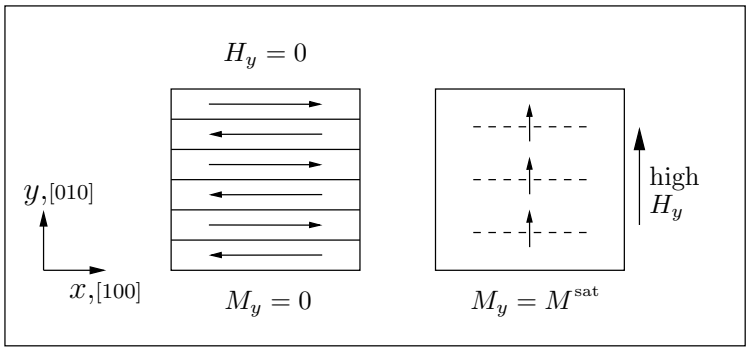

Fig. 5. Magnetization of the single variant specimen along the hard axis.

Since the magnetization vectors in both domains are equally unfavorable with respect to the applied field, no domain wall motion mechanism is available to accommodate the magnetization along the [010]-direction. The magnetization in both domains must be rotated away from the common easy axis. The rotation of the magnetization within a martensitic variant requires work against the magnetocrystalline anisotropy energy. The amount of energy expended in activating this mechanism is higher than that associated with domain wall motion. The [010]-direction is therefore the hard axis for this material. The magnetization of the MSMA specimen along directions in between [100] and [010], requires an intermediate amount of energy and involves the activation of both mechanisms. Unlike the motion of 180° domain

walls, the rotation of the magnetization is associated with ordinary magnetostriction, i. e. the crystal elongates in the direction of the rotating magnetization vector [19, 21].

Fig. 6 qualitatively shows the resulting magnetization curves for the easy [100] and the hard [010]-directions. The coordinate axes are normalized by the saturation magnetization M^{sat} and an arbitrary maximum applied field value H^{max}, respectively. Data for the magnetization of constrained MSMA single crystals have been reported by Tickle and James [63], Cui et al. [28], Shield [30], Lickhachev and Ullakko [64] and Hezcko [65].

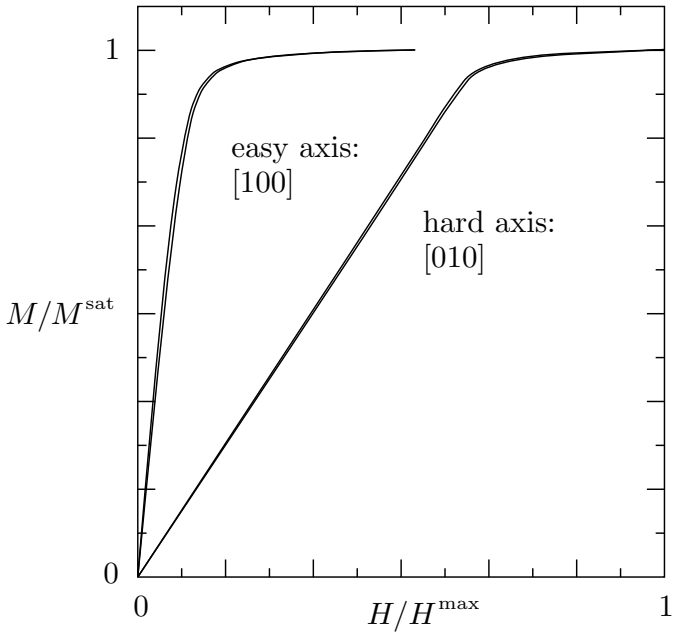

Fig. 6. Qualitative magnetization curves of the single variant MSMA specimen magnetized along the compression and perpendicular axes. For quantitative experimental results [63].

The magnetization curves in Fig. 6 are explained by the mechanisms discussed in the context of Figs. 4 and 5. Recall that the mechanism for alignment with the applied field is the domain wall motion, in the easy axis case, and rotation of the

magnetization vectors, in the hard axis case. According to O'Handley [20], the energy per unit volume u_a needed to saturate a material in a particular direction is given by

$$u_a = \mu_0 \int_0^{M^{\text{sat}}} H(M)\,\mathrm{d}M \ . \tag{1.1}$$

It is clearly seen that by this measure the energy required to magnetize the material to saturation along the hard axis does in fact require much more energy.

Furthermore, it is observed that the hystereses for both magnetization curves are almost negligible. This is expected for the hard axis magnetization curve, since the magnetization rotation in is a reversible process. Magnetic domain wall motion on the other hand can be associated with dissipation. Permanent magnets, for example, are made from materials that exhibit a strong internal resistance to magnetic domain wall motion, due to micro-scale pinning sites and other phenomena [8, 19, 20], which leads to large hysteresis effects. In MSMAs, however, the magnetic domain wall motion appears to be associated with only a very small amount of dissipation.

3. Magnetization by variant reorientation

In MSMAs the variant reorientation process provides an additional mechanism to change the magnetization of the material. This is due to the fact that the magnetic easy axes in the martensitic variants have different directions with respect to a global coordinate system. In the presence of an external field the structural rearrangement is therefore always coupled to a magnetization change. If the reorientation process is initiated by mechanical loading instead of applying a magnetic field, and the applied field is constant, the variant reorientation is in fact the only mechanism that changes the magnetization.

In this mechanism, however, when the applied stress level is more than 6 MPa [66], the MAE does not suffice to overcome the energy required for twin boundary

motion (Fig. 7a). Magnetic field favored martensitic variant does not grow and field induced macroscopic shape change is not observed. The limited availability of MAE restricts the variant reorientation mechanism to work above certain stress level.

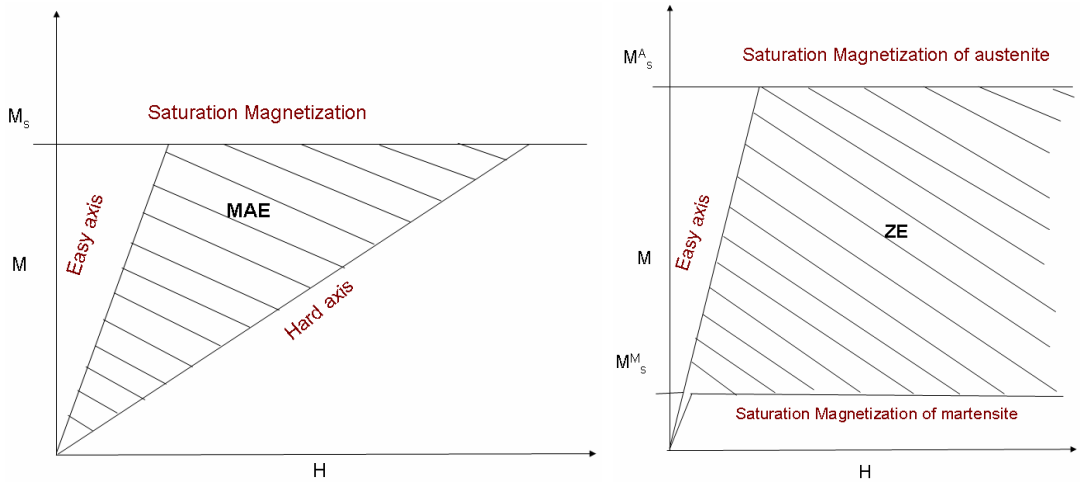

(a) (b)

Fig. 7. Schematic representation of available magnetic energy. (a) MAE for variant reorientation and (b) ZE for phase transformation.

4. Magnetization by phase transformation

The second possible mechanism to change magnetization is the magnetic field induced phase transformation. The main requirement for the field-induced phase transformation is that the magnetic driving energy must be sufficient to move the phase front. The limitation of available magnetic energy and thus low blocking stress in field-induced variant reorientation can be overcome by magnetic field induced martensitic phase transformation. This mechanism is analogous to the temperature induced martensitic transformation in conventional SMAs. The Zeeman energy (ZE), which depends on the difference between the saturation magnetizations of the austenitic and martensitic phases (Fig. 7b), is converted to mechanical energy in the magnetic

field induced phase transformation. In NiMnCoIn material system, the Zeeman energy is large because the austenitic phase is ferromagnetic and martensitic phase is antiferromagnetic. The available magnetic energy (ZE) involved in FIPT is much higher than the magnetic energy (MAE) associated with the variant reorientation mechanism. Karaca et al [2] showed that the ZE in $Ni_{45}Mn_{36.5}Co_5In_{13.4}$ is one order of magnitude higher than the MAE of NiMnGa alloys. This unique characteristic of high available magnetic energy in the FIPT can lead to large MFIS and high actuation stresses. Moreover unlike MAE, ZE is independent on crystal orientation and provides an opportunity to utilize polycrystals for actuator application [49]. Another advantage of this material is that it may work at room temperature.

D. Literature review of MSMA models

Several models have been proposed in the literature to describe the constitutive response related to the magnetic field-induced variant reorientation. The approach most commonly taken is the minimization of a free energy function characterizing the system to find equilibrium configurations for given temperature, stress and magnetic field.

The model presented by James and Wuttig [29] is based on a *constrained theory of micromagnetics* (see also [67–69]). The terms contributing to the free energy in their model are the Zeeman energy, the magnetostatic energy and the elastic energy. The magnetization is assumed to be fixed to the magnetic easy axis of each martensitic variant because of high magnetic anisotropy. The microstructural deformations and the resulting macroscopic strain and magnetization response are predicted by detecting low-energy paths between initial and final configurations. They conclude that the typical strains observed in martensite, together with the typical easy axes observed

in ferromagnetic materials lead to layered domain structures that are simultaneously mechanically and magnetically compatible.

O'Handley [70, 71] proposed a 2-D model in which two variants are separated by a single twin boundary and each variant itself consists of a single magnetic domain. The local magnetization is not necessarily constrained to the crystallographic easy axis. Depending on the magnitude of the magnetic anisotropy, either the magnetic anisotropy difference (low magnetic anisotropy case) or the Zeeman energy (high magnetic anisotropy case) are identified as the driving forces for twin boundary motion. For the intermediate anisotropy case a parametric study is conducted showing the influence of varying elastic and magnetic anisotropy energies. All cases assume an initial variant distribution that implies a remnant magnetization.

Likhachev and Ullakko [64] presented a model which identifies the magnetic anisotropy energy difference in the two variant twinned-martensite microstructure as the main driving force for the reorientation process. The free energies associated with magnetizing a single variant martensite along the magnetic easy and hard axes are computed from integration over the experimental magnetization curves. The driving force for twin boundary motion is proposed to be the derivative of the difference between the two free energy terms with respect to the martensitic variant volume fraction. They argue that, regardless of the physical nature of the driving force, twin boundary motion should be initiated at equivalent load levels. With this assumption experimentally obtained detwinning-under-stress data in addition to the magnetization data are used to predict the MSMA constitutive behavior associated with field-induced variant reorientation.

Hirsinger and Lexcellent [72, 73] introduced the outline of a non-equilibrium thermodynamics based model. The free energy contains chemical, mechanical, magnetic and thermal contributions. The magnetic term is given by the Zeeman energy. Two

internal state variables, the martensitic variant volume fraction and the magnetic domain volume fraction, are introduced to represent the influence of the microstructure. The rate independent dissipative nature of their approach motivates the definition of driving forces for the twin boundary motion and the domain wall motion.

Kiefer and Lagoudas formulated a continuum thermodynamics-based phenomenological constitutive model for MSMAs with internal state variables describing the evolution of the crystallographic and magnetic microstructures. Their approach is aimed at capturing the hysteretic effects associated with the magnetic field-induced reorientation of martensitic twins and the resulting loading history dependence of the material response. Emphasis is also placed on modeling the nonlinear and stress-level-dependent nature of the magnetic field-induced strain and magnetization response. The Kiefer and Lagoudas model mainly distinguishes itself from the Hirsinger and Lexcellent approach by allowing the magnetization vectors to rotate away from the magnetic easy axes, which leads to much more accurate predictions of the magnetization response. Details of the model development were reported in [3, 74–77]. Experimental characterization of MSMA response and the model validation were presented in [1]. The focus of this particular paper was placed on estimating the maximum MSMA actuator work output, both theoretically and experimentally. Furthermore, the numerical analysis of nonlinear magnetostatic boundary value problems for MSMAs was described in [78, 79]. More recently, stability analysis of magnetostatic boundary value problems for MSMAs was presented in [80].

Faidley et al. [8] proposed an extension of an earlier version of the Kiefer and Lagoudas model [74] to predict the reversible strain effect in Ni-Mn-Ga with collinear field and stress. In their approach, internal restoring forces orthogonal to the applied field are attributed to pinning sites which elastically deform twin boundaries. Tan and Elahinia [81] utilized the Kiefer and Lagoudas model to study the dynamic response

of MSMA actuators. Glavatska et al. [82] proposed a constitutive model for the martensitic twin rearrangement based on a statistical approach. The rearrangement of twins and resulting macroscopic strain is assumed to be triggered by magnetic field-induced micro-stresses originating from magnetoelastic interactions. The probability for the rearrangement of the twins in which the stresses are near the critical stress is described through a statistical distribution. This model was utilized by Chernenko et al.[83, 84], who also followed a microscopic approach to the magnetic field-induced deformation of martensite in MSMAs.

Another model that uses the principles of statistical physics has been proposed by Buchelnikov and Bosko [85] who extended a model derived by Govindjee and Hall [86] for conventional shape memory alloys. Their model derivation follows what is referred to as a *multi-well approach*. They identify four phases, the cubic austenite and the three tetragonal variants. These phases can, in principle, transform into any of the other phases under the influence of temperature, stress and magnetic field. The rate of transformation between the different phases is assumed to be proportional to the net probability that one phase will overcome the energetic barrier required to transform to a second phase. The free energy expression that is utilized to compute the energetic barrier consists of elastic, thermal and magnetic energy terms. The magnetic energy consists of the magnetic anisotropy energy, the magnetostatic energy of the demagnetization field and the Zeeman energy.

Smith et al. recently proposed a unified framework for modeling hysteresis in ferroic materials [87], which briefly discusses the subject of magnetic shape memory alloys. A detailed comparison of many of the described models can be also found in the recent paper by Kiang and Tong [88].

A general approach to phenomenological modeling of the loading history dependent constitutive response of materials undergoing phase transformation, detwinning,

or variant reorientation has widely been utilized in the literature on conventional shape memory alloys [86, 89–97]. A detailed review of the modeling of shape memory alloys has recently been published by Patoor et al. [98] and Lagoudas et al. [99]. Since the austenite to martensite phase transformation in SMAs is induced by cooling or the application of mechanical forces, the independent state variables in this case are usually chosen to be temperature and stress. In phenomenological constitutive modeling the system can be characterized by a macroscopic free energy expression which is a function of these independent state variables. A common approach of incorporating path dependence and dissipation is through the introduction of internal state variables [100], whose evolution then accounts for the loading history dependence of the material behavior. Motivated by the crystallographic microstructure of martensite, a common choice for an internal state variable is the martensitic volume fraction. Constitutive equations, which relate the dependent state variables to the independent ones, follow directly from applying the well-known *Coleman and Noll procedure* [101] commonly used in phenomenological modeling. The dependent state variables, such as the strain or entropy, are themselves also functions of the internal state variables through the constitutive relations and depend therefore on the loading history. The lack of apparent intrinsic time scales (diffusionless, thermoelastic phase transformation) makes the shape memory effect subject to rate independent modeling. This approach lends itself to the introduction of transformation functions, similar to yield functions of rate-independent plasticity models, which govern the onset and termination of the phase transformation [102]. Transformation hardening functions account for the interactions of different phases during the transformation process, which influence the activation of the phase transformation. The evolution of transformation strain is related to the evolution of the martensitic volume fraction and its direction is given by a postulated transformation tensor [91].

The variant reorientation process in magnetic shape memory alloys is, from a modeling standpoint, also similar to the detwinning (i. e. self-accommodated to detwinned martensite) and reorientation (i. e. change in the selection of martensitic variants under changes in the stress state) phenomena that are observed in conventional shape memory alloys [95, 103–106].

Many works have been done so far on the interaction of electromagnetic field with a mechanical medium. In the recent work of Drofman and Ogden [107, 108], they developed a theory of nonlinear magneto elasticity for magneto sensitive elastomers. A parallel development of electro sensitive elastomers, based on the interaction between electric fields and mechanical deformation can be obtained in [109]. A detail study of electrostatic forces on large deformations of polarizable material is given in [110, 111]. A continuum theory for deformable ferromagnetic materials can be found in [112]. A theory for the equilibrium response of magnetoelastic membranes under pressure and applied magnetic field is formulated in [113, 114]. The variational formulations for general magneto-mechanical materials have been proposed by many authors and can be found in [115–119].

E. Outline of the present research

The research presented in this dissertation is focused on the following main objectives.

1. We develop a continuum mechanics based modeling framework (chapter II) to describe a general coupled electromagnetic and mechanical responses for MSMAs through finite deformation analysis. The MSMA constitutive equations are derived in a thermodynamic consistent way. Material symmetry is considered for finite and continuous group of symmetry.

2. In chapter III, motivated by experiments, we develop a phenomenological model

to capture the magneto-thermo-mechanical material responses for FIPT. A detailed model calibration procedure is presented here.

3. A brief introduction of microstructure-based phenomenological model (Kiefer-Lagoudas) for variant reorientation is introduced in chapter IV. We show that the general model can also be able to predict variant reorientation MSMA responses as a special case.

4. We solve a coupled magneto-mechanical boundary value problem for MSMAs in chapter V. We demonstrate how a numerical process can take into account the demagnetization effect for a non ellipsoid specimen shape. Moreover, effect of magnetic body force and magnetic body couple on mechanical stress is investigated.

5. Finally we present the stability analysis of the coupled magneto-mechanical system in chapter VI.

CHAPTER II

A CONTINUUM DESCRIPTION OF ELECTROMAGNETIC INTERACTION WITH SOLIDS

The material responses of MSMAs can be considered as a consequence of coupling between electromagnetic and mechanical field variables. When we consider electromagnetic interaction with a continuum, in addition to the *short range* forces which are determined by the local state of the medium, the magnetization interacts with the self field. We assume in the stress hypothesis that this electromagnetic interaction together with the short range interaction will be described by a system of stress [120–122]. Such a decomposition of the stress is not unique. Extensive work on different electromagnetic formulations like two dipole models, Lorentz model, statistical model etc. had been proposed in the literature [123–125] on different notion of breaking up *long range* and *short range* forces. Depending on different formulations, expressions of local stress and Maxwell stress differ, though the net effect always give the same total stress. It is extremely important for a phenomenological approach to select a particular model which is close to the experiment. We consider that the total traction is the sum of material and magnetic traction. We assume in the stress hypothesis that the electromagnetic interaction together with the *short range* interaction describes a system of stress. We will call it *total stress* [122, 126]. Since *total stress* obeys *Cauchy's theorem*, we will consider that the total stress is the *Cauchy stress*.

In this work, we propose a Gibbs free energy for a MSMA material system, where the stress, electromagnetic field and temperature are the controllable dependent variables. We also consider tensor, vector and scalar valued internal variables to capture the magneto-mechanical dissipative behaviors. The Gibbs free energy formulation facilitates to calibrate the model from typical experiments, considered for the MS-

MAs. Though MSMAs are magnetic material, it can interact with electric field when operated under high frequency application. This motivates us to start formulation in a generalized electromagnetic and mechanical framework, where we perform a systematic and rigorous nonlinear finite deformation analysis to combine the Maxwell equations and the mechanical conservation laws.

We consider a finite deformation based analysis of electromagnetically active dissipative material systems. Our major aim is to obtain the *integrity basis*[1] for the Gibbs free energy. We deduce the integrity basis for single crystal by considering *finite symmetry restrictions*. The integrity basis differs in the parent phase and martensitic phase due to different crystalline symmetry. The symmetry restrictions for the evolution equations of the lower symmetric phases are investigated. Finally we consider *continuous symmetry* for polycrystalline materials to take into account anisotropy in the constitutive equations and evolution equations by introducing *structural tensors*. An evolution of a structural tensor is proposed to capture the effect of the evolution of texturing due to changes in the microstructure during phase transformation and reorientation.

A. General balance equations

We express the volume balance and surface balance laws of mechanics for a part $\mathcal{P}_t \subset \Omega_t$ in the following general form

$$\frac{d}{dt}\int_{\mathcal{P}_t} \psi dv = \int_{\partial\mathcal{P}_t} \Phi_\psi \mathbf{n} da + \int_{\mathcal{P}_t} \sigma_\psi dv, \tag{2.1}$$

[1] An integrity basis is a set of polynomials, each invariant under the group of transformations, such that any polynomial function invariant under the group is expressible as a polynomial in elements of the integrity basis [127].

$$\frac{d}{dt}\int_{\partial P_t}\Psi\cdot\mathbf{n}da=\int_{\partial^2\mathcal{P}_t}\Xi_\Psi\cdot\mathbf{t}ds+\int_{\partial\mathcal{P}_t}\Sigma_\Psi\cdot\mathbf{n}da, \tag{2.2}$$

We denote $\mathbf{n}$, the outward unit normal to the boundary $\partial\mathcal{P}_t$ of the region $\mathcal{P}_t$ in the current configuration and $\mathbf{t}$ is the unit tangent to a boundary curve on $\partial\mathcal{P}_t$, oriented in the direct sence about $\mathbf{n}$. The quantity ψ and σ_ψ are the tensor of order p, and Φ_ψ is a tensor field of order p+1 [124, 128, 129] and in the equation (2.2), $\mathbf{\Psi},\mathbf{\Xi}_\Psi,\mathbf{\Sigma}_\Psi$ are the vectors. We consider up to $p=2$.

The material time derivative is denoted by $\frac{d}{dt}$ or by a dot and the spatial time derivative is denoted by $\frac{\partial}{\partial t}$. By using transport theorem, the first term of the equation (2.1) can be written as [129, 130]

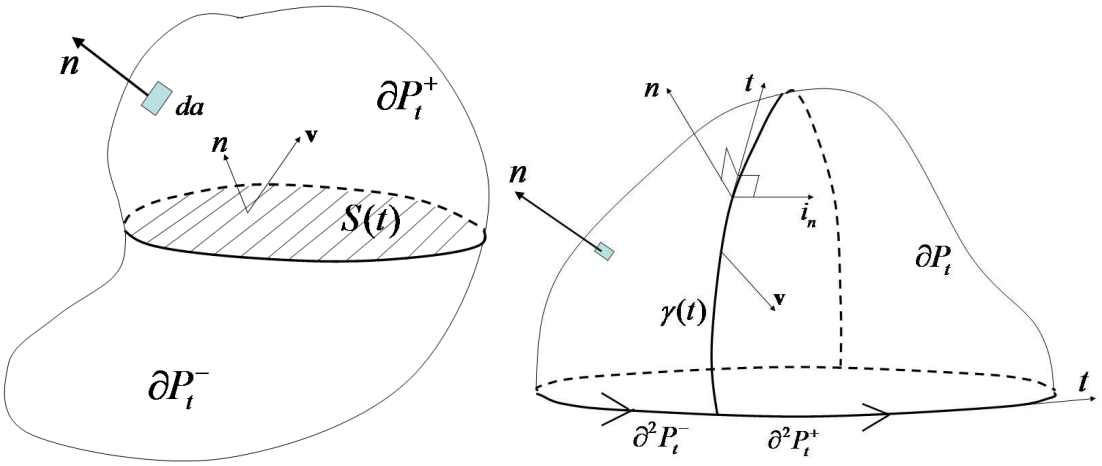

(a) (b)

Fig. 8. (a) Moving discontinuous surface $\mathcal{S}(t)$ and (b) moving discontinuous line $\gamma(t)$.

$$\frac{d}{dt}\int_{\mathcal{P}_t}\psi dv=\int_{\mathcal{P}_t}\frac{\partial\psi}{\partial t}dv+\int_{\partial\mathcal{P}_t}\psi\dot{\mathbf{x}}\cdot\mathbf{n}da-\int_{\mathcal{S}}[\![\psi]\!](\mathbf{v}\cdot\mathbf{n})da. \tag{2.3}$$

Similarly the first term of equation (2.2) can be written as [124]

$$\frac{d}{dt}\int_{\partial\mathcal{P}_t}\mathbf{\Psi}\cdot\mathbf{n}da=\int_{\partial\mathcal{P}_t}\overset{*}{\mathbf{\Psi}}\cdot\mathbf{n}da+\int_\gamma[\![\mathbf{\Psi}\times(\dot{\mathbf{x}}-\mathbf{v})]\!]\cdot\mathbf{t}ds. \tag{2.4}$$

Here, $\mathcal{S}$ is an oriented smooth surface in the material region $\mathcal{P}_t$ (Fig. 8a) and singular surface relative to a field A, defined on $\mathcal{P}_t$ and smooth on $\mathcal{P}_t - \mathcal{S}$. A suffers a jump discontinuity across $\mathcal{S}$. The jump condition is defined as

$$[\![A]\!] = A^+ - A^- \tag{2.5}$$

where A^+ and A^- are the one-side limits from the two regions $\mathcal{P}_t^+$ and $\mathcal{P}_t^-$ of $\mathcal{P}_t$, separated by $\mathcal{S}$. The velocity of $\mathcal{S}$ is $\mathbf{v}$. We call the point $\mathbf{x}$ is *singular* if it is a point on the singular surface and *regular* if it lies on the region where all the tensor functions are smooth. We denote the convective time derivative of the vector $\mathbf{\Psi}$ by

$$\overset{*}{\mathbf{\Psi}} = \dot{\mathbf{\Psi}} + \mathbf{\Psi}\nabla \cdot \dot{\mathbf{x}} - (\nabla \otimes \dot{\mathbf{x}})\mathbf{\Psi} \tag{2.6}$$

$$\Rightarrow \overset{*}{\mathbf{\Psi}} = \dot{\mathbf{\Psi}} - \mathbf{L}\mathbf{\Psi} + \mathbf{\Psi}(\mathrm{tr}\,(\mathbf{L})). \tag{2.7}$$

Where, $\mathbf{L} = \nabla \otimes \dot{\mathbf{x}}$ is the velocity gradient.

Similar argument can be used to an material surface $\partial\mathcal{P}_t$ containing a discontinuous line $\gamma(t)$, moving with an velocity $\mathbf{v}$ on $\partial\mathcal{P}_t$ (Fig. 8b) and the jump condition is given by (2.5). Substituting (2.3) in (2.1), we get

$$\int_{\mathcal{P}_t} \frac{\partial \psi}{\partial t} dv + \int_{\partial\mathcal{P}_t} \psi \dot{\mathbf{x}} \cdot \mathbf{n} da - \int_{\mathcal{S}} [\![\psi]\!](\mathbf{v} \cdot \mathbf{n}) da = \int_{\partial\mathcal{P}_t} \Phi_\psi \mathbf{n} da + \int_{\mathcal{P}_t} \sigma_\psi dv \tag{2.8}$$

Similarly, substituting (2.4) in (2.2), we get

$$\int_{\partial\mathcal{P}_t} \overset{*}{\mathbf{\Psi}} \cdot \mathbf{n} da + \int_\gamma [\![\mathbf{\Psi} \times (\dot{\mathbf{x}} - \mathbf{v})]\!] \cdot \mathbf{t} ds = \int_{\partial^2\mathcal{P}_t} \Xi_\Psi \cdot \mathbf{t} ds + \int_{\partial\mathcal{P}_t} \Sigma_\Psi \cdot \mathbf{n} da \tag{2.9}$$

1. Field equations and jump conditions

We obtain the local balance at a regular point from (2.8) and (2.9) by considering the regions where $\mathcal{P}_t \cap \mathcal{S} = 0$ and $\partial\mathcal{P}_t \cap \gamma = 0$ respectively. The divergence theorem

gives us

$$\int_{\mathcal{P}_t} \{\frac{\partial \psi}{\partial t} + \nabla \cdot (\psi \otimes \dot{\mathbf{x}} - \Phi_\psi) - \sigma_\psi\} dv = 0, \tag{2.10}$$

and by using Stokes' theorem we get

$$\int_{\partial \mathcal{P}_t} \{\overset{*}{\mathbf{\Psi}} - \nabla \times \mathbf{\Xi}_\Psi - \mathbf{\Sigma}_\Psi\} \cdot \mathbf{n} da = 0. \tag{2.11}$$

We obtain the field equations at a regular point with the help of localization theorem [130]

$$\frac{\partial \psi}{\partial t} + \nabla \cdot (\psi \otimes \dot{\mathbf{x}} - \Phi_\psi) - \sigma_\psi = 0, \tag{2.12}$$

$$\overset{*}{\mathbf{\Psi}} - \nabla \times \mathbf{\Xi}_\Psi - \mathbf{\Sigma}_\Psi = 0. \tag{2.13}$$

The notation $\psi \otimes \dot{\mathbf{x}}$ should be understood as $\psi \dot{\mathbf{x}}$ when ψ is a scalar quantity.

The jump conditions are obtained in the following way. We consider a singular point $\mathbf{x} \in \mathcal{S}$. We take the limit by shrinking $\partial {\mathcal{P}_t}^+$ and $\partial {\mathcal{P}_t}^-$ down to $\mathcal{S}$ in such a way that the volume of $\mathcal{P}_t$ tends to zero, while the area remains unchanged and $\lim_{v \to 0} \int_{\mathcal{P}_t} \sigma_\psi dv = \int_{\mathcal{S}} \chi \mathbf{n} da$ exists. Here χ is the surface density of a physical quantity on the singular surface $\mathcal{S}$. Under this condition, (2.8) reduces to

$$\begin{aligned} \int_{\mathcal{S}} \{ [\![\psi(\dot{\mathbf{x}} - \mathbf{v}) \cdot \mathbf{n}]\!] - [\![\Phi_\psi]\!] \mathbf{n} \} da &= \int_{\mathcal{S}} \chi \mathbf{n} da \\ \Rightarrow \int_{\mathcal{S}} \{ [\![\psi(\dot{\mathbf{x}} - \mathbf{v}) \cdot \mathbf{n}]\!] - [\![\Phi_\psi]\!] \mathbf{n} - \chi \mathbf{n} \} da &= 0. \end{aligned} \tag{2.14}$$

Since the integral is smooth on $\mathcal{S}$, the integrand must vanish at $\mathbf{x}$. We obtain,

$$[\![\psi \otimes (\dot{\mathbf{x}} - \mathbf{v}) - \Phi_\psi]\!] \mathbf{n} = \chi \mathbf{n}. \tag{2.15}$$

Similarly, by shrinking $\partial^2 {\mathcal{P}_t}^+$ and $\partial^2 {\mathcal{P}_t}^-$ down to $\gamma(t)$ in such a way that the area

of $\partial\mathcal{P}_t$ tends to zero, while the length of the line segment remains unchanged and $\lim_{a\to 0}\int_{\partial\mathcal{P}_t}\Sigma_\Psi\cdot\mathbf{n}da=\int_\gamma\boldsymbol{\kappa}\cdot\mathbf{i_n}ds$ exists, (2.9) becomes

$$\int_\gamma\{[\![\boldsymbol{\Xi}_\Psi]\!]-[\![\boldsymbol{\Psi}\times(\dot{\mathbf{x}}-\mathbf{v})]\!]\}\cdot\mathbf{t}ds=-\int_\gamma\boldsymbol{\kappa}\cdot\mathbf{i_n}ds. \tag{2.16}$$

Where $\boldsymbol{\kappa}$ is the current per unit length, $\mathbf{i_n}=\mathbf{t}\times\mathbf{n}$ is the unit binormal vector and $\mathbf{t}=\mathbf{n}\times\mathbf{i_n}$ (Fig 8b). Continuing (2.16) we write

$$\begin{aligned}\int_\gamma\{[\![\boldsymbol{\Xi}_\Psi]\!]-[\![\boldsymbol{\Psi}\times(\dot{\mathbf{x}}-\mathbf{v})]\!]\}\cdot(\mathbf{i_n}\times\mathbf{n})ds&=\int_\gamma\boldsymbol{\kappa}\cdot\mathbf{i_n}ds\\ \int_\gamma\{\mathbf{n}\times([\![\boldsymbol{\Xi}_\Psi]\!]-[\![\boldsymbol{\Psi}\times(\dot{\mathbf{x}}-\mathbf{v})]\!])\}\cdot\mathbf{i_n}\mathbf{ds}&=\int_\gamma\boldsymbol{\kappa}\cdot\mathbf{i_n}\mathbf{ds}.\end{aligned} \tag{2.17}$$

[2]So the local form can be written as,

$$\mathbf{n}\times([\![\boldsymbol{\Xi}_\Psi]\!]-[\![\boldsymbol{\Psi}\times(\dot{\mathbf{x}}-\mathbf{v})]\!])=\boldsymbol{\kappa}. \tag{2.18}$$

We are now ready to recover the electromagnetic and mechanical conservation laws from the general form of the balance laws. In the next subsection, we will consider the electromagnetic system, followed by the mechanical system.

2. Electromagnetic conservation laws

We denote the magnetic induction by $\mathbf{b}$, the electric field $\mathbf{e}$, the magnetic field $\mathbf{h}$, the electric displacement $\mathbf{d}$, the magnetization vector $\mathbf{m}$ and the polarization vector $\mathbf{p}$ in the deformed configuration and in the *rest frame*. We select deformed configuration because Maxwell equations are convenient to express. The free charge (surface) and the free current (conductive) density of the body are denoted by q_f and $\mathbf{j}_f$.

The magnetization vector $\mathbf{m}$ and the polarization vector $\mathbf{p}$ are related through

[2]We use the following identity: $\mathbf{A}\cdot(\mathbf{B}\times\mathbf{C})=\mathbf{B}\cdot(\mathbf{C}\times\mathbf{A})=\mathbf{C}\cdot(\mathbf{A}\times\mathbf{B})$.

the following constitutive relations.

$$\mathbf{p} = \mathbf{d} - \epsilon_{\mathbf{0}}\mathbf{e}, \quad \mathbf{m} = \mathbf{b}/\mu_{\mathbf{0}} - \mathbf{h}. \tag{2.19}$$

When the body deforms, let us consider a generic point $P \in \Omega_t$ moves with a velocity $\dot{\mathbf{x}}$. At this moving point, we denote the electro magnetic variables $\{\widetilde{\mathbf{e}}, \widetilde{\mathbf{h}}, \widetilde{\mathbf{b}}, \widetilde{\mathbf{m}}\}$ with respect to a *rest frame*. The rest frame variables, through the *Galilean transformation*, can be written in the following forms

$$\begin{aligned} \widetilde{\mathbf{j}}_f &= \mathbf{j}_f - \dot{\mathbf{x}} q_f, \qquad \widetilde{\mathbf{b}} = \mathbf{b} - c^{-2}\dot{\mathbf{x}} \times \mathbf{e}, \\ \widetilde{\mathbf{e}} &= \mathbf{e} + \dot{\mathbf{x}} \times \mathbf{b}, \quad \widetilde{\mathbf{h}} = \mathbf{h} - \dot{\mathbf{x}} \times \mathbf{d}, \\ \widetilde{\mathbf{m}} &= \mathbf{m} + \dot{\mathbf{x}} \times \mathbf{p}. \end{aligned} \tag{2.20}$$

In general, $\{\widetilde{\mathbf{b}}, \widetilde{\mathbf{e}}, \widetilde{\mathbf{h}}, \widetilde{\mathbf{m}}\}$ obeys *Lorentz transformation*. The Maxwell equations are invariant under Lorentz group of transformation in *Minkowsky space*. But the mechanical responses are not invariant under Lorentz transformation. They are invariant under *Euclidean transformation*. This mismatching of the electromagnetic and mechanical invariance can be solved in *non relativistic* case. It can be shown that under this approximation, $o(|\dot{\mathbf{x}}|^2/c^2)$, where c is the speed of light, the requirement of invariance of the material response under Euclidean transformation is equivalent to the requirement of the Lorentz transformation [123]. So in the non-relativistic limit, $\widetilde{\mathbf{b}} \simeq \mathbf{b}$. We model in this framework, which is also known as *Maxwell Minkowski* formulation.

We follow the substitutions, as shown in the Table I, in the general balance equations to obtain the Maxwell equations and jump conditions. In the table, σ_s is the surface charge density, $\mathbf{K}$ is the surface current density, current per unit width perpendicular to the flow and $\widetilde{\mathbf{K}} = \mathbf{K} - \sigma_s \mathbf{v}$. The local form of the Maxwell equations

Equations (2.12,2.15)	ψ	Φ_ψ	σ_ψ	χ
Gauss law (electric)	0	$-\mathbf{d}$	q_f	σ_s
Gauss law (magnetic)	0	$\mathbf{b}$	0	0
Equations (2.13,2.18)	$\boldsymbol{\Psi}$	$\boldsymbol{\Xi}_\Psi$	$\boldsymbol{\Sigma}_\Psi$	$\boldsymbol{\kappa}$
Ampere's law	$\mathbf{d}$	$\widetilde{\mathbf{h}}$	$-\widetilde{\mathbf{j}}_f$	$\widetilde{\mathbf{K}}$
Faraday's law	$-\mathbf{b}$	$\widetilde{\mathbf{e}}$	0	0

Table I. Electromagnetic field variables

are given by

$$\nabla \cdot \mathbf{d} = q_f \tag{2.21a}$$

$$\nabla \cdot \mathbf{b} = 0 \tag{2.21b}$$

$$\nabla \times \widetilde{\mathbf{h}} - \overset{*}{\mathbf{d}} = \widetilde{\mathbf{j}}_f \tag{2.21c}$$

$$\nabla \times \widetilde{\mathbf{e}} = -\overset{*}{\mathbf{b}}. \tag{2.21d}$$

Similarly, the jump conditions are given by (2.18)

$$\mathbf{n} \cdot [\![\mathbf{d}]\!] = \sigma_s \tag{2.22a}$$

$$\mathbf{n} \cdot [\![\mathbf{b}]\!] = 0 \tag{2.22b}$$

$$\mathbf{n} \times [\![\widetilde{\mathbf{h}} - \mathbf{d} \times (\dot{\mathbf{x}} - \mathbf{v})]\!] = \widetilde{\mathbf{K}} \tag{2.22c}$$

$$\mathbf{n} \times [\![\widetilde{\mathbf{e}} + \mathbf{b} \times (\dot{\mathbf{x}} - \mathbf{v})]\!] = 0. \tag{2.22d}$$

The third condition can be further simplified to

$$\mathbf{n}\times\big[\!\big[\widetilde{\mathbf{h}}-\mathbf{d}\times(\dot{\mathbf{x}}-\mathbf{v})\big]\!\big]=\widetilde{\mathbf{K}}$$
$$\Rightarrow \mathbf{n}\times\big[\!\big[\mathbf{h}+\mathbf{d}\times\mathbf{v}\big]\!\big]=\widetilde{\mathbf{K}}$$
$$\Rightarrow \mathbf{n}\times\big[\!\big[\mathbf{h}\big]\!\big]+\mathbf{n}\times\big[\!\big[\mathbf{d}\times\mathbf{v}\big]\!\big]=\widetilde{\mathbf{K}}$$
$$\Rightarrow \mathbf{n}\times\big[\!\big[\mathbf{h}\big]\!\big]+(\mathbf{n}\cdot\mathbf{v})\big[\!\big[\mathbf{d}\big]\!\big]-\mathbf{v}(\big[\!\big[\mathbf{d}\big]\!\big]\cdot\mathbf{n})=\widetilde{\mathbf{K}}$$
$$\Rightarrow \mathbf{n}\times\big[\!\big[\mathbf{h}\big]\!\big]+(\mathbf{n}\cdot\mathbf{v})\big[\!\big[\mathbf{d}\big]\!\big]-\mathbf{v}\sigma_{\mathbf{s}}=\widetilde{\mathbf{K}}\quad\text{(By using (2.22a))}$$
$$\Rightarrow \mathbf{n}\times\big[\!\big[\mathbf{h}\big]\!\big]+(\mathbf{n}\cdot\mathbf{v})\big[\!\big[\mathbf{d}\big]\!\big]=\widetilde{\mathbf{K}}+\mathbf{v}\sigma_{\mathbf{s}}$$

Or[3]

$$\mathbf{n}\times\big[\!\big[\mathbf{h}\big]\!\big]+(\mathbf{v}\cdot\mathbf{n})\big[\!\big[\mathbf{d}\big]\!\big]=\mathbf{K}. \tag{2.23}$$

Similarly, equation (2.22d) can be simplified as

$$\mathbf{n}\times\big[\!\big[\mathbf{e}\big]\!\big]-(\mathbf{v}\cdot\mathbf{n})\big[\!\big[\mathbf{b}\big]\!\big]=\mathbf{0}. \tag{2.24}$$

3. Mechanical conservation laws

	ψ	Φ_ψ	σ_ψ	χ
Mass	ρ	0	0	0
L momentum	$\rho\mathbf{g}$	$\boldsymbol{\sigma}$	$\rho\mathbf{f}^b$	0
A momentum	$(\mathbf{x}-\mathbf{x}_0)\wedge\rho\mathbf{g}$	$(\mathbf{x}-\mathbf{x}_0)\wedge\boldsymbol{\sigma}$	$(\mathbf{x}-\mathbf{x}_0)\wedge\rho\mathbf{f}^b$	0
Energy	$\rho u+\frac{1}{2}\rho\dot{\mathbf{x}}\cdot\dot{\mathbf{x}}$	$-\mathbf{q}+\boldsymbol{\sigma}^T\dot{\mathbf{x}}-(\widetilde{\mathbf{e}}\times\widetilde{\mathbf{h}})$	$\rho r^h+\rho\dot{\mathbf{x}}\cdot\mathbf{f}^b$	0
	$+\frac{1}{2}(\epsilon_0\mathbf{e}\cdot\mathbf{e}+\frac{1}{\mu_0}\mathbf{b}\cdot\mathbf{b})$			0

Table II. Mechanical field variables

[3] At step three of the above procedure, we use the following identity: $\mathbf{A}\times(\mathbf{B}\times\mathbf{C})=\mathbf{B}(\mathbf{A}\cdot\mathbf{C})-\mathbf{C}(\mathbf{A}\cdot\mathbf{B})$.

Mechanical conservation laws and boundary conditions are obtained from equations (2.12) and (2.15) with the substitutions, given in Table II. Here, ρ is the mass density, $\boldsymbol{\sigma}$ is the total stress generated due to combined magneto-mechanical effect, $\mathbf{f}^b$ is the nonmagnetic body force density, $\mathbf{g} = \dot{\mathbf{x}} + \frac{\epsilon_0}{\rho}\mathbf{e} \times \mathbf{b}$ is the generalized momentum density, $\mathbf{x}_0$ is the position vector of the point where the moment is considered, u is the internal energy density, $\frac{1}{2}\dot{\mathbf{x}} \cdot \dot{\mathbf{x}}$ is the kinetic energy density and $\frac{1}{2}(\epsilon_0 \mathbf{e} \cdot \mathbf{e} + \frac{1}{\mu_0}\mathbf{b} \cdot \mathbf{b})$ is the electromagnetic energy density of the free space. r^h is the heat supply due to external source, $\mathbf{q}$ is the heat flux and $(\widetilde{\mathbf{e}} \times \widetilde{\mathbf{h}})$ is the electro-magnetic energy flux. Using *Poynting theorem* in a moving frame and denoting the Poynting vector $\widetilde{\mathbf{S}} = (\widetilde{\mathbf{e}} \times \widetilde{\mathbf{h}})$ we can write

$$-\nabla \cdot \widetilde{\mathbf{S}} = \widetilde{\mathbf{j}}_f \cdot \widetilde{\mathbf{e}} + \widetilde{\mathbf{h}} \cdot \overset{*}{\mathbf{b}} + \widetilde{\mathbf{e}} \cdot \overset{*}{\mathbf{d}}. \tag{2.25}$$

The conservation laws of mass, linear momentum and angular momentum become

$$\dot{\rho} + \rho \nabla \cdot \dot{\mathbf{x}} = 0 \tag{2.26a}$$

$$\nabla \cdot \boldsymbol{\sigma} + \rho \mathbf{f}^{\mathbf{b}} = \rho \dot{\mathbf{g}} \tag{2.26b}$$

$$\mathrm{skw}\,(\boldsymbol{\sigma}) = \mathrm{skw}\,(\rho \mathbf{g} \otimes \dot{\mathbf{x}}) \tag{2.26c}$$

and the jump conditions

$$\big[\!\big[\rho(\dot{\mathbf{x}} - \mathbf{v})\big]\!\big]\mathbf{n} = 0$$

$$\big[\!\big[\rho \mathbf{g} \otimes (\dot{\mathbf{x}} - \mathbf{v}) - \boldsymbol{\sigma}\big]\!\big]\mathbf{n} = 0 \tag{2.27a}$$

$$\big[\!\big[(\mathbf{x} - \mathbf{x}_0) \wedge \rho \mathbf{g} \otimes (\dot{\mathbf{x}} - \mathbf{v}) - (\mathbf{x} - \mathbf{x}_0) \wedge \boldsymbol{\sigma}\big]\!\big]\mathbf{n} = 0. \tag{2.27b}$$

We will discus detail calculation of the reduction of the energy equation to a simplified form. The calculations up to (2.37) are mostly followed by Kovetz formulation [131]. The derivation is straight forward but one needs a careful book keeping of different

terms. The Conservation of energy can be obtained by substituting the last row of Table.II in (2.12),

$$\frac{\partial}{\partial t}(\rho u + \frac{1}{2}\rho\dot{\mathbf{x}}\cdot\dot{\mathbf{x}} + \frac{\epsilon_0}{2}\mathbf{e}\cdot\mathbf{e} + \frac{1}{2\mu_0}\mathbf{b}\cdot\mathbf{b}) + \nabla\cdot[(\rho u + \frac{1}{2}\rho\dot{\mathbf{x}}\cdot\dot{\mathbf{x}} + \frac{\epsilon_0}{2}\mathbf{e}\cdot\mathbf{e} + \frac{1}{2\mu_0}\mathbf{b}\cdot\mathbf{b})\dot{\mathbf{x}} - (-\mathbf{q} + \boldsymbol{\sigma}^T\dot{\mathbf{x}} - \widetilde{\mathbf{e}}\times\widetilde{\mathbf{h}})] - (\rho r^h + \rho\dot{\mathbf{x}}\cdot\mathbf{f}^b) = 0 \tag{2.28}$$

If we denote a scalar by ϕ, then with the help of mass conservation (2.26a) we can write

$$\frac{\partial\rho\phi}{\partial t} + \nabla\cdot(\rho\phi\dot{\mathbf{x}}) = \rho\dot{\phi}, \tag{2.29}$$

If we denote $\phi = u + \frac{1}{2}\rho\dot{\mathbf{x}}\cdot\dot{\mathbf{x}} + \frac{\epsilon_0}{2\rho}\mathbf{e}\cdot\mathbf{e} + \frac{1}{2\mu_0\rho}\mathbf{b}\cdot\mathbf{b}$ then (2.28), with the help of (2.29), reduces to

$$\begin{aligned}&\rho\frac{d}{dt}(u + \frac{1}{2}\dot{\mathbf{x}}\cdot\dot{\mathbf{x}} + \frac{\epsilon_0}{2\rho}\mathbf{e}\cdot\mathbf{e} + \frac{1}{2\mu_0\rho}\mathbf{b}\cdot\mathbf{b}) + \nabla\cdot[-(-\mathbf{q} + \boldsymbol{\sigma}^T\dot{\mathbf{x}} - \widetilde{\mathbf{e}}\times\widetilde{\mathbf{h}})]\\ -\ &(\rho r^h + \rho\dot{\mathbf{x}}\cdot\mathbf{f}^b) = 0.\end{aligned} \tag{2.30}$$

Moreover, from the relation $\nabla\cdot(\boldsymbol{\sigma}^T\dot{\mathbf{x}}) = \boldsymbol{\sigma} : \mathbf{L} + \dot{\mathbf{x}}\cdot(\nabla\cdot\boldsymbol{\sigma})$ we get,

$$\begin{aligned}&\rho\dot{u} + \rho\dot{\mathbf{x}}\cdot\ddot{\mathbf{x}} + \rho\frac{d}{dt}(\frac{\epsilon_0}{2\rho}\mathbf{e}\cdot\mathbf{e} + \frac{1}{2\mu_0\rho}\mathbf{b}\cdot\mathbf{b}) + \nabla\cdot\mathbf{q} - \boldsymbol{\sigma} : \mathbf{L} + \nabla\cdot(\widetilde{\mathbf{e}}\times\widetilde{\mathbf{h}})\\ -\ &\rho r^h - \dot{\mathbf{x}}\cdot(\rho\mathbf{f}^b + \nabla\cdot\boldsymbol{\sigma}) = 0.\end{aligned} \tag{2.31}$$

Using (2.26b) and collecting the coefficient of $\dot{\mathbf{x}}$, we get

$$\begin{aligned}&\rho\dot{u} + \rho\frac{d}{dt}(\frac{\epsilon_0}{2\rho}\mathbf{e}\cdot\mathbf{e} + \frac{1}{2\mu_0\rho}\mathbf{b}\cdot\mathbf{b}) + \nabla\cdot\mathbf{q} - \boldsymbol{\sigma} : L + \nabla\cdot(\widetilde{\mathbf{e}}\times\widetilde{\mathbf{h}})\\ -\ &\rho r - \rho\dot{\mathbf{x}}\cdot(\dot{\mathbf{g}} - \ddot{\mathbf{x}}) = 0.\end{aligned} \tag{2.32}$$

We now use the following identity for any scalar ϕ

$$\begin{aligned}\rho\frac{d}{dt}(\frac{\phi}{\rho}) &= \rho(\frac{1}{\rho}\dot{\phi}-\frac{\dot{\rho}}{\rho^2}\phi)\\ &= \dot{\phi}+\frac{\rho\nabla\cdot\dot{\mathbf{x}}}{\rho}\phi\\ &= \dot{\phi}+(L:I)\phi. \end{aligned} \tag{2.33}$$

and rewriting the term $\rho\frac{d}{dt}(\frac{\epsilon_0}{2\rho}\mathbf{e}\cdot\mathbf{e}+\frac{1}{2\mu_0\rho}\mathbf{b}\cdot\mathbf{b})$ in the equation (2.32) with the help of the identity (2.33) to obtain

$$\begin{aligned}&\rho\dot{u}+(\epsilon_0\dot{\mathbf{e}}\cdot\mathbf{e}+\frac{1}{\mu_0}\dot{\mathbf{b}}\cdot\mathbf{b})+\frac{1}{2}(\epsilon_0\mathbf{e}\cdot\mathbf{e}+\frac{1}{\mu_0}\mathbf{b}\cdot\mathbf{b})\mathbf{I}:\mathbf{L}\\ &+\nabla\cdot\mathbf{q}-\boldsymbol{\sigma}:\mathbf{L}+\nabla\cdot(\widetilde{\mathbf{e}}\times\widetilde{\mathbf{h}})-\rho r^h-\rho\dot{\mathbf{x}}\cdot(\dot{\mathbf{g}}-\ddot{\mathbf{x}})=0. \end{aligned} \tag{2.34}$$

Our next task is to expand the *Pointing vector* by using equation (2.25). The detail derivation is given in Appendix C. The expanded form is given by

$$\begin{aligned}&\nabla\cdot(\widetilde{\mathbf{e}}\times\widetilde{\mathbf{h}})=-\widetilde{\mathbf{j}}_f\cdot\widetilde{\mathbf{e}}-(\frac{\mathbf{b}\cdot\dot{\mathbf{b}}}{\mu_0}-\widetilde{\mathbf{m}}\cdot\dot{\mathbf{b}}+\epsilon_0\mathbf{e}\cdot\dot{\mathbf{e}}+\widetilde{\mathbf{e}}\cdot\dot{\mathbf{p}})+\rho\frac{d}{dt}(\frac{\epsilon_0}{\rho}\mathbf{e}\times\mathbf{b})\cdot\dot{\mathbf{x}}\\ -\;&[(\frac{\mathbf{b}\cdot\mathbf{b}}{\mu_0}-\widetilde{\mathbf{m}}\cdot\mathbf{b}+\epsilon_0\mathbf{e}\cdot\mathbf{e}+\widetilde{\mathbf{e}}\cdot\mathbf{p})\mathbf{I}\\ -\;&(\frac{\mathbf{b}\otimes\mathbf{b}}{\mu_0}-\widetilde{\mathbf{m}}\otimes\mathbf{b}+\epsilon_0\mathbf{e}\otimes\mathbf{e}+\widetilde{\mathbf{e}}\otimes\mathbf{p}+\epsilon_0\mathbf{e}\times\mathbf{b}\otimes\dot{\mathbf{x}})]:\mathbf{L} \end{aligned} \tag{2.35}$$

Substituting back (2.35) to (2.34) we get

$$\begin{aligned}&\rho\dot{u}+\nabla\cdot\mathbf{q}-\boldsymbol{\sigma}:\mathbf{L}-\widetilde{\mathbf{j}}_f\cdot\widetilde{\mathbf{e}}+\widetilde{\mathbf{m}}\cdot\dot{\mathbf{b}}-\widetilde{\mathbf{e}}\cdot\dot{\mathbf{p}}-[(\frac{1}{2}\frac{\mathbf{b}\cdot\mathbf{b}}{\mu_0}-\widetilde{\mathbf{m}}\cdot\mathbf{b}+\frac{1}{2}\epsilon_0\mathbf{e}\cdot\mathbf{e}\\ +\;&\widetilde{\mathbf{e}}\cdot\mathbf{p})\mathbf{I}-(\frac{\mathbf{b}\otimes\mathbf{b}}{\mu_0}-\widetilde{\mathbf{m}}\otimes\mathbf{b}+\epsilon_0\mathbf{e}\otimes\mathbf{e}+\widetilde{\mathbf{e}}\otimes\mathbf{p}+\epsilon_0\mathbf{e}\times\mathbf{b}\otimes\dot{\mathbf{x}})]:\mathbf{L}\\ -\;&\rho r^h-\rho\dot{\mathbf{x}}\cdot(\dot{\mathbf{g}}-\ddot{\mathbf{x}}-\frac{d}{dt}\frac{\epsilon_0}{\rho}\mathbf{e}\times\mathbf{b})=0 \end{aligned} \tag{2.36}$$

Since $\mathbf{g} = \dot{\mathbf{x}} + \frac{\epsilon_0}{\rho}\mathbf{e} \times \mathbf{b}$, we rewrite the above equation

$$\begin{aligned} & \rho\dot{u} + \nabla \cdot \mathbf{q} - \boldsymbol{\sigma} : \mathbf{L} - \widetilde{\mathbf{j}}_f \cdot \widetilde{\mathbf{e}} + \widetilde{\mathbf{m}} \cdot \dot{\mathbf{b}} - \widetilde{\mathbf{e}} \cdot \dot{\mathbf{p}} \\ - \quad & [(\frac{1}{2}\frac{\mathbf{b} \cdot \mathbf{b}}{\mu_0} - \widetilde{\mathbf{m}} \cdot \mathbf{b} + \frac{1}{2}\epsilon_0 \mathbf{e} \cdot \mathbf{e} + \widetilde{\mathbf{e}} \cdot \mathbf{p})\mathbf{I} - (\frac{\mathbf{b} \otimes \mathbf{b}}{\mu_0} - \widetilde{\mathbf{m}} \otimes \mathbf{b} + \epsilon_0 \mathbf{e} \otimes \mathbf{e} \\ + \quad & \widetilde{\mathbf{e}} \otimes \mathbf{p} + \epsilon_0 \mathbf{e} \times \mathbf{b} \otimes \dot{\mathbf{x}})] : \mathbf{L} - \rho r^h = 0 \end{aligned} \tag{2.37}$$

We assume that $u(\mathbf{F}, \mathbf{p}, \mathbf{b}, s, \{\zeta\})$, where $\mathbf{F}$ is the deformation gradient, s is the entropy. The set $\{\zeta\}$ represents the collection of tensor valued, vector valued and scalar valued internal variables.

Since in the experiments, it is easier to control the stress, magnetic or electric field and temperature, we will propose a Gibbs free energy with the above mentioned controllable quantities as dependent variables. The Gibbs free energy formulation also provides the constitutive responses in terms of controllable variables and facilitates model calibrations. We perform step by step partial Legendre transformations to change the variable space of u to Gibbs free energy G. First we change the variable from $\mathbf{p}$ to $\widetilde{\mathbf{e}}$. Next we consider quasistatic condition for MSMA by assuming that no electric field is applied. We further change the variable $\mathbf{b}$ to $\mathbf{h}$ and pull back all the controllable variables in the reference configuration. Finally we obtain the full Legendre transformation to the Gibbs free energy. All the steps are shown below:

$$u(\mathbf{F}, \mathbf{p}, \mathbf{b}, s, \{\zeta\}) \longrightarrow \psi(\mathbf{F}, \widetilde{\mathbf{e}}, \mathbf{b}, T, \{\zeta\}) \overset{\mathbf{e}=0,\ \dot{\mathbf{x}}\approx 0}{\longrightarrow} \psi(\mathbf{F}, \mathbf{b}, T, \{\zeta\})$$

$$\longrightarrow \psi_1(\mathbf{F}, \mathbf{h}, T, \{\zeta\}) \overset{\Omega_t \to \Omega_0}{\longrightarrow} \widetilde{\psi}_1(\mathbf{E}, \mathbf{H}, T, \{\mathbb{Z}\}) \longrightarrow G(\mathbf{S}^E, \mathbf{H}, T, \{\mathbb{Z}\}).$$

Here $\mathbf{S}^E$ is the work conjugate of the Green strain $\mathbf{E}$. More detail will be discussed shortly. We will now present more detail calculations for each step of the Legendre

transformation. We first consider

$$\psi(\mathbf{F}, \widetilde{\mathbf{e}}, \mathbf{b}, T, \{\zeta\}) = u - sT - \frac{1}{\rho}\widetilde{\mathbf{e}} \cdot \mathbf{p}. \tag{2.38}$$

Now,

$$\dot{\psi} = \dot{u} - \dot{s}T - s\dot{T} - \frac{1}{\rho}\frac{d}{dt}(\widetilde{\mathbf{e}} \cdot \mathbf{p}) - \frac{\mathbf{L} : \mathbf{I}}{\rho}(\widetilde{\mathbf{e}} \cdot \mathbf{p}). \tag{2.39}$$

Substituting $\rho\dot{u}$ from (2.39) to (2.36) we get,

$$\begin{aligned} & \rho(\dot{\psi} + \dot{s}T - s\dot{T}) + \nabla \cdot \mathbf{q} - \boldsymbol{\sigma} : \mathbf{L} - \widetilde{\mathbf{j}}_f \cdot \widetilde{\mathbf{e}} + \widetilde{\mathbf{m}} \cdot \dot{\mathbf{b}} + \dot{\widetilde{\mathbf{e}}} \cdot \mathbf{p} \\ - \quad & [(\frac{1}{2}\frac{\mathbf{b} \cdot \mathbf{b}}{\mu_0} - \widetilde{\mathbf{m}} \cdot \mathbf{b} + \frac{1}{2}\epsilon_0 \mathbf{e} \cdot \mathbf{e})\mathbf{I} - (\frac{\mathbf{b} \otimes \mathbf{b}}{\mu_0} - \widetilde{\mathbf{m}} \otimes \mathbf{b} + \epsilon_0 \mathbf{e} \otimes \mathbf{e} \\ + \quad & \widetilde{\mathbf{e}} \otimes \mathbf{p} + \epsilon_0 \mathbf{e} \times \mathbf{b} \otimes \dot{\mathbf{x}})] : \mathbf{L} - \rho r^h = 0 \end{aligned} \tag{2.40}$$

We collect the coefficient of $\mathbf{L}$ and define *local stress* by

$$\boxed{\boldsymbol{\sigma}^L = \boldsymbol{\sigma} - \boldsymbol{\sigma}^M} \tag{2.41}$$

and the *electro-magnetic stress* by

$$\begin{aligned} \boldsymbol{\sigma}^M \quad = \quad & [\widetilde{\mathbf{m}} \cdot \mathbf{b} - \frac{1}{2}(\epsilon_0 \mathbf{e} \cdot \mathbf{e} + \frac{\mathbf{b} \cdot \mathbf{b}}{\mu_0})]\mathbf{I} \\ + \quad & \frac{\mathbf{b} \otimes \mathbf{b}}{\mu_0} - \widetilde{\mathbf{m}} \otimes \mathbf{b} + \epsilon_0 \mathbf{e} \otimes \mathbf{e} + \widetilde{\mathbf{e}} \otimes \mathbf{p} + \epsilon_0 \mathbf{e} \times \mathbf{b} \otimes \dot{\mathbf{x}} \end{aligned} \tag{2.42}$$

The local form of the energy balance (2.40) reduces to the following form

$$\rho(\dot{\psi} + \dot{s}T - s\dot{T}) + \nabla \cdot \mathbf{q} - \boldsymbol{\sigma}^L : \mathbf{L} - \widetilde{\mathbf{j}}_f \cdot \widetilde{\mathbf{e}} + \widetilde{\mathbf{m}} \cdot \dot{\mathbf{b}} + \dot{\widetilde{\mathbf{e}}} \cdot \mathbf{p} - \rho r^h = 0. \tag{2.43}$$

The entropy inequality is given by

$$\begin{aligned} \rho\dot{s} \quad & \geqslant \quad \rho r^h/T - \nabla \cdot (\mathbf{q}/T) \, , \\ & \geqslant \quad \rho r^h/T - \nabla \cdot \mathbf{q}/T + \mathbf{q} \cdot \nabla T/T^2. \end{aligned} \tag{2.44}$$

Combining (2.44) and (2.43) we get,

$$\rho(\dot{\psi} - s\dot{T}) - \boldsymbol{\sigma}^L : \mathbf{L} + \widetilde{\mathbf{m}} \cdot \dot{\mathbf{b}} + \dot{\widetilde{\mathbf{e}}} \cdot \mathbf{p} - \widetilde{\mathbf{j}}_f \cdot \widetilde{\mathbf{e}} + \mathbf{q} \cdot \nabla T/T \geqslant 0 \tag{2.45}$$

In a moving frame *Ohms law* is given by $\widetilde{\mathbf{j}}_f = \boldsymbol{\Omega}^{-1}\widetilde{\mathbf{e}}$, were $\boldsymbol{\Omega}$ is the resistivity tensor and positive definite. Similarly from *Fourier law* of heat conduction we have $\mathbf{q} = -\mathbf{K}\nabla T$ where $\mathbf{K}$ is the material thermal conductivity tensor and positive definite. With the help of these two constitutive laws we can rewrite (2.45) as

$$\boxed{\rho(\dot{\psi} - s\dot{T}) - \boldsymbol{\sigma}^L : \mathbf{L} + \widetilde{\mathbf{m}} \cdot \dot{\mathbf{b}} + \dot{\widetilde{\mathbf{e}}} \cdot \mathbf{p} \geqslant 0} \tag{2.46}$$

It should be noted that local stress $\boldsymbol{\sigma}^L$ is mechanical work conjugate of the velocity gradient $\mathbf{L}$. We further rewrite (2.46) in the following form,

$$\begin{aligned} & \rho(\psi_{,\mathbf{F}} : \dot{\mathbf{F}} + \psi_{,\mathbf{b}} \cdot \dot{\mathbf{b}} + \psi_{,\widetilde{\mathbf{e}}} \cdot \dot{\widetilde{\mathbf{e}}} + \psi_{,T}\, \dot{T} + \psi_{,\dot{\mathbf{x}}} \cdot \ddot{\mathbf{x}} + \psi_{,\zeta_i} \cdot \dot{\zeta}_i - s\dot{T}) \\ - \quad & \boldsymbol{\sigma}^L : \dot{\mathbf{F}}\mathbf{F}^{-1} + \widetilde{\mathbf{m}} \cdot \dot{\mathbf{b}} + \mathbf{p} \cdot \dot{\widetilde{\mathbf{e}}} \geqslant \mathbf{0} \end{aligned} \tag{2.47}$$

or

$$\begin{aligned} & (\rho\psi_{,\mathbf{F}} - \boldsymbol{\sigma}^L\mathbf{F}^{-T}) : \dot{\mathbf{F}} + (\rho\psi_{,\mathbf{b}} + \widetilde{\mathbf{m}}) \cdot \dot{\mathbf{b}} + (\rho\psi_{,\widetilde{\mathbf{e}}} + \mathbf{p}) \cdot \dot{\widetilde{\mathbf{e}}} + (\rho\psi_{,T} + \rho s)\dot{T} \\ + \quad & \psi_{,\zeta_i} \cdot \dot{\zeta}_i \geqslant 0. \end{aligned} \tag{2.48}$$

Here ζ_i represents an element of the set $\{\zeta\}$ and the associated '$\cdot$' represents the generalized tensor contraction. Using Colleman Noll maximum entropy principle we

get the following constitutive equations.

$$\boldsymbol{\sigma}^L = \rho\psi_{,\mathbf{F}}\,\mathbf{F}^T \tag{2.49a}$$

$$\widetilde{\mathbf{m}} = -\rho\psi_{,\mathbf{b}} \tag{2.49b}$$

$$\mathbf{p} = -\rho\psi_{,\widetilde{\mathbf{e}}} \tag{2.49c}$$

$$s = -\psi_T \tag{2.49d}$$

$$\psi_{,\zeta_i}\cdot\dot{\zeta}_i \geqslant 0 \tag{2.49e}$$

B. MSMA material system: Magnetized medium

In this section we consider MSMA for which polarization is zero ($\mathbf{p} = \mathbf{0}$) and so $\widetilde{\mathbf{m}} = \mathbf{m}$. This reduces the general expression of the magneto stress ((2.42)) in the following form

$$\begin{aligned}\boldsymbol{\sigma}^M &= [\mathbf{m}\cdot\mathbf{b} - \frac{1}{2}(\epsilon_0\mathbf{e}\cdot\mathbf{e} + \frac{\mathbf{b}\cdot\mathbf{b}}{\mu_0})]\mathbf{I} \\ &+ \frac{\mathbf{b}\otimes\mathbf{b}}{\mu_0} - \mathbf{m}\otimes\mathbf{b} + \epsilon_0\mathbf{e}\otimes\mathbf{e} + \epsilon_0\mathbf{e}\times\mathbf{b}\otimes\dot{\mathbf{x}}\end{aligned} \tag{2.50}$$

It is important to note that though the material system does not have polarization, the electric field $\widetilde{\mathbf{e}}$ can influence the magneto stress due to the coupling of $\mathbf{e}$ with $\mathbf{b}$ and $\dot{\mathbf{x}}$.

Since MSMA experiments are conducted under zero electric field, now and onwards we will consider $\mathbf{e} = 0$. Under these conditions, the magneto stress tensor ((2.42)) reduces to the *Maxwell stress*

$$\boxed{\boldsymbol{\sigma}^M = \boldsymbol{\sigma}^{Mb}(\mathbf{b},\mathbf{m}) = \frac{\mathbf{b}\otimes\mathbf{b}}{\mu_0} - \mathbf{m}\otimes\mathbf{b} + [\mathbf{m}\cdot\mathbf{b} - \frac{1}{2}\frac{\mathbf{b}\cdot\mathbf{b}}{\mu_0}]\mathbf{I}} \tag{2.51}$$

Now we will perform partial Legendre transformation from Ψ to Ψ_1, as discussed in the flow chart of the last section.

1. Magnetic field $\mathbf{h}$ as independent variable: $\psi_1 = \psi_1(\mathbf{F}, \mathbf{h}, T, \{\zeta\})$

First we change the dependent variable $\mathbf{b}$ of $\psi(\mathbf{F}, \mathbf{b}, T, \{\zeta\})$ to $\mathbf{h}$. We are looking for a transformation function $\Phi(\mathbf{b}, \mathbf{h})$ such that

$$\psi_1(\mathbf{F}, \mathbf{h}, T, \{\zeta\}) = \psi(\mathbf{F}, \mathbf{b}, T, \{\zeta\}) + \Phi(\mathbf{b}, \mathbf{h}) \tag{2.52}$$

For MSMAs ($\mathbf{p} = \mathbf{0}$ and $\widetilde{\mathbf{m}} = \mathbf{m}$), (2.49b) becomes

$$\rho\psi_{1,\mathbf{b}} = -\mathbf{m} = (-\frac{\mathbf{b}}{\mu_0} + \mathbf{h}) \tag{2.53}$$

and with the transformed function Ψ_1, we are looking for the following constitutive equation

$$\rho\psi_{1,\mathbf{h}} = -\mu_0\mathbf{m} = (-\mathbf{b} + \mu_0\mathbf{h}) \tag{2.54}$$

Taking the partial derivative of (2.52) and using (2.54) we get,

$$\begin{aligned} \rho\psi_{1,\mathbf{h}} = \Phi_{,\mathbf{h}} &= (-\mathbf{b} + \mu_0\mathbf{h}) \\ \Rightarrow \Phi &= -\mathbf{b}\cdot\mathbf{h} + \frac{\mu_0}{2}\mathbf{h}\cdot\mathbf{h} + \Phi_1(\mathbf{b}) \end{aligned} \tag{2.55}$$

where $\Phi_1(\mathbf{b})$ is an arbitrary function. Similarly taking partial derivative of Ψ_1 with respect to $\mathbf{b}$ we get

$$\begin{aligned} \rho\psi_{1,\mathbf{b}} = \mathbf{0} &= \psi_{,\mathbf{b}} + \Phi_{,\mathbf{b}} \\ \Rightarrow \mathbf{0} &= (-\frac{\mathbf{b}}{\mu_0} + \mathbf{h}) + (-\mathbf{h} + \Phi_{1,\mathbf{b}}) \\ &= -\frac{\mathbf{b}}{\mu_0} + \Phi_{1,\mathbf{b}} \\ \Rightarrow \Phi_1 &= \frac{\mathbf{b}\cdot\mathbf{b}}{2\mu_0}. \end{aligned} \tag{2.56}$$

The integration constant is set to zero by assuming $\Phi_1(\mathbf{0}) = \mathbf{0}$. Substituting back (2.56) in (2.55) we get,

$$\begin{aligned}
\Phi &= -\mathbf{b}\cdot\mathbf{h} + \frac{\mu_0}{2}\mathbf{h}\cdot\mathbf{h} + \frac{\mathbf{b}\cdot\mathbf{b}}{2\mu_0} \\
&= \frac{\mu_0}{2}(\mathbf{h}\cdot\mathbf{h} - 2\frac{\mathbf{b}}{\mu_0}\cdot\mathbf{h} + \frac{\mathbf{b}\cdot\mathbf{b}}{\mu_0^2}) \\
&= \frac{\mu_0}{2}(\mathbf{h} - \frac{\mathbf{b}}{\mu_0})\cdot(\mathbf{h} - \frac{\mathbf{b}}{\mu_0}) \\
&= \frac{\mu_0}{2}\mathbf{m}\cdot\mathbf{m}. \qquad (2.57)
\end{aligned}$$

We perform the following partial Legendre transformation,

$$\boxed{\psi_1(\mathbf{F},\mathbf{h},T,\{\zeta\}) = \psi(\mathbf{F},\mathbf{b},T,\{\zeta\}) + \frac{\mu_0}{2\rho}\mathbf{m}\cdot\mathbf{m}.} \qquad (2.58)$$

Therefore,

$$\dot{\psi_1} = \dot{\psi} + \frac{\mu_0}{\rho}(\dot{\mathbf{m}}\cdot\mathbf{m}) + \frac{\mu_0}{2\rho}(\mathbf{m}\cdot\mathbf{m})\mathbf{I}:\mathbf{L} \quad \text{by (2.33)}$$

and we write

$$\begin{aligned}
&(\psi_{1,\mathbf{F}} : \dot{\mathbf{F}} + \psi_{1,\mathbf{h}}\cdot\dot{\mathbf{h}} + \psi_{1,T}\dot{T} + \psi_{1,\zeta_i}\cdot\dot{\zeta}_i) \\
= \;& (\psi_{,\mathbf{F}} : \dot{\mathbf{F}} + \psi_{,\mathbf{b}}\cdot\dot{\mathbf{b}} + \psi_{,T}\dot{T} + \psi_{,\zeta_i}\cdot\dot{\zeta}_i) \\
+ \;& \frac{\mu_0}{\rho}(\dot{\mathbf{m}}\cdot\mathbf{m}) + \frac{\mu_0}{2\rho}(\mathbf{m}\cdot\mathbf{m})\mathbf{F}^{-T} : \dot{\mathbf{F}}. \qquad (2.59)
\end{aligned}$$

Moreover using the fact that

$$\begin{aligned}
\rho\psi_{,\mathbf{b}}\cdot\dot{\mathbf{b}} + \mu_0(\dot{\mathbf{m}}\cdot\mathbf{m}) &= \rho\psi_{,\mathbf{b}}\cdot\mu_0(\dot{\mathbf{h}} + \dot{\mathbf{m}}) + \mu_0(\dot{\mathbf{m}}\cdot\mathbf{m}) \\
&= (-\mathbf{m})\cdot\mu_0(\dot{\mathbf{h}} + \dot{\mathbf{m}}) + \mu_0(\dot{\mathbf{m}}\cdot\mathbf{m}) \\
&= -\mu_0\mathbf{m}\cdot\dot{\mathbf{h}} \qquad (2.60)
\end{aligned}$$

and comparing the coefficients of the like terms with the help of (2.49a), (2.49b), (2.49d) and (2.49e) we write from (2.59)

$$\begin{aligned}
\boldsymbol{\sigma}^{Lh} &= \boldsymbol{\sigma}^{L} + \frac{\mu_0}{2}(\mathbf{m}\cdot\mathbf{m})\mathbf{I} && \text{(2.61a)}\\
\rho\psi_{1,\mathbf{h}} &= -\mu_0\mathbf{m} && \text{(2.61b)}\\
\psi_{1,T} &= -s && \text{(2.61c)}\\
\psi_{1,\zeta_i} &= \psi_{\zeta_i} && \text{(2.61d)}
\end{aligned}$$

where we define $\boldsymbol{\sigma}^{Lh} = \rho\psi_{1,\mathbf{F}}\mathbf{F}^T$. Since $\boldsymbol{\sigma}^{L} = \boldsymbol{\sigma} - \boldsymbol{\sigma}^{Mb}$ ((2.41)) and using (2.61a) we further write

$$\begin{aligned}
\boldsymbol{\sigma}^{Lh} &= \boldsymbol{\sigma}^{L} + \frac{\mu_0}{2}(\mathbf{m}\cdot\mathbf{m})\mathbf{I}\\
&= \boldsymbol{\sigma} - (\boldsymbol{\sigma}^{Mb} - \frac{\mu_0}{2}(\mathbf{m}\cdot\mathbf{m})\mathbf{I}) && \text{(2.62)}
\end{aligned}$$

and denote

$$\boxed{\boldsymbol{\sigma}^{Mh} = \boldsymbol{\sigma}^{Mb} - \frac{\mu_0}{2}(\mathbf{m}\cdot\mathbf{m})\mathbf{I}} \qquad \text{(2.63)}$$

such that

$$\boxed{\boldsymbol{\sigma}^{Lh} = \boldsymbol{\sigma} - \boldsymbol{\sigma}^{Mh}.} \qquad \text{(2.64)}$$

We change the variable $\mathbf{b}$ to $\mathbf{h}$ of the Maxwell stress $\boldsymbol{\sigma}^{Mb}(\mathbf{b},\mathbf{m})$ (2.51) by using the relation $\mathbf{b} = \mu_0(\mathbf{m}+\mathbf{h})$ and obtain

$$\begin{aligned}
\boldsymbol{\sigma}^{Mb}(\mathbf{h},\mathbf{m}) &= \mu_0(\mathbf{m}+\mathbf{h})\otimes(\mathbf{m}+\mathbf{h}) - \mathbf{m}\otimes\mu_0(\mathbf{m}+\mathbf{h})\\
&+ [\mathbf{m}\cdot\mu_0(\mathbf{m}+\mathbf{h}) - \frac{1}{2}\mu_0(\mathbf{m}+\mathbf{h})\cdot(\mathbf{m}+\mathbf{h})]\mathbf{I}\\
&= \mu_0\mathbf{h}\otimes\mathbf{h} + \mu_0\mathbf{h}\otimes\mathbf{m} + \frac{\mu_0}{2}[\mathbf{m}\cdot\mathbf{m} - \mathbf{h}\cdot\mathbf{h}]\mathbf{I}. && \text{(2.65)}
\end{aligned}$$

ubstituting back $\boldsymbol{\sigma}^{Mb}(\mathbf{h},\mathbf{m})$ in (2.63) we write the Maxwell stress

$$\boxed{\boldsymbol{\sigma}^{Mh} = \mu_0\mathbf{h}\otimes\mathbf{h} + \mu_0\mathbf{h}\otimes\mathbf{m} - \frac{\mu_0}{2}(\mathbf{h}\cdot\mathbf{h})\mathbf{I}.} \tag{2.66}$$

The set of constitutive equations become

$$\begin{aligned}
\boldsymbol{\sigma}^{Lh} &= \rho\psi_{1,\mathbf{F}}\mathbf{F}^T && \text{(2.67a)}\\
\mu_0\mathbf{m} &= -\rho\psi_{1,\mathbf{h}} && \text{(2.67b)}\\
s &= -\psi_{1,T} && \text{(2.67c)}\\
\psi_{1,\zeta_i}\cdot\dot{\zeta}_i &\geqslant 0 && \text{(2.67d)}
\end{aligned}$$

It is worth to mention that, if we use the relation (2.64) in the conservation linear momentum (2.26b) and conservation of angular momentum (2.26c), we get

$$\begin{aligned}
\nabla\cdot\boldsymbol{\sigma}^{Lh} + \mu_0(\nabla\mathbf{h})\mathbf{m} &= \mathbf{0} && \text{(2.68a)}\\
\text{skw}\,(\boldsymbol{\sigma}^{Lh}) &= \mu_0\text{skw}\,(\mathbf{m}\otimes\mathbf{h}) && \text{(2.68b)}
\end{aligned}$$

The above relation is same as in *two-dipole model* [123] when the free current is neglected.

2. Reference configuration: $\psi_1 = \widetilde{\psi}_1(\mathbf{E},\mathbf{H},T,\{\mathbb{Z}\})$

In this subsection, we will describe our formulation in the material configuration. Such a formulation is advantageous to describe the deformation of solids. Moreover, independent field variables become objective in the material configuration. Let $\mathbf{H}$ be the magnetic field vector in Ω_0 such that

$$\begin{aligned}
\mathbf{H} &= \mathbf{F}^T\mathbf{h}, && \text{(2.69)}\\
\mathbf{M} &= (\det\mathbf{F})\mathbf{F}^{-1}\mathbf{m}. && \text{(2.70)}
\end{aligned}$$

In addition

$$\mathbf{E} = \frac{1}{2}(\mathbf{C} - \mathbf{I}), \;\; \mathbf{C} = \mathbf{F^T F}. \tag{2.71}$$

$\{\mathbb{Z}\}$ represents the set of tensor, vector and scalar internal variables, defined in the undeformed configuration. We write,

$$\dot{\psi}_1 \;\; = \;\; \dot{\psi}_1(\mathbf{F}, \mathbf{h}, T, \zeta_i) = \psi_{1,\mathbf{F}} : \dot{\mathbf{F}} + \psi_{1,\mathbf{h}} \cdot \dot{\mathbf{h}} + \psi_{1,T}\dot{T} + \psi_{1,\zeta_i} : \dot{\zeta}_i \tag{2.72}$$

$$\dot{\psi}_1 \;\; = \;\; \dot{\widetilde{\psi}}_1(\mathbf{E}, \mathbf{H}, T, \mathbb{Z}_i) = \widetilde{\psi}_{1,\mathbf{E}} : \dot{\mathbf{E}} + \widetilde{\psi}_{1,\mathbf{H}} \cdot \dot{\mathbf{H}} + \widetilde{\psi}_{1,T}\dot{T} + \widetilde{\psi}_{1,\mathbb{Z}_i} : \dot{\mathbb{Z}}_i \tag{2.73}$$

and

$$\dot{\mathbf{E}} \;\; = \;\; \frac{1}{2}(\dot{\mathbf{F}}^T\mathbf{F} + \mathbf{F}^T\dot{\mathbf{F}}), \tag{2.74a}$$

$$\dot{\mathbf{H}} \;\; = \;\; \dot{\mathbf{F}}^T\mathbf{h} + \mathbf{F}^T\dot{\mathbf{h}}. \tag{2.74b}$$

Since, by definition, $\mathbf{E}$ is symmetric,$\widetilde{\psi}_{1,\mathbf{E}}$ is also symmetric. Using this property we can write,

$$\begin{aligned} \widetilde{\psi}_{1,\mathbf{E}} : \dot{\mathbf{E}} \;\; &= \;\; \widetilde{\psi}_{1,\mathbf{E}} : \frac{1}{2}(\dot{\mathbf{F}}^T\mathbf{F} + \mathbf{F}^T\dot{\mathbf{F}}) \\ &= \;\; \mathbf{F}\widetilde{\psi}_{1,\mathbf{E}} : \dot{\mathbf{F}}. \end{aligned} \tag{2.75}$$

$$\widetilde{\psi}_{1,\mathbf{H}} \cdot \dot{\mathbf{H}} \;\; = \;\; (\mathbf{h} \otimes \widetilde{\psi}_{1,\mathbf{H}}) : \dot{\mathbf{F}} + \mathbf{F}\widetilde{\psi}_{1,\mathbf{H}} \cdot \dot{\mathbf{h}}. \tag{2.76}$$

Substituting equations (2.76) and (2.75) in (2.73) and comparing the coefficients of $\dot{\mathbf{F}}, \dot{\mathbf{h}}, \dot{T}$ we get,

$$\psi_{1,\mathbf{F}} \;\; = \;\; \mathbf{F}\widetilde{\psi}_{1,\mathbf{E}} + (\mathbf{h} \otimes \widetilde{\psi}_{1,\mathbf{H}}) \tag{2.77a}$$

$$\psi_{1,\mathbf{h}} \;\; = \;\; \mathbf{F}\widetilde{\psi}_{1,\mathbf{H}} \tag{2.77b}$$

$$\psi_{1,T} \;\; = \;\; \widetilde{\psi}_{1,T}. \tag{2.77c}$$

From equation (2.61b) we know that $\rho\psi_{1,\mathbf{h}} = -\mu_0\mathbf{m}$ and so,

$$\mathbf{F}\widetilde{\psi}_{1,\mathbf{H}} = -\frac{\mu_0}{\rho}\mathbf{m}. \tag{2.78}$$

Substituting back equation (2.78) in equation (2.77a) we get,

$$\psi_{1,\mathbf{F}} = \mathbf{F}\widetilde{\psi}_{1,\mathbf{E}} - \frac{\mu_0}{\rho}(\mathbf{h}\otimes\mathbf{m})\mathbf{F}^{-T}. \tag{2.79}$$

Next by using equation (2.67a), we write

$$\begin{aligned} \frac{1}{\rho}\boldsymbol{\sigma}^{Lh}\mathbf{F}^{-T} &= \mathbf{F}\widetilde{\psi}_{1,\mathbf{E}} - \frac{\mu_0}{\rho}(\mathbf{h}\otimes\mathbf{m})\mathbf{F}^{-T} \\ \Rightarrow \mathbf{F}\widetilde{\psi}_{1,\mathbf{E}} &= \frac{1}{\rho}(\boldsymbol{\sigma}^{Lh} + \mu_0(\mathbf{h}\otimes\mathbf{m}))\mathbf{F}^{-T}. \end{aligned} \tag{2.80}$$

We define *material stress* $\boldsymbol{\sigma}^E$ such that

$$\boxed{\boldsymbol{\sigma}^E = \boldsymbol{\sigma}^{Lh} + \mu_0\mathbf{h}\otimes\mathbf{m}} \tag{2.81}$$

We further simplify the above expression with respect to the total stress in the following way,

$$\begin{aligned} \boldsymbol{\sigma}^E &= \boldsymbol{\sigma}^{Lh} + \mu_0\mathbf{h}\otimes\mathbf{m} \\ &= (\boldsymbol{\sigma} - \boldsymbol{\sigma}^{Mh}) + \mu_0\mathbf{h}\otimes\mathbf{m} \\ &= \boldsymbol{\sigma} - \boldsymbol{\sigma}^h. \end{aligned} \tag{2.82}$$

The expression for $\boldsymbol{\sigma}^h$ is

$$\boxed{\boldsymbol{\sigma}^h = \mu_0\mathbf{h}\otimes\mathbf{h} - \frac{\mu_0}{2}(\mathbf{h}\cdot\mathbf{h})\mathbf{I}.} \tag{2.83}$$

It should be noted that $\boldsymbol{\sigma}^E$ is symmetric because by definition total stress $\boldsymbol{\sigma}$ is symmetric and according to (2.83), $\boldsymbol{\sigma}^h$ is symmetric. Continuing (2.80) we write,

$$\begin{aligned}\widetilde{\psi}_{1,\mathbf{E}} &= \frac{1}{\rho}\mathbf{F}^{-1}(\boldsymbol{\sigma}^{Lh} + \mu_0(\mathbf{h}\otimes\mathbf{m}))\mathbf{F}^{-T} \\ &= \frac{1}{\rho_0}(\det\mathbf{F})\mathbf{F}^{-1}\boldsymbol{\sigma}^E\mathbf{F}^{-T}. \end{aligned} \tag{2.84}$$

We define material stress in the undeformed configuration by

$$\boxed{\mathbf{S}^E = (\det\mathbf{F})\mathbf{F}^{-1}\boldsymbol{\sigma}^E\mathbf{F}^{-T}.} \tag{2.85}$$

Moreover, it should be noted from (2.78) that

$$\mathbf{F}\widetilde{\psi}_{1,\mathbf{H}} = -\frac{\mu_0}{\rho}\mathbf{m}, \tag{2.86}$$

$$\Rightarrow \widetilde{\psi}_{1,\mathbf{H}} = -\frac{\mu_0}{\rho_0}(\det\mathbf{F})\mathbf{F}^{-1}\mathbf{m}, \quad (\rho_0 = \rho(\det\mathbf{F})) \tag{2.87}$$

$$\Rightarrow \widetilde{\psi}_{1,\mathbf{H}} = -\frac{\mu_0}{\rho_0}\mathbf{M}. \tag{2.88}$$

We use (2.70) in the second step to obtain (2.88). The set of constitutive equations and the dissipative inequality become,

$$\mathbf{S}^E = (\det\mathbf{F})\mathbf{F}^{-1}\boldsymbol{\sigma}^E\mathbf{F}^{-T} = \rho_0\widetilde{\psi}_{1,\mathbf{E}} \tag{2.89a}$$

$$\mu_0\mathbf{M} = -\rho_0\widetilde{\psi}_{1,\mathbf{H}} \tag{2.89b}$$

$$s = -\widetilde{\psi}_{1,T} \tag{2.89c}$$

$$\psi_{1,\mathbb{Z}_i}\cdot\dot{\mathbb{Z}}_i \geqslant 0. \tag{2.89d}$$

3. The Gibbs free energy: $G = G(\mathbf{S}^E, \mathbf{H}, T, \{\mathbb{Z}\})$

This is the final step to obtain the Gibbs free energy with the following Legendre transformation

$$G(\mathbf{S}^E, \mathbf{H}, T, \{\mathbb{Z}\}) = \widetilde{\psi}_1 - \frac{1}{\rho_0}\mathbf{S}^E : \mathbf{E}. \tag{2.90}$$

Now,

$$\begin{aligned}
\dot{G} &= \dot{\widetilde{\psi}}_1 - \frac{1}{\rho_0}\dot{\mathbf{S}}^E : \mathbf{E} - \frac{1}{\rho_0}\mathbf{S}^E : \dot{\mathbf{E}} \\
\Rightarrow G_{,\mathbf{S}^E} : \dot{\mathbf{S}}^E + G_{,\mathbf{H}} \cdot \dot{\mathbf{H}} + G_{,T}\,\dot{T} + G_{,\mathbb{Z}_i} \cdot \dot{\mathbb{Z}}_i &= (\widetilde{\psi}_{1,\mathbf{E}} : \dot{\mathbf{E}} + \widetilde{\psi}_{1,\mathbf{H}} \cdot \dot{\mathbf{H}} + \widetilde{\psi}_{1,T}\dot{T} + \widetilde{\psi}_{1,\mathbb{Z}_i} \cdot \dot{\mathbb{Z}}_i) \\
&- \frac{1}{\rho_0}\dot{\mathbf{S}}^E : \mathbf{E} - \frac{1}{\rho_0}\mathbf{S}^E : \dot{\mathbf{E}} \\
(G_{,\mathbf{S}^E} + \frac{1}{\rho_0}\mathbf{E}) : \dot{\mathbf{S}}^E + (G_{,\mathbf{H}} - \widetilde{\psi}_{1,\mathbf{H}}) \cdot \dot{\mathbf{H}} &+ (G_{,T} - \widetilde{\psi}_{1,T})\dot{T} + G_{,\mathbb{Z}_i} \cdot \dot{\mathbb{Z}}_i \\
&= \widetilde{\psi}_{1,\mathbf{E}} : \dot{\mathbf{E}} - \frac{1}{\rho_0}\mathbf{S}^E : \dot{\mathbf{E}} + \widetilde{\psi}_{1,\mathbb{Z}_i} \cdot \dot{\mathbb{Z}}_i \\
&= \widetilde{\psi}_{1,\mathbb{Z}_i} \cdot \dot{\mathbb{Z}}_i
\end{aligned} \tag{2.91}$$

This implies

$$-(G_{,\mathbf{S}^E} + \frac{1}{\rho_0}\mathbf{E}) : \dot{\mathbf{S}}^E - (G_{,\mathbf{H}} - \widetilde{\psi}_{1,\mathbf{H}}) \cdot \dot{\mathbf{H}} - (G_{,T} - \widetilde{\psi}_{1,T})\dot{T} - G_{,\mathbb{Z}_i} \cdot \dot{\mathbb{Z}}_i \geqslant 0 \tag{2.92}$$

So, the constitutive equations are

$$\begin{aligned}
\mathbf{E} &= -\rho_0 G_{,\mathbf{S}^E} \\
G_{,\mathbf{H}} &= \widetilde{\psi}_{1,\mathbf{H}} \\
G_{,T} &= \widetilde{\psi}_{1,T}
\end{aligned} \tag{2.93}$$

and from Eqs. (2.89b), (2.89c), (2.89d) we get,

$$\mathbf{E} = -\rho_0 G_{,\mathbf{S}^E} \tag{2.94a}$$

$$\mu_0 \mathbf{M} = -\rho_0 G_{,\mathbf{H}} \tag{2.94b}$$

$$s = -G_{,T} \tag{2.94c}$$

$$-\rho G_{,\mathbb{Z}_i} \cdot \dot{\mathbb{Z}}_i \geqslant 0. \tag{2.94d}$$

where

$$
\begin{aligned}
\mathbf{S}^E &= \frac{\rho_0}{\rho}\mathbf{F}^{-1}[\boldsymbol{\sigma}^E]\mathbf{F}^{-T} \ , \\
&= \frac{\rho_0}{\rho}\mathbf{F}^{-1}[\boldsymbol{\sigma} - \boldsymbol{\sigma}_h]\mathbf{F}^{-T} \ , \\
&= \frac{\rho_0}{\rho}\mathbf{F}^{-1}[\boldsymbol{\sigma} - [\mu_0\mathbf{h}\otimes\mathbf{h} - \frac{1}{2}\mu_0(\mathbf{h}\cdot\mathbf{h})\mathbf{I}]]\mathbf{F}^{-T} \ , \\
&= \frac{\rho_0}{\rho}\mathbf{F}^{-1}[\boldsymbol{\sigma} - [\mu_0(\mathbf{F}^{-T}\mathbf{H})\otimes(\mathbf{F}^{-T}\mathbf{H}) - \frac{1}{2}\mu_0((\mathbf{F}^{-T}\mathbf{H})\cdot(\mathbf{F}^{-T}\mathbf{H}))\mathbf{I}]]\mathbf{F}^{-T} \ , \\
&= \mathbf{S} - \frac{\rho_0}{\rho}[\mu_0\mathbf{C^{-1}H}\otimes\mathbf{C^{-1}H} - \mathbf{\frac{1}{2}}\mu_\mathbf{0}(\mathbf{H}\cdot\mathbf{C^{-1}H})\mathbf{C^{-1}}] \ , \qquad (2.95) \\
&= \mathbf{S} - \frac{\rho_0}{\rho}\mathbf{S}_H(\mathbf{C},\mathbf{H}) \ .
\end{aligned}
$$

In the next subsection, we will introduce the set of internal variables $\{\mathbb{Z}\}$.

4. Internal state variables

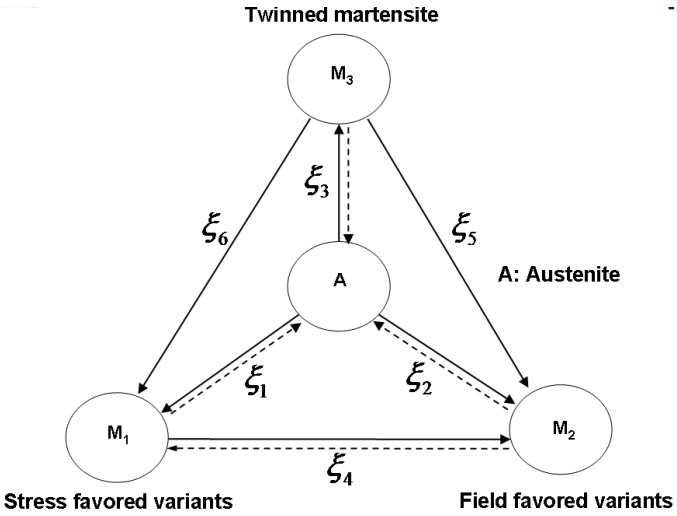

Fig. 9. Schematic of inter-phase transitions

We denote stress favored martensitic variants by M_1, field favored and twinned martensitic variants by M_2 and M_3, respectively (Fig. 9). The austenitic phase is denoted by A. The volume fractions of M_1, M_2 and M_3, produced during phase

transformation from A, are denoted by ξ_1, ξ_2 and ξ_3. We denote the reorientation volume fraction of M_2 from M_1 by ξ_4, of M_2 from M_3 by ξ_5, and of M_1 from M_3 by ξ_6. The productions of volume fractions ξ_i, from different phases are schematically presented in Fig. 9. The three phase transformations $A \leftrightarrow M_1$, $A \leftrightarrow M_2$, $A \leftrightarrow M_3$ and the field induced variant reorientation $M_1 \leftrightarrow M_2$ can be generated both directions. However, reorientation from stress favored variants M_1 and field favored variants M_2 to twinned martensitic variant M_3 is not energetically favorable and $\dot{\xi}_5$, $\dot{\xi}_6$ may only occur in one direction. We select the set of six scalar internal variables ξ_i $(i = 1..6)$, to describe the phase state of the material. The total volume fractions of M_1, M_2, M_3 are denoted by c_1, c_2, c_3 and the volume fraction of the austenitic phase (A) is denoted by c_4. The rate $\dot{c}_i$ of each volume fraction is obtained by summing up the reaction rates $\dot{\xi}_j$ [91], i.e,

$$\dot{c}_i = \nu_{ij}\dot{\xi}_j. \tag{2.96}$$

where,

$$\nu_{ij} = \begin{bmatrix} 1 & 0 & 0 & -1 & 0 & 1 \\ 0 & 1 & 0 & 1 & 1 & 0 \\ 0 & 0 & 1 & 0 & -1 & -1 \\ -1 & -1 & -1 & 0 & 0 & 0 \end{bmatrix}. \tag{2.97}$$

The volume fractions are subjected to the following constraints,

$$\sum_i^4 \dot{c}_i = 0, \quad \sum_i^4 c_i = 1, \quad \text{and} \quad 0 \leq c_i \leq 1.$$

If the initial volume fractions of M_1, M_2, M_3 and A are c_{01}, c_{02}, c_{03} and c_{04} respectively, we can write

$$c_i = c_{0i} + \nu_{ij}\xi_j, \tag{2.98}$$

We further assume the *inelastic strain* $\mathbf{E}^I$ and *internal magnetization* $\mathbf{M}^I$, generated during structural transformation, are the tensor valued and vector valued internal variables. We extend the idea of inelastic strain to the generation of internal magnetization vector $\mathbf{M}^I$. This internal magnetization may take into account the phenomenological effect of different micro-magnetic mechanism like rotation of magnetization vector and evolution of magnetic domain walls. Finally, we consider the mixing energy g of the transformation and reorientation as an internal variable. This yields the complete set of internal variables as $\{\mathbb{Z}\} = \{\mathbf{E}^I, \mathbf{M}^I, \xi_i, g\}$.

Rest of the subsection, we will discuss the evolution laws for the internal state variables. Following additive decomposition [132, 133], the inelastic strain rate $\dot{\mathbf{E}}^I$, produced during phase transformation and variant reorientation, can be written as

$$\dot{\mathbf{E}}^I = \dot{\mathbf{E}}^t + \dot{\mathbf{E}}^r, \tag{2.99}$$

where, $\mathbf{E}^t$ is the transformation strain due to phase transformation and $\mathbf{E}^r$ is the reorientation strain produced during variant reorientation. We further assume that the transformation and reorientation strain rates obey the following flow rules

$$\dot{\mathbf{E}}^t = \sum_{i=1}^{3} \mathbf{\Lambda}_i^t \dot{\xi}_i, \tag{2.100a}$$

$$\dot{\mathbf{E}}^r = \sum_{i=4}^{6} \mathbf{\Lambda}_i^r \dot{\xi}_i \tag{2.100b}$$

The tensors $\mathbf{\Lambda}_i^t$ and $\mathbf{\Lambda}_i^r$ describe the direction and magnitude of the strain generated during phase transformation and variant reorientation, respectively.

Similarly we consider that the rate of magnetization vector $\dot{\mathbf{M}}^I$ can be decomposed in the following way,

$$\dot{\mathbf{M}}^I = \dot{\mathbf{M}}^t + \dot{\mathbf{M}}^r, \tag{2.101}$$

Here, $\dot{\mathbf{M}}^t$ is generated during phase transformation and $\dot{\mathbf{M}}^r$ is generated during reorientation. We assume the following flow rules

$$\dot{\mathbf{M}}^t = \sum_{i=1}^{3} \boldsymbol{\gamma}_i^t \dot{\xi}_i, \tag{2.102a}$$

$$\dot{\mathbf{M}}^r = \sum_{i=4}^{6} \boldsymbol{\gamma}_i^r \dot{\xi}_i, \tag{2.102b}$$

where the vectors $\boldsymbol{\gamma}_i^t$ and $\boldsymbol{\gamma}_i^r$ take into account the direction and magnitude of the internal magnetization due to the microstructural changes.

The evolution of the interaction or mixing energy, $\dot{g}$, between the parent phase and martensitic phase during phase transformation ($\dot{g}^t$) and among the martensitic variants during variant reorientation ($\dot{g}^r$) can be represented by

$$\dot{g} = \dot{g}^t + \dot{g}^r, \tag{2.103}$$

and we assume the following flow rules

$$\dot{g}^t = \sum_{i=1}^{3} f_i^t \dot{\xi}_i, \tag{2.104a}$$

$$\dot{g}^r = \sum_{i=4}^{6} f_i^r \dot{\xi}_i, \tag{2.104b}$$

where f_i s are the hardening functions. Thus, the Gibbs free energy with the set of external ($\{\mathbf{S}^E, \mathbf{H}, T\}$) and internal ($\{\mathbb{Z}\} = \{\mathbf{E}^I, \mathbf{M}^I, \xi_i, g\}$) state variables is given by

$$G = G(\mathbf{S}^E, \mathbf{H}, T, \mathbf{E}^I, \mathbf{M}^I, \xi_i, g). \tag{2.105}$$

C. Material symmetry

After defining the Gibbs free energy and the evolution equations one needs to consider material symmetry. MSMAs are single crystals or polycrystals which may exhibit

finite or *continuous symmetry*, respectively. In this section we discuss a brief introduction on finite and continuous symmetries for a *scalar function* with an arbitrary number of tensor arguments. The arguments of the scalar function may be *polar tensors*, *axial tensors*, *i-tensors* and *c-tensors*. Polar tensors do not change sign under improper rotation while axial tensors do. Tensors of any order that are invariant under time inversion are known as i-tensors and tensors whose components change sign with time reversal are known as c-tensors. The methods will then be extended for any tensor function.

1. Finite symmetry for magneto-crystalline material

The point groups for crystals are known as *classical point groups*[4]. We denote the classical group by $\mathscr{G}$. Since a reversal of time changes the sign of the current and hence reverses the direction of the magnetic moment vector in magnetic materials, we need an additional *time-inversion* operation τ. When this operator acts on a classical point group, it is possible to find a new group, known as *magnetic point groups* [134]. In this group, half of the elements of the ordinary point group $\mathscr{G}$ are multiplied by the time-inversion operator τ. The other half forms a subgroup, $\mathscr{H}$, of $\mathscr{G}$. The magnetic point group, $\mathscr{M}$, can be written as

$$\mathscr{M} = \mathscr{H} + \tau(\mathscr{G} - \mathscr{H}).$$

Ferromagnetic, antiferromagnetic, ferrimagnetic and weak ferromagnetic materials belong to this group. For a general case, we denote the magnetic point group by

$$\mathscr{M} = \{\mathscr{M}^{\alpha}\}$$

[4] A brief introduction on finite symmetry and point groups is presented in Appendix B.

for $\alpha = 1, .., n$ where n is the order of the group. The representation of the group is thus given by

$$T(\mathscr{M}) = \{T(\mathscr{M}^{\alpha})\}.$$

If we denote the *fully reduced* representation of T by Γ, then

$$\Gamma = \bigoplus_{i=1}^{r} n_i \Gamma^{(i)}, \tag{2.106}$$

where $\Gamma^{(1)}, ...\Gamma^{(r)}$ are the *irreducible representation* of $\mathscr{M}$. We use the *orthogonality of characters* (B.4) to obtain the coefficients n_i of equation (2.106) [135].

a. Determination of polynomial integrity basis

After defining a magnetic point group $\mathscr{M}$, we consider the problem of generating an integrity basis for a scalar valued tensor function $W(\mathbf{X}, \mathbf{Y}, ...)$ so that it is invariant under $\mathscr{M}$ [135–137]. If $\mathbf{A} \in \{\mathbf{X}, \mathbf{Y}, ...\}$ and $\mathbf{Q} \in \{T(\mathscr{M})\}$ then the following transformation holds true

$$A'_{ijk...n} = (-1)^p (\det \mathbf{Q}) Q_{ip} Q_{jq} ... Q_{nu} A_{pqr...u}.$$

In the above transformation, $p = 1$ for c-tensors and $p = 0$ for i-tensors. $\det \mathbf{Q} = 1$ for polar tensors and $\det \mathbf{Q} = -1$ for axial tensors.

Given a magnetic point group, we now determine the *basic quantities* of $\mathbf{X}, \mathbf{Y}, ...$ Let

$$\mathbf{u} = [u_1, ..., u_m]^T = [X_1, ...X_p, Y_1, ..., Y_q, ...]^T$$

denote the column vector whose entries are the independent components of $\mathbf{X}$, $\mathbf{Y}, ...$ For example, $X_1, ..., X_p$ are the p independent components of the tensor $\mathbf{X}$. We set

$W(\mathbf{u}) := W(\mathbf{X},\, \mathbf{Y}, ...)$ and the restrictions imposed on the scalar function are

$$W(\mathbf{u}) = W(\mathscr{T}_k \mathbf{u}) \quad (k = 1, ..., n)$$

where $\{\mathscr{T}_k\}$ are m-dimensional matrix representation of $\{T(\mathscr{M})\}$. The representation $\{\mathscr{T}_k\}$ can be decomposed into *irreducible representations* associated with the group $\{\mathscr{M}\}$. We denote these representations by $\{\Gamma_k^{(1)},\ \Gamma_k^{(2)}....\}$. Thus, we are looking for a *similarity transformation* with a non-singular $m \times m$ matrix $\mathbf{R}$ such that

$$\mathbf{R}\mathscr{T}_k\mathbf{R}^{-1} = \bigoplus_{i=1}^{r} n_i \Gamma_k^{(i)} \quad (k = 1, ..., n),$$

where

$$\mathbf{Ru} = \begin{bmatrix} \mathbf{u}^{(1)} \\ \mathbf{u}^{(2)} \\ \vdots \\ \mathbf{u}^{(r)} \end{bmatrix}, \quad \mathbf{u}^{(1)} = \begin{bmatrix} u_1^{(1)} \\ u_2^{(1)} \\ \vdots \\ u_{n_1}^{(1)} \end{bmatrix}, \quad \mathbf{u}^{(2)} = \begin{bmatrix} u_1^{(2)} \\ u_2^{(2)} \\ \vdots \\ u_{n_2}^{(2)} \end{bmatrix}, ..., \mathbf{u}^{(r)} = \begin{bmatrix} u_1^{(r)} \\ u_2^{(r)} \\ \vdots \\ u_{n_r}^{(r)} \end{bmatrix} .$$

We can then express the scalar function as

$$W(\mathbf{u}) = P(\mathbf{u}^{(1)},\, \mathbf{u}^{(2)}, ..., \mathbf{u}^{(r)}) = P(\Gamma_k^{(1)}\mathbf{u}^{(1)},\, \Gamma_k^{(2)}\mathbf{u}^{(2)}, ..., \Gamma_k^{(r)}\mathbf{u}^{(r)}).$$

The set $\{\mathbf{u}^{(1)}, \mathbf{u}^{(2)}, ..., \mathbf{u}^{(r)}\}$, associated with $\{\Gamma_k^{(1)}, \Gamma_k^{(2)}, ..., \Gamma_k^{(r)}\}$, forms the *carrier space* for the irreducible representation and the elements of the set are known as *basic quantities*.

Let $I_1, ..., I_s$ be the polynomials in the basic quantities $\{\mathbf{u}^{(1)}, \mathbf{u}^{(2)}, ..., \mathbf{u}^{(r)}\}$ such that $I_1, ..., I_s$ are each invariant under $\mathscr{M}$ and such that every function $P(\mathbf{u}^{(1)},\, \mathbf{u}^{(2)}, ..., \mathbf{u}^{(r)})$, which is invariant under $\mathscr{M}$, can be expressed as a functions of $I_1, ..., I_s$. The $I_1, ..., I_s$ are said to form an *integrity basis*, invariant under $\mathscr{M}$. The elements of integrity basis of degree 1, 2, 3 are given by [136]

Degree 1 :

$$J_1(\mathbf{u}^{(1)}),\ J_2(\mathbf{u}^{(2)}), ..., J_r(\mathbf{u}^{(r)}).$$

Degree 2 :

$$J_{11}(\mathbf{u}^{(1)}, \mathbf{u}^{(1)}),\ J_{12}(\mathbf{u}^{(1)}, \mathbf{u}^{(2)}), ...$$

Degree 3 :

$$J_{111}(\mathbf{u}^{(1)}, \mathbf{u}^{(1)}, \mathbf{u}^{(1)}),\ J_{112}(\mathbf{u}^{(1)}, \mathbf{u}^{(1)}, \mathbf{u}^{(2)}), ...$$

2. Continuous symmetry for magneto-noncrystalline material

In the previous subsection, we presented the results of integrity basis with complete generality for the crystallographic point groups. This was possible because a finite group has a finite number of irreducible representation $\Gamma^{(1)}, ..., \Gamma^{(r)}$. A group containing an infinite number of continuous elements is called a *continuous group*. The number of irreducible representations associated with the continuous group is not finite. There is no way to present a general result compared to those given for finite group. This problem has been discussed by Rivlin and Spencer for the $O(3)$ and $SO(3)$. Their procedure makes extensive use of Cayley-Hamilton identity to generate integrity basis. Integrity basis for a scalar valued tensor functions $W(\mathbf{X}, \mathbf{Y}, ...)$ can be obtained by following Rivlin and Spensor [138, 139]. More results of invariants and integrity basis can be found in [127, 140]. A comprehensive study is available in the review paper by Zheng [141].

A non-crystal type material can be classified into four types: *isotropic*, *transversely isotropic*, *icosahedral* and *non-crystal dihedral* [142] which belong to a continuous group. In this study we consider only transverse isotropy, whose symmetry

groups can be classified into five groups: $\mathscr{A}=\{C_\infty,\ C_{\infty v},\ C_{\infty h},\ D_\infty,\ D_{\infty h}\}$. The transverse isotropy of a scalar function can be considered by introducing *structural tensors* to its arguments and then considering the function as an isotropic one. The structural tensors of the five different groups are presented in Table. III, where

Continuous groups	Structural tensors
C_∞	$\mathbf{e}_3$, $\mathbf{P}$
$C_{\infty v}$	$\mathbf{e}_3$
$C_{\infty h}$	$\mathbf{e}_3 \otimes \mathbf{e}_3$, $\mathbf{N}_3$
D_∞	$\mathbf{e}_3 \otimes \mathbf{e}_3$, $\mathbf{P}$
$D_{\infty h}$	$\mathbf{e}_3 \otimes \mathbf{e}_3$

Table III. Structural tensors for different groups of transverse isotropy

$$\begin{aligned}
\mathbf{P} &= \mathbf{e}_1 \otimes \mathbf{e}_2 \otimes \mathbf{e}_3 - \mathbf{e}_2 \otimes \mathbf{e}_1 \otimes \mathbf{e}_3 + \mathbf{e}_2 \otimes \mathbf{e}_3 \otimes \mathbf{e}_1 - \mathbf{e}_3 \otimes \mathbf{e}_2 \otimes \mathbf{e}_1 \\
&+ \mathbf{e}_3 \otimes \mathbf{e}_1 \otimes \mathbf{e}_2 - \mathbf{e}_1 \otimes \mathbf{e}_3 \otimes \mathbf{e}_2, \\
\mathbf{N}_3 &= \mathbf{e}_1 \otimes \mathbf{e}_2 - \mathbf{e}_2 \otimes \mathbf{e}_1.
\end{aligned}$$

The preferred unit direction of transverse isotropy is given by $\mathbf{e}_3$. We denote two unit orthogonal directions with respect to $\mathbf{e}_3$ by $\mathbf{e}_1$ and $\mathbf{e}_2$.

3. Symmetry restrictions for general constitutive relations

So far, we have considered a tensor valued scalar function of the form $W(\mathbf{X},\ \mathbf{Y}, ...)$. In this section we focus on the most general constitutive form

$$T_{i_1....i_n} = T_{i_1....i_n}(\mathbf{A},\ \mathbf{B}, ...)$$

which is invariant under $\{\mathscr{M}\}$ or $\{\mathscr{A}\}$. We convert the tensor valued function by introducing an arbitrary tensor $\mathbf{t}$, which has same order and symmetry properties as

T. We define a scalar V such that

$$V = t_{i_1....i_n} T_{i_1....i_n}$$

and $V = V(\mathbf{t}, \mathbf{A}, \mathbf{B}, ...)$ is linear in $\mathbf{t}$. Now one can find the *integrity basis* for V with the arguments $\mathbf{t}, \mathbf{A}, \mathbf{B}, ...$ as described in the previous subsection. Let the set $\{I\}$, with elements $I_1, ..., I_r$ of the integrity basis, be independent of $\mathbf{t}$ and the set $\{L\}$, with elements $L_1, ..., L_m$, be linear in $\mathbf{t}$ and the rest of the elements are of higher order in $\mathbf{t}$. Since V is linear in $\mathbf{t}$ it may be represented by

$$V = \sum_{p=1}^{m} c_p(I_1, ..., I_r) L_p,$$

where c_p's are scalar polynomials. Then the generalized form of the constitutive relation, which is invariant under $\{\mathscr{M}\}$, can be written as

$$\begin{aligned} T_{i_1....i_n} = \frac{\partial V}{\partial t_{i_1....i_n}} &= \sum_{p=1}^{m} c_p(I_1, ..., I_r) \frac{\partial L_p}{\partial t_{i_1....i_n}} \\ &= \sum_{p=1}^{m} c_p(I_1, ..., I_r) \mathscr{D}^p_{i_1....i_n}, \end{aligned} \tag{2.107}$$

where

$$\mathscr{D}^p_{i_1....i_n} = \frac{\partial L_p}{\partial t_{i_1....i_n}}.$$

We denote the set $\{\mathscr{D}\}$ by $\{\frac{\partial L_1}{\partial t_{i_1....i_n}}, \frac{\partial L_2}{\partial t_{i_1....i_n}} .... \frac{\partial L_m}{\partial t_{i_1....i_n}}\}$.

D. Constitutive equations for MSMAs

After describing a generalized method for obtaining integrity basis in the previous section, we now apply it to the Gibbs free energy and evolution equations for MSMAs. The finite symmetry group is considered for single crystal MSMA while continuous symmetry is considered for polycrystals and multi-variant materials.

The general form of the Gibbs free energy for an MSMA system can be written as

$$G = G(\mathbf{S}^E, \mathbf{H}, T, \mathbf{E}^I, \mathbf{M}^I, \xi_i, g, \{\mathbb{S}\}). \tag{2.108}$$

where $\mathbf{S}^E$, $\mathbf{E}^I$ are the *polar, second order, symmetric, i*-tensors and $\mathbf{H}$, $\mathbf{M}^I$ are the *axial c*-vectors. The anisotropy for a continuous symmetry group is considered by introducing structural tensors $\{\mathbb{S}\}$. For the transverse isotropic case, the elements of $\{\mathbb{S}\}$ can be obtained from Tab. III. It should be noted that for finite symmetry we do not need to consider any structural tensor.

Let Υ_ϕ be the integrity basis of (2.108) which may be split such that

$$\Upsilon_\phi = \Upsilon_{\phi I} \bigcup \Upsilon_{\phi P} \quad \text{and} \quad \Upsilon_{\phi I} \bigcap \Upsilon_{\phi P} = \emptyset.$$

Here, $\Upsilon_{\phi I}$ contains the elements of the integrity basis with at least one internal variable and $\Upsilon_{\phi P}$ is the set of the remaining elements. Based on the above arguments, we propose

$$G(\Upsilon_\phi, T, \xi_i, g) = \sum_{j=1}^{4} c_j(\xi_i) G_{P_j}(\Upsilon_{\phi P}, T) + G_I(\Upsilon_{\phi I}, T) + G_{mix}(g) \tag{2.109}$$

We denote the sets obtained by taking partial derivative of the elements of Υ_ϕ with respect to $\mathbf{H}$, $\mathbf{S}^E$, $\mathbf{E}^I$ and $\mathbf{M}^I$ by $\Upsilon_{\mathbf{H}}$, $\Upsilon_{\mathbf{S}^E}$, $\Upsilon_{\mathbf{E}^I}$ and $\Upsilon_{\mathbf{M}^I}$, respectively. In addition, for continuous symmetry we denote $\Upsilon_{\{\mathbb{S}\}}$ as the partial derivative of Υ_ϕ with respect to $\{\mathbb{S}\}$. The expression of the strain $\mathbf{E}$, the magnetization vector $\mathbf{M}$ and the entropy

s can be written in the following ways (equations (2.94a) to (2.94c))

$$\begin{aligned}
\mathbf{E} &= -\rho_0 G_{,\mathbf{S}^E} = \sum_{\mathbf{T_a}\in\boldsymbol{\Upsilon}_{\mathbf{SE}}} \alpha_a(\Upsilon_\phi)\mathbf{T_a}, && (2.110a)\\
\bar{\mathbf{M}} &= -\frac{\rho_0}{\mu_0} G_{,\mathbf{H}} = \sum_{\mathbf{v}_b\in\boldsymbol{\Upsilon}_{\mathbf{H}}} \beta_b(\Upsilon_\phi)\mathbf{v}_b, && (2.110b)\\
s &= -\rho_0 G_{,T} && (2.110c)
\end{aligned}$$

Moreover[5], the entropy inequality becomes

$$\boldsymbol{\pi}_{E^I} : \dot{\mathbf{E}}^I + \boldsymbol{\pi}_{M^I} : \dot{\mathbf{M}}^I + \pi_{\xi_i}\dot{\xi}_i + \pi_g \dot{g} + \boldsymbol{\pi}_{\{\mathbb{S}\}} : \{\dot{\mathbb{S}}\} \geq 0, \tag{2.111}$$

where we denote

$$\begin{aligned}
\boldsymbol{\pi}_{E^I} &= -\rho_0 G_{,\mathbf{E}^I} = \sum_{\mathbf{R_a}\in\boldsymbol{\Upsilon}_{\mathbf{E^I}}} \chi_a(\Upsilon_\phi)\mathbf{R_a}\\
\boldsymbol{\pi}_{M^I} &= -\rho_0 G_{,\mathbf{M}^I} = \sum_{\mathbf{u_b}\in\boldsymbol{\Upsilon}_{\mathbf{M^I}}} \varphi_b(\Upsilon_\phi)\mathbf{u}_b\\
\pi_{\xi_i} &= -\rho_0 G_{,\xi_i}\\
\pi_g &= -\rho_0 G_{,g}\\
\boldsymbol{\pi}_{\{\mathbb{S}\}} &= -\rho_0 G_{,\{\mathbb{S}\}} = \sum_{\mathbf{U_c}\in\boldsymbol{\Upsilon}_{\{\mathbb{S}\}}} \omega_c(\Upsilon_\phi)\mathbf{U_c}.
\end{aligned}$$

The rate $\dot{\mathbf{E}}^I$, $\dot{\mathbf{M}}^I$ and $\dot{g}$ can be obtained from the evolution equations (2.99), (2.101) and (2.103).

Considering the evolution equations for the inelastic strain (equations (2.100a) and (2.100b)), we assume that transformation and reorientation occur due to the deviatoric part ($\mathbf{S}'^E$) of the stress $\mathbf{S}^E$, field, temperature and structural tensor (for

[5]It should be noted that from equation (2.94b), the magnetization $\mathbf{M} = (\det\mathbf{F})\mathbf{F}^T\bar{\mathbf{M}}$.

continuous symmetry only). Then $\mathbf{\Lambda}_v^\beta$ can be represented as

$$(\Lambda_{ij}^\beta)_v = (\Lambda_{ij}^\beta)_v(\mathbf{S'}^E, \mathbf{H}, T, \{\mathbb{S}\}),$$

where as for the evolution of the magnetization and mixing energy equation we can write

$$(\gamma_i^\beta)_v = (\gamma_i^\beta)_v(\mathbf{S'}^E, \mathbf{H}, T, \{\mathbb{S}\}),$$

and

$$f_v^\beta = f_v^\beta(\mathbf{S'}^E, \mathbf{H}, T, \{\mathbb{S}\}).$$

Here $\beta = t$ for transformation, $\beta = r$ for reorientation and v may vary from 1 to 6. Following subsection 3, we further write

$$(\Lambda_{ij}^\beta)_v = \sum_{p=1}^{m} c_{p_v}(I_1, ..., I_r)(\mathscr{D}_{ij}^p)_v. \tag{2.112}$$

Similarly, from the evolution equation for the internal magnetization (equations (2.102a) and (2.102b)), we can write for any generic $\boldsymbol{\gamma}_v^\beta$,

$$(\gamma_i^\beta)_v = \sum_{p=1}^{m} c'_{p_v}(I_1, ..., I_r)(\mathscr{D}_i^p)_v, \tag{2.113}$$

and for the hardening function

$$(f^\beta)_v = c''_{p_v}(I_1, ..., I_r). \tag{2.114}$$

We further focus on continuous symmetry for which one needs to know about the evolution of structural tensors. Since the direction of texturing, which is denoted by $\mathbf{e}_3$, may change due to the microstructural change during phase transformation and variant reorientation, the structural tensors evolve with the change in the direction

of $\mathbf{e}_3$. Let $\mathbf{\Sigma} \in \{\mathbb{S}\}$ and

$$\mathbf{\Sigma} = \mathbf{\Sigma}(\mathbf{e}_1, \mathbf{e}_2, \mathbf{e}_3).$$

The rate of change of the structural tensor can then be represented by

$$\dot{\mathbf{\Sigma}} = \mathbf{\Xi}(\mathbf{e}_1, \mathbf{e}_2, \mathbf{e}_3, \dot{\mathbf{e}}_3). \tag{2.115}$$

We can express $\mathbf{e}_3$ with respect to the *directional cosines* such that $\mathbf{e}_3 = (\cos\alpha_1, \cos\alpha_2, \cos\alpha_3)^T$ and

$$\dot{\mathbf{e}}_3 = -(\sin\alpha_1(\dot{\alpha}_1), \sin\alpha_2(\dot{\alpha}_2), \sin\alpha_3(\dot{\alpha}_3))^T.$$

The evolution of the α_j (j=1,3) may be related with the evolution of the volume fractions such that

$$\dot{\alpha}_j \;\; = \;\; \sum_{i=1}^{3} \Theta_{ij}^{t} \dot{\xi}_i + \sum_{i=3}^{6} \Theta_{ij}^{r} \dot{\xi}_i. \tag{2.116}$$

Here Θ_{ij}^{β} are scalars that take into account the change in α_i due to changes in ξ_j.

E. Integrity basis of the Gibbs free energy for finite symmetry

Our next objective is to find out the elements of Υ_ϕ for MSMA material systems which belong to a specific class of symmetry group. For finite symmetry, we consider *field induced phase transformation* and *variant reorientation* in a single crystal specimen. We demonstrate continuous symmetry for polycrystalline MSMAs.

1. Field Induced Phase Transformation (FIPT)

Austenitic phase: We consider FIPT in a NiMnCoIn *single crystal* which has a ferromagnetic austenitic phase. The austenitic phase is cubic and it is a well known fact

that cubic symmetry does not support ferromagnetism [134, 143, 144]. For example, the symmetry of *bcc* α-iron is often thought to be cubic, but is tetragonal due to the axially symmetric magnetic moment [145]. Similarly, a reduction in the symmetry of the Ni crystal structure occurs from fcc to trigonal ($3\underline{m}$) due to the alignment of the magnetic moment along the [111] direction. The Cu_2MnAl Heusler alloy has the $L2_1$ chemical structure and belongs to $Fm3m$ space group even though the magnetic point group of this compound, like Ni, is $3\underline{m}$ [143].

In the present case, the NiMnCoIn crystal exhibits $L2_1$ type Heusler structure with the $Fm3m$ *space group* [146]. The magnetic point group has not been reported to date. Since the crystal structure and space group of NiMnCoIn resembles Cu_2MnAl Heusler alloy, we consider that the ferromagnetic austenitic phase belongs to $3\underline{m}$ magnetic point group.

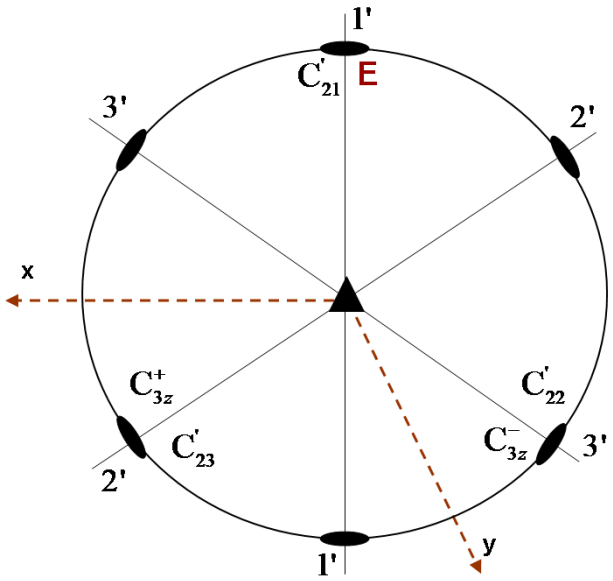

Fig. 10. Stereographic representation of the symmetry elements and reference axes for $3m$ point group.

Figure 10 represents the $3m$ point group in *stereographic projections*. The notation of the diagram follows from [144]. The triangle at the center (▲) represents

$3\underline{m}$	E	S_1	S_2	$\tau(R_1)$	$\tau(R_1S_1)$	$\tau(R_1S_2)$
$\Gamma^{(1)}$	1	1	1	1	1	1
$\Gamma^{(2)}$	1	1	1	-1	-1	-1
$\Gamma^{(3)}$	E	A	B	$-F$	$-G$	$-H$

Table IV. The irreducible representation of 3$\underline{\text{m}}$

the 3-fold rotations along the z axis which is perpendicular to the plane of the paper and obey the right-hand rule. A solid ellipse denotes 2-fold rotations along the $i' - i'$ axis ($i = 1, 2, 3$). The alpha-numeric labeling of the symmetry operations are placed on the figure in the position to which the letter E is taken by that operation. $C_{3z}^{\pm}$ represents $360^o/3$ anticlockwise/clockwise rotation along the z axis and C'_{2i} is the 180^o rotation along the $i' - i'$ axis. It should be noted that x and y axes are not orthogonal. The angle between them is 120^o. All the components of the magneto-mechanical variables for the austenitic phase will be presented with respect to the above mentioned coordinate frame.

The *irreducible representation* for $3\underline{m}$ is given in Table IV. The top row of Table IV represents the *matrix representation* of the symmetry operations of this group. They are E: identity, R_i: reflection on x^i plane, S_1: rotation through $2\pi/3$ clockwise about x^3, S_2: rotation through $2\pi/3$ anticlockwise about x^3 and τ is the time inversion operator. We denote $\{x^1 = x, x^2 = y, x^3 = z\}$ and the form of the matrices can be found in [135]. The *irreducible representation* (last row of Table IV) are defined in terms of the matrices

Type	Decomposition
Axial c-vectors	$\Gamma^{(1)} \oplus \Gamma^{(3)}$
Polar i-tensors	$2\Gamma^{(1)} \oplus 2\Gamma^{(3)}$

Table V. Decomposition of magneto-mechanical quantities of 3$\underline{\underline{\text{m}}}$ magnetic point group

$\Gamma^{(1)}$	H_3	$S^E_{11}+S^E_{22},\ S^E_{33}$
$\Gamma^{(2)}$		
$\Gamma^{(3)}$	(H_1, H_2)	$(S^E_{13}, S^E_{23}),\ (2S^E_{12}, S^E_{11}-S^E_{22})$

Table VI. The basic quantities of 3$\underline{\text{m}}$

$$E=\begin{bmatrix}1 & 0\\ 0 & 1\end{bmatrix},\quad A=\begin{bmatrix}-\frac{1}{2} & \frac{\sqrt{3}}{2}\\ -\frac{\sqrt{3}}{2} & -\frac{1}{2}\end{bmatrix},\quad B=\begin{bmatrix}-\frac{1}{2} & -\frac{\sqrt{3}}{2}\\ \frac{\sqrt{3}}{2} & -\frac{1}{2}\end{bmatrix},\quad F=\begin{bmatrix}1 & 0\\ 0 & -1\end{bmatrix}$$
$$G=\begin{bmatrix}-\frac{1}{2} & \frac{\sqrt{3}}{2}\\ \frac{\sqrt{3}}{2} & \frac{1}{2}\end{bmatrix},\quad H=\begin{bmatrix}-\frac{1}{2} & -\frac{\sqrt{3}}{2}\\ -\frac{\sqrt{3}}{2} & \frac{1}{2}\end{bmatrix}.$$

The decompositions of *axial c-vectors* and *polar i-tensors* are given in the Table V.

We assume that the austenitic phase is magneto-elastic and the Gibbs free energy for this phase depends on the stress, magnetic field and temperature. The Gibbs free energy can then be represented by

$$G = G_A(\mathbf{S}^E,\, \mathbf{H},\, T).$$

The basic quantities for the above arguments are given in Table VI. We write

$$\Gamma^{(1)}: \quad \left\{u_1^{(1)},\, u_2^{(1)},\, u_3^{(1)}\right\} = \left\{H_3,\ S^E_{11}+S^E_{22},\, S^E_{33}\right\}$$
$$\Gamma^{(3)}: \quad \left\{\mathbf{u}_1^{(3)},\, \mathbf{u}_2^{(3)},\, \mathbf{u}_3^{(3)}\right\} = \left\{\begin{bmatrix}H_1\\ H_2\end{bmatrix},\ \begin{bmatrix}S^E_{13}\\ S^E_{23}\end{bmatrix},\ \begin{bmatrix}2S^E_{12}\\ S^E_{11}-S^E_{22}\end{bmatrix}\right\}$$

The multilinear elements of the integrity bases, in terms of the basic quantities, are given by

$$\begin{aligned} &\text{Degree 1:} \qquad u_i^{(1)} \quad (i=1,3) \\ &\text{Degree 2:} \qquad \mathbf{u}_i^{(3)} \cdot \mathbf{u}_j^{(3)} \quad (i,j=1,3). \end{aligned}$$

Martensitic phase: The single crystal *antiferromagnetic* martensitic phase of this material is $14M$ monoclonic [50, 146]. The monoclinic martensitic phase belongs to $2/m$ (C_{2h}) classical point group. The three magnetic point groups of $2/m$ are $\underline{2}/\underline{m}$, $2/\underline{m}$, $\underline{2}/m$. The magnetic group of NiMnCoIn martensitic phase has not been reported in the literature so far.

The integrity basis for each magnetic point group is different. We need to identify the group which is closest to the observed material response. For example, any material belonging to group $\underline{2}/\underline{m}$ is a ferromagnetic material [134, 147]. Thus, we eliminate this group for the antiferromagnetic martensitic phase. Now, both $2/\underline{m}$, $\underline{2}/m$ are antiferromagnetic and it can be shown that the integrity bases for magneto-mechanical coupling up to second order are the same for $2/\underline{m}$ and $\underline{2}/m$ [135]. We select $\underline{2}/m$ to proceed.

The stereographic representation of $2/m$ is presented in Fig. 11. The notation is the same as described for the austenitic phase. The irreducible representation for $\underline{2}/m$ is given in Table VII. The matrices of the symmetric operations are E: identity, C: inversion, R_i: reflection on x^i plane, D_i: rotation of π anticlockwise about x^i. The decompositions of *axial c-vectors* and *polar i-tensors* are presented in Table VIII. We consider the martensitic phase to be magneto-elastic and the Gibbs free energy for

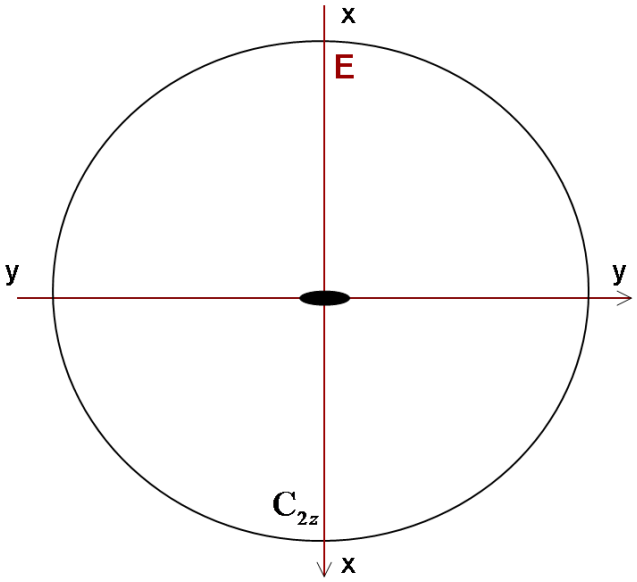

Fig. 11. Stereographic representation of the symmetry elements and reference axes for $2/m$ point group.

this phase is assumed to be

$$G = G_M(\mathbf{S}^E, \mathbf{H}, T).$$

The basic quantities for the above arguments are given in Table IX and we write

$\underline{2}/m$	E	$\tau(D_3)$	R_3	$\tau(C)$
$\Gamma^{(1)}$	1	1	1	1
$\Gamma^{(2)}$	1	1	-1	-1
$\Gamma^{(3)}$	1	-1	1	-1
$\Gamma^{(4)}$	1	-1	-1	1

Table VII. The irreducible representation of $\underline{2}$/m

Type	Decomposition
Axial c-vectors	$2\Gamma^{(2)} \oplus \Gamma^{(3)}$
Polar i-tensors	$4\Gamma^{(1)} \oplus 2\Gamma^{(4)}$

Table VIII. Decomposition of magneto-mechanical quantities of $\underline{2}$/m magnetic point group

$\Gamma^{(1)}$	$S^E_{11}, S^E_{22}, S^E_{33}, S^E_{12}$	
$\Gamma^{(2)}$		H_1, H_2
$\Gamma^{(3)}$		H_3
$\Gamma^{(4)}$	S^E_{32}, S^E_{31}	

Table IX. The basic quantities of ($\underline{2}$/m)

$$\Gamma^{(1)}: \quad \left\{u_1^{(1)},\, u_2^{(1)},\, u_3^{(1)},\, u_4^{(1)}\right\} = \left\{S^E_{11}, S^E_{22}, S^E_{33}, S^E_{12}\right\}$$
$$\Gamma^{(2)}: \quad \left\{u_1^{(2)},\, u_2^{(2)}\right\} = \{H_1, H_2\}$$
$$\Gamma^{(3)}: \quad \left\{u_1^{(3)}\right\} = \{H_3\}$$
$$\Gamma^{(4)}: \quad \left\{u_1^{(4)},\, u_2^{(4)}\right\} = \left\{S^E_{23}, S^E_{31}\right\}$$

The multilinear elements of the integrity basis, in terms of the basic quantities, are given by

Degree 1: $\quad u_i^{(1)} \quad (i = 1, 4)$

Degree 2: $\quad u_j^{(2)} u_k^{(2)},\ u_l^{(3)} u_m^{(3)},\ u_r^{(4)} u_s^{(4)} \quad (j, k = 1, 2; l, m = 1, 1; r, s = 1, 2).$

Transforming phase: The stress favored martensitic variant is nucleated from the austenitic phase under high stress and low magnetic field, since austenitic field is

$\Gamma^{(1)}$	$S_{11}^E, S_{22}^E, S_{33}^E, S_{12}^E$		$E_{11}^I, E_{22}^I, E_{33}^I, E_{12}^I$		
$\Gamma^{(2)}$		H_1, H_2		M_1^I, M_2^I	
$\Gamma^{(3)}$		H_3		M_3^I	
$\Gamma^{(4)}$	S_{32}^E, S_{31}^E		E_{32}^I, E_{31}^I		

Table X. The basic quantities of ($\underline{2}$/m) for transformation

only stable at high field. We consider that only the stress favored single crystal martensitic variant exists. Nucleation of the new phase causes inelastic deformation and the change in strain and magnetization are taken into account through the set of internal variables. The internal variables for this case are inelastic strain $\mathbf{E}^I$, internal magnetization $\mathbf{M}^I$ and volume fraction ξ_1 of the martensitic phase. The evolution of $\mathbf{E}^I$ and $\mathbf{M}^I$ are related to that of ξ_1 through transformation tensor $\mathbf{\Lambda}_1^t$ and transformation vector $\boldsymbol{\gamma}_1^t$, respectively. The Gibbs free energy for this phase is given by

$$G = G_I(\mathbf{S}^E,\, \mathbf{H},\, T,\, \mathbf{E}^I,\, \mathbf{M}^I).$$

Since the nucleating phase is martensite, we impose symmetry restrictions of $\underline{2}/m$ on the Gibbs free energy function. The orientation of the martensitic variant is the same as Fig. 11 and the basic quantities are given in Table X. We write

$$\begin{aligned}
\Gamma^{(1)}: \quad & \left\{u_1^{(1)},\, u_2^{(1)},\, u_3^{(1)},\, u_4^{(1)}\right\} = \left\{S_{11}^E, S_{22}^E, S_{33}^E, S_{12}^E\right\} \\
& \left\{u_5^{(1)},\, u_6^{(1)},\, u_7^{(1)},\, u_8^{(1)}\right\} = \left\{E_{11}^I, E_{22}^I, E_{33}^I, E_{12}^I\right\} \\
\Gamma^{(2)}: \quad & \left\{u_1^{(2)},\, u_2^{(2)},\, u_3^{(2)},\, u_4^{(2)}\right\} = \left\{H_1, H_2,\, M_1^I, M_2^I\right\} \\
\Gamma^{(3)}: \quad & \left\{u_1^{(3)},\, u_2^{(3)}\right\} = \left\{H_3,\, M_3^I\right\} \\
\Gamma^{(4)}: \quad & \left\{u_1^{(4)},\, u_2^{(4)},\, u_3^{(4)},\, u_4^{(4)}\right\} = \left\{S_{23}^E, S_{31}^E,\, E_{23}^I, E_{31}^I\right\}.
\end{aligned}$$

$\Gamma^{(1)}$	$S'^E_{11}, S'^E_{22}, S'^E_{33}, S'^E_{12}$	$t_{11}, t_{22}, t_{33}, t_{12}$
$\Gamma^{(2)}$		
$\Gamma^{(3)}$		
$\Gamma^{(4)}$	S'^E_{32}, S'^E_{31}	t_{32}, t_{31}

Table XI. The basic quantities of ($\underline{2}$/m) for strain evolution

The multilinear elements of the integrity bases, in terms of basic quantities, are given by

Degree 1: $u_i^{(1)} \quad (i = 1, 8)$

Degree 2: $u_j^{(2)} u_k^{(2)},\ u_l^{(3)} u_m^{(3)},\ u_r^{(4)} u_s^{(4)} \quad (j, k = 1, 4; l, m = 1, 2; r, s = 1, 4).$

Since the phase transformation occurs due to deviatoric part ($\mathbf{S}'^E$) of the stress $\mathbf{S}^E$, we further consider the strain evolution equation in the following form

$$\dot{E}^I_{ij} = (\Lambda^t_{ij})_1(\mathbf{S}'^E)\dot{\xi}_1.$$

As described in subsection 3, we construct $V = V(\mathbf{t}, \mathbf{S}'^{\mathbf{E}})$ and the basic quantities are given in Table XI. We write

$$\begin{aligned}
\Gamma^{(1)}: \quad & \left\{u_1^{(1)},\ u_2^{(1)},\ u_3^{(1)},\ u_4^{(1)}\right\} = \left\{S'^E_{11}, S'^E_{22}, S'^E_{33}, S'^E_{12}\right\} \\
& \left\{u_5^{(1)},\ u_6^{(1)},\ u_7^{(1)},\ u_8^{(1)}\right\} = \left\{t_{11}, t_{22}, t_{33}, t_{12}\right\} \\
\Gamma^{(4)}: \quad & \left\{u_1^{(4)},\ u_2^{(4)},\ u_3^{(4)},\ u_4^{(4)}\right\} = \left\{S'^E_{23}, S'^E_{31},\ t_{23}, t_{31}\right\}.
\end{aligned}$$

Elements of the integrity bases are

Degree 1: $u_1^{(1)},\ u_2^{(1)},\ u_3^{(1)},\ u_4^{(1)},\ u_5^{(1)},\ u_6^{(1)},\ u_7^{(1)},\ u_8^{(1)}$

Degree 2: $(u_1^{(4)})^2,\ (u_2^{(4)})^2,\ (u_3^{(4)})^2,\ (u_4^{(4)})^2,\ u_1^{(4)}u_2^{(4)},\ u_1^{(4)}u_3^{(4)},\ u_1^{(4)}u_4^{(4)},$
$u_2^{(4)}u_3^{(4)},\ u_2^{(4)}u_4^{(4)},\ u_3^{(4)}u_4^{(4)}$

Following subsection 3, we find that $\{I\} = \{u_1^{(1)},\, u_2^{(1)},\, u_3^{(1)},\, u_4^{(1)}, (u_1^{(4)})^2,\, (u_2^{(4)})^2,\, u_1^{(4)}u_2^{(4)}\}$ are independent of $\mathbf{t}$ and $\{L\} = \{u_5^{(1)},\, u_6^{(1)},\, u_7^{(1)},\, u_8^{(1)},\, u_1^{(4)}u_3^{(4)}, u_1^{(4)}u_4^{(4)},\, u_2^{(4)}u_3^{(4)},\, u_2^{(4)}u_4^{(4)}\}$ are linear in $\mathbf{t}$. Then the elements of the set $\{\mathscr{D}_{ij}\} = \frac{\partial\{L\}}{\partial t_{ij}}$ are given by

$$\frac{\partial u_5^{(1)}}{\partial t_{ij}} = \begin{bmatrix} 1 & 0 & 0 \\ 0 & 0 & 0 \\ 0 & 0 & 0 \end{bmatrix}, \frac{\partial u_6^{(1)}}{\partial t_{ij}} = \begin{bmatrix} 0 & 0 & 0 \\ 0 & 1 & 0 \\ 0 & 0 & 0 \end{bmatrix}, \frac{\partial u_7^{(1)}}{\partial t_{ij}} = \begin{bmatrix} 0 & 0 & 0 \\ 0 & 0 & 0 \\ 0 & 0 & 1 \end{bmatrix}, \frac{\partial u_8^{(1)}}{\partial t_{ij}} = \begin{bmatrix} 0 & 1 & 0 \\ 1 & 0 & 0 \\ 0 & 0 & 0 \end{bmatrix},$$

$$\frac{\partial (u_1^{(4)}u_3^{(4)})}{\partial t_{ij}} = \begin{bmatrix} 0 & 0 & 0 \\ 0 & 0 & S_{23}'^E \\ 0 & S_{23}'^E & 0 \end{bmatrix}, \frac{\partial (u_1^{(4)}u_4^{(4)})}{\partial t_{ij}} = \begin{bmatrix} 0 & 0 & S_{23}'^E \\ 0 & 0 & 0 \\ S_{23}'^E & 0 & 0 \end{bmatrix},$$

$$\frac{\partial (u_2^{(4)}u_3^{(4)})}{\partial t_{ij}} = \begin{bmatrix} 0 & 0 & 0 \\ 0 & 0 & S_{31}'^E \\ 0 & S_{31}'^E & 0 \end{bmatrix}, \frac{\partial (u_2^{(4)}u_4^{(4)})}{\partial t_{ij}} = \begin{bmatrix} 0 & 0 & S_{31}'^E \\ 0 & 0 & 0 \\ S_{31}'^E & 0 & 0 \end{bmatrix}$$

and we can write

$$(\Lambda_{ij}^t)_1 = \sum_{p=1}^{8} c_{p_1}(\{I\})(\mathscr{D}_{ij}^p)_1.$$

Similarly, for the internal magnetization, the evolution equation is

$$\dot{M}_i^I = (\gamma_i^t)_1(\mathbf{S}'^E)\dot{\xi}_1$$

and we construct $V = V(\mathbf{r}, \mathbf{S'^E})$. The basic quantities are given in Table XII and so

$$\begin{aligned}
\Gamma^{(1)}: &\quad \left\{u_1^{(1)},\, u_2^{(1)},\, u_3^{(1)},\, u_4^{(1)}\right\} = \left\{S_{11}'^E,\, S_{22}'^E,\, S_{33}'^E,\, S_{12}'^E\right\} \\
\Gamma^{(2)}: &\quad \left\{u_1^{(2)},\, u_2^{(2)}\right\} = \{r_1,\, r_2\} \\
\Gamma^{(3)}: &\quad \left\{u_1^{(3)}\right\} = \{r_3\} \\
\Gamma^{(4)}: &\quad \left\{u_1^{(4)},\, u_2^{(4)}\right\} = \left\{S_{32}'^E,\, S_{31}'^E\right\}.
\end{aligned}$$

$\Gamma^{(1)}$	$S'^E_{11}, S'^E_{22}, S'^E_{33}, S'^E_{12}$		
$\Gamma^{(2)}$		r_1	r_2
$\Gamma^{(3)}$		r_3	
$\Gamma^{(4)}$	S'^E_{32}, S'^E_{31}		

Table XII. The basic quantities of ($\underline{2}$/m) for magnetization evolution

Among the elements of the integrity basis, only $\{L\} = \{u_1^{(2)}, u_2^{(2)}, u_1^{(3)}\}$ are linear in $\mathbf{r}$. So the elements of $\{\mathscr{D}_i\} = \frac{\partial\{L\}}{\partial r_i}$ are

$$\frac{\partial u_1^{(2)}}{\partial r_i} = \begin{bmatrix} 1 \\ 0 \\ 0 \end{bmatrix}, \quad \frac{\partial u_2^{(2)}}{\partial r_i} = \begin{bmatrix} 0 \\ 1 \\ 0 \end{bmatrix}, \quad \frac{\partial u_1^{(3)}}{\partial r_i} = \begin{bmatrix} 0 \\ 0 \\ 1 \end{bmatrix}.$$

It should be noted that there is no stress dependence on the elements of $\{\mathscr{D}\}$. Finally we write

$$(\gamma_i^t)_1 = \sum_{p=1}^{3} c'_{p1}(\{I\})(\mathscr{D}_i^p)_1.$$

Here $\{I\}$ is the same as described for $\mathbf{\Lambda}_1^t$.

2. Field induced variant reorientation

The most widely used material for this mechanism is Ni_2MnGa. The martensitic phase has 10M structure and belongs to $I4/mmm$ space group. The classical point group is $4/mmm$ (D_{4h}). The five magnetic point groups are $\underline{4}/\underline{mmm}m, 4/\underline{m}mm, \underline{4}/mm\underline{m}, 4/\underline{mmm}$ and $4/m\underline{mm}$. Among them only $4/m\underline{mm}$ is ferromagnetic and rest of the members are antiferromagnetic [134]. So we consider $4/m\underline{mm}$ to develop the integrity basis.

There are three possible variants for tetragonal martensite. We denote variant-3 to be that which has its shorter length (c) along the z direction. The x and y axes

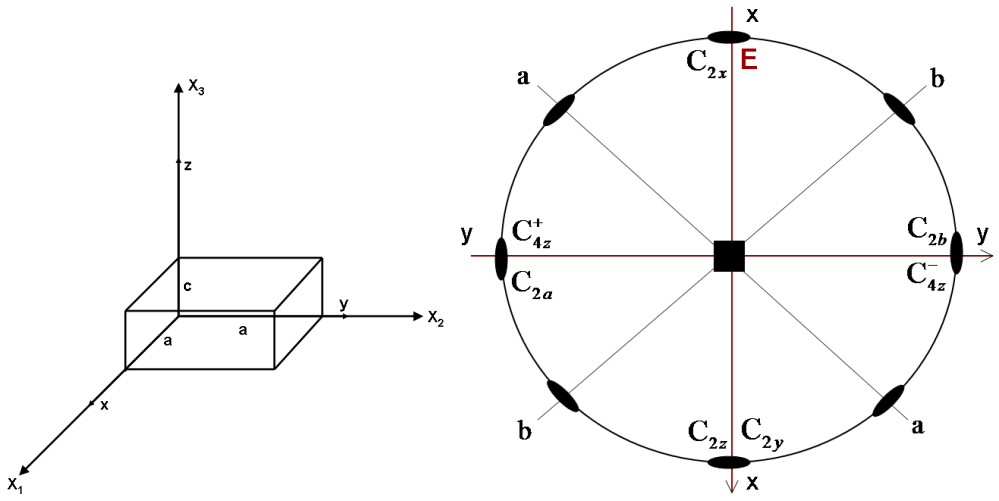

(a) (b)

Fig. 12. (a) Orientation of variant-3 with x, y, z comprising the body fixed (local) coordinate system and X_1, X_2, X_3 defining the global coordinate system (b) Stereographic representation of the symmetry elements and local reference axes for $4/mmm$ point group.

are along the longer side with length a (Fig. 12a). The stereographic representation of the group elements of $4/mmm$ is presented in Fig. 12(b). The notation is the same as described in the previous subsection. The filled square (■) at the center represents the 4-fold rotations about the z axis. The irreducible representation is given in Tables XIII and XIV, where the matrices

$$E = \begin{bmatrix} 1 & 0 \\ 0 & 1 \end{bmatrix}, \quad F = \begin{bmatrix} 1 & 0 \\ 0 & -1 \end{bmatrix}, \quad K = \begin{bmatrix} 0 & 1 \\ 1 & 0 \end{bmatrix}, \quad L = \begin{bmatrix} 0 & 1 \\ -1 & 0 \end{bmatrix}.$$

The magneto-mechanical decompositions are presented in Table XV and the basic quantities are given in Table XVI. The components of the basic quantities are presented with respect to the orientation of the crystal as given in Fig. 12(a). They

$4/m\underline{mm}$	E	$\tau(D_1)$	$\tau(D_2)$	D_3	$\tau(CT_3)$	R_1T_3	R_2T_3	$\tau(R_3T_3)$
$\Gamma^{(1)}$	1	1	1	1	1	1	1	1
$\Gamma^{(2)}$	1	-1	-1	1	-1	1	1	-1
$\Gamma^{(3)}$	1	-1	-1	1	1	-1	-1	1
$\Gamma^{(4)}$	1	1	1	1	-1	-1	-1	-1
$\Gamma^{(5)}$	E	F	$-F$	$-E$	$-K$	$-L$	L	K
$\Gamma^{(1')}$	1	1	1	1	1	1	1	1
$\Gamma^{(2')}$	1	-1	-1	1	-1	1	1	-1
$\Gamma^{(3')}$	1	-1	-1	1	1	-1	-1	1
$\Gamma^{(4')}$	1	1	1	1	-1	-1	-1	-1
$\Gamma^{(5')}$	E	F	$-F$	$-E$	$-K$	$-L$	L	K

Table XIII. The irreducible representation of 4/m$\underline{\text{mm}}$: part-1

$4/m\underline{mm}$	C	$\tau(R_1)$	$\tau(R_2)$	R_3	$\tau(T_3)$	D_1T_3	D_2T_3	$\tau(D_3T_3)$
$\Gamma^{(1)}$	1	1	1	1	1	1	1	1
$\Gamma^{(2)}$	1	-1	-1	1	-1	1	1	-1
$\Gamma^{(3)}$	1	-1	-1	1	1	-1	-1	1
$\Gamma^{(4)}$	1	1	1	1	-1	-1	-1	-1
$\Gamma^{(5)}$	E	F	$-F$	$-E$	$-K$	$-L$	L	K
$\Gamma^{(1')}$	-1	-1	-1	-1	-1	-1	-1	-1
$\Gamma^{(2')}$	-1	1	1	-1	1	-1	-1	1
$\Gamma^{(3')}$	-1	1	1	-1	-1	1	1	-1
$\Gamma^{(4')}$	-1	-1	-1	-1	1	1	1	1
$\Gamma^{(5')}$	$-E$	$-F$	F	E	K	L	$-L$	$-K$

Table XIV. The irreducible representation of 4/m$\underline{\text{mm}}$: part-2

Type	Decomposition
Axial c-vectors	$\Gamma^{(1)} \oplus \Gamma^{(5)}$
Polar i-tensors	$2\Gamma^{(1)} \oplus \Gamma^{(3)} \oplus \Gamma^{(4)} \oplus \Gamma^{(5)}$

Table XV. Decomposition of msgneto-mechanical quantities of 4/m$\underline{\text{mm}}$ magnetic point group

$\Gamma^{(1)}$	H_3	M_3^I	$S_{11}^E + S_{22}^E,\ S_{33}^E$	$E_{11}^I + E_{22}^I,\ E_{33}^I$
$\Gamma^{(2)}$				
$\Gamma^{(3)}$			S_{12}^E	E_{12}^I
$\Gamma^{(4)}$			$S_{11}^E - S_{22}^E$	$E_{11}^I - E_{22}^I$
$\Gamma^{(5)}$	$(H_2,\ -H_1)$	$(M_2,\ -M_1)$	$(S_{23}^E,\ -S_{31}^E)$	$(E_{23}^I,\ -E_{31}^I)$
$\Gamma^{(1')}$				
$\Gamma^{(2')}$				
$\Gamma^{(3')}$				
$\Gamma^{(4')}$				
$\Gamma^{(5')}$				

Table XVI. The basic quantities of 4/m$\underline{\text{mm}}$

are

$$\Gamma^{(1)}: \quad \left\{u_1^{(1)},\, u_2^{(1)},\, u_3^{(1)},\, u_4^{(1)},\, u_5^{(1)},\, u_6^{(1)}\right\} = \{H_3,\, M_3^I,\, S_{11}^E + S_{22}^E,\, S_{33}^E,\, E_{11}^I + E_{22}^I,\, E_{33}^I\}$$

$$\Gamma^{(3)}: \quad \left\{u_1^{(3)},\, u_2^{(3)}\right\} = \left\{S_{12}^E,\, E_{12}^I\right\}$$

$$\Gamma^{(4)}: \quad \left\{u_1^{(4)},\, u_2^{(4)}\right\} = \left\{S_{11}^E - S_{22}^E,\, E_{11}^I - E_{22}^I\right\}$$

$$\Gamma^{(5)}: \quad \left\{\mathbf{u}_1^{(5)},\, \mathbf{u}_2^{(5)},\, \mathbf{u}_3^{(5)},\, \mathbf{u}_4^{(5)}\right\} = \left\{\begin{bmatrix} H_2 \\ -H_1 \end{bmatrix}, \begin{bmatrix} M_2^I \\ -M_1^I \end{bmatrix}, \begin{bmatrix} S_{23}^E \\ -S_{31}^E \end{bmatrix}, \begin{bmatrix} E_{23}^I \\ -E_{31}^I \end{bmatrix}\right\}.$$

The elements of the integrity basis are given by

$$\text{Degree 1:} \quad u_i^{(1)} \quad (i = 1, 6) \tag{2.117}$$

$$\text{Degree 2:} \quad u_l^{(3)} u_m^{(3)},\ u_r^{(4)} u_s^{(4)},\ \mathbf{u}_i^{(5)} \cdot \mathbf{u}_j^{(5)} \quad (l, m, r, s = 1, 2; i, j = 1, 4). \tag{2.118}$$

Variant-1 and variant-2: Variant-1 (shorter axis is along the X_1 direction) is selected by applying traction on the single crystal along X_1. The orientation of the initial configuration of variant-1 is presented in Fig. 13. The variant-2 has its shorter length along the X_2 direction. When the magnetic field intensity is high enough along the direction of spontaneous magnetization (X_2), variant-2 becomes preferred. We assume that these two structural phases are magneto-elastic and the Gibbs free energy is assumed to have the following form

$$G_\alpha = G_\alpha(\mathbf{S}^E, \mathbf{H}, T), \tag{2.119}$$

where $\alpha = M_1$ for variant-1 and $\alpha = M_2$ for variant-2. Since the orientations of variant-1 and variant-2 are different than variant-3, the basic quantities are also dif-

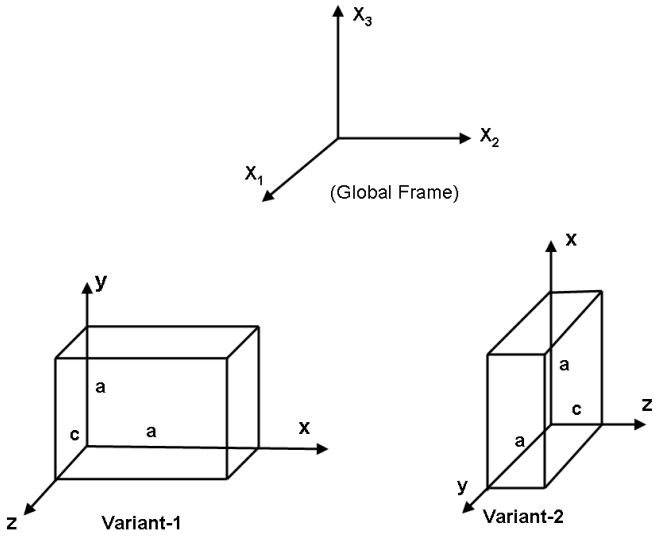

Fig. 13. Orientations of variant-1 and variant-2

ferent. Changes in the local coordinate systems for the variant-1 and variant-2 can be taken into account by changing the indices such that

$$\begin{bmatrix} 1 \to 2 \\ 2 \to 3 \\ 3 \to 1 \end{bmatrix} \quad \text{and} \quad \begin{bmatrix} 1 \to 3 \\ 2 \to 1 \\ 3 \to 2 \end{bmatrix} \tag{2.120}$$

respectively. The left columns are for the local index and the right columns indicate the global index. The integrity basis can then be directly derived from (2.117).

Nucleating phase of Variant 2 : The initial phase of the single crystal MSMA is the stress favored variant-1 and with the application of magnetic field, the field favored variant-2 nucleates. During the nucleation process, the two variants coexist and form a twinned structure. The internal strain and magnetization thus generated are taking into account by considering the internal variables $\mathbf{E}^I$ and $\mathbf{M}^I$. We assume

$\Gamma^{(1)}$	$S'^E_{33}+S'^E_{11},\ S'^E_{22}$	$t_{33}+t_{11},\ t_{22}$
$\Gamma^{(2)}$		
$\Gamma^{(3)}$	S'^E_{31}	t_{31}
$\Gamma^{(4)}$	$S'^E_{33}-S'^E_{11}$	$t_{33}-t_{11}$
$\Gamma^{(5)}$	$(S'^E_{12},\ -S'^E_{23})$	$(t_{12},\ -t_{23})$

Table XVII. The basic quantities of 4/mmm for strain evolution

the Gibbs free energy of the mixing phase by

$$G_I = G_I(\mathbf{S}^E, \mathbf{H}, \mathbf{E}^I, \mathbf{M}^I, T). \tag{2.121}$$

Since variant-2 is nucleating, symmetry restrictions associated with variant-2 are considered. Integrity basis can be obtained from (2.117) with suitable coordinate transformations.

We write the strain evolution equation for nucleation of variant-2 as

$$\dot{E}^I_{ij} = (\Lambda^r_{ij})_4(\mathbf{S}'^E)\dot{\xi}_4.$$

As described in subsection 3, we construct $V = V(\mathbf{t}, \mathbf{S}'^{\mathbf{E}})$ and the basic quantities are given by (Table. XVII)

$$\begin{aligned}
\Gamma^{(1)}: &\quad \left\{u^{(1)}_1,\ u^{(1)}_2,\ u^{(1)}_3,\ u^{(1)}_4\right\} = \left\{S'^E_{33}+S'^E_{11},\ S'^E_{22},\ t_{33}+t_{11},\ t_{22}\right\}\\
\Gamma^{(3)}: &\quad \left\{u^{(3)}_1,\ u^{(3)}_2\right\} = \left\{S'^E_{31},\ t_{31}\right\}\\
\Gamma^{(4)}: &\quad \left\{u^{(4)}_1,\ u^{(4)}_2\right\} = \left\{S'^E_{33}-S'^E_{11},\ t_{33}-t_{11}\right\}\\
\Gamma^{(5)}: &\quad \left\{\mathbf{u}^{(5)}_1,\ \mathbf{u}^{(5)}_2\right\} = \left\{\begin{bmatrix} S'^E_{12}\\ -S'^E_{23}\end{bmatrix},\ \begin{bmatrix} t_{12}\\ -t_{23}\end{bmatrix}\right\}.
\end{aligned}$$

$\Gamma^{(1)}$	r_2	$S'^E_{33}+S'^E_{11},\, S'^E_{22}$
$\Gamma^{(2)}$		
$\Gamma^{(3)}$		S'^E_{31}
$\Gamma^{(4)}$		$S'^E_{33}-S'^E_{11}$
$\Gamma^{(5)}$	$(r_1,\, -r_3)$	$(S'^E_{12},\, -S'^E_{23})$

Table XVIII. The basic quantities of 4/mmm for magnetization evolution

Here $\{I\}=\{u_1^{(1)},\, u_2^{(1)},\, u_1^{(3)},\, u_1^{(4)}\, \mathbf{u}_1^{(5)}\cdot\mathbf{u}_1^{(5)}\}$ is independent of $\mathbf{t}$ and $\{L\}=\{u_3^{(1)},\, u_4^{(1)}, u_1^{(3)}u_2^{(3)},\, u_1^{(4)}u_2^{(4)},\, \mathbf{u}_1^{(5)}\cdot\mathbf{u}_2^{(5)}\}$ are linear in $\mathbf{t}$. Then the elements of the set $\{\mathscr{D}_{ij}\}$ are given by

$$\frac{\partial u_3^{(1)}}{\partial t_{ij}}=\begin{bmatrix}1&0&0\\0&0&0\\0&0&1\end{bmatrix},\quad \frac{\partial u_4^{(1)}}{\partial t_{ij}}=\begin{bmatrix}0&0&0\\0&1&0\\0&0&0\end{bmatrix},\quad \frac{\partial (u_1^{(3)}u_2^{(3)})}{\partial t_{ij}}=\begin{bmatrix}0&0&S'^E_{31}\\0&0&0\\S'^E_{31}&0&0\end{bmatrix},$$

$$\frac{\partial (u_1^{(4)}u_2^{(4)})}{\partial t_{ij}}=\begin{bmatrix}-(S'^E_{33}-S'^E_{11})&0&0\\0&0&0\\0&0&(S'^E_{33}-S'^E_{11})\end{bmatrix},\frac{\partial (\mathbf{u}_1^{(5)}\cdot\mathbf{u}_2^{(5)})}{\partial t_{ij}}=\begin{bmatrix}0&S'^E_{12}&0\\S'^E_{12}&0&S'^E_{23}\\0&S'^E_{23}&0\end{bmatrix}.$$

We may write

$$(\Lambda^r_{ij})_4=\sum_{p=1}^{5}c_{p_4}(\{I\})(\mathscr{D}^p_{ij})_4.$$

Similarly, the magnetization evolution equation for nucleation of variant-2 is given by

$$\dot{M}^I_i=(\gamma^r_i)_4(\mathbf{S}'^E)\dot{\xi}_4.$$

We construct $V=V(\mathbf{r},\mathbf{S}'^{\mathbf{E}})$ and the basic quantities are given by (Table. XVIII)

$$\Gamma^{(1)}: \quad \left\{u_1^{(1)},\, u_2^{(1)},\, u_3^{(1)}\right\} = \left\{r_2,\, S'^E_{33} + S'^E_{11},\, S'^E_{22}\right\}$$

$$\Gamma^{(5)}: \quad \left\{\mathbf{u}_1^{(5)},\, \mathbf{u}_2^{(5)}\right\} = \left\{ \begin{bmatrix} r_1 \\ -r_3 \end{bmatrix}, \begin{bmatrix} S'^E_{12} \\ -S'^E_{23} \end{bmatrix} \right\}.$$

For this case, $\{I\} = \{u_2^{(1)},\, u_3^{(1)}, \mathbf{u}_2^{(5)} \cdot \mathbf{u}_2^{(5)}\}$ is independent of $\mathbf{r}$ and $\{L\} = \{u_1^{(1)}, \mathbf{u}_1^{(5)} \cdot \mathbf{u}_2^{(5)}\}$ is linear in $\mathbf{r}$. So

$$\frac{\partial u_1^{(1)}}{\partial r_i} = \begin{bmatrix} 0 \\ 1 \\ 0 \end{bmatrix}, \quad \frac{\partial(\mathbf{u}_1^{(5)} \cdot \mathbf{u}_2^{(5)})}{\partial r_i} = \begin{bmatrix} S'^E_{12} \\ 0 \\ S'^E_{23} \end{bmatrix}$$

and we write

$$(\gamma_i^r)_4 = \sum_{p=1}^{2} c'_{p_4}(\{I\})(\mathscr{D}_i^p)_4.$$

where $\{\mathscr{D}_i\} = \frac{\partial\{L\}}{\partial r_i}$.

F. Integrity basis of the Gibbs free energy for continuous symmetry

We have already discussed anisotropy for a single crystal, single variant MSMAs by considering finite symmetry. However, anisotropy may exist in a specimen due to the polycrystalline nature of the presence of multiple variants of the martensitic phase. The variants may have some preferred directions of anisotropy.

We confine our analysis by considering transverse isotropy which belongs to $D_{\infty h}$ group for which the *structural tensor* has the form $\mathbf{e}_3 \otimes \mathbf{e}_3$, where $\mathbf{e}_3$ is the preferred unit direction of texturing (Subsection: 2). We consider $\mathbf{A}_m = \mathbf{a}\otimes\mathbf{a}$ as the mechanical structural tensor and $\mathbf{A}_f = \mathbf{f}\otimes\mathbf{f}$ as the magnetic structural tensor. The unit vectors $\mathbf{a}$ and $\mathbf{f}$ are the direction of mechanical and magnetic anisotropy, respectively. Moreover, $\mathbf{A}_m$ and $\mathbf{A}_f$ may evolve during loading due to microstructural change.

We assume that the mechanical transverse anisotropy is predominant in the directional tensor of the inelastic strain. Thus, $\mathbf{\Lambda}_i^\beta = \mathbf{\Lambda}_i^\beta(\mathbf{S'}^E, \mathbf{a}\otimes\mathbf{a}, \mathbf{H})$. Similarly the directional vector for magnetization evolution $\boldsymbol{\gamma}_i^\beta(\mathbf{S'}^E, \mathbf{f}\otimes\mathbf{f}, \mathbf{H})$ is dominated by the magnetic transverse anisotropy. We consider $\mathbf{a} = (\cos\alpha_1^m,$
$\cos\alpha_2^m, \cos\alpha_3^m)^T$ and $\mathbf{f} = (\cos\alpha_1^f, \cos\alpha_2^f, \cos\alpha_3^f)^T$, where $(\alpha_1, \alpha_2, \alpha_3)$ are the angles made by the unit directional vector with the global axes. Denoting $\mathbf{r}$ as either $\mathbf{a}$ or $\mathbf{f}$, we can write

$$[\mathbf{r}\otimes\mathbf{r}]_{ij} = \begin{bmatrix} \cos^2\alpha_1 & \cos\alpha_1\cos\alpha_2 & \cos\alpha_1\cos\alpha_3 \\ \cos\alpha_1\cos\alpha_2 & \cos^2\alpha_2 & \cos\alpha_2\cos\alpha_3 \\ \cos\alpha_1\cos\alpha_3 & \cos\alpha_2\cos\alpha_3 & \cos^2\alpha_3 \end{bmatrix}. \tag{2.122}$$

By taking the time derivative of (2.122), one can write

$$\begin{aligned} (\mathbf{a}\,\dot{\otimes}\,\mathbf{a}) &= \mathbf{L}^m(\alpha_i^m, \dot{\alpha}_i^m), \\ (\mathbf{f}\,\dot{\otimes}\,\mathbf{f}) &= \mathbf{L}^f(\alpha_i^f, \dot{\alpha}_i^f), \end{aligned}$$

and the evolution equations for α are defined through equation (2.116)

$$\dot{\alpha}_j^m = \sum_{i=1}^{3}\Theta_{ij}^{tm}\dot{\xi}_i + \sum_{i=3}^{6}\Theta_{ij}^{rm}\dot{\xi}_i, \tag{2.123a}$$

$$\dot{\alpha}_j^f = \sum_{i=1}^{3}\Theta_{ij}^{tf}\dot{\xi}_i + \sum_{i=3}^{6}\Theta_{ij}^{rf}\dot{\xi}_i. \tag{2.123b}$$

Here $\Theta_{ij}^{\beta m}$ ($\beta = t$ for transformation, $\beta = r$ for reorientation) are scalars that take into account the change in α_i due to change in ξ_j. Moreover, we assume $\Theta_{ij}^{\beta m}(\mathbf{S'}^E, \mathbf{H}, \mathbf{a}\otimes\mathbf{a}, \mathbf{f}\otimes\mathbf{f})$, $\Theta_{ij}^{\beta f}(\mathbf{S'}^E, \mathbf{H}, \mathbf{a}\otimes\mathbf{a}, \mathbf{f}\otimes\mathbf{f})$ and hardening function $f_i^\beta(\mathbf{S'}^E, \mathbf{H}, \mathbf{a}\otimes\mathbf{a}, \mathbf{f}\otimes\mathbf{f})$ depend on both mechanical and magnetic anisotropy. The isotropic scalar invariants are presented in Table. XIX. Thus, we consider

Arguments	Invariant/s (j)	
$\mathbf{H}$	$j_1 = \mathbf{H} \cdot \mathbf{H}$	
$\mathbf{S'}^E$	$j_2 = \mathrm{tr}\,(\mathbf{S'}^E)^2$	$j_3 = \mathrm{tr}\,(\mathbf{S'}^E)^3$
$\mathbf{H}, \mathbf{S'}^E$	$j_4 = \mathbf{H} \cdot \mathbf{S'}^E\mathbf{H}$	$j_5 = \mathbf{H} \cdot \mathbf{S'}^{E^2}\mathbf{H}$
$\mathbf{H}, \mathbf{a} \otimes \mathbf{a}$	$j_6 = \mathbf{H} \cdot (\mathbf{a} \otimes \mathbf{a})\mathbf{H}$	
$\mathbf{H}, \mathbf{f} \otimes \mathbf{f}$	$j_7 = \mathbf{H} \cdot (\mathbf{f} \otimes \mathbf{f})\mathbf{H}$	
$\mathbf{S'}^E, \mathbf{a} \otimes \mathbf{a}$	$j_8 = \mathrm{tr}\,(\mathbf{S'}^E(\mathbf{a} \otimes \mathbf{a}))$	$j_9 = \mathrm{tr}\,(\mathbf{S'}^{E^2}(\mathbf{a} \otimes \mathbf{a}))$
$\mathbf{S'}^E, \mathbf{f} \otimes \mathbf{f}$	$j_{10} = \mathrm{tr}\,(\mathbf{S'}^E(\mathbf{f} \otimes \mathbf{f}))$	$j_{11} = \mathrm{tr}\,(\mathbf{S'}^{E^2}(\mathbf{f} \otimes \mathbf{f}))$
$\mathbf{H}, \mathbf{S'}^E, \mathbf{a} \otimes \mathbf{a}$	$j_{12} = \mathbf{H} \cdot \mathbf{S'}^E(\mathbf{a} \otimes \mathbf{a})\mathbf{H}$	
$\mathbf{H}, \mathbf{S'}^E, \mathbf{f} \otimes \mathbf{f}$	$j_{13} = \mathbf{H} \cdot \mathbf{S'}^E(\mathbf{f} \otimes \mathbf{f})\mathbf{H}$	

Table XIX. Isotropic scalar invariants for $\mathbf{S'}^E, \mathbf{a} \otimes \mathbf{a}, \mathbf{f} \otimes \mathbf{f}, \mathbf{H}$

Arguments	Invariant/s	
$\mathbf{H}$	$\mathbf{H}$	
$\mathbf{H}, \mathbf{S'}^E$	$\mathbf{S'}^E\mathbf{H}$	$\mathbf{S'}^{E^2}\mathbf{H}$
$\mathbf{H}, \mathbf{f} \otimes \mathbf{f}$	$(\mathbf{f} \otimes \mathbf{f})\mathbf{H}$	
$\mathbf{H}, \mathbf{S'}^E, \mathbf{f} \otimes \mathbf{f}$	$\mathbf{S'}^E(\mathbf{f} \otimes \mathbf{f})\mathbf{H}$	$(\mathbf{f} \otimes \mathbf{f})\mathbf{S'}^E\mathbf{H}$

Table XX. Isotropic vector invariants for $\mathbf{S'}^E, \mathbf{f} \otimes \mathbf{f}, \mathbf{H}$

Arguments	Invariant/s	
0	$\mathbf{I}$	
$\mathbf{H}$	$\mathbf{H}\otimes\mathbf{H}$	
$\mathbf{S'}^E$	$\mathbf{S'}^E$	$\mathbf{S'}^{E^2}$
$\mathbf{a}\otimes\mathbf{a}$	$(\mathbf{a}\otimes\mathbf{a})$	
$\mathbf{H},\mathbf{S'}^E$	$\mathbf{H}\otimes\mathbf{S'}^E\mathbf{H}+\mathbf{S'}^E\mathbf{H}\otimes\mathbf{H}$	$\mathbf{S'}^E\mathbf{H}\otimes\mathbf{S'}^E\mathbf{H}$
$\mathbf{H},\mathbf{a}\otimes\mathbf{a}$	$\mathbf{H}\otimes(\mathbf{a}\otimes\mathbf{a})\mathbf{H}+(\mathbf{a}\otimes\mathbf{a})\mathbf{H}\otimes\mathbf{H}$	$(\mathbf{a}\otimes\mathbf{a})\mathbf{H}\otimes(\mathbf{a}\otimes\mathbf{a})\mathbf{H}$
$\mathbf{S'}^E,\mathbf{a}\otimes\mathbf{a}$	$\mathbf{S'}^E(\mathbf{a}\otimes\mathbf{a})+(\mathbf{a}\otimes\mathbf{a})\mathbf{S'}^E$	$(\mathbf{a}\otimes\mathbf{a})\mathbf{S'}^E(\mathbf{a}\otimes\mathbf{a})$
	$\mathbf{S'}^E(\mathbf{a}\otimes\mathbf{a})\mathbf{S'}^E$	

Table XXI. Isotropic tensor invariants for $\mathbf{S'}^E,\mathbf{a}\otimes\mathbf{a},\mathbf{H}$

$$
\begin{aligned}
f_i^\beta &= f_i^\beta(j_1,j_2..,j_{13})\\
\Theta_{ij}^{\beta m} &= \Theta_i^{\beta m}(j_1,j_2..,j_{13})\\
\Theta_{ij}^{\beta f} &= \Theta_i^{\beta f}(j_1,j_2..,j_{13})
\end{aligned}
$$

The integrity basis for a tensor function is presented in Table. XXI and $\mathbf{\Lambda}_i^\beta$ can be written as

$$
\begin{aligned}
\mathbf{\Lambda}_i^\beta &= t_1\mathbf{I}+t_2\mathbf{H}\otimes\mathbf{H}+t_3\mathbf{S'}^E+t_4\mathbf{S'}^{E^2}+t_5(\mathbf{a}\otimes\mathbf{a})\\
&+ t_6(\mathbf{H}\otimes\mathbf{S'}^E\mathbf{H}+\mathbf{S'}^E\mathbf{H}\otimes\mathbf{H})+t_7\mathbf{S'}^E\mathbf{H}\otimes\mathbf{S'}^E\mathbf{H}\\
&+ t_8(\mathbf{H}\otimes(\mathbf{a}\otimes\mathbf{a})\mathbf{H}+(\mathbf{a}\otimes\mathbf{a})\mathbf{H}\otimes\mathbf{H})+t_9(\mathbf{a}\otimes\mathbf{a})\mathbf{H}\otimes(\mathbf{a}\otimes\mathbf{a})\mathbf{H}\\
&+ t_{10}(\mathbf{S'}^E(\mathbf{a}\otimes\mathbf{a})+(\mathbf{a}\otimes\mathbf{a})\mathbf{S'}^E)+t_{11}(\mathbf{a}\otimes\mathbf{a})\mathbf{S'}^E(\mathbf{a}\otimes\mathbf{a})\\
&+ t_{12}\mathbf{S'}^E(\mathbf{a}\otimes\mathbf{a})\mathbf{S'}^E, \qquad (2.124)
\end{aligned}
$$

where

$$t_i = t_i(j_1,j_2,j_3,j_4,j_5,j_6,j_8,j_9,j_{12}).$$

Similarly, the integrity basis for a vector function is given in Table. XX and the form is given below

$$\begin{aligned}\boldsymbol{\gamma}_i^{\beta} &= s_1\mathbf{H} + s_2\mathbf{S}'^{E}\mathbf{H} + s_3\mathbf{S}'^{E^2}\mathbf{H} + s_4(\mathbf{f}\otimes\mathbf{f})\mathbf{H} + s_5\mathbf{S}'^{E}(\mathbf{f}\otimes\mathbf{f})\mathbf{H} \\ &+ s_6(\mathbf{f}\otimes\mathbf{f})\mathbf{S}'^{E}\mathbf{H}, \end{aligned} \tag{2.125}$$

where,

$$s_i = s_i(j_1, j_2, j_3, j_4, j_5, j_7, j_{10}, j_{11}, j_{13}).$$

G. Applications of the theory

In this section, we propose a specific form of the Gibbs free energy and explicit expressions of the magneto-mechanical constitutive equations are derived. A specific loading path is selected to further reduce the constitutive equations to a simpler form. We will consider two examples to demonstrate the impact of considering symmetry restrictions in the modeling. Variant reorientation for a single crystal will be considered followed by an example of phase transformation in a polycrystalline MSMA.

1. Field induced variant reorientation

We consider the stress favored martensitic variant reorients to the field favored variant, for which $\xi_1 = \xi_2 = \xi_3 = \xi_5 = \xi_6 = 0$ (Fig. 9) and $c_3 = c_4 = 0$. The reorientation process begins with a stress favored variant (M_1) ,i.e, $c_{01} = 1$ and $c_{02} = c_{03} = c_{04} = 0$. The reduced form of the kinematic relation (2.98) becomes

$$c_1 = 1 - \xi_4, \tag{2.126}$$

$$c_2 = \xi_4. \tag{2.127}$$

We denote the Gibbs free energy of the variant-1 and the variant-2 by G_{P_1} and G_{P_2} respectively. The Gibbs free energy of the reorienting phase is denoted by $G_{P_1 \to P_2}$. We write

$$G(\Upsilon_\phi, T, \xi_4, g) = G_{P_1}(\Upsilon_{\phi P}, T) + G_{P_1 \to P_2}(\Upsilon_\phi, T, \xi_4, g),$$

where

$$\begin{aligned} G_{P_1 \to P_2}(\Upsilon_\phi, T, \xi_4, g) &= \xi_4[G_{P_2}(\Upsilon_{\phi P}, T) - G_{P_1}(\Upsilon_{\phi P}, T)] \\ &+ G_I(\Upsilon_{\phi I}) + G_{mix}(g). \end{aligned}$$

$$G(\Upsilon_\phi, T, \xi_4, g) = G_M(\Upsilon_{\phi P}, T) + G_I(\Upsilon_{\phi I}, T) + G_{mix}(g) \tag{2.128}$$

a. Variant 1:

As described in the subsection 2, the arguments of the Gibbs free energy of the variants are $\mathbf{S}^E, \mathbf{H}$ and T (2.119). The invariant form of the Gibbs free energy for variant-1 can be written as

$$G_{P_1} = G_{P_1}(\Upsilon_{\phi P}, T),$$

where the elements of the integrity basis $\Upsilon_{\phi P}$ are

$$\begin{aligned} &I_1 = H_1, \quad I_2 = H_2^2 + H_3^2, \quad I_3 = S_{22}^E + S_{33}^E, \quad I_4 = S_{11}^E \\ &I_5 = [S_{31}^E]^2 + [S_{12}^E]^2, \quad I_6 = [S_{23}^E]^2, \quad I_7 = S_{22}^E S_{33}^E, \quad I_8 = H_2 S_{12}^E + H_3 S_{31}^E. \end{aligned}$$

The elements of the integrity basis are obtained from (2.118) and using (2.120)(a). We consider elastic and magnetic energies with quadratic dependence on stress and field, respectively, while only terms of first degree in stress and field are considered

for the magneto-mechanical coupling energy. Under these assumptions, G_{P_1} can be expanded as

$$G_{P_1}(I_1, I_2, I_3, I_4, I_5, I_6, I_7, I_8) = G_0^1 - \frac{1}{\rho_0}(a_1 I_1 + a_2 I_1^2 + a_3 I_2 + a_4 I_3^2 + a_5 I_4^2 + a_6 I_5 + a_7 I_6 + a_8 I_7 + a_9 I_8 + a_{10} I_1 I_3 + a_{11} I_1 I_4 + a_{12} I_3 I_4). \tag{2.129}$$

With this definition, we return to (2.110a) and (2.110b) and write[6]

$$\begin{aligned}
\mathbf{E}_1 &= -\rho_0 G_{P_1,\mathbf{S}^E} \\
&= 2a_4 I_3 I_{3,\,\mathbf{S}^E} + 2a_5 I_4 I_{4,\,\mathbf{S}^E} + a_6 I_{5,\,\mathbf{S}^E} + a_7 I_{6,\,\mathbf{S}^E} + a_8 I_{7,\,\mathbf{S}^E} \\
&+ a_9 I_{8,\,\mathbf{S}^E} + a_{10} I_1 I_{3,\,\mathbf{S}^E} + a_{11} I_1 I_{4,\,\mathbf{S}^E} + a_{12}(I_3 I_{4,\,\mathbf{S}^E} + I_4 I_{3,\,\mathbf{S}^E}) \\
&= (2a_5 I_4 + a_{12} I_3 + a_{11} I_1)\mathbf{i}\otimes\mathbf{i} + 2(2a_6 S_{12}^E + a_9 H_2)\ \mathrm{Sym}[\mathbf{i}\otimes\mathbf{j}] \\
&+ (2a_4 I_3 + a_8 S_{33}^E + a_{12} I_4 + a_{10} I_1)\mathbf{j}\otimes\mathbf{j} + 4a_7 S_{23}^E\ \mathrm{Sym}[\mathbf{j}\otimes\mathbf{k}] \\
&+ 2(2a_6 S_{31}^E + a_9 H_3)\ \mathrm{Sym}[\mathbf{k}\otimes\mathbf{i}] + (a_8 S_{22}^E + a_{12} I_4 + a_{10} I_1 + 2a_4 I_3)\mathbf{k}\otimes\mathbf{k}
\end{aligned} \tag{2.130}$$

and

$$\begin{aligned}
\mu_0 \mathbf{M}_1 &= -\rho_0 G_{P_1,\mathbf{H}} \\
&= a_1 I_{1,\,\mathbf{H}} + 2a_2 I_1 I_{1,\,\mathbf{H}} + a_3 I_{2,\,\mathbf{H}} + a_9 I_{8,\,\mathbf{H}} + (a_{10} I_3 + a_{11} I_4) I_{1,\,\mathbf{H}} \\
&= (a_1 + 2a_2 H_1 + a_{10}(S_{22}^E + S_{33}^E) + a_{11} S_{11}^E)\mathbf{i} + (2a_3 H_2 + a_9 S_{12}^E)\mathbf{j} \\
&+ (2a_3 H_3 + a_9 S_{31}^E)\mathbf{k}.
\end{aligned} \tag{2.131}$$

[6]The symmetric part of a second order tensor $\mathbf{A}$ is denoted by $\mathrm{Sym}[\mathbf{A}] = \frac{1}{2}(\mathbf{A} + \mathbf{A}^T)$.

The unit vectors along the global X_1, X_2, X_3 axes are denoted by $\mathbf{i}, \mathbf{j}, \mathbf{k}$, respectively.

b. Variant-2

Like variant-1, the Gibbs free energy of variant-2 may be taken as

$$G_{P_2} = G_{P_2}(\Upsilon_{\phi P}, T),$$

where $\Upsilon_{\phi P}$ has the following elements:

$$J_1 = H_2, \quad J_2 = H_3^2 + H_1^2, \quad J_3 = S_{33}^E + S_{11}^E, \quad J_4 = S_{22}^E,$$
$$J_5 = [S_{12}^E]^2 + [S_{23}^E]^2, \quad J_6 = [S_{31}^E]^2, \quad J_7 = S_{33}^E S_{11}^E, \quad J_8 = H_3 S_{23}^E + H_1 S_{12}^E$$

The elements of the integrity basis are obtained from (2.118) and (2.120)(b). It should be noted that the elements of the integrity basis of variant-2 are different than variant-1 due to different orientation. Considering similar assumptions of magento-mechanical energy for variant-1, G_{P_2} can be expanded as

$$G_{P_2}(J_1, J_2, J_3, J_4, J_5, J_6, J_7, J_8) = G_0^2 - \frac{1}{\rho_0}(b_1 J_1 + b_2 J_1^2 + b_3 J_2 + b_4 J_3^2$$
$$+ b_5 J_4^2 + b_6 J_5 + b_7 J_6 + b_8 J_7 + b_9 J_8 + b_{10} J_1 J_3 + b_{11} J_1 J_4 + b_{12} J_3 J_4). \quad (2.132)$$

Like variant-1, we can write

$$\begin{aligned}
\mathbf{E}_2 &= -\rho_0 G_{P_2,\mathbf{S}^E} \\
&= 2b_4 J_3 J_{3,\,\mathbf{S}^E} + 2b_5 J_4 J_{4,\,\mathbf{S}^E} + b_6 J_{5,\,\mathbf{S}^E} + b_7 J_{6,\,\mathbf{S}^E} + b_8 J_{7,\,\mathbf{S}^E} \\
&+ b_9 J_{8,\,\mathbf{S}^E} + b_{10} J_1 J_{3,\,\mathbf{S}^E} + b_{11} J_1 J_{4,\,\mathbf{S}^E} + b_{12}(J_3 J_{4,\,\mathbf{S}^E} + J_4 J_{3,\,\mathbf{S}^E}) \\
&= (2b_4 J_3 + b_8 S^E_{33} + b_{12} J_4 + b_{10} J_1)\mathbf{i}\otimes\mathbf{i} + 2(2b_6 S^E_{12} + b_9 H_1)\ \mathrm{Sym}[\mathbf{i}\otimes\mathbf{j}] \\
&+ (2b_5 J_4 + b_{12} J_3 + b_{11} J_1)\mathbf{j}\otimes\mathbf{j} + 2(2b_6 S^E_{23} + b_9 H_3)\ \mathrm{Sym}[\mathbf{j}\otimes\mathbf{k}] \\
&+ 4b_7 S^E_{31}\ \mathrm{Sym}[\mathbf{k}\otimes\mathbf{i}] + (2b_4 J_3 + b_8 S^E_{11} + b_{12} J_4 + b_{10} J_1)\mathbf{k}\otimes\mathbf{k}. \qquad (2.133)
\end{aligned}$$

and

$$\begin{aligned}
\mu_0 \mathbf{M}_2 &= -\rho_0 G_{P_2,\mathbf{H}} \\
&= b_1 J_{1,\,\mathbf{H}} + 2b_2 J_1 J_{1,\,\mathbf{H}} + b_3 J_{2,\,\mathbf{H}} + b_9 J_{8,\,\mathbf{H}} + (b_{10} J_3 + b_{11} J_4) J_{1,\,\mathbf{H}} \\
&= (2b_3 H_1 + b_9 S^E_{12})\mathbf{i} + (b_1 + 2b_2 H_2 + b_{10}(S^E_{33} + S^E_{11}) + b_{11} S^E_{22})\mathbf{j} \\
&+ (2b_3 H_3 + b_9 S^E_{23})\mathbf{k}. \qquad (2.134)
\end{aligned}$$

c. Reorienting phase of Variant 2 :

The arguments of the Gibbs free energy of the reorienting phase are $\mathbf{S}^E, \mathbf{H}, \mathbf{E}^I$, $\mathbf{M}^I$, and T (2.121). The Gibbs free energy with respect to the invariants can be considered as

$$G_I = G_I(\Upsilon_{\phi I}, T).$$

where the elements of the set $\Upsilon_{\phi I}$ are (using (2.117), (2.118) and (2.120)b)

$$K_1 = S^E_{33} + S^E_{11}, \quad K_2 = S^E_{22}, \quad K_3 = E^r_{33} + E^r_{11}, \quad K_4 = E^r_{22}$$

$$K_5 = H_2, \quad K_6 = M^r_2, \quad K_7 = [S^E_{12}]^2 + [S^E_{23}]^2, \quad K_8 = [S^E_{31}]^2$$

$$K_9 = S^E_{33}S^E_{11}, \quad K_{10} = [E^r_{12}]^2 + [E^r_{23}]^2, \quad K_{11} = [E^r_{31}]^2$$

$$K_{12} = E^r_{33}S^E_{11}, \quad K_{13} = S^E_{31}E^r_{31}, \quad K_{14} = [S^E_{33} - S^E_{11}][E^r_{33} - E^r_{11}]$$

$$K_{15} = E^r_{12}S^E_{12} + E^r_{23}S^E_{23}, \quad K_{16} = H^2_3 + H^2_1, \quad K_{17} = [M^r_3]^2 + [M^r_1]^2,$$

$$K_{18} = H_3M^r_3 + H_1M^r_1.$$

In the present context, where only variant reorientation takes place, $\mathbf{E}^I = \mathbf{E}^r$ and $\mathbf{M}^I = \mathbf{M}^r$. Further considering first order coupling between stress and inelastic strain and between field and internal magnetization, the expanded form of the Gibbs free energy can be written as

$$\begin{aligned} & G_I(K_1, K_2, K_3, K_4, K_5, K_6, K_{12}, K_{13}, K_{14}, K_{15}, K_{18}) \\ = \;& G^I_0 - \frac{1}{\rho_0}(c_1K_1K_3 + c_2K_1K_4 + c_3K_2K_3 + c_4K_2K_4 + c_5K_5K_6 \\ + \;& c_6K_{12} + c_7K_{13} + c_8K_{14} + c_9K_{15} + c_{10}K_{18}). \end{aligned} \tag{2.135}$$

The constitutive equations are written as

$$\begin{aligned}
\bar{\mathbf{E}}^I &= -\rho_0 G_{I,\mathbf{S}^E} \\
&= c_1 K_3 K_{1,\,\mathbf{S}^E} + c_2 K_4 K_{1,\,\mathbf{S}^E} + c_3 K_3 K_{2,\,\mathbf{S}^E} + c_4 K_4 K_{2,\,\mathbf{S}^E} \\
&+ c_6 K_{12,\,\mathbf{S}^E} + c_7 K_{13,\,\mathbf{S}^E} + c_8 K_{14,\,\mathbf{S}^E} + c_9 K_{15,\,\mathbf{S}^E} \\
&= [c_1(E^r_{33}+E^r_{11}) + c_2 E^r_{22} - c_8(E^r_{33}-E^r_{11}) + c_6 E^r_{33}]\mathbf{i}\otimes\mathbf{i} + 2c_9 E^r_{12}\ \mathrm{Sym}[\mathbf{i}\otimes\mathbf{j}] \\
&+ [c_3(E^r_{33}+E^r_{11}) + c_4 E^r_{22}]\mathbf{j}\otimes\mathbf{j} + 2c_9 E^r_{23}\ \mathrm{Sym}[\mathbf{j}\otimes\mathbf{k}] + 2c_7 E^r_{31}\ \mathrm{Sym}[\mathbf{k}\otimes\mathbf{i}] \\
&+ [c_1(E^r_{33}+E^r_{11}) + c_2 E^r_{22} + c_8(E^r_{33}-E^r_{11})]\mathbf{k}\otimes\mathbf{k} \qquad (2.136)
\end{aligned}$$

and

$$\begin{aligned}
\mu_0\bar{\mathbf{M}}^I &= -\rho_0 G_{I,\mathbf{H}} \\
&= c_5 K_6 K_{5,\,\mathbf{H}} + c_{10} K_{18,\,\mathbf{H}} \\
&= c_5 M^r_2 \mathbf{j} + c_{10}(M^r_1\mathbf{i} + M^r_3\mathbf{k}). \qquad (2.137)
\end{aligned}$$

We write the strain evolution equation as

$$\dot{\mathbf{E}}^r = \mathbf{\Lambda}^r_4(\mathbf{S}'^E)\dot{\xi}_4.$$

For the present case we could write $\{I\} = \{S'^E_{33}+S'^E_{11},\ S'^E_{22},\ (S'^E_{31})^2,\ (S'^E_{33}-S'^E_{11})^2,\ (S'^E_{12})^2+(S'^E_{23})^2\}$. The elements of the set $\{\mathscr{D}\}$ are given by

$$\mathscr{D}^1 = \mathbf{i}\otimes\mathbf{i} + \mathbf{k}\otimes\mathbf{k}, \quad \mathscr{D}^2 = \mathbf{j}\otimes\mathbf{j}, \quad \mathscr{D}^3 = 2S'^E_{31}\ \mathrm{Sym}[\mathbf{i}\otimes\mathbf{k}],$$

$$\mathscr{D}^4 = (S'^E_{33}-S'^E_{11})(\mathbf{k}\otimes\mathbf{k} - \mathbf{i}\otimes\mathbf{i}), \quad \mathscr{D}^5 = 2S'^E_{12}\ \mathrm{Sym}[\mathbf{i}\otimes\mathbf{j}] + 2S'^E_{23}\ \mathrm{Sym}[\mathbf{j}\otimes\mathbf{k}].$$

Spanning $\mathbf{\Lambda}_4^r$ in terms of the elements of $\{\mathscr{D}\}$, we write

$$\begin{aligned}\mathbf{\Lambda}_4^r &= c_{14}(\mathbf{i}\otimes\mathbf{i}+\mathbf{k}\otimes\mathbf{k})+c_{24}\mathbf{j}\otimes\mathbf{j}+2c_{34}S_{31}'^E\ \mathrm{Sym}[\mathbf{i}\otimes\mathbf{k}]\\ &+ c_{44}(S_{33}'^E-S_{11}'^E)(\mathbf{k}\otimes\mathbf{k}-\mathbf{i}\otimes\mathbf{i})+2c_{54}(S_{12}'^E\ \mathrm{Sym}[\mathbf{i}\otimes\mathbf{j}]+S_{23}'^E\ \mathrm{Sym}[\mathbf{j}\otimes\mathbf{k}])\end{aligned}$$

Similarly, the magnetization evolution equation is given by

$$\dot{\mathbf{M}}^r=\boldsymbol{\gamma}_4^r(\mathbf{S}'^E)\dot{\xi}_4.$$

for which $\{I\}=\{S_{33}'^E+S_{11}'^E,\ (S_{12}'^E)^2+(S_{23}'^E)^2\}$ and

$$\mathscr{D}^1=\mathbf{j},\quad \mathscr{D}^2=S_{12}'^E\mathbf{i}+S_{23}'^E\mathbf{k}.$$

The expression for $\boldsymbol{\gamma}$ is then given by

$$\boldsymbol{\gamma}_4^r=c_{14}'\mathbf{j}+c_{24}'(S_{12}'^E\mathbf{i}+S_{23}'^E\mathbf{k}).$$

The final forms of the strain and magnetization constitutive equations are written as

$$\mathbf{E} = -\rho_0 G_{,\mathbf{S}^E}=\mathbf{E}_1+\xi_4(\Delta\mathbf{E})+\bar{\mathbf{E}}^I \tag{2.138}$$

$$\mu_0\mathbf{M} = -\rho_0 G_{,\mathbf{H}}=\mathbf{M}_1+\xi_4(\Delta\mathbf{M})+\bar{\mathbf{M}}^I, \tag{2.139}$$

where $\Delta\mathbf{E}=\mathbf{E}_2-\mathbf{E}_1$ and $\Delta\mathbf{M}=\mathbf{M}_2-\mathbf{M}_1$.

d. A specific magneto-mechanical loading path

We consider a single variant (variant-1) is under axial traction along the X_1 direction and magnetic field is applied along the X_2 direction. Under these magneto-mechanical loading conditions, we assume $\mathbf{S}^E=S_{11}^E\mathbf{i}\otimes\mathbf{i}$ and $\mathbf{H}=H_2\mathbf{j}$ and the strain constitutive

equations may be reduced to

$$\begin{aligned}
\mathbf{E}_1 &= 2a_5 S_{11}^E \mathbf{i}\otimes\mathbf{i} + 2a_9 H_2 \ \mathrm{Sym}[\mathbf{i}\otimes\mathbf{j}] + a_{12} S_{11}^E \mathbf{j}\otimes\mathbf{j} + a_{12} S_{11}^E \mathbf{k}\otimes\mathbf{k},\\
\mathbf{E}_2 &= (2b_4 S_{11}^E + b_{10} H_2)\mathbf{i}\otimes\mathbf{i} + (b_{12} S_{11}^E + b_{11} H_2)\mathbf{j}\otimes\mathbf{j}\\
&+ ((2b_4 + b_8) S_{11}^E + b_{10} H_2)\mathbf{k}\otimes\mathbf{k},\\
\mathbf{\Lambda}_4^r &= (d_1 + d_4 S_{11}'^E)\mathbf{i}\otimes\mathbf{i} + d_2 \mathbf{j}\otimes\mathbf{j} + (d_1 - d_4 S_{11}'^E)\mathbf{k}\otimes\mathbf{k}.
\end{aligned}$$

We have the following remarks on the strain constitutive equations:

- Variant-1 has a shear component due to the presence of magnetic field.
- The remaining strain components for variant-1 are uncoupled from the field.
- Variant-2 does not have any shear component.
- All the diagonal terms of variant-2 are coupled with magnetic field.
- $\mathbf{\Lambda}_4^r$ does not contain any off diagonal terms.

Next, considering the magnetization constitutive response, the reduced form can be written as

$$\begin{aligned}
\mathbf{M_1} &= (a_1 + a_{11} S_{11}^E)\mathbf{i} + 2a_3 H_2 \mathbf{j},\\
\mathbf{M}_2 &= (b_1 + 2b_2 H_2 + b_{10} S_{11}^E)\mathbf{j},\\
\boldsymbol{\gamma}_4^r &= p_1 \mathbf{j}.
\end{aligned}$$

Further assuming p_1 is constant, the internal magnetization can be written as

$$\bar{\mathbf{M}}^I = p_1 \xi_4 \mathbf{j}.$$

Thus being consistent with the symmetry restrictions, we have the following remarks on the simplified magnetic constitutive equation:

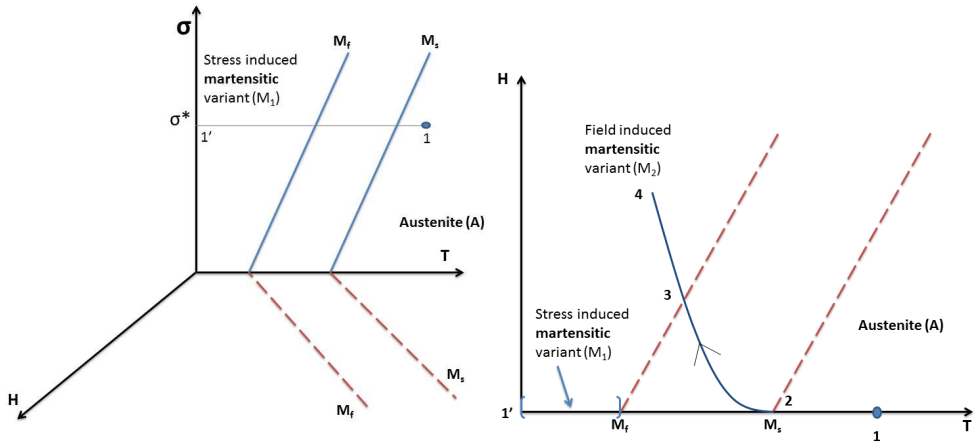

(a) (b)

Fig. 14. (a) Schematic representation of a stress-field-temperature phase diagram with the projections of the martensitic start (M_s) and martensitic finish (M_f) surfaces on the $\sigma - H$ and $H - T$ planes. (b) Magneto-thermal loading path on the $H - T$ plane.

- The X_1 magnetization component of variant-1 is coupled with the stress but the other component is not.
- X_1 magnetization component is not present in variant-2.
- $\boldsymbol{\gamma}_4^r$ is restricted to have no X_1 component.

2. Field induced phase transformation

We consider field induced phase transformation in a *polycrystalline* MSMA where the austenitic phase is *paramagnetic* and martensitic phase is *ferromagnetic* [148]. Initially, the specimen is at a high temperature under compressive loading without any magnetic field and completely austenitic. The initial state is denoted by point-1 in Fig. 14(a), while Fig. 14(b) presents the phase lines on the $H - T$ plane at a stress level σ^*. A specific magneto-thermal loading path is also schematically shown in Fig. 14(b). From point-1, the temperature decreases to point-2 still under zero

magnetic field. A magnetic field $H = f(T)$ is then applied and the martensitic transformation ends at point-3 where field induced martensitic variant (M_2) is present due to the high magnetic field. Between point-2 and point-3 both stress favored and field favored variants nucleate while stress favored variants reorient to the field favored ones. The direction of the texturing of the stress favored variant is denoted by $\mathbf{a}_i$ and the texturing direction at point-3 is denoted by $\mathbf{a}_f$. As a result of the transformation and reorientation of this process (point 2 to 3) the direction of texturing continuously changes from $\mathbf{a}_i$ to $\mathbf{a}_f$. We introduce a structural tensor $\mathbf{A} = \mathbf{a} \otimes \mathbf{a}$ in the Gibbs free energy to take into account the directionality of the magneto-mechanical responses along $\mathbf{a}$. The polycrystalline austenitic phase is assumed to be isotropic.

We simplify the analysis by considering no reorientation from M_1 to M_2, i.e, $\xi_4 = 0$. Moreover, $\xi_3 = \xi_5 = \xi_6 = 0$. Under these conditions, the volume fractions of the stress induced martensitic phase, field induced martensitic phase and austenitic phase can be deduced from (2.98) as

$$\begin{aligned} c_1 &= \xi_1, \\ c_2 &= \xi_2, \\ c_4 &= 1 - (\xi_1 + \xi_2). \end{aligned}$$

We assume the initial phase is fully austenitic ,i.e, $c_{04} = 1$. Denoting $\xi_1 + \xi_2 = \xi$, the volume fractions of the total martensitic and austenitic phases can be written as

$$\begin{aligned} c_1 + c_2 &= \xi, \\ c_4 &= 1 - \xi. \end{aligned}$$

We denote the Gibbs free energy of the austenitic and the martensitic phases by G_{P_4} and $G_{P_1} = G_{P_2} = G_{P_m}$, respectively. The Gibbs free energy of the transforming phase

is denoted by $G_{P_4 \to P_m}$. Thus, from (2.109), we write

$$G(\Upsilon_\phi, T, \xi, g) = G_{P_4}(\Upsilon_{\phi P}, T) + G_{P_4 \to P_m}(\Upsilon_\phi, T, \xi, g),$$

where

$$\begin{aligned} G_{P_4 \to P_m}(\Upsilon_\phi, T, \xi, g) &= \xi[G_{P_m}(\Upsilon_{\phi P}, T) - G_{P_4}(\Upsilon_{\phi P}, T)] \\ &+ G_I(\Upsilon_{\phi I}) + G_{mix}(g). \end{aligned}$$

We consider the following assumptions on the integrity basis for this study.

1. The martensitic and austenitic phases are linear thermoelastic. Therefore, G has a second order dependence on $\mathbf{S}^E$. Moreover, G only depends on first order coupling between $\mathbf{S}^E$ and T.

2. G depends only on the first order coupling of $\mathbf{E}^t$ and $\mathbf{S}^E$. We assume that the inelastic deformation is an isochoric process and generation of transformation strain $\mathbf{E}^t$ is proportional to the deviatoric stress. This means $\mathrm{tr}\,(\mathbf{E}^t) = 0$. We also assume that G depends only on the first order coupling of $\mathbf{M}^t$ and $\mathbf{H}$.

3. In general, magnetostriction in MSMAs is not observed. Quadratic coupling of the magnetic field $\mathbf{H}$ with the $\mathbf{S}^E$ and $\mathbf{E}^t$ is therefore neglected.

Under these assumptions, we consider Υ_ϕ to be composed of the following set of nine invariants

$$\begin{aligned} I_1 &= \mathbf{H} \cdot \mathbf{H}, \qquad I_2 = \mathrm{tr}\,(\mathbf{S}^E), \qquad I_3 = \mathrm{tr}\,(\mathbf{S}^{E^2}), \\ I_4 &= (\mathbf{H} \cdot \mathbf{a})^2, \qquad I_5 = \mathbf{a} \cdot \mathbf{S}^E \mathbf{a}, \qquad I_6 = \mathbf{a} \cdot \mathbf{S}^{E^2} \mathbf{a}, \\ I_7 &= \mathrm{tr}\,(\mathbf{S}^E \mathbf{E}^t), \qquad I_8 = \mathrm{tr}\,(\mathbf{S}^E (\mathbf{a} \otimes \mathbf{a}) \mathbf{E}^t), \quad I_9 = \mathbf{M}^t \cdot \mathbf{H}. \end{aligned} \tag{2.140}$$

We assume $G_{P_4} = G_{P_4}(I_1, I_2, I_3, T)$ for the isotropic austenitic phase. The Gibbs

free energy of the transversely isotropic martensitic phase is denoted by $G_{P_m} = G_{P_m}(I_1, I_2, I_3, I_4, I_5, I_6, T)$. We assume that the energy associated with inelastic transformation is given by $G_I = G_I(\Upsilon_{\phi I}) = G_I(I_7, I_8, I_9)$. The Gibbs free energies for the austenitic and martensitic phases can be expanded up to second degree of the elements of the integrity basis. We consider a general expression

$$\begin{aligned}
G_{P\alpha}(I_1, I_2, I_3, I_4, I_5, I_6, T) &= G_0^\alpha - \frac{1}{\rho}(a_1^\alpha I_1 + a_2^\alpha I_1^2) - \frac{1}{\rho}(a_3^\alpha I_2 + a_4^\alpha I_2^2) \\
&-\frac{1}{\rho}(a_5^\alpha I_3 + a_6^\alpha I_3^2) - \frac{1}{\rho}(a_7^\alpha I_4 + a_8^\alpha I_4^2) - \frac{1}{\rho}(a_9^\alpha I_5 + a_{10}^\alpha I_5^2) \\
&-\frac{1}{\rho}(a_{11}^\alpha I_6 + a_{12}^\alpha I_6^2) - \frac{1}{\rho}(a_{13}^\alpha(\Delta T) + a_{14}^\alpha(\Delta T)^2) - \frac{1}{\rho}(a_{15}^\alpha I_1 I_2 + a_{16}^\alpha I_1 I_3 \\
&+a_{17}^\alpha I_1 I_4 + a_{18}^\alpha I_1 I_5 + a_{19}^\alpha I_1 I_6 + a_{20}^\alpha I_1 \Delta T) - \frac{1}{\rho}(a_{21}^\alpha I_2 I_3 + a_{22}^\alpha I_2 I_4 \\
&+a_{23}^\alpha I_2 I_5 + a_{24}^\alpha I_2 I_6 + a_{25}^\alpha I_2 \Delta T) - \frac{1}{\rho}(a_{26}^\alpha I_3 I_4 + a_{27}^\alpha I_3 I_5 + a_{28}^\alpha I_3 I_6 \\
&+a_{29}^\alpha I_3 \Delta T) - \frac{1}{\rho}(a_{30}^\alpha I_4 I_5 + a_{31}^\alpha I_4 I_6 + a_{32}^\alpha I_4 \Delta T) \\
&-\frac{1}{\rho}(a_{33}^\alpha I_5 I_6 + a_{34}^\alpha I_5 \Delta T) - \frac{1}{\rho} a_{35}^\alpha I_6 \Delta T. \qquad (2.141)
\end{aligned}$$

where $-\frac{1}{\rho}$ is a normalizing factor, T_0 is a reference temperature and $\Delta T = T - T_0$. The austenitic phase and the martensitic phase are denoted by $\alpha = 4$ and $\alpha = m$ respectively.

The inelastic energy G_I can be expanded up to second degree of the elements of the integrity basis as

$$\begin{aligned}
G_I(I_7, I_8, I_9) &= G_0^I - \frac{1}{\rho}(b_1 I_7 + b_2 I_7^2) - \frac{1}{\rho}(b_3 I_8 + b_4 I_8^2) \\
&-\frac{1}{\rho}(b_5 I_9 + b_6 I_9^2) - \frac{1}{\rho}(b_7 I_7 I_8 + b_8 I_7 I_9 + b_9 I_8 I_9). \qquad (2.142)
\end{aligned}$$

Finally we consider the mixing energy as

$$G^{mix}(g) = -\frac{1}{\rho} g. \qquad (2.143)$$

Since we assume that the elastic energy functions for the austenitic and martensitic phases depend only on the quadratic power of the stress, we neglect I_2, I_3^2, I_5, I_6^2, $I_2I_3, I_2I_6,\ I_3I_5, I_3I_6,\ I_5I_6$. Moreover, we consider the magneto-mechanical coupling energy where the order of the stress components is one and so $I_1I_3, I_1I_6,\ I_3I_4, I_4I_6$ are neglected. Under these assumptions (2.141) reduces to

$$\begin{aligned}
G_{P\alpha}(I_1,I_2,I_3,I_4,I_5,I_6,T) &= G_0^\alpha - \frac{1}{\rho}(a_1^\alpha I_1 + a_2^\alpha I_1^2) - \frac{1}{\rho}a_4^\alpha I_2^2 - \frac{1}{\rho}a_5^\alpha I_3 \\
&-\frac{1}{\rho}(a_7^\alpha I_4 + a_8^\alpha I_4^2) - \frac{1}{\rho}a_{10}^\alpha I_5^2 - \frac{1}{\rho}a_{11}^\alpha I_6 - \frac{1}{\rho}(a_{13}^\alpha(\Delta T) + a_{14}^\alpha(\Delta T)^2) \\
&-\frac{1}{\rho}(a_{15}^\alpha I_1I_2 + a_{17}^\alpha I_1I_4 + a_{18}^\alpha I_1I_5) - \frac{1}{\rho}a_{20}^\alpha I_1\Delta T - \frac{1}{\rho}(a_{22}^\alpha I_2I_4 \\
&+a_{23}^\alpha I_2I_5 + a_{25}^\alpha I_2\Delta T) - \frac{1}{\rho}a_{29}^\alpha I_3\Delta T - \frac{1}{\rho}(a_{30}^\alpha I_4I_5 + a_{32}^\alpha I_4\Delta T) \\
&-\frac{1}{\rho}a_{34}^\alpha I_5\Delta T - \frac{1}{\rho}a_{35}^\alpha I_6\Delta T, \qquad (2.144)
\end{aligned}$$

for which

$$\begin{aligned}
\mathbf{E}^\alpha &= -\rho_0 G_{P\alpha,\mathbf{S}^E} \\
&= (2a_4^\alpha I_2 + a_{15}^\alpha I_1 + a_{22}^\alpha I_4 + a_{23}^\alpha I_5 + a_{25}^\alpha\Delta T)\mathbf{I} + 2(a_5^\alpha + a_{29}^\alpha\Delta T)\mathbf{S}^E \\
&+ (2a_{10}^\alpha I_5 + a_{23}^\alpha I_2 + a_{18}^\alpha I_1 + a_{30}^\alpha I_4 + a_{34}^\alpha\Delta T)(\mathbf{a}\otimes\mathbf{a}) \\
&+ (a_{11}^\alpha + a_{35}^\alpha\Delta T)[\mathbf{S}^E(\mathbf{a}\otimes\mathbf{a}) + (\mathbf{a}\otimes\mathbf{a})\mathbf{S}^E], \qquad (2.145)
\end{aligned}$$

$$\begin{aligned}
\mu_0\mathbf{M}^\alpha &= -\rho_0 G^{P\alpha}{}_{,\mathbf{H}} \\
&= 2(a_1^A + 2a_2^A I_1 + a_{15}^A I_2 + a_{17}^A I_4 + a_{18}^A I_5 + a_{20}^A\Delta T)\mathbf{H} \\
&+ 2(a_7^\alpha + 2a_8^\alpha I_4 + a_{17}^\alpha I_1 + a_{22}^\alpha I_2 + a_{30}^\alpha I_5 + a_{32}^\alpha\Delta T)(\mathbf{H}\cdot\mathbf{a})\mathbf{a}. \qquad (2.146)
\end{aligned}$$

It should be noted that for the austenitic phase ($\alpha = 4$), I_4, I_5, I_6 and $\mathbf{a}$ are zero.

In the transforming state, we consider only first order coupling between stress and transformation strain and between magnetic field and internal magnetization

such that

$$G_I(I_7, I_8, I_9) = G_I^0 - \frac{1}{\rho}(b_1 I_7 + b_3 I_8 + b_5 I_9). \tag{2.147}$$

The strain response of the transforming phase is given by

$$\begin{aligned} \bar{\mathbf{E}}^I &= -\rho_0 G_{I,\mathbf{S}^E} = b_1 I_{7,\,\mathbf{S}^E} + b_3 I_{8,\,\mathbf{S}^E} \\ &= b_1 \mathbf{E}^t + b_3 \mathrm{Sym}[(\mathbf{a}\otimes\mathbf{a})\mathbf{E}^t]. \end{aligned} \tag{2.148}$$

We consider $\mathbf{\Lambda}_1^t = \mathbf{\Lambda}_2^t = \mathbf{\Lambda}^t$ such that $\dot{\mathbf{E}}^t = \mathbf{\Lambda}^t \dot{\xi}$. Assuming that $\mathbf{\Lambda}^t(\mathbf{S}^E, \mathbf{a}\otimes\mathbf{a})$ has a linear dependence in stress, equation (2.124) can be simplified to

$$\begin{aligned} \mathbf{\Lambda}^t &= t_1\mathbf{I} + t_3\mathbf{S'}^E + t_5(\mathbf{a}\otimes\mathbf{a}) + t_{10}(\mathbf{S'}^E(\mathbf{a}\otimes\mathbf{a}) + (\mathbf{a}\otimes\mathbf{a})\mathbf{S'}^E) \\ &+ t_{11}(\mathbf{a}\otimes\mathbf{a})\mathbf{S'}^E(\mathbf{a}\otimes\mathbf{a}). \end{aligned} \tag{2.149}$$

In a similar way, for magnetic response we can write

$$\begin{aligned} \bar{\mathbf{M}}^I &= -\rho_0 G_{I,\mathbf{H}} = b_5 I_{9,\,\mathbf{H}} \\ &= b_5 \mathbf{M}^t. \end{aligned}$$

We consider $\boldsymbol{\gamma}_1^t = \boldsymbol{\gamma}_1^t = \boldsymbol{\gamma}^t$ so that $\dot{\mathbf{M}}^t = \boldsymbol{\gamma}^t \dot{\xi}$. Assuming $\boldsymbol{\gamma}_1^t(\mathbf{S}^E, \mathbf{H}, \mathbf{a}\otimes\mathbf{a})$ has a linear dependence in stress, equation (2.125) can be simplified to

$$\boldsymbol{\gamma}^t = s_1\mathbf{H} + s_2\mathbf{S'}^E\mathbf{H} + s_4(\mathbf{a}\otimes\mathbf{a})\mathbf{H} + s_5\mathbf{S'}^E(\mathbf{a}\otimes\mathbf{a})\mathbf{H} + s_6(\mathbf{a}\otimes\mathbf{a})\mathbf{S'}^E\mathbf{H}. \tag{2.150}$$

The final forms of the strain and magnetization constitutive equations are written as

$$\mathbf{E} = -\rho_0 G_{,\mathbf{S}^E} = \mathbf{E}^4 + \xi_1(\Delta\mathbf{E}) + \bar{\mathbf{E}}^I \tag{2.151}$$

$$\mu_0\mathbf{M} = -\rho_0 G_{,\mathbf{H}} = \mathbf{M}_4 + \xi_1(\Delta\mathbf{M}) + \bar{\mathbf{M}}^I,, \tag{2.152}$$

where

$$\bar{\mathbf{M}} \;=\; -\rho_0 G_{,\mathbf{H}} = \mathbf{M}_1 + \xi_1(\Delta\mathbf{M}) + \bar{\mathbf{M}}^I,$$

$\Delta\mathbf{E} = \mathbf{E}^m - \mathbf{E}^4$ and $\Delta\mathbf{M} = \mathbf{M}_m - \mathbf{M}_4$.

a. A specific magneto-mechanical loading path

We consider a specimen that is initially entirely in the austenitic phase and under axial traction along the X_1 direction with a magnetic field applied along the X_2 direction. Under these loading conditions, $\mathbf{S}^E = S^E_{11}\mathbf{i}\otimes\mathbf{i}$ and $\mathbf{H} = H_2\mathbf{j}$. At the beginning when the field is low, only the stress favored variant is nucleated with the decrease in temperature. The direction of the transverse anisotropy is then along the *unit direction* $\mathbf{a}_i = (1,0,0)^T$ at the initial condition. At high field, the direction changes to $\mathbf{a}_f = (0,1,0)^T$ due to the presence of field favored variants.

Our main focus in this subsection is on the evolution of the structural tensor. We assume that $\mathbf{a} = (\cos\beta, \sin\beta, 0)$, where β is the angle with the $(1,0,0)$ direction. The structural tensor may be then written as

$$[\mathbf{a}\otimes\mathbf{a}]_{ij} = \begin{bmatrix} \cos^2\beta & \cos\beta\sin\beta & 0 \\ \cos\beta\sin\beta & \sin^2\beta & 0 \\ 0 & 0 & 0 \end{bmatrix}.$$

and the time derivative as

$$[\mathbf{a}\dot{\otimes}\mathbf{a}]_{ij} = \begin{bmatrix} -\sin 2\beta & \cos 2\beta & 0 \\ \cos 2\beta & \sin 2\beta & 0 \\ 0 & 0 & 0 \end{bmatrix}\dot{\beta}.$$

The evolution of the angle β can be written from (2.123) in a simple form

$$\dot{\beta} = \Theta \dot{\xi}.$$

If Θ is assumed to be constant, then $\beta = \Theta\xi + c$. Moreover from the fact that $\beta = 0$ at $\xi = 0$ and $\beta = \frac{\pi}{2}$ at $\xi = 1$, one can find $\Theta = \frac{\pi}{2}$ and $c = 0$.

Finally, we have the following remarks:

- The internal strain tensor $\bar{\mathbf{E}}^I$ is different than the transformation strain $\mathbf{E}^t$, which is used as an internal variable (2.148).

- $\boldsymbol{\gamma}^t$ can not *only* be a function of $\mathbf{S}^E$. The stress is always coupled with the magnetic field (2.150).

- The intensity of multi-field coupling may be high. The influence of magnetic field on stress has been reported to be more than 15% compared to the stress level under a no field condition by solving a simplified magneto-mechanical boundary value problem for MSMA [149].

CHAPTER III

FIELD INDUCED PHASE TRANSFORMATION (FIPT)

In this chapter, a continuum based model of the magnetic Field Induced Phase Transformation (FIPT) for Magnetic Shape Memory Alloys (MSMA) is developed. Hysteretic material behaviors are considered through the introduction of internal state variables. A Gibbs free energy is proposed using group invariant theory and the coupled constitutive equations are derived in a thermodynamically consistent way. We assume the material is isotropic in this formulation and this is a special case of the generalized one which was discussed in the previous chapter. Moreover, small strain approximation is assumed to avoid much complexities in the model calibration. An experimental procedure of FIPT in NiMnCoIn MSMA single crystals, which can operate under high blocking stress, is described. The model is then reduced to a 1-D form and the material parameter identification from the experimental results is discussed. Model predictions of magneto-thermo-mechanical loading conditions are presented and compared to experiments.

A. Continuum description and thermodynamic framework

We aim to propose a phenomenological modeling for FIPT from the experimental observations. Magneto-mechanical experimental conditions are schematically presented in Fig. 15(a). In the experiments, a magnetic field $\mathbf{H}_a$ is applied through a superconducting magnet while the specimen is held under compressive stress at a constant temperature. The magnetic field is applied coaxially with the mechanical load. Initially, the specimen is in antiferromagnetic martensitic phase. After a critical applied magnetic field is reached, ferromagnetic austenitic phase nucleates and phase transformation completes with further increase in magnetic field. The specimen returns

to the martensitic phase again when the magnetic field decreases below a critical value, characteristic of the material. Fig. 15(b) presents the corresponding average magneto-mechanical material responses. Due to dissipative nature of the magneto-mechanical phase transformation (FIPT), hysteretic loops are observed. The detailed experimental procedure will be discussed in Section D, while Fig. 15 presented here to motivate the proposed constitutive model.

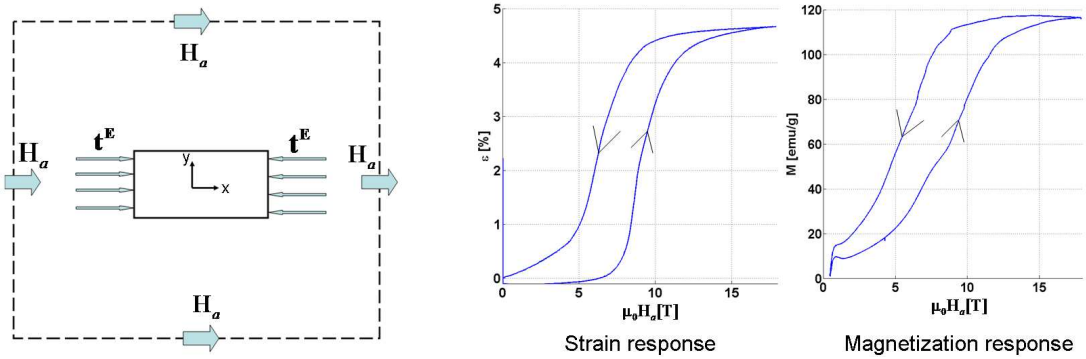

(a) (b)

Fig. 15. (a) Applied boundary conditions. The traction t^E is applied on the specimen along the same direction of the applied magnetic field H_a. The temperature of the specimen and the ambient are maintained at T_0. (b) Mechanical and magnetization hysteretic responses of $Ni_{45.7}Mn_{16.5}Co_5In_{13.5}$ single crystal specimen.

1. Constitutive equations

The constitutive response of MSMAs undergoing a FIPT will depend on state variables such as appropriate measures of stress and magnetic field and also internal state variables to account for loading path dependence due to the hysteretic response caused by dissipation. We assume that the internal energy $u(\boldsymbol{\varepsilon}, \mathbf{M}, s, \{\zeta\})$, where $\boldsymbol{\varepsilon}$ is the total strain, $\mathbf{M}$ is the magnetization, s is the entropy and $\{\zeta\}$ is the set of internal

state variables.

We consider the following internal state variables $\{\zeta\} = \{\boldsymbol{\varepsilon}^t, \mathbf{M}^t, \xi, g\}$ to take into account the dissipative behavior. $\boldsymbol{\varepsilon}^t$ is the *transformation strain* tensor, $\mathbf{M}^t$ is the *transformation magnetization* vector, ξ is the *martensitic volume fraction* and g is the *mixing energy* of the two phases during transformation. $\mathbf{M}^t$ takes into account the phenomenological effect of different micro-magnetical mechanisms e.g. rotation of magnetization vector and evolution of magnetic domain walls.

We write the rate form of the local energy balance ([123], based on two-dipole model, equation 3.3.9) as

$$\rho\dot{u} = \underbrace{\boldsymbol{\sigma}^E : \mathbf{L}}_{Mechanical} - \underbrace{\nabla \cdot \mathbf{q}}_{Thermal} + \underbrace{\mu_0 \mathbf{H} \cdot \dot{\mathbf{M}}}_{Magnetic} + \underbrace{\rho r^h}_{Heat\ source} \tag{3.1}$$

where ρ is the mass density, $\boldsymbol{\sigma}^E = \boldsymbol{\sigma} + \mu_0 \mathbf{H} \otimes \mathbf{M}$ [123, 124] is the mechanical part of the Cauchy stress $\boldsymbol{\sigma}$, $\mathbf{L} = \nabla \otimes \mathbf{v}$ is the velocity gradient, $\mathbf{v}$ is the velocity, $\mathbf{q}$ is the heat flux, μ_0 is the permeability of the free space, $\mathbf{H}$ is the magnetic field vector and r^h is the heat supply due to an external source. The magnetic field $\mathbf{H}$ represents the total magnetic field at a material point. $\mathbf{H}$ may be different from $\mathbf{H}_a$ due to *demagnetization effect* which will be discussed in Section C.

The free charge and the free current density of the body are neglected in this study. The small strain approximation is assumed and the total strain is given by $\boldsymbol{\varepsilon} = \frac{1}{2}(\nabla \mathbf{u} + (\nabla \mathbf{u})^T)$, where $\mathbf{u}$ is the displacement vector. Thus the strain rate $\dot{\boldsymbol{\varepsilon}}$, is equal to the symmetric part of the velocity gradient $\mathbf{L}$, $\mathbf{D}$ ($\dot{\boldsymbol{\varepsilon}} = \mathbf{D}$). Due to the presence of the body couple, $\mathrm{skw}\,\boldsymbol{\sigma} = \mu_0 \mathrm{skw}\,(\mathbf{M} \otimes \mathbf{H})$ [123] so that $\boldsymbol{\sigma}^E$ is symmetric. As a result, (3.1) can be written as

$$\rho\dot{u} = \boldsymbol{\sigma}^E : \dot{\boldsymbol{\varepsilon}} - \nabla \cdot \mathbf{q} + \mu_0 \mathbf{H} \cdot \dot{\mathbf{M}} + \rho r^h. \tag{3.2}$$

Since the experiments are field, temperature and stress controlled (Fig. 15(a)), we wish to write the free energy in terms of these state variables. Thus, a Legendre transformation is used to obtain the Gibbs free energy G from u. The Legendre transformation is given by

$$G(\boldsymbol{\sigma}^E, \mathbf{H}, T, \{\zeta\}) = u - sT - \frac{1}{\rho}\boldsymbol{\sigma}^E : \boldsymbol{\varepsilon} - \frac{\mu_0}{\rho}\mathbf{H}\cdot\mathbf{M}. \tag{3.3}$$

All the experiments are performed in quasistatic conditions and the free energy function does not depend on the rate of magnetic field and temperature. Considering the Clausius-Duhem entropy inequality

$$\rho\dot{s} \geqslant \frac{\rho r^h}{T} - \nabla\cdot(\frac{\mathbf{q}}{T}), \tag{3.4}$$

and combining (3.4), (3.2), (3.3) we get,

$$\rho(\dot{G} + s\dot{T}) + \dot{\boldsymbol{\sigma}}^E : \boldsymbol{\varepsilon} + \mu_0\mathbf{M}\cdot\dot{\mathbf{H}} \geqslant 0. \tag{3.5}$$

Using the Coleman and Noll procedure [101], the following constitutive equations are obtained

$$\begin{aligned}
\boldsymbol{\varepsilon} &= -\rho G_{,\boldsymbol{\sigma}^E} && \text{(3.6a)}\\
\mathbf{M} &= -\frac{\rho}{\mu_0}G_{,\mathbf{H}} && \text{(3.6b)}\\
s &= -G_{,T} && \text{(3.6c)}\\
-\rho G_{,\zeta_i}\cdot\dot{\zeta}_i &\geqslant 0, && \text{(3.6d)}
\end{aligned}$$

where the subscript 'comma' denotes the partial derivative. Expanding the entropy inequality (3.6d), we get

$$\boldsymbol{\pi}_{\boldsymbol{\varepsilon}^t} : \dot{\boldsymbol{\varepsilon}}^t + \boldsymbol{\pi}_{\mathbf{M}^t}\cdot\dot{\mathbf{M}}^t + \pi_\xi\dot{\xi} + \pi_g\dot{g} \geq 0. \tag{3.7}$$

The thermodynamic driving forces are denoted by

$$\begin{aligned}
\boldsymbol{\pi}_{\boldsymbol{\varepsilon}^t} &= -\rho G_{,\boldsymbol{\varepsilon}^t} \\
\boldsymbol{\pi}_{\mathbf{M}^t} &= -\rho G_{,\mathbf{M}^t} \\
\pi_\xi &= -\rho G_{,\xi} = -\rho(G^M - G^A) = -\rho \Delta G \\
\pi_g &= -\rho G_{,g}.
\end{aligned}$$

The inelastic strain $\boldsymbol{\varepsilon}^t$ is related to the evolution of the martensitic volume fraction through the following flow rule

$$\dot{\boldsymbol{\varepsilon}}^t = \boldsymbol{\Lambda}^t \dot{\xi}. \tag{3.8}$$

The transformation tensor $\boldsymbol{\Lambda^t}$ takes into account the direction and magnitude of the generated strain during phase transformation, the specific form of which will be given in subsection 3. Similarly, we assume the following evolution equation for the transformation magnetization

$$\dot{\mathbf{M}}^t = \boldsymbol{\gamma}^t \dot{\xi} \tag{3.9}$$

where $\boldsymbol{\gamma}^t$ takes into account the direction and magnitude of the internal magnetization during the evolution of ξ. The evolution of g is related to the evolution of ξ by

$$\dot{g} = f^t \dot{\xi}, \tag{3.10}$$

where f^t is a hardening function. If (3.8), (3.9) and (3.10) are substituted in to (3.7), we get

$$\boldsymbol{\pi}_{\boldsymbol{\varepsilon}^t} : \boldsymbol{\Lambda}^t \dot{\xi} + \boldsymbol{\pi}_{\mathbf{M}^t} \cdot \boldsymbol{\gamma}^t \dot{\xi} + \pi_\xi \dot{\xi} + \pi_g f^t \dot{\xi} \geq 0,$$

or,

$$\pi^t \dot{\xi} \geq 0,$$

where the total thermodynamic driving force π^t due to phase transformation is given by

$$\pi^t = \boldsymbol{\pi}_{\boldsymbol{\varepsilon}^t} : \boldsymbol{\Lambda}^t + \boldsymbol{\pi}_{\mathbf{M}^t} \cdot \boldsymbol{\gamma}^t + \pi_\xi + \pi_g f^t. \tag{3.11}$$

The following transformation function, Φ^t, is then introduced,

$$\Phi^t := \begin{cases} \pi^t - Y^t, & \dot{\xi} > 0 \\ -\pi^t - Y^t, & \dot{\xi} < 0 \end{cases}, \qquad \Phi^t \leq 0, \tag{3.12}$$

where Y^t is a positive scalar associated with the internal dissipation during phase transformation and can be found from calibration. The proposed transformation function is similar to the transformation function used with conventional shape memory behavior [92, 102]. It is assumed that the constraints of the transformation process follows the principle of maximum dissipation and can be expressed in terms of the Kuhn Tucker type conditions [150]

$$\Phi^t \leq 0, \quad \Phi^t \dot{\xi} = 0\,. \tag{3.13}$$

2. Representation of the Gibbs free energy

We denote the Gibbs free energy of the austenitic phase and the martensitic phase by G^A and G^M respectively. The Gibbs free energy of the transforming phase is denoted by $G^{A\to M}$. We write

$$G(\boldsymbol{\sigma}^E, \mathbf{H}, T, \boldsymbol{\varepsilon}^t, \mathbf{M}^t, \xi, g) = G^A(\boldsymbol{\sigma}^E, \mathbf{H}, T) + G^{A\to M}(\boldsymbol{\sigma}^E, \mathbf{H}, T, \boldsymbol{\varepsilon}^t, \mathbf{M}^t, \xi, g),$$

where

$$\begin{aligned} G^{A\to M}(\boldsymbol{\sigma}^E, \mathbf{H}, T, \boldsymbol{\varepsilon}^t, \mathbf{M}^t, \xi, g) &= \xi[G^M(\boldsymbol{\sigma}^E, \mathbf{H}, T) - G^A(\boldsymbol{\sigma}^E, \mathbf{H}, T)] \\ &+ G^I(\boldsymbol{\sigma}^E, \mathbf{H}, \boldsymbol{\varepsilon}^t, \mathbf{M}^t) + G^{mix}(g). \end{aligned}$$

G^I and G^{mix} are the Gibbs free energy due to the magneto-inelastic deformation and the energy due to the mixing of the two phases during transformation. We determine the *integrity basis* of the scalar function G for two tensor state variables $\{\boldsymbol{\sigma}^E, \boldsymbol{\varepsilon}^t\}$ and two vector state variables $\{\mathbf{M}^t, \mathbf{H}\}$. The list of the all elements of the integrity basis can be found in [127, 140, 141]. The magneto-mechanical anisotropy due to crystalline symmetry of the single crystal specimen is not considered at the present moment. We consider following assumptions on the integrity basis for this study.

1. The martensitic and austenitic phases are linear thermoelastic and so G has a second order dependence on $\boldsymbol{\sigma}^E$. Moreover, G only depends on first order coupling between $\boldsymbol{\sigma}^E$ and T.

2. G depends only on the first order coupling of $\boldsymbol{\varepsilon}^t$ and $\boldsymbol{\sigma}^E$. We assume that the inelastic deformation is an isochoric process and generation of transformation strain $\boldsymbol{\varepsilon}^t$ is proportional to the deviatoric stress. This means $\mathrm{tr}\,(\boldsymbol{\varepsilon}^t) = 0$. We also assume that G depends only on the first order coupling of $\mathbf{M}^t$ and $\mathbf{H}$.

3. In general, magnetostriction in MSMAs is not observed. Thus quadratic coupling of the magnetic field $\mathbf{H}$ with the $\boldsymbol{\sigma}^E$ and $\boldsymbol{\varepsilon}^t$ is neglected.

These assumptions result in the following set of five invariants:

$$\begin{aligned} I_1 &= \mathbf{H}\cdot\mathbf{H}, \qquad I_2 = \mathrm{tr}\,(\boldsymbol{\sigma}^E), \qquad I_3 = \mathrm{tr}\,(\boldsymbol{\sigma}^{E^2}), \\ I_4 &= \mathrm{tr}\,(\boldsymbol{\sigma}^E\boldsymbol{\varepsilon}^t), \qquad I_5 = \mathbf{M}^t\cdot\mathbf{H}. \end{aligned} \tag{3.14}$$

Since the austenitic and martensitic phases are independent of internal variables, we assume $G^A = G^A(I_1, I_2, I_3, T)$ and $G^M = G^M(I_1, I_2, I_3, T)$. We assume that the energy associated with inelastic deformation is given by $G^I = G^I(I_4, I_5)$. The Gibbs free energies for the austenitic and martensitic phases can be expanded up to second degree of the elements of the integrity basis in the following way

$$\begin{aligned} G^\alpha(I_1, I_2, I_3, T) = G_0^\alpha &- \frac{1}{\rho}(a_1^\alpha I_1 + a_2^\alpha I_1^2) - \frac{1}{\rho}(a_3^\alpha I_2 + a_4^\alpha I_2^2) - \frac{1}{\rho}(a_5^\alpha I_3 + a_6^\alpha I_3^2) \\ &- \frac{1}{\rho}(a_7^\alpha(\Delta T) + a_8^\alpha(\Delta T)^2) - \frac{1}{\rho}(a_9^\alpha I_1 I_2 + a_{10}^\alpha I_1 I_3 + a_{11}^\alpha I_1 \Delta T) \\ &- \frac{1}{\rho}(a_{12}^\alpha I_2 I_3 + a_{13}^\alpha I_2 \Delta T) - \frac{1}{\rho} a_{14}^\alpha I_3 \Delta T. \end{aligned} \tag{3.15}$$

where $-\frac{1}{\rho}$ is a normalizing factor, $\Delta T = T - T_0$ and T_0 is a reference temperature. The austenitic phase and the martensitic phase are denoted by $\alpha = A$ and $\alpha = M$ respectively. The inelastic energy G^I can be expanded up to degree one (assumption 2) of the elements of the integrity basis as

$$G^I(I_4, I_5) = G_0^I - \frac{1}{\rho} b_1 I_4 - \frac{1}{\rho} b_2 I_5. \tag{3.16}$$

Finally we consider the mixing energy as

$$G^{mix}(g) = -\frac{1}{\rho} g. \tag{3.17}$$

After we write down (3.15) to (3.17), we need to produce equations (3.6a) to (3.6d). Next section will provide the expressions of the constitutive equations.

B. Reduced form of magneto-thermo-mechanical constitutive response

In this section, magneto-mechanical coupling in the austenitic phase and martensitic phase will be discussed first. Then, we will derive the material constitutive responses for the transforming phase.

1. Austenitic phase

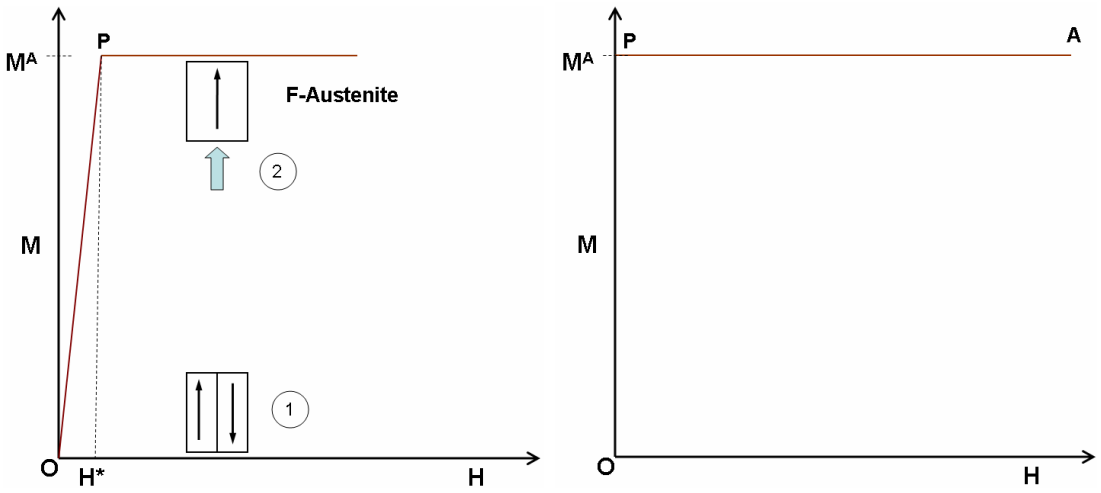

Fig. 16. Schematic representation of magnetization vs. field response of (a) an ideal ferromagnetic response and (b) approximated ferromagnetic response. Magnetic field is applied along the direction of the easy axis.

As shown in Fig. 16a, the magnetization in the austenitic phase is zero at no field condition. This is due to the fact that, at the mesoscale, spontaneous magnetization vectors alter their direction in the successive magnetic domain and the average macroscale magnetization becomes zero (label 1). When magnetic field is applied along the direction of the *easy axis* [1], which is $\hat{\mathbf{n}}$ for the present case, the domain walls disappear almost instantly and the austenitic phase saturates at M^A (label 2) [151]. We thus neglect the variation OP and model the saturation magnetization of the austenitic phase by the horizontal line PA (Fig. 16b). It should be noted that, when the direction of the applied field changes, the direction of the saturation magnetization vector also changes (Fig. 17a). The behavior is similar to a *sgn* function and

[1]The spontaneous magnetization of a ferromagnetic material prefers to align in certain directions. These directions are known as *easy axis*.

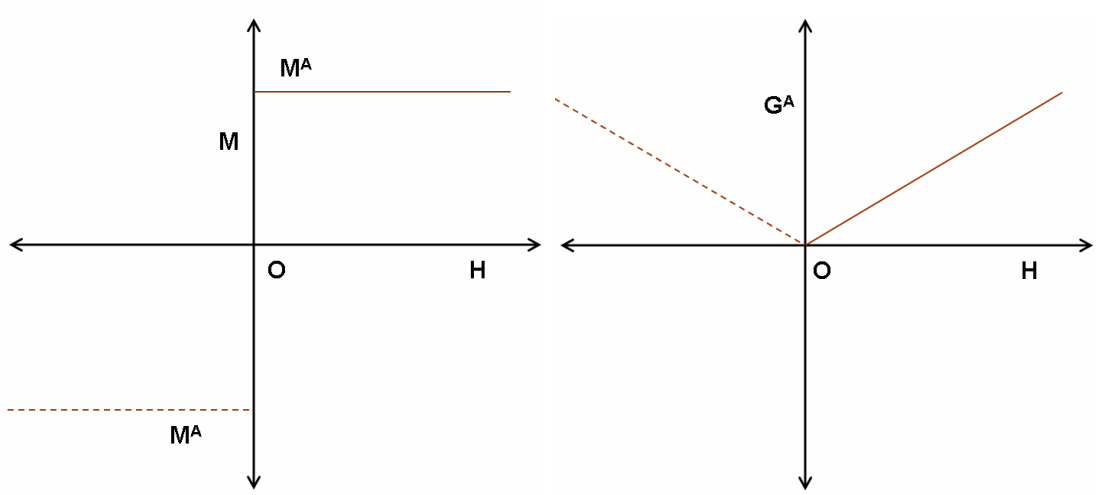

(a) (b)

Fig. 17. Schametic of the (a) magnetization response and (b) corresponding Gibbs free energy of the austenitic phase.

odd in $\mathbf{H}$. This magnetization behavior suggests that the Gibbs free energy should be a *linear even function* of $\mathbf{H}$ (see Fig. 17b). But the invariant theory says that the minimum degree of $\mathbf{H}$ in the Gibbs free energy function is two due to the presence of the invariant element $I_1 = \mathbf{H} \cdot \mathbf{H}$. To solve this issue, we propose to describe the dependency of the Gibbs free energy with a new invariant $\widetilde{I}_1 = \sqrt{I_1} = \sqrt{\mathbf{H} \cdot \mathbf{H}}$. When we differentiate $\tilde{I}_1$ with respect to $\mathbf{H}$ for the expression of the magnetization response we get

$$\widetilde{I}_{1,\mathbf{H}} = \frac{\mathbf{H}}{\sqrt{\mathbf{H} \cdot \mathbf{H}}} = \frac{\mathbf{H}}{|\mathbf{H}|} = \hat{\mathbf{n}}$$

where, $\hat{\mathbf{n}}$ is the unit vector along the direction of magnetic field $\mathbf{H}$. $\hat{\mathbf{n}}$ becomes a null vector when $\mathbf{H}$ becomes zero. Thus, we replace I_1 by $\tilde{I}_1$.

Since experiments are performed at sufficiently low temperatures below T_c, we assumed a linear relationship between saturation magnetization and temperature.

Moreover, the experiments have shown almost a linear relationship between the saturation magnetization of austenite and externally applied stress, the reason of which is not fully known, therefore, in our analysis we have assumed a linear relationship between saturation magnetization and applied stress. Experimental data for the uniaxial loading condition will be presented in the subsection 1. The magnetization constitutive response (3.6b) of the austenitic phase can be written as

$$\mu_0 \mathbf{M}^A = (\hat{a}_1^A + a_9^A \mathrm{tr}\,(\boldsymbol{\sigma}^E) + a_{11}^A T)\hat{\mathbf{n}}, \tag{3.18}$$

where $\hat{a}_1^A = a_1^A - a_{11}^A T_0$. We consider the *mechanical response* of the austenitic phase as linear elastic. The energy function depends only on the quadratic power of stress and the strain response (3.6a) can be written as

$$\boldsymbol{\varepsilon}^A = 2a_4^A \mathrm{tr}\,(\boldsymbol{\sigma}^E)\mathbf{I} + 2a_5^A \boldsymbol{\sigma}^E + a_{13}^A \mathbf{I}\Delta T + a_9^A(\sqrt{\mathbf{H}\cdot\mathbf{H}})\mathbf{I}. \tag{3.19}$$

We can identify that a_4^A, a_5^A are the two elastic constants for isotropic material and a_{13}^A, is the thermal expansion coefficients. Since the austenitic phase is thermoelastic, we consider $\alpha_{14}^A = 0$.

Finally considering the fact that for isochoric and incompressible materials, entropy change is given by

$$\rho(s^A - s_0^A) = c^A \ln(\frac{T}{T_0})$$

where s_0^A and T_0 are the specific entropy and the reference temperature. c^A $(= c_v^A = c_p^A)$ is the specific heat of the austenitic phase. Expanding the logarithmic term and considering the first degree we get

$$\ln(\frac{T}{T_0}) \approx \frac{T - T_0}{T_0}.$$

So,

$$\rho s^A = \rho s_0^A + \frac{c^A}{T_0}(T - T_0).$$

The entropy equation (3.6c) is then written as

$$\rho s^A = \rho s_0^A + a_{11}^A \sqrt{\mathbf{H} \cdot \mathbf{H}} + a_{13}^A \mathrm{tr}\,(\boldsymbol{\sigma}^E) + \frac{c^A}{T_0}(\Delta T), \tag{3.20}$$

where $a_7^A = \rho s_0^A$ and $a_8^A = \frac{c^A}{2T_0}$.

2. Martensitic phase

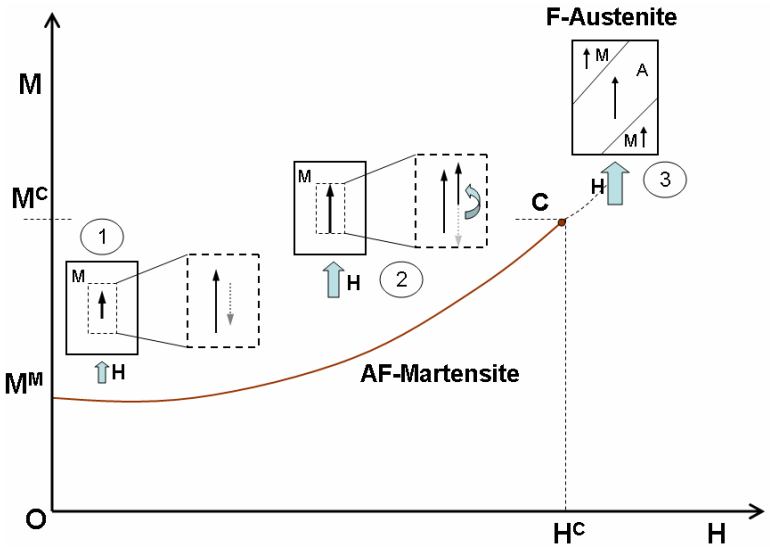

Fig. 18. Schematic of Anti-ferromagnetic (AF) magnetization vs. field response of the martensitic phase

The anti-ferromagnetic martensitic phase has lower saturation magnetization than the austenitic phase. But the magnetization of an anti-ferromagnet can increase beyond saturation under the influence of a strong magnetic field [152, 153]. This phenomenon, also known as *meta-magnetic transition*, is generally observed in anti-ferromagnetic materials. Figure 18 depicts this phenomena in detail. The martensitic

phase reaches saturation M^M at a very small magnetic field (label 1). The saturation magnetization of the anti-ferromagnetic material is low due to the fact that electronic spin of the constituent atoms in a crystal structure opposes each other. We consider the direction $\hat{\mathbf{n}}$ of applied field is along the direction of the spin axis. When applied field intensity increases, the electron spin axis, which opposes the magnetic field, changes direction and the overall magnetization [153] increases (label 2). This mechanism is also known as *spin flop* mechanism. The increase may continue up to a certain critical magnetic field, where nucleation of ferromagnetic austenitic phase becomes energetically favorable. Point C denotes the beginning of the nucleation of the austenitic phase at a critical field H^C. We denote the increased saturation magnetization by M^C at H^C. We also assume that the saturation magnetization of the martensitic phase in the mixture of martensite and austenite remains at M^C. We neglect the implicit coupling of magnetization with stress and temperature in the martensitic phase. Moreover we consider up to quadratic power of the magnetic field (i.e. considering $\widetilde{I}_1$ and $\widetilde{I}_1^{\,2}$) in the Gibbs free energy (3.15) to take account the spin flop mechanism. The form of magnetization response (3.6b) is given by

$$\mu_0 \mathbf{M}^M = a_1^M \hat{\mathbf{n}} + 2a_2^M \mathbf{H}. \tag{3.21}$$

Moreover, the martensitic phase has a similar mechanical response to the austenitic phase and we can immediately write

$$\boldsymbol{\varepsilon}^M = 2a_4^M \mathrm{tr}\,(\boldsymbol{\sigma}^E)\mathbf{I} + 2a_5^M \boldsymbol{\sigma}^E + a_{13}^M \mathbf{I}\Delta T. \tag{3.22}$$

Similarly, the entropy equation is written as

$$\rho s^M = \rho s_0^M + a_{13}^M \mathrm{tr}\,(\boldsymbol{\sigma}^E) + \frac{c^M}{T_0}(\Delta T). \tag{3.23}$$

3. Transforming phase

The strain response of the transforming phase is given by

$$\boldsymbol{\varepsilon}^I = -\rho G^I_{,\boldsymbol{\sigma}^E} = b_1 \boldsymbol{\varepsilon}^t.$$

We assume that the evolution of transformation strain (3.8) generates only from the evolution of total martensitic volume fraction. The directions of the evolution are given as

$$\boldsymbol{\Lambda}^t = \begin{cases} E^{cur}(\bar{\sigma}^E)(\frac{3}{2}\boldsymbol{\sigma}'^E/\bar{\sigma}^E), & \dot{\xi} > 0 \\ \frac{\mathbf{E}^{t-r}}{\xi^r}, & \dot{\xi} < 0 \end{cases} \tag{3.24}$$

During forward reorientation ($\dot{\xi} > 0$), the transformation strain is generated in the direction of deviatoric stress $\boldsymbol{\sigma}'^E$, which is normalized by the Mises equivalent stress $\bar{\sigma}^E = \sqrt{(3/2\boldsymbol{\sigma}'^E : \boldsymbol{\sigma}'^E)}$. E^{cur} is the magnitude of the maximum transformation strain. During full reverse transformation ($\dot{\xi} < 0$), the transformation strain generated by the previous forward transformation must be recovered. This motivates the form of $\boldsymbol{\Lambda}^t$ during reverse transformation, where $\mathbf{E}^{t-r}$ denotes the transformation strain at transformation reversal i.e the state at which the most recent forward transformation ended. The scalar ξ^r is the martensitic volume fraction at the transformation reversal and is used for normalization.

The magnetization response is simply given by

$$\mu_0 \mathbf{M}^I = -\rho G^I_{,\mathbf{H}} = b_2 \mathbf{M}^t. \tag{3.25}$$

The directions of the evolution of magnetization can be expressed as,

$$\boldsymbol{\gamma}^t = \begin{cases} {}^{\mathbf{t}}\boldsymbol{\Gamma}^{\mathbf{f}}, & \dot{\xi} > 0 \\ {}^{\mathbf{t}}\boldsymbol{\Gamma}^{\mathbf{r}}, & \dot{\xi} < 0 \end{cases} \tag{3.26}$$

Here, ${}^{\mathbf{t}}\mathbf{\Gamma}^{\mathbf{f}}$ and ${}^{\mathbf{t}}\mathbf{\Gamma}^{\mathbf{r}}$ are the directions of internal magnetization during forward and reverse transformation. These two vectors are determined experimentally and procedure of finding them is discussed in subsection E. We will determine the values in the next section. The evolution of the mixing energy g is related with the hardening function f^t, which is proposed in the following form

$$f^t = \begin{cases} -A(I_2, I_3)(\pi - \cos^{-1}(2\xi - 1)) + B(I_2, I_3), & \dot{\xi} > 0 \\ -C(I_2, I_3)(\pi - \cos^{-1}(2\xi - 1)) + D(I_2, I_3), & \dot{\xi} < 0 \end{cases} . \tag{3.27}$$

Here A, B, C, D are the hardening parameters to be determined experimentally. Since all the experiments are performed with a uniaxial mechanical and magnetic loading, we need to reduce the model in one dimension for model calibrations.

C. 1-D reduction of the constitutive model

We reduce the model to 1-D where the stress and magnetic field are applied in the x-direction, (Fig. 15a) i.e. $\hat{\mathbf{n}} = (1, 0, 0)^T$. It is assumed that the uniaxial mechanical stress σ^E_{xx} and magnetic field H_x are uniformly distributed inside the prismatic specimen. However a uniaxial applied field can be affected by the demagnetization effect due to the non-ellipsoid geometry of the specimen [19, 20]. The applied magnetic field H_a is different than the field at a material point. So, we consider that the applied magnetic field H_a is the total magnetic field H_x at a generic material point to derive the constitutive equations. The experimental data correction due to demagnetization effect is discussed in Appendix F1.

1. Magnetization response

The magnetization constitutive equation (3.6b) reduces in the 1-D to

$$M_x = M_x^A + \xi(M_x^M - M_x^A) + M_x^I, \tag{3.28}$$

and therefore (3.18), (3.21) and (3.25) become

$$\mu_0 M_x^A = \hat{a}_1^A + a_9^A \sigma_{xx}^E + a_{11}^A T, \tag{3.29a}$$

$$\mu_0 M_x^M = \begin{cases} a_1^M + 2a_2^M H_x, & \text{for } \xi = 1 \text{ and } H_x \leq H^C, \\ \mu_0 M^C, & \text{for } \xi \in (0,1). \end{cases} \tag{3.29b}$$

$$\mu_0 M_x^I = b_2 \gamma_x^t \xi = \widetilde{\gamma}_x^t \xi. \tag{3.29c}$$

2. Mechanical response

The 1-D form of the mechanical response (3.6a) can be written as

$$\varepsilon_{xx} = \varepsilon_{xx}^A + \xi(\varepsilon_{xx}^M - \varepsilon_{xx}^A) + \varepsilon_{xx}^I. \tag{3.30}$$

In view of (3.30), (3.19), (3.22) and (3.24) become

$$\varepsilon_{xx}^A = 2(a_4^A + a_5^A)\sigma_{xx}^E + a_{13}^A \Delta T + a_9^A H_x, \tag{3.31a}$$

$$\varepsilon_{xx}^M = 2(a_4^M + a_5^M)\sigma_{xx}^E + a_{13}^M \Delta T, \tag{3.31b}$$

$$\varepsilon_{xx}^I = b_1 \varepsilon_{xx}^t, \tag{3.31c}$$

where

$$\varepsilon_{xx}^t = \int_0^\xi \Lambda_{xx}^t d\xi. \tag{3.32}$$

The expression of Λ^t_{xx} can be obtained from (3.24) in the following way. We write $\boldsymbol{\sigma}^E = \sigma^E_{xx}\mathbf{e_x}\otimes\mathbf{e_x}$. So, $\boldsymbol{\sigma'}^E = \boldsymbol{\sigma}^E - \frac{1}{3}\mathrm{tr}\,(\boldsymbol{\sigma}^E)\mathbf{I} = \frac{2}{3}\sigma^E_{xx}\mathbf{e}_x\otimes\mathbf{e}_x - \frac{1}{3}\sigma^E_{xx}\mathbf{e}_y\otimes\mathbf{e_y} - \frac{1}{3}\sigma^E_{xx}\mathbf{e}_z\otimes\mathbf{e}_z$. This implies that $\|\boldsymbol{\sigma'}^E\| = \boldsymbol{\sigma'}^E : \boldsymbol{\sigma'}^E = \frac{2}{3}(\sigma^E{}_{xx})^2$ and consequently $\bar{\sigma}^E = \sqrt{\frac{3}{2}\|\boldsymbol{\sigma'}^E\|} = |\sigma^E_{xx}|$. Therefore, from (3.24) we obtain $\Lambda^t_{xx} = E^{cur}\frac{3}{2}\frac{\frac{2}{3}\sigma^E_{xx}}{|\sigma^E_{xx}|} = E^{cur}\mathrm{sgn}(\sigma^E_{xx})$.

We assumed in subsection 3 that E^{cur} depends on the stress level only. This means that E^{cur} is the same for the temperature-induced or field-induced phase transformation. Motivated by experiments, we approximate $E^{cur}(|\sigma^E|)$ using following sigmoid function

$$E^{cur}(|\sigma^E|) = \frac{a}{1+e^{-(|\sigma^E|-m)/s}} + c. \tag{3.33}$$

Here m is the point of inflection and $1/s$ is the growth rate of the curve. The two parameters a and c are to be determined from the experiments.

3. Thermodynamic driving force

The thermodynamic driving force (3.11) for the field induced phase transformation in 1-D loading condition is given by

$$\pi^t = \pi_{\varepsilon^t}\Lambda^t_{xx} + \pi_\xi + \pi_g f^t, \tag{3.34}$$

where

$$\pi_{\varepsilon^t} = \sigma^E_{xx}, \tag{3.35a}$$

$$\pi_\xi = -\rho(G^M - G^A) = -\rho\Delta G, \tag{3.35b}$$

$$\pi_g = 1. \tag{3.35c}$$

We rewrite the transformation function (3.12) and the Kuhn Tucker conditions (3.13) as

$$\Phi^t = \text{sgn}(\dot{\xi})\pi^t - Y^t, \tag{3.35d}$$

$$\Phi^t \leq 0, \ \Phi^t\dot{\xi} = 0. \tag{3.35e}$$

Moreover, equation (3.35b) can be expanded as

$$-\rho\Delta G = \frac{1}{2}\Delta[\frac{1}{2E}](\sigma^E_{xx})^2 + \mu_0\Delta M H_x + \Delta[a_{13}]\sigma^E_{xx}(T - T_0) + \rho\Delta s_0 T - \rho\Delta u_0, \tag{3.36}$$

where $\Delta[\cdot] = [\cdot]^M - [\cdot]^A$ and $\rho u_0^A = \rho G_0^A + \rho s_0^A T_0$. We assume $c^M = c^A$ and so $\Delta c = 0$. It should be reminded that $\Delta M = (M^C - M_x^A)$, since at the beginning and after completion of phase transformation, the martensitic phase is at its saturation magnetization value M^C.

This is the end of modeling part and we have reached a point where we need to determine the unknown material and model parameters. Next, we will discuss experimental detail of FIPT with a specific loading path. The model will be then calibrated from the experimental data.

D. Experimental procedure for FIPT

In this section, we first briefly describe the experimental setup and the preparation of the specimen tested. A magneto-thermo-mechanical loading path is designed to capture the FIPT responses. A selection of experimental responses are presented at the end of this section.

1. Experimental setup and specimen preparation

A micro-magneto-thermo-mechanical testing system (micro-MTM) was exclusively designed and fabricated for direct measurements of MFIS during FIPT under different constant stress levels and temperatures. The miniature stress stage is presented in Fig. 19. The micro-MTM's body and inner components are made of precipitation hardened nonmagnetic Cu-Be and can apply compressive loads on specimens using a specially designed screw-driven 316L stainless steel Belleville springs. The spring design and stacking sequence allowed achieving near constant stress levels during temperature changes due to the differences between the thermal expansion coefficient (+/- 5 MPa variation in the temperature range of interest). The entire micro-MTM device is 10 mm in diameter and 50 mm long. Displacements during magnetic FIPT are measured using a miniature capacitive sensor with an accuracy of ± 0.0001 mm that is capable of measuring the displacements at temperatures as low as 4.2 K and magnetic fields as high as 18 Tesla. The experimental setup is schematically shown in Fig. 20. More detail on the set up are given in [154]. The micro-MTM was placed in a custom designed extraction type superconducting magnet to obtain magnetization and MFIS measurements of the NiMnCoIn specimens under magnetic fields from 0 to 18 Tesla and test temperatures ranging from 4.2 to 250 K under different stress levels.

$Ni_{45}Mn_{36.5}Co_5In_{13.5}$ ingots were synthesized using vacuum induction melting and single crystals were grown in a He atmosphere using the Bridgman technique. The composition of the single crystals was determined to be $Ni_{45.7}Mn_{35.6}Co_{4.8}In_{13.8}$ using wavelength-dispersive spectroscopy (WDS). The difference between the nominal and actual compositions is thought to be due to Mn evaporation during single crystal growth. The single crystal samples were then cut into rectangular prisms with

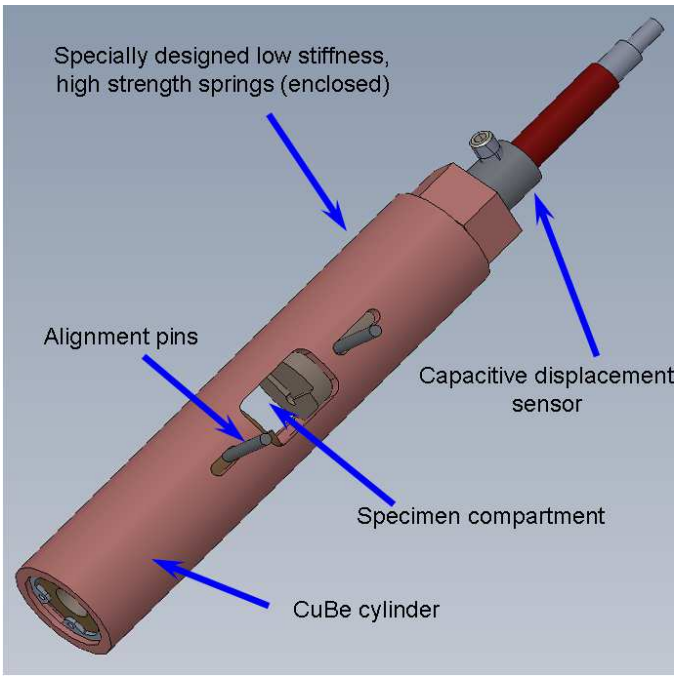

Fig. 19. Miniature stress stage with 10 mm in diameter and 50 mm long

dimensions of 2mm × 2mm × 4mm using electro-discharge machining to assure that both magnetic field and stress can be applied along known crystallographic directions. The [100] direction indicates the long axis of the rectangular prisms. The specimens were homogenized at 900^0C for 24 h under vacuum, water quenched and then heat treated at 500^0C for 1 h under vacuum to achieve ordering in the samples that resulted in martensitic transformation temperatures below room temperature. The thermo-magnetic response of the crystals was characterized using a superconducting quantum interference device (SQUID) magnetometer that can apply magnetic fields up to 18 Tesla.

2. Experimental loading path

We perform a specific experiment for a particular thermo-magneto- mechanical loading condition. The loading paths are described in Fig. 21, where T is the temperature,

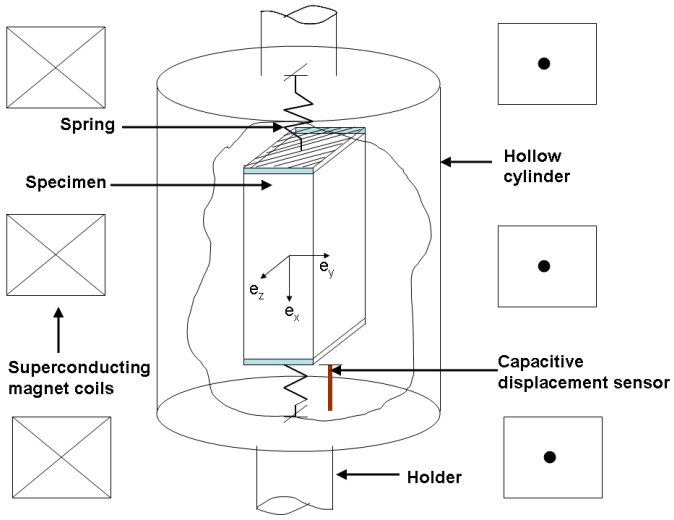

Fig. 20. Schematic of the micro-MTM setup. e_x, e_y, e_z are the unit vectors along the x, y, z directions. The ($\bullet$) and ($\times$) in the superconducting magnet coil denote current out of and current into the plane of the paper.

H_a is the applied magnetic field and σ^E is the mechanical stress. The four critical magnetic fields for forward phase transformation start and finish and the reverse phase transformation start and finish are denoted by H_s^M, H_f^M, H_s^A and H_f^A respectively. Similarly, the four critical temperatures are denoted by T_s^M, T_f^M, T_s^A and T_f^A. Since Cauchy stress for a magneto-mechanical system is magnetic field dependent [123, 124], we denote σ^E as the Cauchy stress with no magnetic field or the mechanical part of the Cauchy stress. We measure all tractions from the $\sigma^E - T$ plane at H_a=0.

The specimen initially is in the austenitic phase at room temperature (300 K). The initial traction $\bar{\sigma}_A$ on the specimen at room temperature and zero magnetic field is found to be -60 MPa. The initial state of the specimen is denoted by point 1 in Fig. 21. During the cooling process, the spring becomes stiffer and the traction increases up to point 2. Forward transformation starts at point 2, and the length of the specimen consequently shrinks during the path 2-3. The shortening of the length relaxes some spring loads and the traction decreases. After point 3, the traction increases up to

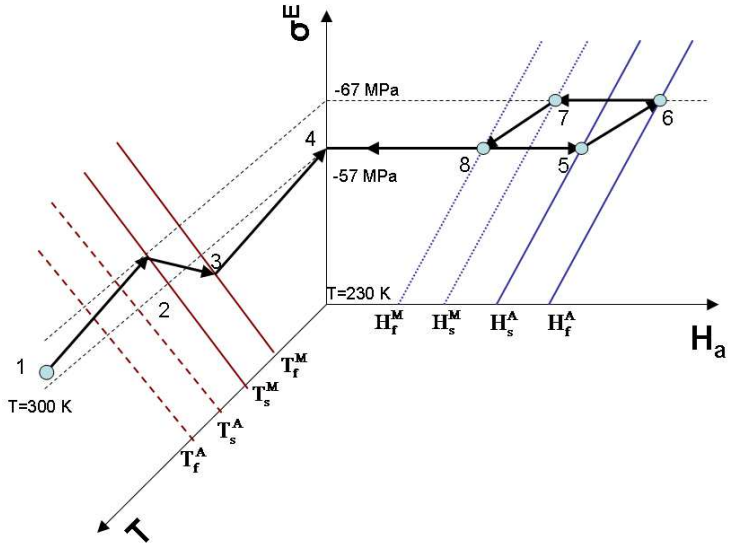

Fig. 21. Schematic of the experimental loading path. The experimentally controlled parameters are temperature, applied magnetic field and mechanical stress. The inclined parallel lines are the projections of the phase surfaces on the stress-field and stress-temperature parametric planes.

point 4 due to the increase in spring stiffness. The specimen is cooled down to T=230 K at point 4. At this point, the specimen is fully transformed to the martensitic phase. Next the temperature is held constant at 230 K and the magnetic field is gradually applied. At point 5, transformation to the austenitic phase is initiated due to magnetic field which completes at point 6. Through the transformation, the traction increases up to point 6, where the specimen recovers its initial length. Upon subsequently decreasing the magnetic field, the reverse phase transformation begins at point 7. After that, by further decreasing of the magnetic field, the specimen starts to shrink and the magnitude of the traction gradually drops. Phase transformation completes at point 8 when further field is removed. The tractions at the beginning and end of the reverse/forward field induced phase transformation are estimated to be -57 MPa and -67 MPa, respectively. It is experimentally observed that the spring

stiffness increases as the temperature decreases and so the traction at point 4 and point 6 increases. Tractions in the martensitic and austenitic phases (point 4 and 6) at 230 K, 200 K and 150 K are listed in Table. XXII.

Initial:	point 1	Final:	point 4	point 6
T [K]	$\bar{\sigma}_A$ [MPa]	T [K]	σ_M [MPa]	σ_A [MPa]
300	-60	230	-57	-67
	-100		-100	-110
300	-60	200	-60	-70
	-100		-103	-113
300	-100	150	-112	-122

Table XXII. Variations of traction levels on the martensitic and austenitic phase at different temperatures.

3. Experimental results

A typical experimental response of strain vs field as well as magnetization vs field are presented in Fig. 22. We observe nearly 5% strain recovery during the field induced reverse transformation (Fig. 22a). The magnetization saturates close to 120 emu/g (Fig. 22b). It should be noted that from 0 to $\mu_0 H_s^A$=7 T no MFIS is observed but magnetization continuously increases. This increase in magnetization may be due to *meta-magnetic phenomenon* (subsection 2). After 7 T, austenitic phase nucleates and MFIS is observed. The magnetization at $\mu_0 H^C = \mu_0 H_s^A = 7$ T can be identified as $M^C = 40$ emu/g (Fig. 18). If we investigate the magnetization response at -100 MPa (Fig. 23(b)), it is observed that the slope of the curve changes drastically around 10 T. This is probably due to the termination of spin-flop mechanism and nucleation of the austenitic phase. The magnetization M^C at this point is also 40 emu/g. Thus we

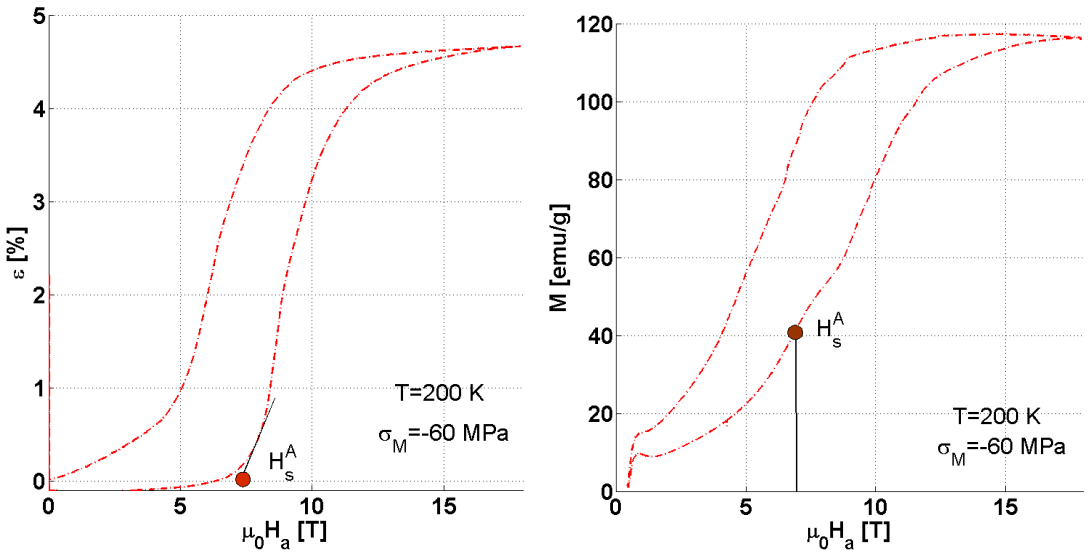

(a) (b)

Fig. 22. Experimental responses of (a) strain vs field and (b) magnetization vs field at 200 K and at a stress level -60 MPa in the martensitic phase.

assume that M^C=40 emu/g remains constant irrespective of stress and temperature level.

In the Fig. 23(a) we observe that maximum strain increases with the increase in applied stress level. This is due to the fact that low stress is not sufficient to bias only single martensitic variant. At high stress level, the volume fraction of the stress favored martensitic variant increases and so the maximum transformation strain. Moreover from Fig. 23(b) we observe that saturation magnetization of the austenitic phase decreases with the increase in magnitude of the stress. This may be due to the fact that applied stress influences the ferromagnetic order. The saturation magnetization of the martensitic phase, M^M, remains constant at 15 emu/g.

Given the 1-D constitutive relations (Section C), the following model parameters must be identified: (A) magnetic, (B) mechanical and (C) thermodynamic, listed

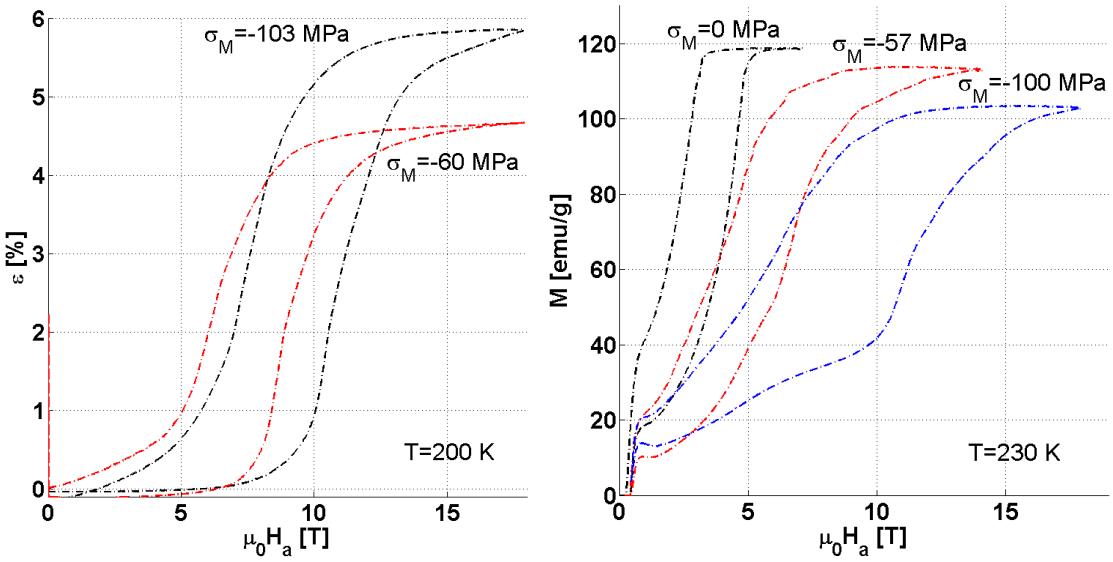

(a) (b)

Fig. 23. Experimental responses of (a) strain vs field and (b) magnetization vs field at 200 K and at a stress level -57 MPa in the martensitic phase.

in Table. XXIII. The experiments required to identify the model parameters are described in the next section.

E. Identification of material parameters

All the material properties that will be used to identify the model parameters are determined from experiments. We follow the sequences I to V in Table. XXIII to identify the model parameters. At the end of this section, results of all required experimental parameters and their values are given in Table. XXIV and Table. XXV, respectively.

Model parameters
(A)-Magnetic
(I): $\hat{a}_1^A$, a_9^A, a_{11}^A
(II): a_1^M, a_2^M, $\widetilde{\gamma}_x^t$
(B)-Mechanical
(III): $(a_4^A + a_5^A)$, a_{13}^A, $(a_4^M + a_5^M)$, a_{13}^M
(IV): a, c, m, s
(C)-Thermodynamic
(V): $\rho\Delta s_0, \rho\Delta u_0, A, B, C, D, Y^t$

Table XXIII. Required model parameters.

1. Magnetic parameters

a. Group I

We are looking for calibrating the constants $\{\hat{a}_1^A, a_9^A, a_{11}^A\}$ of the austenitic phase from the magneto-mechanical and magneto-thermal experimental responses as shown in Fig. 24. Based on these experimental data, we consider the following linear system

$$\begin{bmatrix} 1 & \sigma_1 & T_1 \\ 1 & \sigma_1 & T_2 \\ 1 & \sigma_2 & T_3 \end{bmatrix} \begin{pmatrix} \hat{a}_1^A \\ a_9^A \\ a_{11}^A \end{pmatrix} = \mu_0 \begin{pmatrix} M_1 \\ M_2 \\ M_3 \end{pmatrix}. \tag{3.37}$$

We consider two temperatures T_1=300 K and T_2=340 K at $\sigma_1 = \sigma_A = 0$ for which the *mass magnetizations* are M_1=102 emu/g and M_2=90 emu/g respectively (Fig. 24(a)). Here we denote the stress level in the austenitic phase by σ_A. We convert mass

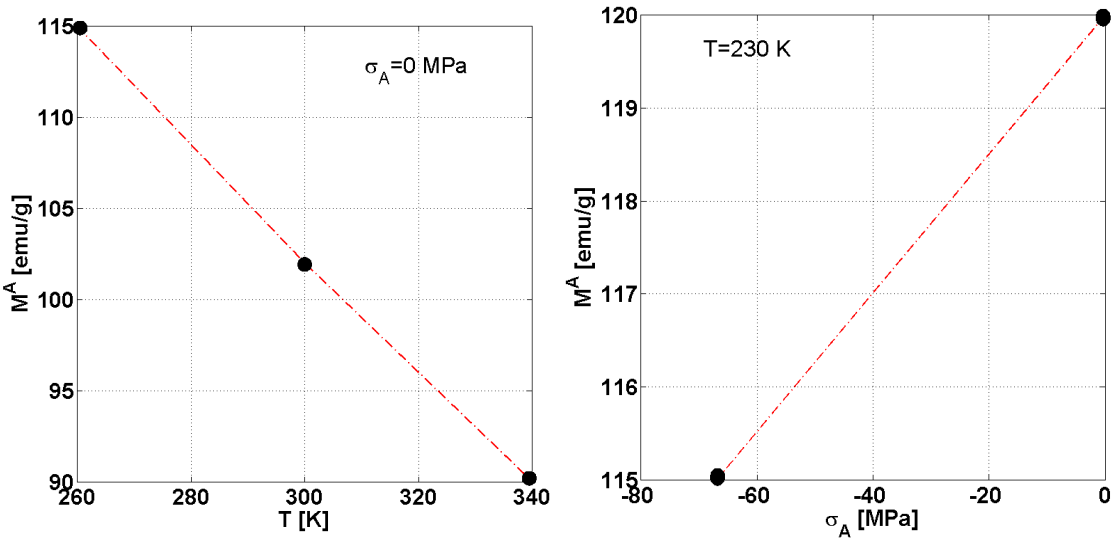

(a) (b)

Fig. 24. Variation of saturation magnetization of the austenitic phase with (a) temperature at zero stress and (b) compressive stress at $T = 230K$.

magnetization to *volume magnetization* and consider M_1=102ρ A/m and M_2=90ρ A/m, where ρ (kg/m^3) is the density of the material[2]. Using the first two equations of (3.37), we obtain

$$\hat{a}_1^A = \mu_0 \frac{M_1 T_2 - M_2 T_1}{T_2 - T_1}, \qquad a_{11}^A = \mu_0 \frac{M_1 - M_2}{T_1 - T_2}. \tag{3.38}$$

In addition, we select the saturation magnetization $M_3 = M_\sigma^A$=115ρ A/m at $\sigma_2 = \sigma_A$=-67 MPa and $T_3 = 230$ K (Fig. 24(b)) to calculate a_9^A. We write from the last

[2]**Units:** The units of magnetization (magnetic field), stress and temperature in SI system are $[A/m]$, $[Pa]$ and $[K]$ respectively. However the experimental data for this study are recorded in the unit of [emu/g](=10^{-3}A.m^2). If ρ [kg/m^3] is the density of the material then 1[emu/g]=1 A.m^2/kg=[A/m]/[kg/m^3]. This means that multiplying ρ to the magnetization value in the [emu/g] unit, we get magnetization in the [A/m] unit. Moreover μ_0=$4\pi\times10^{-7}$ N/A^2, 1[T]=[N/A^2].[A/m]=[N/A.m] and [T].[A/m]=[Pa].

row of (3.37),

$$a_9^A = \frac{\mu_0 M_\sigma^A - (\hat{a}_1^A + a_{11}^A T_3)}{\sigma_A}.$$

By denoting $(\hat{a}_1^A + a_{11}^A T_3) = \mu_0 M_0^A$, the zero stress saturation magnetization at $T =$ 230 K, we reduce the above expression as

$$a_9^A = \mu_0 \frac{M_\sigma^A - M_0^A}{\sigma_A}. \tag{3.39}$$

b. Group II

Considering the martensitic phase, we obtain

$$a_1^M = \mu_0 M^M, \tag{3.40}$$

at $H_x = 0$. Knowing the fact that due to spin flop phenomena (sec 2) the increased saturation magnetization at $H_x = H^C$ is $M_x^M = M^C$ (Fig. 18), we can write from (3.29b)

$$\mu_0 M^C = \mu_0 M^M + 2a_2^M H^C$$

and obtain

$$a_2^M = \mu_0 \frac{M^C - M^M}{2H^C}. \tag{3.41}$$

As per discussion in subsection 3, the values of the constant material properties M^C and M^M are 40 emu/g and 15 emu/g, respectively. Finally, by evaluating (3.28) at $\xi = 1$, we get

$$M^C = M^C + \widetilde{\gamma}_x^t, \Rightarrow \widetilde{\gamma}_x^t = 0, \tag{3.42}$$

which means the magnetization changes due to presence of ferromagnetic austenitic phase in the phase mixture.

2. Mechanical parameters

a. Group III

We identify the elastic modulus of the austenitic and martensitic phase (3.31a, 3.31b) by $E^A = 2(a_4^A + a_5^A)$ and $E^M = 2(a_4^M + a_5^M)$, respectively. The values (E^A=12 GPa, E^M=25 GPa) are obtained from a pseudoelastic test [2]. So,

$$a_4^A + a_5^A = \frac{E^A}{2}, \tag{3.43}$$

$$a_4^M + a_5^M = \frac{E^M}{2}. \tag{3.44}$$

The thermal expansion coefficients can be identified as $\alpha^A = a_{13}^A$ and $\alpha^M = a_{13}^M$. The thermal expansion of both phases are negligible i.e. $\alpha^M = \alpha^A \approx 0$. The coefficient of H_x (3.31a) has already been determined in the magnetization response and equals to a_9^A (3.39).

b. Group IV

The constants a and c of equation (3.33) are calculated by assuming that

$$\lim_{|\sigma^E|\to\infty} E^{cur}(|\sigma^E|) = E_{max}, \quad \lim_{|\sigma^E|\to 0} E^{cur}(|\sigma^E|) = E_{min}.$$

With these two conditions, we determine

$$a = (1 + e^{-m/s})(E_{max} - E_{min}) \tag{3.45}$$

$$c = (1 + e^{-m/s})E_{min} - e^{-m/s}E_{max}. \tag{3.46}$$

From Fig. 25, we consider $E_{min} = 0$, E_{max}=5.5% and the values of m and s are 50

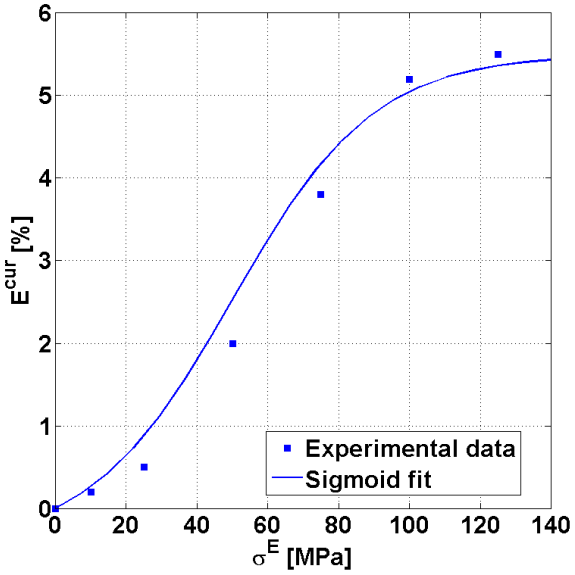

Fig. 25. Maximum strain versus stress response of the martensitic phase transformation. The dots are the experimental values [2] and the continuous line is the fit.

and 20, respectively. Since, at the end of transformation we get maximum inelastic deformation which is equal to the maximum transformation strain, then $b_1 = 1$. In this study we always consider complete phase transformation. Thus for the reverse transformation, $\xi^r = 1$ (equation (3.24)).

3. Thermodynamic parameters

a. Group V

We calibrate $\rho\Delta s_0$ by using Clausius-Clapeyron relation, which can be obtained by applying the consistency condition to (3.35d). Taking the time derivative of (3.35d) we get $\dot{\pi}^t = 0$ and at the critical values, when $\dot{\xi} = 0$, we can write

$$\pi^t{}_{,\sigma^E_{xx}}\, \dot{\sigma}^E_{xx} + \pi^t{}_{,H_x}\, \dot{H}_x + \pi^t{}_{,T}\, \dot{T} = 0. \tag{3.47}$$

Since the stress is kept constant ($\dot{\sigma}^E_{xx}$=0) at the start and end of forward and reverse transformation,

$$\frac{dH_x}{dT} = -\frac{\pi^t,_T}{\pi^t,_{H_x}} = -\frac{\rho\Delta s_0 - a^A_{11}H_x}{\mu_0\Delta M}$$

The presence of the magnetic field variable H_x in the term $a^A_{11}H_x$ adds additional complexity to model calibration. We assume this value is small enough[3] compared to the $\rho\Delta s_0$ such that

$$\frac{dH_x}{dT} \approx -\frac{\rho\Delta s_0}{\mu_0\Delta M}.$$

Moreover, we consider the average $\langle\mu_0\frac{dH_x}{dT}\rangle$ slope (Fig. 26) and assume that it is constant at all stress levels. Thus $\rho\Delta s_0$ is found to be

$$\rho\Delta s_0 = -\langle\mu_0\frac{dH_x}{dT}\rangle\Delta M. \tag{3.48}$$

From the experiments (Fig. 26) conducted in $H-T$ plane, we calculate the average slope $\langle\mu_0\frac{dH_x}{dT}\rangle$=-13.6 T/K. If we calculate the corresponding entropy change, we get $\rho\Delta s_0$=8.725 MPa/K, which is significantly higher than $a^A_{11}H_x$=0.04 MPa/K and thus supports our assumption.

Finally, we need to know the remaining parameters A, B, C, D, Y^t, which we assume to be independent of stress, and $\rho\Delta u_0$. From the Kuhn Tucker condition (3.35e) we get two conditions at the beginning and end of forward transformation:

$$\pi^t(\sigma_A, H^M_s, T_c) - Y^t = 0, \qquad \text{for } \dot{\xi} > 0, \quad \text{at } \xi = 0 \tag{3.49a}$$

$$\pi^t(\sigma_M, H^M_f, T_c) - Y^t = 0, \qquad \text{for } \dot{\xi} > 0, \quad \text{at } \xi = 1. \tag{3.49b}$$

[3]We first calculate the value of this term at an arbitrary large magnetic field, say μ_0H_x=20 T. This value is more than the maximum magnetic field (μ_0H_x=18 T) that can be applied in the experimental test setup. At this condition, a value of $a^A_{11}H_x$=0.04 MPa/K is obtained.

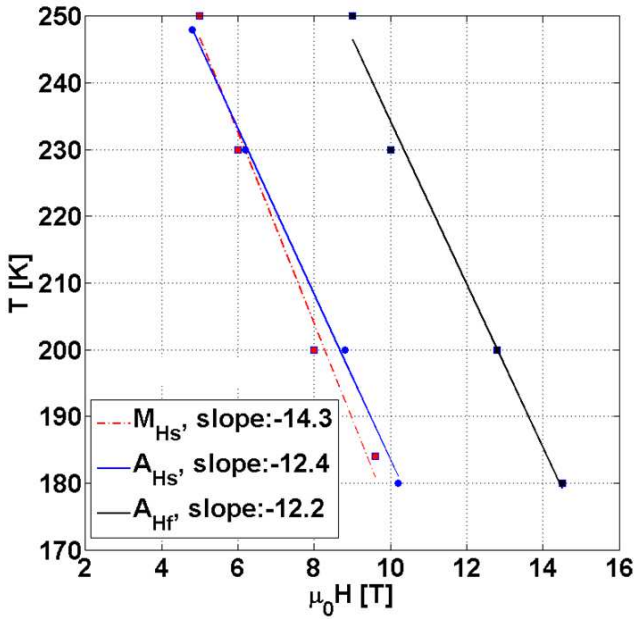

Fig. 26. Experimental results of the temperature vs field dependence. We assume equal slopes at all stress level. M_{Hs} is the locus of the martensitic start temperature at a given magnetic field. Similarly, A_{Hs} and A_{Hf} are the locus of the austenitic start and finish temperature, respectively.

Similarly, for reverse transformation we get two more equations,

$$\pi^t(\sigma_M, H_s^A, T_c) + Y^t = 0, \qquad \text{for } \dot{\xi} < 0, \quad \text{at } \xi = 1 \tag{3.50a}$$

$$\pi^t(\sigma_A, H_f^A, T_c) + Y^t = 0, \qquad \text{for } \dot{\xi} < 0, \quad \text{at } \xi = 0. \tag{3.50b}$$

The thermodynamic driving force π^t (3.34) for the forward transformation becomes,

$$\pi^t = |\sigma_{xx}^E| E^{cur} + \frac{1}{2}\Delta(\frac{1}{E})(\sigma_{xx}^E)^2 + \mu_0 \Delta M H_x + \rho \Delta s_0 T - \rho \Delta u_0 + f^t, \tag{3.51}$$

while for the reverse transformation

$$\pi^t = \sigma_{xx}^E E_{xx}^{t-r} + \frac{1}{2}\Delta(\frac{1}{E})(\sigma_{xx}^E)^2 + \mu_0 \Delta M H_x + \rho \Delta s_0 T - \rho \Delta u_0 + f^t. \tag{3.52}$$

The four critical magnetic fields, H_s^A, H_f^A, H_s^M and H_f^M are obtained from Fig. 27

in the following ways. According to the experimental observation (subsection 3),

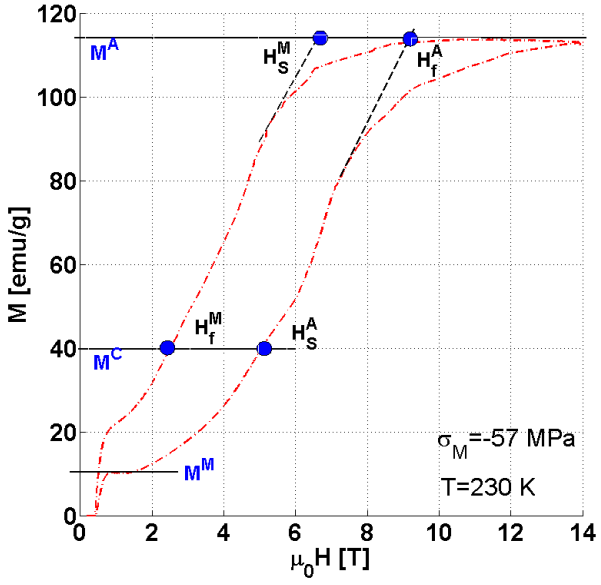

Fig. 27. Experimental results of the magnetization-field response at constant stress σ_M=-57 MPa and at constant temperature $T = 230K$.

the values of M^M=15 emu/g and M^C=40 emu/g are assumed to be constant at any stress and temperature level. We identify H_s^A and H_f^M from the intersection of the horizontal line M^C=40 emu/g, whereas H_f^A and H_s^M are obtained by tangent intersection method. Their values are given in Tab. XXV. Finally, the continuity of the hardening function [92] gives us

$$\int_0^1 f^t\Big|_{\dot{\xi}>0} d\xi = \int_0^1 f^t\Big|_{\dot{\xi}<0} d\xi. \tag{3.53}$$

Solving the five equations (3.49a) to (3.50b) and (3.53), we obtain the five unknowns, $A, \widetilde{B}, C, \widetilde{D}$ and Y^t. Detailed derivations are given in Appendix E1. It should be noted that we introduce a new constant $\widetilde{B} = B + \rho\Delta u_0$ and $\widetilde{D} = D + \rho\Delta u_0$ such that B and D absorb the term $\rho\Delta u_0$. All material properties are summarized in Tab. XXV. Moreover, we consider a cubic dependence of stress on the hardening

Experimental material parameters
(A)-Magnetic
(I): $\{\sigma_1,\, M_1,\, M_2,\, T_1, T_2\}$, $\{\sigma_2,\, M_3,\, T_3\}$
(II): $M^M,\, M^C,\, H^C$
(B)-Mechanical
(III): $E^A,\, \alpha^A,\, E^M,\, \alpha^M$
(IV): E_{max}, E_{min}
(C)-Thermodynamic
(V): $\frac{dH}{dT},\, H_s^A,\, H_f^A,\, H_s^M,\, H_f^M$

Table XXIV. Required material parameters.

parameters A and B [4] i.e, $A(\sigma_{xx}^E) = A_1 + A_2\sigma_{xx}^{E^3}$ and $\widetilde{B}(\sigma_{xx}^E) = \widetilde{B}_1 + B_2\sigma_{xx}^{E^3}$. We consider the constant hardening parameters C and D for the reverse transformation. The stress dependence assumption on A and $\widetilde{B}$ are based on experimental observations. We calibrate the constants $A_1, A_2,\ \widetilde{B}_1$ and B_2 in the following ways. We already know the values of $A(\sigma_{xx}^E = -57)$ and $\widetilde{B}(\sigma_{xx}^E = -57)$. Moreover, we select an additional experiment, the magnetization response at 0 MPa and 230 K, to calibrate the stress dependence components of A_1, A_2 and $\widetilde{B}_1, B_2$. We consider $\mu_0 H_s^M$=3 T and $\mu_0 H_f^M$=0.5 T from the experiment and use (E.1) and (E.2) to find the values of $\widetilde{B}(\sigma_{xx}^E = 0)$ and $A(\sigma_{xx}^E = 0)$. So we write $A_1 = A(\sigma_{xx}^E = 0)$, $A_2 = \frac{A(\sigma_{xx}^E=-57) - A(\sigma_{xx}^E=0)}{(\sigma_{xx}^E=-57)^3}$ and $\widetilde{B}_1 = \widetilde{B}(\sigma_{xx}^E = 0)$, $B_2 = \frac{B(\sigma_{xx}^E=-57) - \widetilde{B}(\sigma_{xx}^E=0)}{(\sigma_{xx}^E=-57)^3}$.

[4] Recall that in (3.27) we assumed $A(I_2, I_3)$, $B(I_2, I_3)$...etc. Here we are considering $A(I_2) = A_1 + A_2 I_2^3$ and $B(I_2) = B_1 + B_2 I_2^3$.

F. Model simulations and predictions

We first discuss model simulations and then model predictions are compared with experiments in (a), (b) and (c) for magnetization-field, strain-field and magnetization-temperature data, respectively. In subsection 3 we perform parametric studies with different magneto-thermo-mechanical loading conditions. Finally the model predictions of magneto-thermo-mechanical phase surfaces are presented.

1. Model simulations

The summary of the material constitutive equations are given in Tab. XXXIII. One needs to know the evolution of ξ to generate analytic solutions of the constitutive responses. The evolution of ξ is obtained from the Khun Tucker condition (3.35e) and the detailed derivations are given in Appendix 4. The expressions of ξ for the forward and reverse transformation are given as

Forward transformation ($\dot{\xi} > 0$):

$$\xi = \frac{1}{2} + \frac{1}{2}\cos(f_1|\sigma^E_{xx}|E^{cur} + f_2(\sigma^E_{xx})^2 + f_3 H_x + f_4 T + f_5) \tag{3.54}$$

Reverse transformation ($\dot{\xi} < 0$):

$$\xi = \frac{1}{2} + \frac{1}{2}\cos(r_1\sigma^E_{xx}E^{t-r} + r_2(\sigma^E_{xx})^2 + r_3 H_x + r_4 T + r_5). \tag{3.55}$$

Here f_i and r_i are constants and the values are given in the Appendix 4.

The reader should recall that the magnitude of the traction varies about 10 MPa during phase transformation due to the deflection of the springs. We discretize this difference, denoted by δS, by the number of n incremental steps. We assume that the stress remains constant at each increment. We write at increment $(n+1)$,

$\sigma_{xx}^{E^{n+1}} = \sigma_{xx}^{E^n} + \frac{\delta S}{n}$, $E^{cur^{n+1}} = E^{cur}(\sigma_{xx}^{E^{n+1}})$ and $\epsilon_{xx}^{t^{n+1}} = \Lambda_{xx}^{t}(\sigma_{xx}^{E^{n+1}})\xi^{n+1}$. The initial condition of the problem is $\sigma_{xx}^{E^0} = \sigma_A$ or $\sigma_{xx}^{E^0} = \sigma_M$, depending on the forward and the reverse transformation.

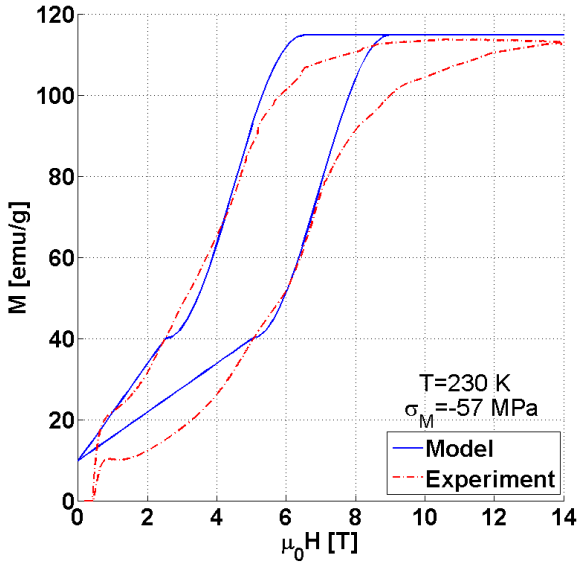

Fig. 28. Model simulation of magnetization response at 230 K and σ_M=-57 MPa.

We simulate the magnetization response at the calibration stress σ_M=-57 MPa and temperature 230 K. The result is shown in Fig. 28. The solid line is the modeled result and the dotted line is the experimental data. Moreover, the difference between the applied field and internal field is small due to *demagnetization effect* for this particular magnetic loading direction. An estimation of this error is presented in Appendix F1 by assuming uniformly distributed magnetic field inside the specimen. So we present all the model predictions by considering internal magnetic field is nearly equal to applied magnetic field.

A kink is observed at the end of forward transformation (around 2.5 T in the figure). This appears due to the trigonometric hardening function. The transition can be made smooth by improving the trigonometric hardening function or by introducing

different hardening functions. Further details about the smooth transitioning in the modeling of conventional shape memory alloys can be found in [155].

2. Model predictions

a. Magnetization-field prediction

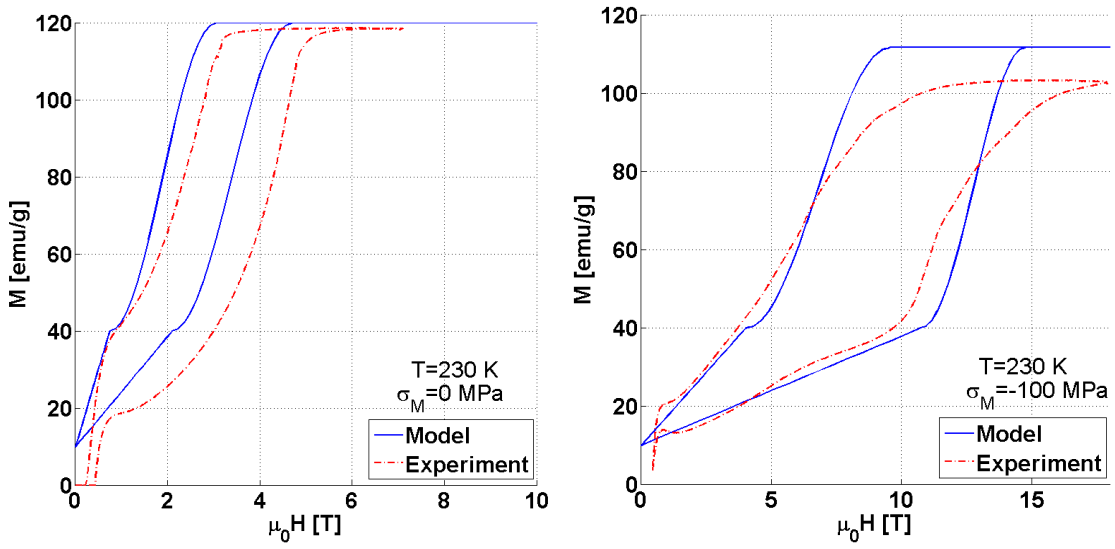

(a) (b)

Fig. 29. Model predictions of magnetization responses (a) at 230 K and σ_M=-57 MPa and (b) at 230K and σ_M=-100 MPa.

The model prediction of the magnetization response at 0 MPa and 230 K is given in Fig. 29(a). The predicted saturation magnetization at 0 MPa is close to the experiment. The prediction of magnetization at σ_M=-100 MPa is presented in Fig. 29(b). In this prediction, the variation of magnetization (linear part) in the martensitic phase are captured well, whereas the model over predicts the saturation magnetization of the austenitic phase a small amount.

b. Strain-field prediction

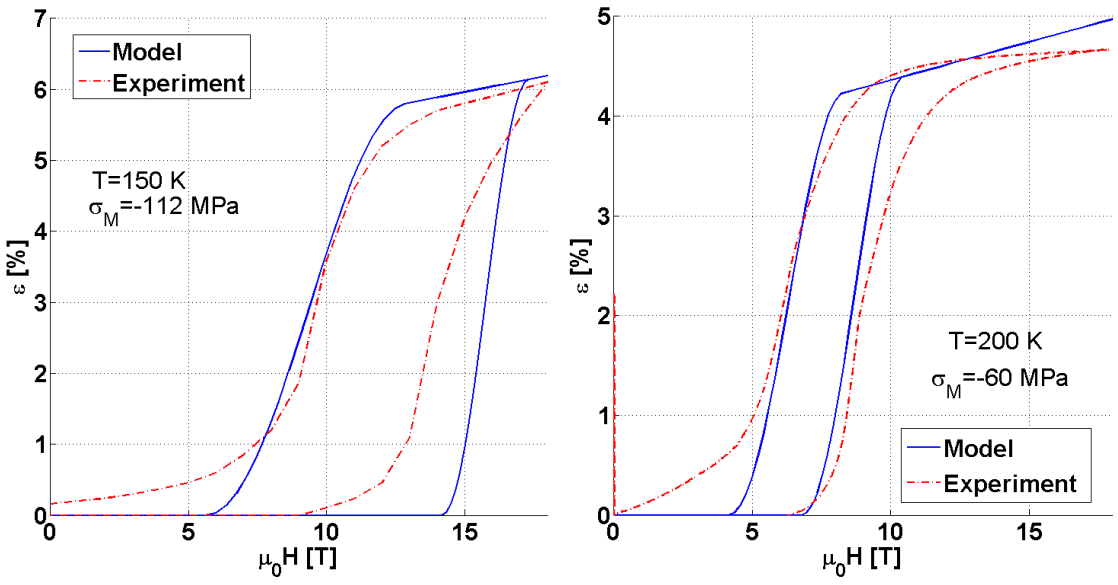

(a) (b)

Fig. 30. (a) Field induced strain prediction at (a) T=150 K at σ_M=-112 MPa and (b) T=200 K at σ_M=-60 MPa.

We predict the strain responses at temperature T=150 K with σ_M=-112 MPa and at T=200 K with σ_M=-60 MPa in Fig. 30. The maximum transformation strain for FIPT at -112 MPa is about 6%, where under same mechanical traction the maximum strain is about 5% (Fig. 25), when the specimen is used as SMA (i.e. a thermomechanical material). Similarly, for a stress level of -60 MPa, the maximum transformation strain for FIPT is nearly 4.5% (Fig. 30b) while for conventional shape memory effect it is around 3% (Fig. 25). It is observed experimentally that the strain in the austenitic phase increases with the increase in magnetic field. The model prediction is able to capture this linear trend. This is due the coupling of stress with the saturation magnetization of the austenitic phase. The term $a_9^A H_x$ in (3.31a) contributes significantly to the overall strain response. For example, taking an arbitrary

value of $\mu_0 H_x$=10 T, we get $a_9^A H_x$=0.6%.

c. Magnetization-temperature prediction

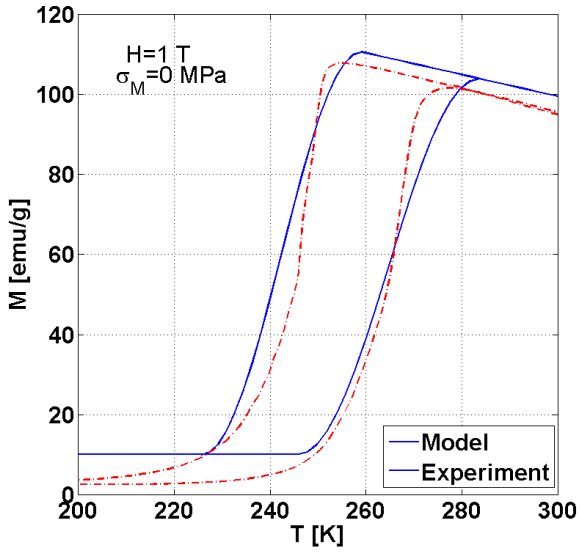

Fig. 31. Predictions of magnetization responses at constant field ($\mu_0 H$=1 T) and constant stress (0 MPa).

We also predict the magneto-thermal response at 0 MPa and under a constant magnetic field H_c=1 T (Fig. 31a). The four critical temperatures are calculated by using the following equations.

$$\pi^t(H_c, T_s^M) - Y^t = 0, \qquad \text{for } \dot{\xi} > 0, \quad \text{at } \xi = 0$$
$$\pi^t(H_c, T_f^M) - Y^t = 0, \qquad \text{for } \dot{\xi} > 0, \quad \text{at } \xi = 1$$

and

$$\pi^t(H_c, T_s^A) + Y^t = 0, \qquad \text{for } \dot{\xi} < 0, \quad \text{at } \xi = 1$$
$$\pi^t(H_c, T_f^A) + Y^t = 0, \qquad \text{for } \dot{\xi} < 0, \quad \text{at } \xi = 0$$

The predicted temperatures are given in Table. XXVII. We assume that at a com-

parative small field of 1 T, the magnetization of martensitic phase does not increase beyond M^M due to spin flop phenomena i.e we consider $M^C = M^M$.

3. Results for various magneto-thermo-mechanical loading paths

a. Magneto-mechanical model predictions

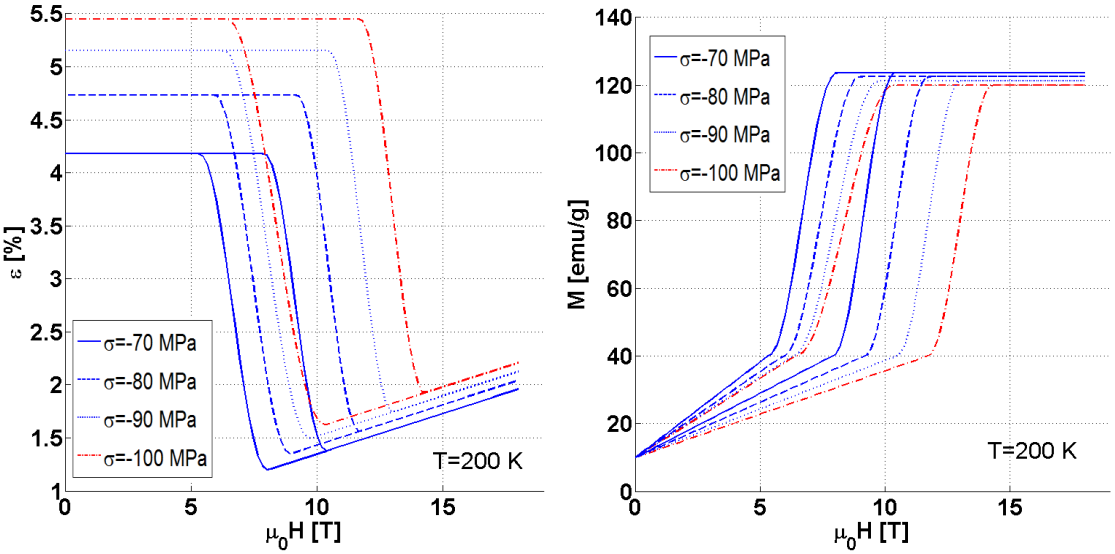

(a) (b)

Fig. 32. (a) Model predictions of strain-field responses and (b) magnetization-field responses at different stress levels and at constant temperature T=200 K.

Finally we present a few model predictions of magneto-mechanical behaviors of these material system. The strain-field responses at different stress levels at a constant temperature are presented in Fig. 32a. We select a constant temperature T=200 K and vary the stress level from -70 MPa to -100 MPa. In this demonstration, we consider austenite as the reference state and the vertical axis represents the compressive strain due to martensitic phase transformation. In the austenitic phase, the strain linearly decreases with the magnetic field due to the magneto-mechanical coupling.

The magnetization response is presented in Fig. 32(b). The saturation magnetization decreases with the increase in stress level due to the magneto-mechanical coupling in the austenitic phase. The strain-field and magnetization-field responses

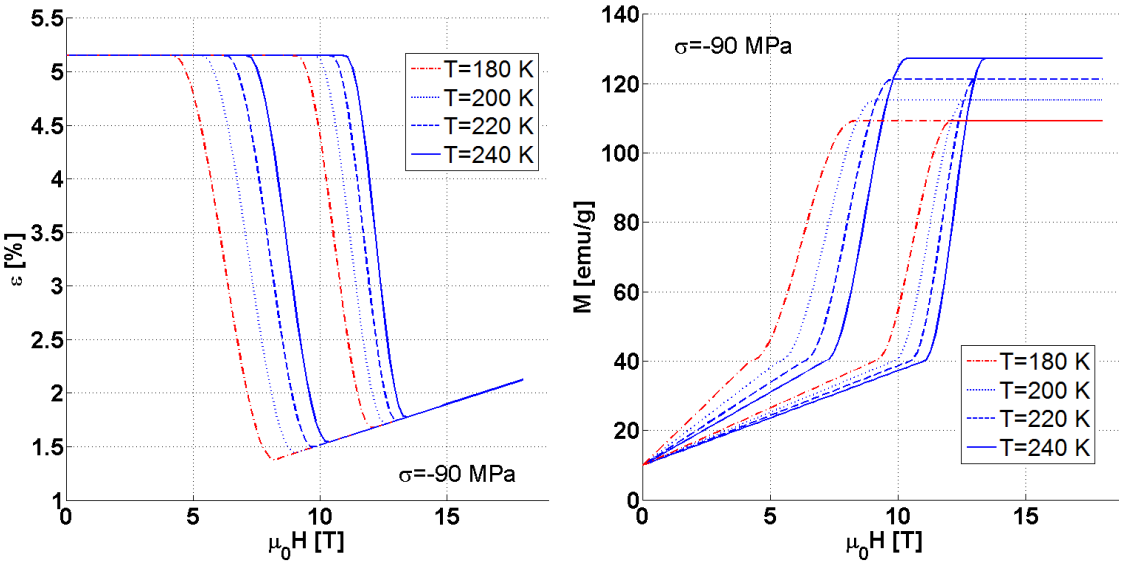

(a) (b)

Fig. 33. (a) Model predictions of strain-field responses and (b) magnetization-field responses at different temperatures and at constant stress σ=-90 MPa.

at different temperature and constant stress are presented in Fig. 33. In this case, the traction is kept constant at -90 MPa and the temperature is varied from 180 K to 240 K with a 20 K interval. The influence of temperature on saturation magnetization is clearly observed in Fig. 33(b).

b. Magneto-thermo-mechanical model predictions

We demonstrate the model's capability to capture magneto-thermo-mechanical coupling by selecting a magneto-thermal loading path as shown in Fig. 34. In this figure the low temperature, low field condition denotes the martenstic phase and the

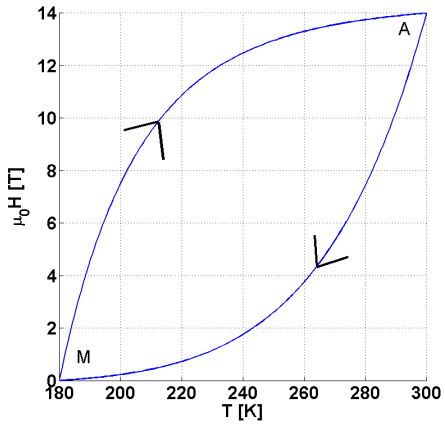

Fig. 34. Magneto-thermal loading path at constant stress σ=-80 MPa.

high temperature, high field denotes the austenitic phase. For forward transformation (M→A), we increase the temperature gradually from 180 K to 300 K and the magnetic field changes as indicated on the path with the forward arrow. Similarly, for reverse transformation (A→M), we follow the alternative path. We consider the following equations for the magneto-thermal loading path

$$\mu_0 H = \begin{cases} m_1 T^{n_1} + c_1 \,, & M \to A \\ \\ m_2 T^{n_2} + c_2 \,, & A \to M \end{cases} \tag{3.56}$$

We considered n_1=9 for the forward loading and n_2=-7 for the reverse loading condition. The constants m_1, c_1 and m_2, c_2 are obtained from the two end point conditions of the Fig. 34. We predict the strain-field-temperature response and magnetization-field-temperature responses of this material in Fig. 35.

4. Magneto-thermo-mechanical transformation surfaces

The stress-field phase diagram at 230 K is presented in Fig. 36(a). The projections of four transformation surfaces on the stress-field plane at 230 K are presented by the four curves. These curves are plotted by using (3.35d). Similarly, the stress-

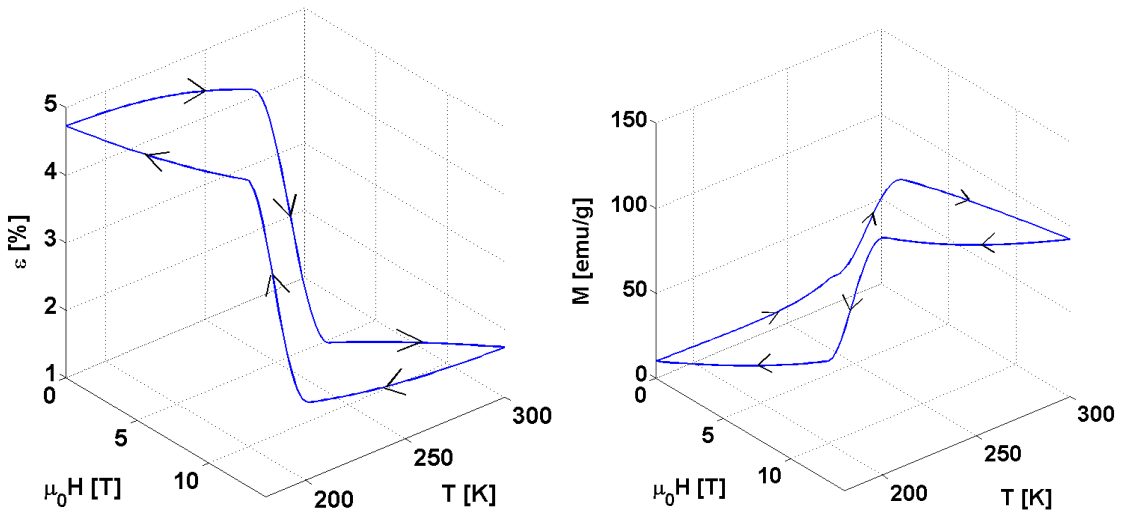

(a) (b)

Fig. 35. (a) Model predictions of strain-field-temperature response and (b) magnetization-field-temperature response at constant stress σ=-80 MPa.

temperature phase diagram at 0 T is given in Fig. 36(b). As we assume that the forward transformation depends on the higher order stress, the locus of H_f^M, H_s^M and T_f^M, T_s^M behaves different than the locus of H_f^A, H_s^A and T_f^A, T_s^A. Moreover, the difference between H_f^M, H_s^M (or T_f^M, T_s^M) at a constant stress level increases rapidly with the increase in stress. This kind of response is sometimes observed in thermo-mechanical SMAs where increasing stress expands the temperature difference between martensitic start and martensitic finish temperatures [156]. The model predictions of 3-D (magneto-thermo-mechanical) austenitic and the martensitic finish surfaces are given in Fig. 37.

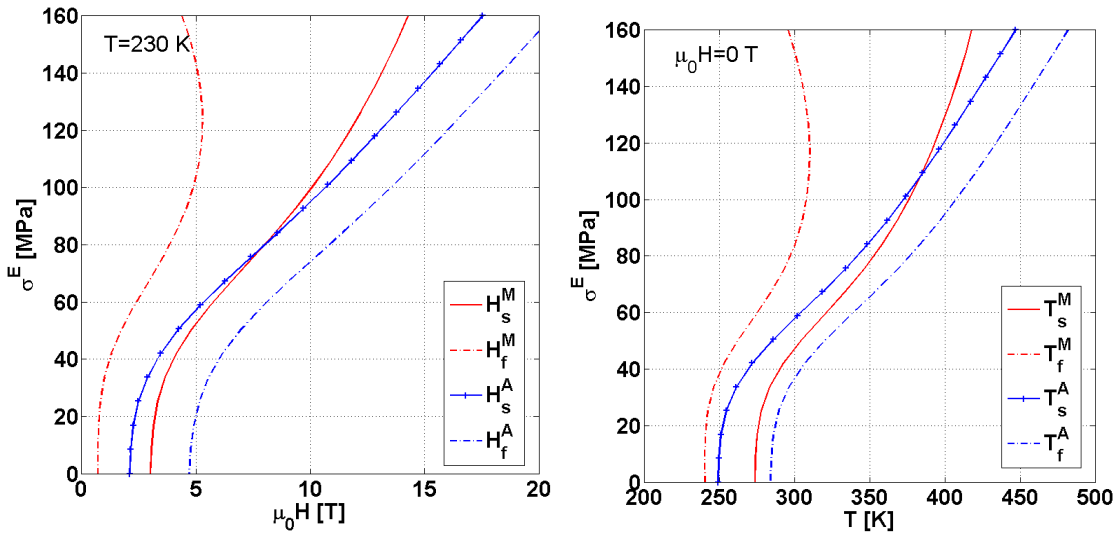

(a) (b)

Fig. 36. (a) Model prediction of stress-field phase diagram at 230 K and (b) model prediction of stress-temperature phase diagram at $\mu_0 H$=0 T.

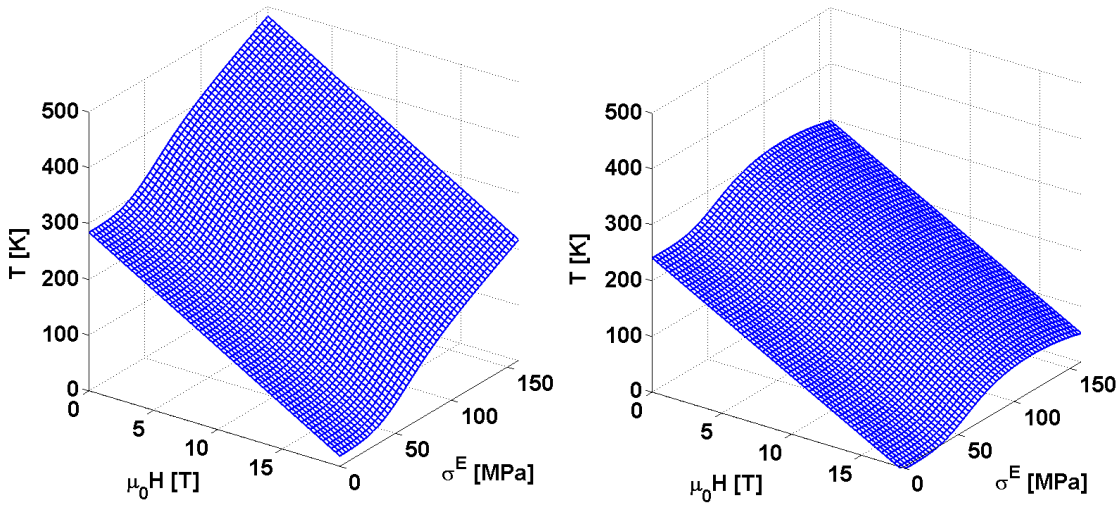

(a) (b)

Fig. 37. 3D phase diagram: (a) austenitic finish surface and (b) martensitic finish surface.

1. Saturation magnetization of the austenitic phase (Fig. 24)

M_1=102ρ A/m, M_2=90ρ A/m, T_1=300 K, T_2=340 K, at $\sigma_1 = \sigma_A$=0 MPa

$M_3 = M_\sigma^A$=115ρ A/m at $\sigma_2 = \sigma_A$=-67 MPa, T_3=230 K and M_0^A=120ρ A/m

(ρ=8020 kg/m^3)

2. Saturation magnetization of the martensitic phase (Fig. 27)

M^M=15ρ A/m, M^C= 40ρ A/m at

$H^C = H_f^M$ for forward transformation

$H^C = H_s^A$ for reverse transformation

and $\widetilde{\gamma}_x^t = 0$

3. Pseudoelastic response and thermal expansion coefficients

$E^A = 12\,\text{GPa},\ E^M = 25\,\text{GPa},\ \alpha^M = \alpha^A \approx 0$

4. Maximum transformation strain (Fig. 25)

$E_{min} = 0,\ E_{max} = 5.5,\ m = 50,\ s = 20,\ b_1$=1, ξ^r=1

5. Magnetic field-temperature slope (Fig. 26)

$\mu_0 \frac{dH_x}{dT}$=-13.6 T/K

6. Critical magnetic fields (Fig. 27)

$\mu_0 H_s^M = 6.5$ T, $\mu_0 H_f^M = 2.5$ T, $\mu_0 H_s^A = 5.0$ T, $\mu_0 H_f^A = 9.0$ T

at $T = 230K$ and $\sigma_M = -57$ MPa

Table XXV. Measured material properties from different magneto-thermo-mechanical experiments.

Magnetization response:

$$M_x = M_x^A + \xi(M_x^M - M_x^A).$$

$$\mu_0 M_x^A = \hat{a}_1^A + a_9^A \sigma_{xx}^E + a_{11}^A T$$

$$\mu_0 M_x^M = a_1^M + a_2^M H_x, \qquad \text{for } \xi = 1 \text{ and } H_x \leq H^C$$

$$= \mu_0 M^C, \qquad \text{for } \xi \in (0,1)$$

Strain response:

$$\varepsilon_{xx} = \varepsilon_{xx}^A + \xi(\varepsilon_{xx}^M - \varepsilon_{xx}^A) + \varepsilon_{xx}^I$$

$$\varepsilon_{xx}^A = \tfrac{1}{E^A}\sigma_{xx}^E + a_9^A H_x, \ \varepsilon_{xx}^M = \tfrac{1}{E^M}\sigma_{xx}^E$$

$$\varepsilon_{xx}^I = \Lambda_{xx}^t \xi = E^{cur}(|\sigma^E|)\xi$$

$$E^{cur}(|\sigma^E|) = \tfrac{a}{1+e^{-(|\sigma^E|-m)/s}} + c$$

Model parameters:

$$\hat{a}_1^A = \mu_0 \tfrac{M_1 T_2 - M_2 T_1}{T_2 - T_1}, \qquad a_9^A = \mu_0 \tfrac{M_\sigma^A - M_0^A}{\sigma_A}, \qquad a_{11}^A = \mu_0 \tfrac{M_1 - M_2}{T_1 - T_2}.$$

$$a_1^M = \mu_0 M^M, \qquad a_2^M = \mu_0 \tfrac{M^C - M^M}{H_c}$$

$$a = (1 + e^{m/s})(E_{max} - E_{min}), \quad c = (1 - e^{m/s})E_{min} - e^{m/s}E_{max}$$

Table XXVI. Summary of the 1-D constitutive equations.

	T_s^A	T_f^A	T_s^M	T_f^M
Experimental data	250	280	260	220
Model predictions	246	284	259	225

Table XXVII. Critical temperatures [K] at 0 MPa and 1 T

CHAPTER IV

FIELD INDUCED VARIANT REORIENTATION

If an external field is applied, it is energetically favorable for the magnetization vectors to align with the applied field. In MSMAs three competing mechanisms are available to achieve this alignment. The first two, the *magnetic domain wall motion* and the *magnetization vector rotation* are common to all ferromagnetic materials and shall be discussed shortly. The third mechanism, which is unique for magnetic shape memory alloys, is the magnetic field-driven *reorientation of martensitic variants*. This is possible since the preferred axes of the tetragonal variants are mutually perpendicular, such that an external magnetic field can be used to favor certain variants over others. The induced redistribution of variants leads to the observed macroscopic shape change.

A. Experiments on MSMAs for variant reorientation

An experimental setup designed to measure magnetic field-induced strains in MSMAs following the basic principle qualitatively described in the preceding paragraphs is shown in Fig. 38 [1, 66]. The setup consists of a 2T electromagnet, which is adjustably mounted on a mechanical load frame such that the directions of applied force and magnetic field are perpendicular. The specimen is held in place by non-magnetic grips. A polymer chamber, which encloses the grips and specimen, is filled with nitrogen gas for cooling. As depicted in Fig. 38(b), temperature, deformation, and magnetic field measurements are taken by a thermocouple, a capacitive displacement sensor and a Hall probe. Similar experiments have been reported by Tickle [63, 151], Heczko [47], Shield [30] and others.

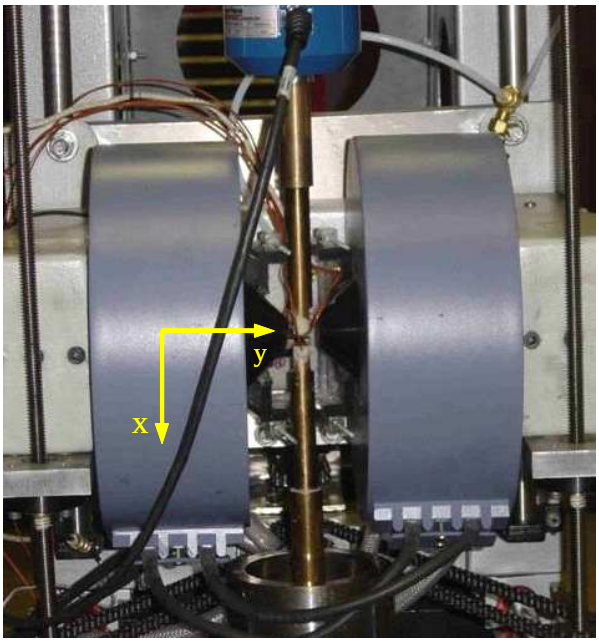

(a) Detail of the test setup showing the electromagnets, the grips and the load cell on the MTS frame, with the polymer chamber removed.

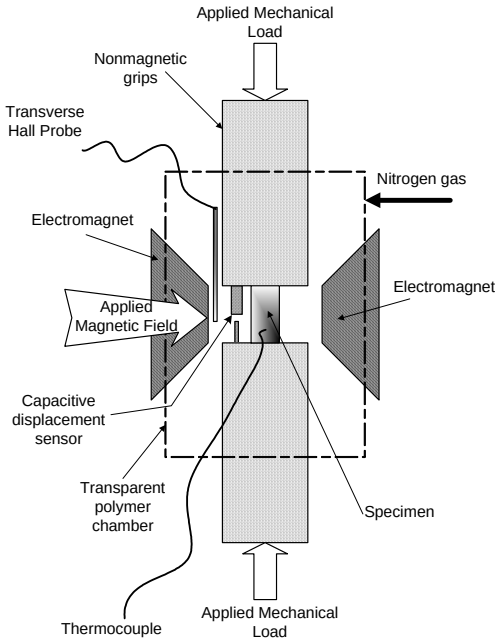

(b) Schematic showing the components of test setup as well as the applicable mechanical and magnetic load directions.

Fig. 38. Magneto-thermo-mechanical setup used for MFIS measurements [1, 66]

Magnetic field-induced strain data obtained from measurements on this test frame are plotted in Fig. 39 for second magnetic field cycles. The figure shows the magnetic field-induced strain as a function of the magnetic field, not the total strain, such that all curves start at the origin. The observed response is nonlinear and hysteretic, which indicates that there is considerable dissipation associated with the variant reorientation. The achievable field-induced reorientation strain and the shape of the hysteresis loops show the strong stress level dependence.

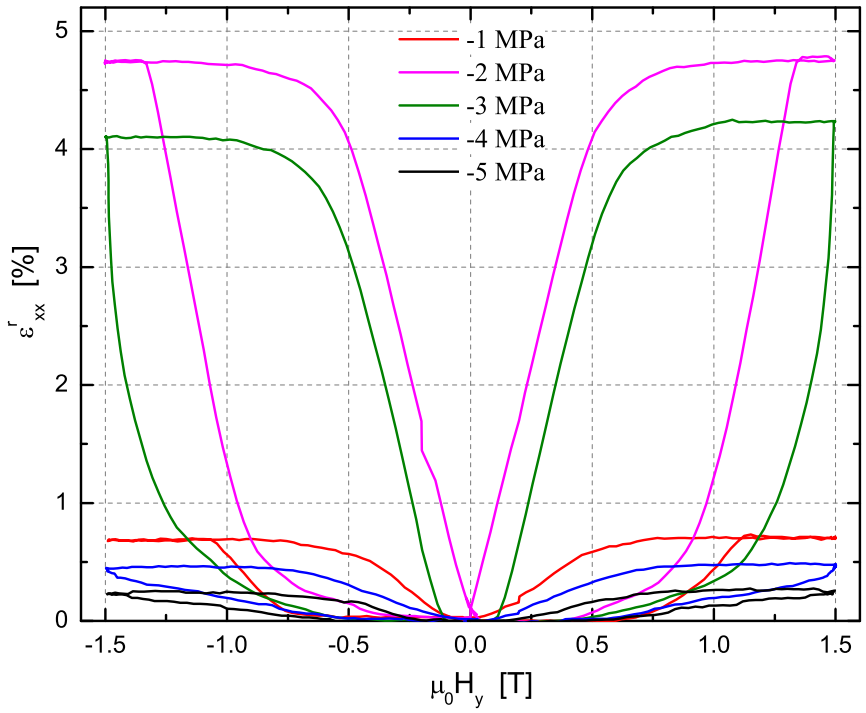

Fig. 39. Evolution of the MFIS in a Ni_2MnGa single crystal at different stress levels during the second magnetic cycle. Data taken from [1].

B. Microstructure based MSMA modeling

For a MSMA, the magnetization vector is identified through an appropriate phenomenological model [1, 3]. The model is based on the Gibbs free energy function G, in which the Cauchy stress tensor $\boldsymbol{\sigma}$ and the magnetic field strength $\boldsymbol{H}$ are the independent state variables. The loading history dependence of the constitutive behavior, caused by dissipation associated with variant rearrangement, is introduced through the evolution of internal state variables. The chosen internal state variables are the variant volume fraction ξ, the magnetic domain volume fraction α and the magnetization rotation angles $\theta_i (i{=}1{,}4)$. Such configurations have been observed experimentally in Ni-Mn-Ga [157–160]. Corresponding micrographs are shown in Fig. 40(b). An ide-

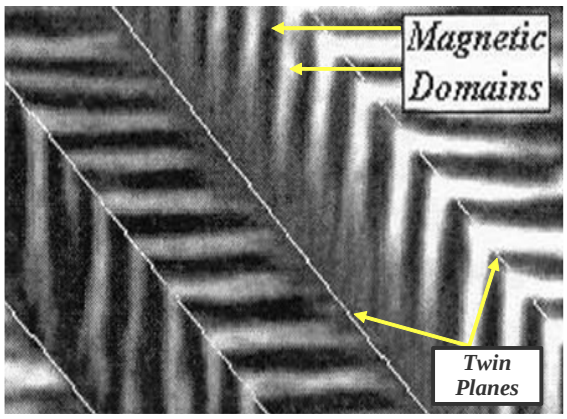

(a) Magneto-optical images using the magnetic garnet film technique as observed by Likhachev et al. [157].

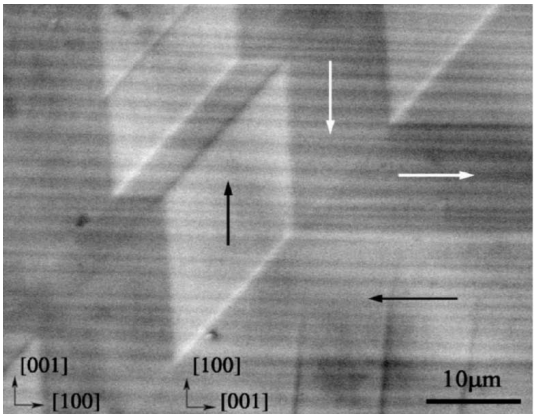

(b) Scanning electron microscopy (SEM) images taken by Ge et al. [158].

alized microstructural representation of the twinned martensitic phase is given in Figure 40. Two martensitic variants, variant-1 with volume fraction, ξ, and variant-2 with volume fraction, $1-\xi$, form 90^o magnetic domain walls and each variant contains 180^o domain walls. The volume fractions of 180^o magnetic domain wall in variant-1 and variant-2 are represented in Figure 40 by domain-1 and domain-2 and denoted by α and $1-\alpha$ respectively.

The specific form of the Gibbs free energy is given by [3]

$$\begin{aligned} G(\boldsymbol{\sigma}, \boldsymbol{H}, T, \boldsymbol{\varepsilon}^r, \xi, \alpha, \theta_i) = \; & -\frac{1}{2\rho}\boldsymbol{\sigma} : \mathcal{S}\boldsymbol{\sigma} - \frac{1}{\rho}\boldsymbol{\sigma} : \boldsymbol{\varepsilon}^r - \frac{\mu_0}{\rho}\boldsymbol{M}\cdot\boldsymbol{H} + \frac{1}{\rho}f(\xi,\alpha) \\ & + \{\xi(1-\alpha)G_2^{an}(\theta_2) + (1-\xi)(1-\alpha)G_1^{an}(\theta_1) \\ & + \xi\alpha G_4^{an}(\theta_4) + (1-\xi)\alpha G_3^{an}(\theta_3)\} + G_0(T), \end{aligned} \tag{4.1}$$

where ρ, $\mathcal{S}$, $\boldsymbol{\varepsilon}^r$, f, G_k^{an} and G_0 are the density, the effective compliance tensor, the reorientation strain tensor, a hardening function, the magnetocrystalline anisotropy energy of the k^{th} domain and a reference state energy respectively. The free energy

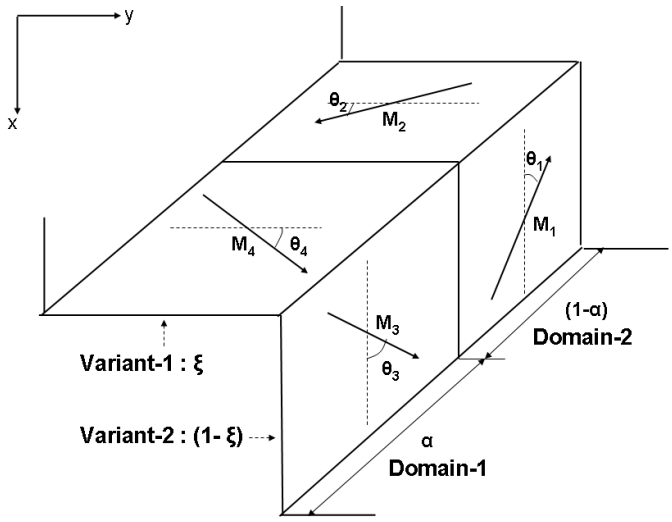

Fig. 40. Schematic representation of the microstructure showing the coexistence of martensitic variants and magnetic domains [3].

function (4.1) is comprised of the elastic strain energy, the Zeeman energy, a mixing term, the magnetocrystalline anisotropy energy, and a reference state energy. The Zeeman or external field energy aims to align the internal magnetization with the externally applied magnetic field. The magnetocrystalline anisotropy energy can be viewed as the energy stored in the material due to the work done by an applied field in rotating the magnetization away from the magnetic easy axes.

The internal variables ξ, α and θ_i can in general be connected with energy dissipation. Experimental results [63] show that the hysteresis for the single variant MSMA crystal specimen with respect to the magnetic easy axis and hard axis are almost negligible. This observation was expected for the case of the hard axis magnetization response, since the dominant mechanism, related with the magnetization rotation θ_i, is a reversible process. With regard to the easy axis magnetization, magnetic domain wall motion is the most important mechanism that can be associated with dissipation. Permanent magnets, for example, exhibit large hysteresis effects

due to micro-scale pinning sites and other phenomena [19, 20]. In MSMA, however, the magnetic domain wall motion appears to be associated with a very small amount of dissipation.

The dissipation in MSMAs is mainly due to variant reorientation mechanism which is caused due to the change in ξ, allowing to neglect the α dependency of the hardening function f. From the free energy expression (4.1) the constitutive equations are derived in a thermodynamically consistent manner, such that the magnetization constitutive equation becomes

$$\boldsymbol{M} = -\frac{\rho}{\mu_0}\frac{\partial G}{\partial \boldsymbol{H}}. \tag{4.2}$$

By using the Gibbs energy function (4.1) and the 1^{st} law of thermodynamics, Coleman-Noll entropy principle obeys the following inequality

$$\boldsymbol{\pi}^r : \dot{\boldsymbol{\varepsilon}}^r + \pi_\xi \dot{\xi} + \pi_\alpha \dot{\alpha} + \sum_i^4 \pi_{\theta_i} \dot{\theta}_i \geq 0 \tag{4.3}$$

where $\boldsymbol{\pi}^r = -\rho\frac{\partial G}{\partial \boldsymbol{\varepsilon}^r}$, $\pi_\xi = -\rho\frac{\partial G}{\partial \xi}$, $\pi_\alpha = -\rho\frac{\partial G}{\partial \alpha}$, $\pi_{\theta_i} = -\rho\frac{\partial G}{\partial \theta_i}$ are the thermodynamic driving forces. As the rotation of magnetization vector and magnetic domain wall motion do not have any dissipation effect [63], we have $\pi_{\theta_i} = 0$, $\pi_\alpha = 0$.

1. Explicit Form of Magnetization Constitutive Equations

In this section we present a special reduced form of magnetization constitutive equations in 2-D, consistent with the experiment, to capture some main features of the MSMAs. In a typical experiment, a martensitic MSMA sample is subjected to a constant mechanical load along the long axis, which is the x-axis, and subsequently to a perpendicular magnetic field in the y-axis. The stress is assumed to be uniaxial and uniform inside the specimen. The effects of magnetic body force and magnetic body

couple are neglected in the present work and the fully-coupled magnetomechanical problem, where stress is allowed to vary pointwise, will be studied in a subsequent paper. The x-component of the applied magnetic field is zero. However, the magnetic field along the x direction due to the magnetization of the body is assumed to be small and the dependence $\boldsymbol{M}(H_x)$ is neglected. So the magnetization components are assumed to have the form of $M_x = M_x(H_y)$ and $M_y = M_y(H_y)$. Under these conditions, the general 3-D magnetostatic problem can be reduced to a simpler 2-D problem by considering the components of the field variables in the following form

$$\boldsymbol{H} = \{H_x, H_y, 0\}, \boldsymbol{M} = \{M_x, M_y, 0\}, \boldsymbol{B} = \{B_x, B_y, 0\}. \tag{4.4}$$

We also assume that the only non-zero stress component is σ_{xx}, which is uniform and constant inside the specimen during the experiment.

In the martensitic phase (Figure 40), $\boldsymbol{M}_1$,$\boldsymbol{M}_2$, $\boldsymbol{M}_3$,$\boldsymbol{M}_4$ represent the magnetization vectors of variant-2 in domain-2, variant-1 in domain-2, variant-2 in domain-1 and variant-1 in domain-1 respectively. θ_i represents the corresponding rotation of the magnetization vector $\boldsymbol{M}_i$ from the magnetic easy axis (dotted line). If $\boldsymbol{M}$ is the total magnetization vector contributed from each variant and domain volume fraction, then

$$\boldsymbol{M} = (1-\xi)\{(1-\alpha)\boldsymbol{M}_1 + \alpha\boldsymbol{M}_3\} + \xi\{(1-\alpha)\boldsymbol{M}_2 + \alpha\boldsymbol{M}_4\}, \tag{4.5}$$

where

$$\boldsymbol{M}_1 = M^{sat}(-\cos\theta_1\boldsymbol{e}_x + \sin\theta_1\boldsymbol{e}_y), \boldsymbol{M}_2 = M^{sat}(\sin\theta_2\boldsymbol{e}_x - \cos\theta_2\boldsymbol{e}_y), \tag{4.6}$$

$$\boldsymbol{M}_3 = M^{sat}(\cos\theta_3\boldsymbol{e}_x + \sin\theta_3\boldsymbol{e}_y), \boldsymbol{M}_4 = M^{sat}(\sin\theta_4\boldsymbol{e}_x + \cos\theta_4\boldsymbol{e}_y), \tag{4.7}$$

and M^{sat} represents the saturation magnetization. The rotation angles are directly re-

lated with the the anisotropy energy. An explicit form of magnetocrystalline anisotropy energy for uniaxial symmetry is usually given by [161],

$$G_i^{an} = K_1 \sin^2 \theta_i. \tag{4.8}$$

where K_1 is the coefficient to be determined from magnetization measurement and θ is the rotation angle between the magnetization and the easy axis.

We will now present the expressions of magnetization vector before reorientation, during reorientation and after reorientation.

1. **Before Reorientation**

   Before reorientation starts we only have stress-favored variant in the initial configuration. Since the MSMA specimen does not have any remnant magnetization before applying the magnetic field, only 180^o domain walls exist. When the magnetic field is applied along the y-direction, the hard axis of the stress-favored variant, the magnetization vectors start rotating in each domain. The domain walls do not move since there is no magnetic field acting along the easy axis of the stress-favored variant. The x component of the magnetization vector in the adjacent domain alters the direction and cancels out when added and gives zero resultant magnetization. On the other hand, the y components of the magnetization vectors are added up and give a resultant magnetization.

   In this region, we have $\xi = 0$ and $\alpha = \frac{1}{2}$. Moreover, from $\pi_{\theta_1} = \pi_{\theta_3} = 0$ we get $\sin\theta_1 = \sin\theta_3 = \frac{\mu_0 M^{sat}}{2\rho K_1} H_y$.

   Equation (4.5) gives the magnetization vector,

$$\boldsymbol{M} = \frac{1}{2}(\boldsymbol{M}_1 + \boldsymbol{M}_3) = M^{sat} \sin\theta_1 \boldsymbol{e}_y \quad \text{or } \boldsymbol{M} = \frac{\mu_0 (M^{sat})^2}{2\rho K_1} H_y \boldsymbol{e}_y. \tag{4.9}$$

The above result shows that we only have y component of the magnetization vector in the macroscopic scale.

2. **During Reorientation**

Once the critical field for the variant reorientation has been reached, the field-favored variant nucleates and a sharp change in the slope of magnetization curve occurs. In this configuration the magnetic domain wall motion is initiated due to the formation of 90^0 domain and it is assumed that the unfavorable magnetic domains in the field-favored variant are eliminated simultaneously with the activation of the reorientation process due to comparative high magnetic field [14, 151].

Here, $\alpha = 1$ and equations $\pi_{\theta_3} = \pi_{\theta_4} = 0$ lead to $\sin\theta_3 = \frac{\mu_0 M^{sat}}{2\rho K_1} H_y$ and $\theta_4 = 0$. Considering the above results, the expression for the macroscopic magnetization vector $\boldsymbol{M}$ (Equation (4.5)) is given below.

$$\begin{gathered}\boldsymbol{M} = (1-\xi)\boldsymbol{M}_3 + \xi\boldsymbol{M}_4 = \\ M^{sat}((1-\xi)\cos\theta_3 + \xi\sin\theta_4)\boldsymbol{e}_x + M^{sat}((1-\xi)\sin\theta_3 + \xi\cos\theta_4)\boldsymbol{e}_y,\end{gathered} \tag{4.10}$$

and by substituting the expression of θ_3 and θ_4, we get

$$\boldsymbol{M} = (1-\xi)\sqrt{1 - (\frac{\mu_0 M^{sat}}{2\rho K_1} H_y)^2}\boldsymbol{e}_x + (1-\xi)\frac{\mu_0 M^{sat}}{2\rho K_1} H_y \boldsymbol{e}_y. \tag{4.11}$$

The expression of ξ can be obtained from the equation $\pi_\xi = 0$ by using Kuhn-Tucker loading conditions and a specific form of hardening function. More detail derivation is given in [3]. Here we will present the evolution equation of ξ for a constant applied traction during the forward reorientation process. The

expression is given below,

$$\xi = \frac{1}{2}\cos\left[F_1\left(\frac{(\mu_0 M^{sat})^2}{2\rho K_1}H_y^2 - \mu_0 M^{sat} H_y\right) + F_2 + \pi\right] + \frac{1}{2}. \tag{4.12}$$

The model parameters F_1 and F_2 are functions of M^{sat}, ρK_1, $H_y^{s(1,2)}$, $H_y^{f(1,2)}$. Here we introduce two more new material parameters $H_y^{s(1,2)}$ and $H_y^{f(1,2)}$, which denote the beginning and the end of the reorientation process. These parameters can be found from experiments.

3. **After Reorientation**

   After complete reorientation, only field induced martensitic variant is present and the magnetization process becomes saturated. The magnetization vectors are aligned along the applied magnetic field, which is the easy axis of the field-favored variant.

   In this situation we have $\xi = 1$ and $\alpha = 1$. Equation $\pi_{\theta_4} = 0$ gives $\theta_4 = 0$ and the magnetization vector is given by

$$\boldsymbol{M} \;=\; \boldsymbol{M}_4 = M^{sat}\sin\theta_4 \boldsymbol{e}_x + M^{sat}\cos\theta_4 \boldsymbol{e}_y = M^{sat}\boldsymbol{e}_x. \tag{4.13}$$

In its present form, the proposed model could be extended to a 3-D formulation for polycrystal MSMAs, assuming isotropic behavior. Currently, the model is implemented in a 2-D form and calibrated from experiments on single crystal MSMAs [47]. A proper 3-D implementation for single crystal MSMAs requires additional constants to account for the anisotropic behavior. Once a 3-D single crystal model is developed, we can use micromechanic techniques in order to produce a model suitable for polycrystals.

Specific relations between the constants F_1 and F_2 and the model parameters

M^{sat}, ρK_1, $H_y^{s(1,2)}$, $H_y^{f(1,2)}$, σ^* and $\varepsilon^{r,max}$, namely the saturation magnetization, the magnetocrystalline anisotropy constant, the critical field values for the start and finish of the forward reorientation process, the blocking stress and the maximum reorientation strain are given in [77]. The model parameters must be identified from experiments. The specific calibration used in the following simulations is based on experimental data reported in [1]. The resulting parameter values are listed in Table XXVIII.

Table XXVIII. Material parameters calibrated for the $Ni_{51.1}Mn_{24.0}Ga_{24.9}$ composition tested at a compressive stress level of -2 MPa [1].

Material Parameters					
Quantity	Value	Unit	Quantity	Value	Unit
ρK_1	700.0	$\mathrm{kJm^{-3}}$	$\mu_0 H_y^{s(1,2)}$	0.9	T
M^{sat}	742.4	$\mathrm{kAm^{-1}}$	$\mu_0 H_y^{f(1,2)}$	1.85	T
$\varepsilon^{r,max}$	5.65	%	$\mu_0 H_y^{s(2,1)}$	0.75	T
σ^*	-2.0	MPa	$\mu_0 H_y^{f(2,1)}$	-0.17	T

The predicted magnetization response curves are plotted in Fig. 41 and may be explained in the following way. Initially, the sample consists of the stress-favored variant and two oppositely magnetized domains of equal volume fraction separated by 180° domain walls, such that it is macroscopically unmagnetized. When magnetic field is applied along the y-direction, the hard axis of the stress-favored variant, the magnetization vectors start to rotate in each domain. The x-components of the magnetization vectors in the adjacent domains cancel each other, while their y-components add up. Once the critical field for the variant reorientation has been reached, the field-favored variant nucleates and magnetization curve becomes nonlinear. As pointed out

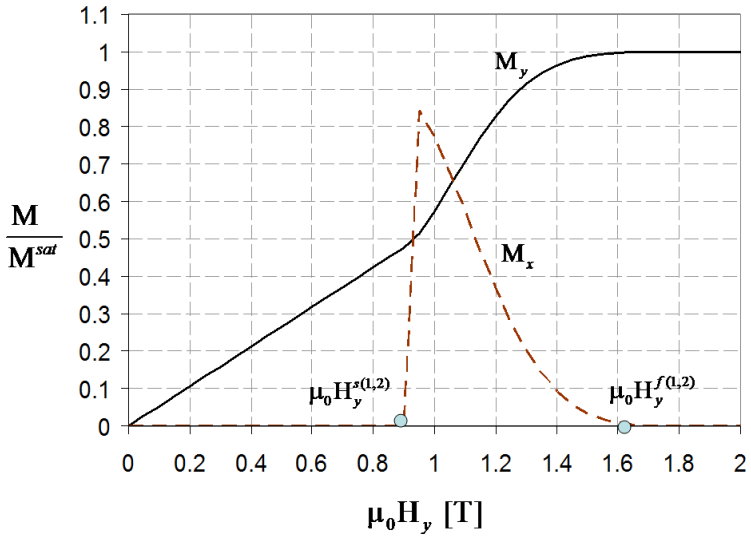

Fig. 41. The x and y-components of the predicted magnetization response.

above, it is assumed that unfavorable magnetic domains are eliminated simultaneously with the activation of the reorientation process due to comparatively high magnetic field (see also [14, 151]). This results in a sharp increase of the M_x-component of the predicted magnetization curve. After the reorientation process is completed, only the single-domain, field-favored variant remains and the magnetic saturation level is reached with the magnetization vector fully-aligned along the applied field direction, which coincides with the easy axis of the field-favored variant.

C. Variant reorientation model from the generalized framework

In this section we show that the generalized model (as discussed in chapter II) is capable to capture the key features of variant reorientation. The major difference in this approach from the Kiefer-Lagoudas model is that there are no micro scale

variables θ_i or α, as discussed in the previous section. We consider the stress favored martensitic variant reorients to the field favored variant, for which $\xi_1 = \xi_2 = \xi_3 = 0$ and $c_3 = c_4 = 0$. The reorientation process begins with stress favored variant (M_1)

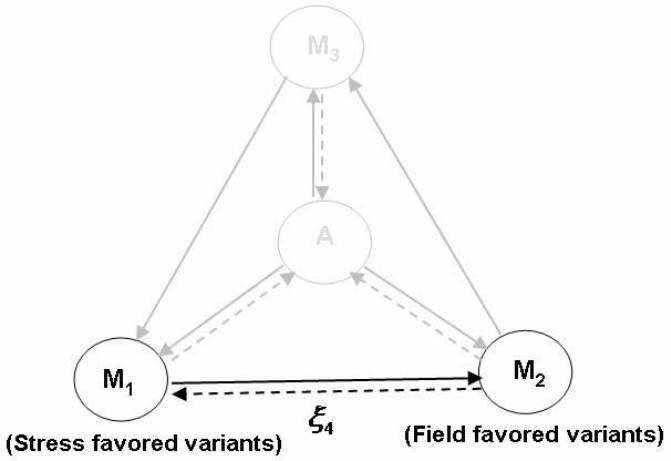

Fig. 42. Schematic diagram of the reorientation process.

i.e $c_{01} = 1$ and $c_{02} = c_{03} = 0$. The kinematic diagram reduces to Fig. 42 and the reduced form of Eq. (2.98) becomes

$$c_1 = 1 - \xi_4, \tag{4.14}$$

$$c_2 = \xi_4. \tag{4.15}$$

We consider the martensitic phase is isotropic and from (2.109) we get

$$G(\Upsilon_\phi, T, \xi_4, g) = G_M(\Upsilon_{\phi P}, T) + G_I(\Upsilon_{\phi I}, T) + G_{mix}(g). \tag{4.16}$$

Here we also consider the material is isotropic with a small strain approximation. The integrity basis

$$\begin{aligned} I_1 &= \mathbf{H}\cdot\mathbf{H}, \qquad I_2 = \mathrm{tr}\,(\boldsymbol{\sigma}^E), \qquad I_3 = \mathrm{tr}\,(\boldsymbol{\sigma}^{E^2}), \\ I_4 &= \mathrm{tr}\,(\boldsymbol{\sigma}^E\boldsymbol{\varepsilon}^I), \qquad I_5 = \mathbf{M}^I\cdot\mathbf{H}. \end{aligned} \tag{4.17}$$

is considered to study variant reorientation mechanism and we propose following form of the Gibbs free energy.

$$\begin{aligned} G^M &= \frac{\nu^M}{2\rho_0\mathbb{E}^M} I_2^2 - \frac{1+\nu^M}{2\rho_0\mathbb{E}^M} I_3 - \frac{1}{\rho_0} a_2^M I_1 + u_0^M(T_0) \\ &= \frac{\nu^M}{2\rho_0\mathbb{E}^M} \mathrm{tr}\,(\boldsymbol{\sigma}^E)^2 - \frac{1+\nu^M}{2\rho_0\mathbb{E}^M} \mathrm{tr}\,(\boldsymbol{\sigma}^{E^2}) - \frac{1}{\rho_0} a_2^M (\mathbf{H}\cdot\mathbf{H}) + u_0^M(T_0), \end{aligned} \tag{4.18a}$$

$$\begin{aligned} G^I &= -\frac{1}{\rho_0} b_1 I_4 - \frac{1}{\rho_0} I_5, \\ &= -\frac{1}{\rho_0} b_1 \mathbf{H}\cdot\mathbf{M}^I - \frac{1}{\rho_0} \mathrm{tr}\,(\boldsymbol{\sigma}^E \mathbf{E}^I) \end{aligned} \tag{4.18b}$$

$$G^{mix} = -\frac{1}{\rho_0} g. \tag{4.18c}$$

We simplify the flow rules, given in (2.100a) by

$$\dot{\mathbf{E}}^I = \dot{\mathbf{E}}^r = \boldsymbol{\Lambda}^r \dot{\xi}_4. \tag{4.19}$$

Similarly from (3.9) and (2.104a) we obtain

$$\dot{\mathbf{M}}^I = \dot{\mathbf{M}}^r = \boldsymbol{\gamma}^r \dot{\xi}_4, \tag{4.20}$$

$$\dot{g} = f^r \dot{\xi}_4. \tag{4.21}$$

where

$$\boldsymbol{\gamma}^r = \begin{cases} {}^{\mathbf{r}}\boldsymbol{\Gamma}^{\mathbf{f}}, & \dot{\xi}_4 > 0 \\ {}^{\mathbf{r}}\boldsymbol{\Gamma}^{\mathbf{r}}, & \dot{\xi}_4 < 0 \end{cases} \tag{4.22}$$

Here, ${}^{\mathbf{r}}\boldsymbol{\Gamma}^{\mathbf{f}}$ and ${}^{\mathbf{r}}\boldsymbol{\Gamma}^{\mathbf{r}}$ are the directions of internal magnetization during the forward and reverse reorientation. Finally the hardening function is proposed by

$$f^r := \begin{cases} -A(\pi - \cos^{-1}(2\xi_4 - 1)) + B, & \dot{\xi}_4 > 0\,, \\ -C(\pi - \cos^{-1}(2\xi_4 - 1)) + D, & \dot{\xi}_4 < 0\,, \end{cases} \tag{4.23}$$

1. Phenomenological description of magnetization response

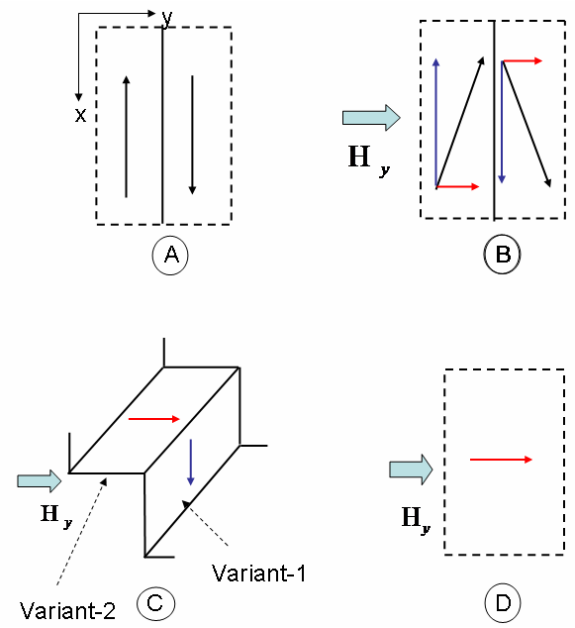

Fig. 43. Schematic representation of micro scale mechanism

As explained in Fig. 43(A), we only have stress favored variant in the initial state. Since the MSMA specimen does not have any remnant magnetization before applying magnetic field, only 180^o domain walls exist and resultant macroscopic magnetization is zero. When magnetic field is applied along the y-direction, the magnetization vectors start rotating in each domain. The x component of the magnetization vector in the adjacent domain alters the direction and cancels out when added and gives zero resultant magnetization. On the other hand, the y components of the magnetization vectors are added up and give a resultant magnetization (Fig. 43(B)). The above mentioned mechanism can be captured phenomenologically from the proposed Gibbs free energy. The magnetization constitutive response, for $\xi_4 = 0$, is given by

$$\mathbf{M} = -\frac{\rho_0}{\mu_0}\frac{\partial G^M}{\partial \mathbf{H}} = \frac{2a_2^M}{\mu_0} H_y \, \mathbf{e}_y. \tag{4.24}$$

Equation (4.24) shows that M_y component varies linearly with H_y. Here we consider the magnetic field at a material point is same as the applied field. We find the

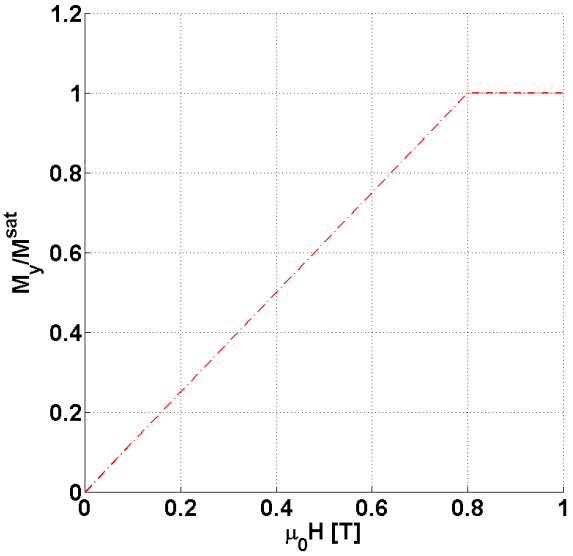

Fig. 44. Magnetization response of stress favored martensitic variant at -3 MPa.

constant $\frac{2a_2^M}{\mu_0}$ from an experiment. Fig. 44 represents the magnetization response of a stress favored martensitic variant, operated under the traction -3 MPa, which is higher than the blocking stress. The single variant reaches saturation by the rotation of magnetization vectors. The slope is represented by K_a such that $K_a = \frac{M_y/M^{sat}}{\mu_0 H_y}$ (Fig. 44) or $\frac{M_y}{H_y} = \mu_0 K_a M^{sat} = \frac{2a_2^M}{\mu_0}$.

Next we consider the magnetization during reorientation. We consider (4.22) where, ${}^{\mathbf{r}}\mathbf{\Gamma}^{\mathbf{f}}$ and ${}^{\mathbf{r}}\mathbf{\Gamma}^{\mathbf{r}}$ are the directions of internal magnetization during the forward and reverse reorientation. We only focus on the forward reorientation in this study. Moreover, ${}^{\mathbf{r}}\mathbf{\Gamma}^{\mathbf{f}}$ is assumed to be constant and we write $\mathbf{M}^I = {}^{\mathbf{r}}\mathbf{\Gamma}^{\mathbf{f}}\xi + \mathbf{P}$, where $\mathbf{P}$ is an arbitrary constant. The two dimensional form is given by

$$M_x = \Gamma_x^f \xi + P_x. \tag{4.25}$$

$$M_y = \Gamma_y^f \xi + P_y. \tag{4.26}$$

Once the critical field for the variant reorientation is reached, the field favored variant nucleates (Fig. 43(C)) and the formation of 90^0 domain wall takes place [14, 151].

When $\xi \to 0^+$, $\mathbf{M} = P_x\ \mathbf{e}_x + P_y\ \mathbf{e}_y$ and the magnetization has a vertical component due to the formation of 90^o domain wall. This means $P_y = M^C$, where $M^C = K_a H_s^{M_2}$ is the magnetization at the critical field $H_s^{M_2}$. Since due to the formation of 90^o domain wall, the magnetization of the stress favored variant $(1 - \xi \approx 1)$ saturates with the magnitude $P_x = \sqrt{M^{sat2} - M^{C2}}$. At the end of variant reorientation ($\xi = 1$, Fig. 43(D)), we have $(\Gamma_x^f + P_x)\ \mathbf{e}_x + (\Gamma_y^f + P_y)\ \mathbf{e}_y = M^{sat}\ \mathbf{e}_y$. This implies, $\Gamma_x^f = -P_x$ and $\Gamma_y^f = M^{sat} - P_y$. We can summarize the solution of the unknown parameters in the following way,

$$P_y = M^C, \qquad P_x = \sqrt{M^{sat2} - M^{C2}} = \alpha\,(\text{say}), \tag{4.27}$$

$$\Gamma_y^f = M^{sat} - P_y = M^{sat} - M^C = \gamma\,(\text{say}), \qquad \Gamma_x^f = -P_x = -\alpha. \tag{4.28}$$

Thus the components of the magnetization are given by

$$M_x = \alpha - \alpha\xi, \tag{4.29}$$

$$M_y = M^C + \gamma\xi. \tag{4.30}$$

2. Phenomenological description of strain response

The directions of the evolution are given as

$$\mathbf{\Lambda}^r = \begin{cases} E^{cur}(\bar{\sigma}^E)(\mathbf{e}_x \otimes \mathbf{e}_x - \mathbf{e}_y \otimes \mathbf{e}_y)\,, & \dot{\xi}_4 > 0 \\ \frac{\mathbf{E}^{t-r}}{\xi^r}\,, & \dot{\xi}_4 < 0 \end{cases} \tag{4.31}$$

Here $\boldsymbol{\sigma}'^E$ is the deviatoric stress, which is normalized by the Mises equivalent stress $\bar{\sigma}^E = \sqrt{(3/2\boldsymbol{\sigma}'^E : \boldsymbol{\sigma}'^E)}$. During full reverse reorientation ($\dot{\xi}_4$), the transformation strain generated by the previous forward transformation must be recovered. This

motivates the form of $\mathbf{\Lambda}^r$ during reverse transformation, where $\mathbf{E}^{t-r}$ denotes the reorientation strain at reorientation reversal i.e the state at which most recent forward reorientation ended. The scalar ξ^r is the martensitic volume fraction at the transformation reversal, used for normalization.

3. Constitutive equations summary

the constitutive equations ((3.6a), (3.6b), and (3.6c)) can be written in the following form,

$$\mathbf{E} = -\frac{\nu}{\mathbb{E}}\mathrm{tr}\,(\boldsymbol{\sigma}^E)\mathbf{I} + \frac{1+\nu}{\mathbb{E}}\boldsymbol{\sigma}^E + \mathbf{E}^I \tag{4.32}$$

$$\mathbf{M} = \begin{cases} (\mu_0 M^{sat} K_a) H_y \, \mathbf{e}_y & \text{for } \xi_4 = 0 \ , \\ -\sqrt{M^{sat\,2} - M^{C\,2}}(1-\xi_4)\ \mathbf{e}_x & \\ +((1-\xi_4)M^C + M^{sat}\xi_4)\ \mathbf{e}_y \ , & \text{for } \xi_4 \in (0,1) \\ M^{sat}\,\mathbf{e}_y & \text{for } \xi_4 = 1 \ . \end{cases} \tag{4.33}$$

$$\rho_0 s = \langle s_0 \rangle + \langle \alpha \rangle \mathrm{tr}\,(\boldsymbol{\sigma}^E) + s_0^A \Delta T - \frac{\langle c \rangle}{T_0}(\Delta T)^2 \tag{4.34}$$

$$\boldsymbol{\pi}_{\mathbf{E}^I} = \boldsymbol{\sigma}^E \tag{4.35}$$

$$\boldsymbol{\pi}_{\mathbf{M}^I} = \mathbf{H} \tag{4.36}$$

$$\pi_\xi = 0 \tag{4.37}$$

$$\pi_g = 1 \tag{4.38}$$

$$\pi^r = \boldsymbol{\pi}_{\mathbf{E}^I} : \mathbf{\Lambda}^r + \boldsymbol{\pi}_{\mathbf{M}^I} : \boldsymbol{\gamma}^r + f^r \tag{4.39}$$

$$\tag{4.40}$$

where,

$$\Phi^r := \begin{cases} \pi^r - Y^r\,, & \dot{\xi} > 0 \\ -\pi^r - Y^r\,, & \dot{\xi} < 0 \end{cases}, \qquad \Phi^r \leq 0 \tag{4.41}$$

$$\Phi^r \leq 0, \quad \Phi^r \dot{\xi} = 0\,. \tag{4.42}$$

4. Model calibration

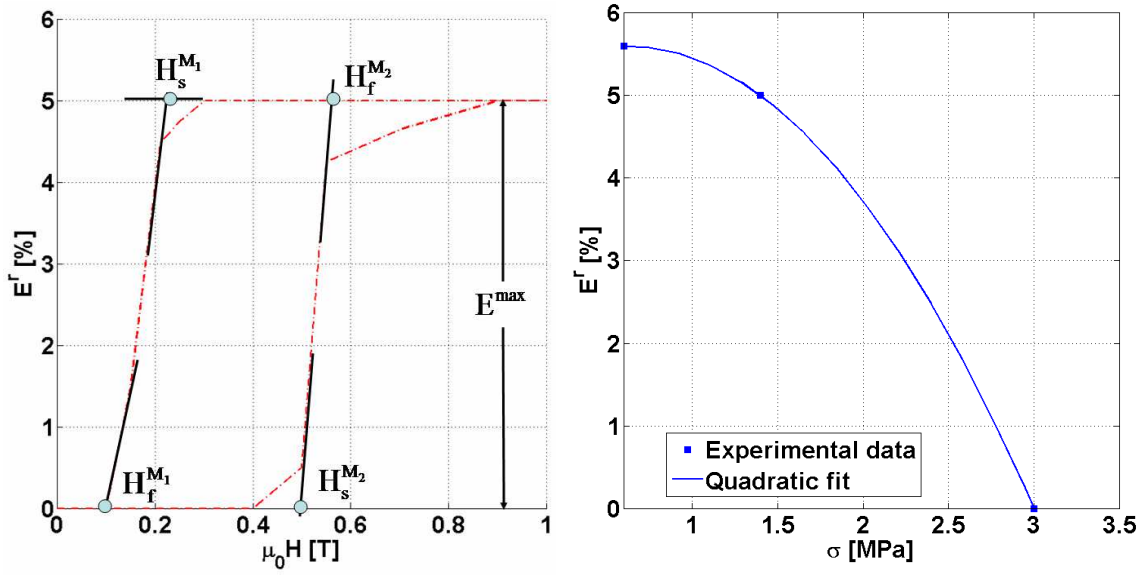

(a) (b)

Fig. 45. (a) Experimental data of strain-field response at -1.4 MPa and (b) maximum reorientation strain at different stress level.

The x-component of the strain response is given by

$$E_{xx} = \frac{1}{\mathbb{E}}\sigma^E_{xx} + E^I_{xx}, \tag{4.43}$$

The four critical magnetic fields (Fig. 45a) are $H_s^{M_2}$, forward reorientation starts, $H_f^{M_2}$, forward reorientation ends, $H_s^{M_1}$, reverse reorientation starts and $H_f^{M_1}$, reverse reorientation ends. The experimental data for maximum strain are given in Fig. 45b. We fit a quadratic curve, which is given by

$$E^{cur}(\bar{\mathbf{S}}^E) = \alpha_1(\bar{S}^E)^2 + \alpha_2\bar{S}^E + \alpha_3. \tag{4.44}$$

$\mu_0 H_s^{M_2} = 0.5$ T, $\mu_0 H_f^{M_2} = 0.58$ T, $\mu_0 H_s^{M_1} = 0.28$ T, $\mu_0 H_f^{M_1} = 0.1$ T
M^{sat} =742 kN/A, $K_a = 1.25$/T, $S_M = -1.4$ MPa,
$\alpha_1 = -0.9896$, $\alpha_2 = 1.2292$, $\alpha_3 = 5.2187$.

Table XXIX. Material constants from magnetization response

a. Thermodynamic driving force

The reduced form of the thermodynamic force (4.39) is given by

$$\pi^r = S^E_{xx}E^{cur} + \mu_0\gamma H_y + f^r. \tag{4.45}$$

We need to know the parameters A, B, C, D, Y^r and $\rho\Delta u_0$. From the Kuhn Tucker condition ((4.41)) we get two conditions at the beginning and two conditions at the

finish of the forward reorientation. They are

$$\pi^r(\sigma^*, H_s^{M_2}) - Y^r = 0, \qquad \text{for } \dot{\xi}_4 > 0, \quad \text{at } \xi_4 = 0 \tag{4.46a}$$

$$\pi^r(\sigma^*, H_f^{M_2}) - Y^r = 0, \qquad \text{for } \dot{\xi}_4 > 0, \quad \text{at } \xi_4 = 1 \tag{4.46b}$$

Similarly, for reverse reorientation we get two more equations,

$$\pi^r(\sigma^*, H_s^{M_1}) + Y^r = 0, \qquad \text{for } \dot{\xi}_4 < 0, \quad \text{at } \xi_4 = 1 \tag{4.47a}$$

$$\pi^r(\sigma^*, H_f^{M_1}) + Y^r = 0, \qquad \text{for } \dot{\xi}_4 < 0, \quad \text{at } \xi_4 = 0 \tag{4.47b}$$

The constant stress level is denoted by σ^*. The continuity of the hardening function [92] gives us

$$\int_0^1 f^r\Big|_{\dot{\xi}_4>0} d\xi_4 = \int_0^1 f^r\Big|_{\dot{\xi}_4<0} d\xi_4. \tag{4.48}$$

Solving the above five equations (from 4.46a to 4.48), we get the solution of five unknowns, $A, \widetilde{B},\ C, \widetilde{D}, Y^r$. It should be noted that we introduce a new constant $\widetilde{B} = B + \rho\Delta u_0$ and $\widetilde{D} = D + \rho\Delta u_0$ since B and D absorbs the term $\rho\Delta u_0$.

5. Model simulation and predictions

The model simulation is presented in Fig. 46(a), followed by the magnetization prediction in Fig. 46(b). The prediction shows good agreement with the experimental results. Model predictions of field induced strain and magnetization are presented in Fig. 47. The model also predicts the increase of critical magnetic fields due to the increase of stress.

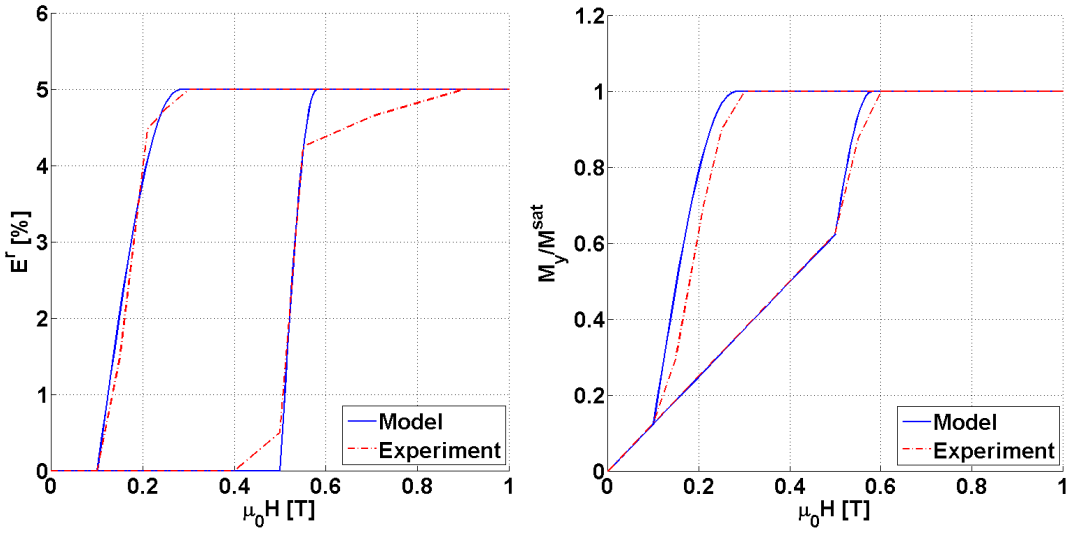

(a) (b)

Fig. 46. (a) Model simulation of strain-field response at -1.4 MPa and (b) model prediction of magnetization response at -1.4 MPa.

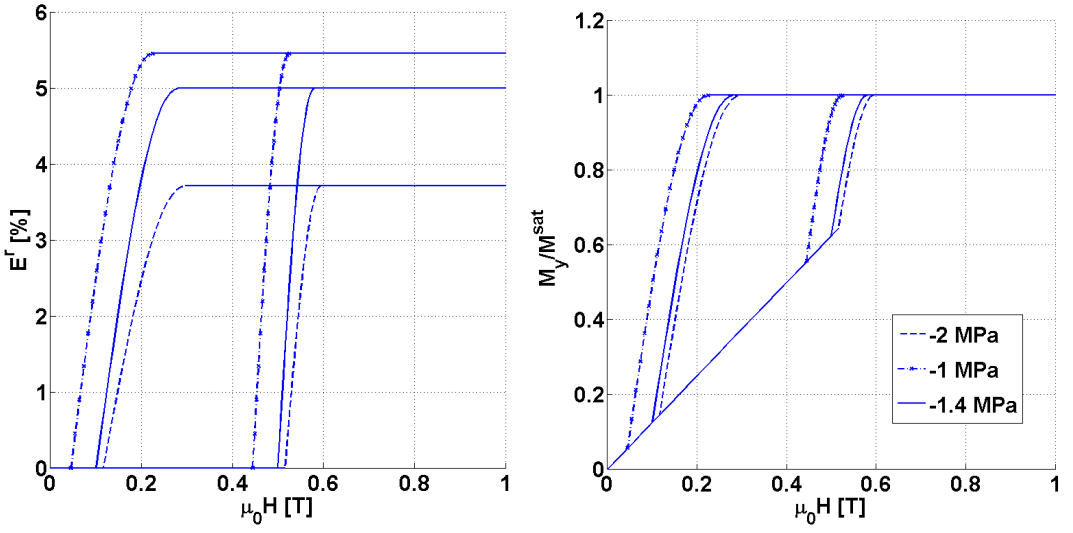

(a) (b)

Fig. 47. (a) Model predictions of strain-field and (b) model predictions of magnetization responses at different stress levels.

CHAPTER V

MAGNETOMECHANICAL BOUNDARY VALUE PROBLEMS FOR MSMAS*

This chapter is concerned with the finite element analysis of boundary value problems involving nonlinear magnetic shape memory behavior, as might be encountered in experimental testing or engineering applications of MSMAs. The presented investigations mainly focus on two aspects: First, nonlinear magnetostatic analysis, in which the nonlinear magnetic properties of the MSMA are predicted by the phenomenological internal variable model previously developed by Kiefer and Lagoudas [3], is utilized to investigate the influence of the demagnetization effect on the interpretation of experimental measurements. An iterative procedure is proposed to deduce the true constitutive behavior of MSMAs from experimental data that typically reflect a sample shape-dependent system response. Secondly, the common assumption of homogeneous Cauchy stress distribution in the MSMA sample is tested. This is motivated by the expectation that the influence of magnetic body forces and body couples caused by field matter interactions may not be negligible in MSMAs that exhibit blocking stresses of well below 10 MPa. To this end, inhomogeneous Maxwell stress distributions are first computed in a post-processing step, based on the magnetic field and magnetization distributions obtained in the magnetostatic analysis. Since the computed Maxwell stress fields, though allowing a first estimation of the magnetic force and couple influence, do not satisfy equilibrium conditions, a finite element analysis of the coupled field equations is performed in a second step to complete

*This chapter is reproduced with the permission from Taylor & Francis for the published work "Finite element analysis of the demagnetization effect and stress inhomogeneities in magnetic shape memory alloy samples" by Krishnendu Haldar, Björn Kiefer and Dimitris C. Lagoudas, Philosophical Magazine Volume 91 Issue 32 (2011), pp. 4126-4157.

the study. It is found that highly non-uniform Cauchy stress distributions result under the influence of magnetic body forces and couples, with magnitudes of the stress components comparable to externally applied bias stress levels.

A. A Concise Review of the Magnetostatic Problem

In the following section basic concepts of magnetostatics in the presence of magnetized matter are summarized to provide the foundation for the analysis of magnetostatic boundary value problems (BVPs) for MSMA materials. For static conditions in stationary bodies and negligible current density, Maxwell's equations in $\mathbb{R}^3$ are reduced to [162, 163]

$$\nabla\cdot\mathbf{B} = 0\ , \quad \text{and} \quad \nabla\times\mathbf{H} = \mathbf{0}\ , \tag{5.1}$$

where $\mathbf{B}$ is the magnetic induction and $\mathbf{H}$ is the magnetic field strength. These two quantities are related through the constitutive relation $\mathbf{B} = \mu_0(\mathbf{H} + \mathbf{M})$, in which μ_0 is the permeability of free space and $\mathbf{M}$ is the magnetization of a material point in a magnetized body, in this case a magnetic shape memory alloy sample. Eqs. (5.1) are subject to the jump conditions

$$[\![\mathbf{B}]\!]\cdot\mathbf{n} = 0\ , \quad [\![\mathbf{H}]\!]\times\mathbf{n} = \mathbf{0}\ , \tag{5.2}$$

on all interfaces, if surface currents are negligible. In Eqs. (5.2), $\mathbf{n}$ denotes the unit normal to the surface of discontinuity.

Taking advantage of the specific form of Eqs. (5.1), the magnetostatic problem is often reformulated, by deriving the magnetic field strength from a scalar potential Φ^m or the magnetic induction from a vector potential $\mathbf{\Phi}^m$. In the latter case $\mathbf{B} = \nabla\times\mathbf{\Phi}^m$ identically satisfies (5.1a). Using the identity $\nabla\times(\nabla\times\mathbf{\Phi}^m) = \nabla(\nabla\cdot\mathbf{\Phi}^m) - \Delta\mathbf{\Phi}^m$, and

the Coulomb gauge $\nabla\cdot\mathbf{\Phi}^m = 0$, (5.1b) takes the form

$$\nabla\times(\mu_0^{-1}\nabla\times\mathbf{\Phi}^m - \mathbf{M}) = \mathbf{0}\ , \quad \text{or} \quad \Delta\mathbf{\Phi}^m = -\mu_0\nabla\times\mathbf{M}\ , \tag{5.3}$$

which is the *vector-valued Poisson equation* for the magnetic potential $\mathbf{\Phi}^m$.

B. Finite Element Analysis of the Nonlinear Magnetostatic Problem

Based on the field equations and the MSMA constitutive relations derived in the previous section we can now proceed with the solution of specific nonlinear magnetostatic boundary value problems using the finite element method. The numerical analysis presented in this paper was performed using the COMSOL Multiphysics finite element software package.

The geometry and boundary conditions of the considered model problem are illustrated in Fig. 48. This particular arrangement is motivated by the experimental set up reported in [1]. The computational domain may be regarded as the gap between the pole pieces of an electromagnet of dimensions $26\,\text{mm}\times 26\,\text{mm}\times 26\,\text{mm}$ for which a uniform magnetic field of up to 2 T can be applied. Typical specimen dimensions are $8\,\text{mm}\times 4\,\text{mm}\times 4\,\text{mm}$, or aspect ratios of $2:1:1$, where the long axis is the x-direction.

A spatially constant magnetic potential

$$\Phi^m_x = \Phi^m_y = 0\ ; \quad \Phi^m_z = -\mu_0 H^a_y x\ , \tag{5.4}$$

is applied on all sides of the boundary, such that with (5.3) it follows

$$\begin{aligned}
&\mu_0 H_x = B_x = \frac{\partial\Phi^m_z}{\partial y} - \frac{\partial\Phi^m_y}{\partial z} = 0\ , \quad \mu_0 H_y = B_y = \frac{\partial\Phi^m_x}{\partial z} - \frac{\partial\Phi^m_z}{\partial x} = \mu_0 H^a_y\ ,\\
&\mu_0 H_z = B_z = \frac{\partial\Phi^m_y}{\partial x} - \frac{\partial\Phi^m_x}{\partial y} = 0\ ,
\end{aligned} \tag{5.5}$$

i.e. the desired homogeneous magnetic field in the computational domain in the ab-

sence of the specimen. The presence of the magnetizable sample, of course, perturbs the homogeneity of the applied field.

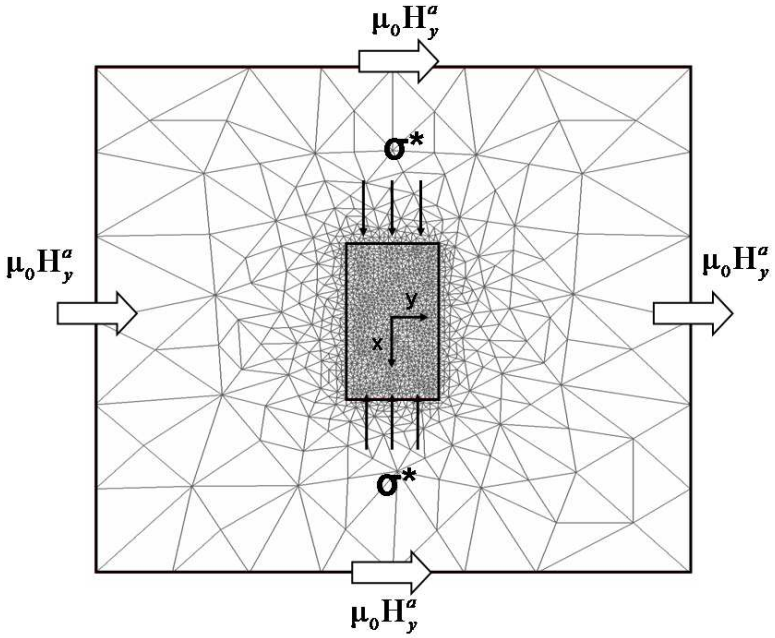

Fig. 48. Domain geometry, mesh and boundary conditions for the magnetostatic problem.

The following comments must be made regarding the usage of the magnetization data in the magnetostatic analysis:

1. The stress is assumed to be uniaxial, at a constant level and spatially homogeneous, since magnetic body forces and magnetic body couples are neglected. The only coupling between the mechanical and the magnetostatic problem at this point is given by the stress level dependence of the magnetic properties. Thus for each stress level the magnetostatic analysis has to be performed in a separate computation.

2. The magnetic field, and thus the magnetization, on the other hand vary spatially inside the rectangular specimen. The magnetic properties predicted by the constitutive model are evaluated at every integration point in the finite element mesh. Since the magnetization nonlinearly depends on the magnetic field, the magnetostatic problem is highly nonlinear. COMSOL Multiphysics provides an appropriate iterative nonlinear solver. The parametric version of this solver was used such that the magnetic field distribution could be computed, while scaling the applied magnetic field from 0 T to 2 T.

3. Although a magnetic potential difference was applied to represent a homogeneous external field whose x-component is zero, see (5.5), the magnetic field in the MSMA specimen is non-uniform and exhibits a non-zero x-component, particularly at the corners of the sample. The constitutive dependency $\mathbf{M}(H_x)$ is assumed to be small and thus neglected.

4. The hysteretic nature of the constitutive response is not addressed in the magnetostatic analysis at this point. To be precise, the hysteresis is not neglected, but the analysis is only carried out for monotonous loading from 0 T to 2 T, not for the removal of the magnetic field.

Numerical results of the finite element analysis are plotted in Fig. 49 in terms of the distribution of the y-component of the magnetic field for the exemplary applied magnetic induction level of 2 T.

It is observed that indeed, due to the non-ellipsoidal shape of the specimen, the magnetic field and thus the magnetization are non-uniform inside the specimen although a constant magnetic induction is applied at the boundary of the computational domain. The presence of the magnetized specimen clearly perturbs the magnetic field in the free space surrounding the sample. From this distribution one can for exam-

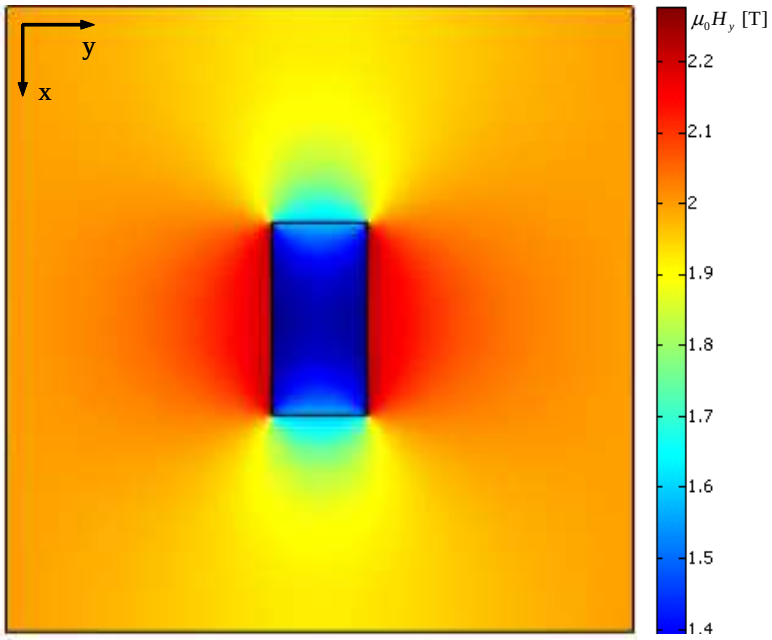

Fig. 49. Distribution of H_y in the computational domain at the applied magnetic field of $\mu_0 H_y^a = 2.0$ T.

ple obtain information to which extent a Hall probe reading, used to measure the applied field, can be expected to be influenced by the sample's magnetic field. The distribution at 2.0 T, at which essentially all of the material has been magnetized to saturation along the y-axis, is symmetric with respect to both axes of the coordinate system.

It again must be emphasized that in the magnetostatic problem the magnetization is allowed to change locally and its value is determined by evaluating the magnetization curve for the magnetic field acting at the particular point. The internal mechanism which leads to the macroscopic magnetization response, namely the evolution of the martensitic variants, the magnetic domains and the magnetization rotation angles as predicted by the constitutive model have been discussed earlier. Such a modeling approach assumes that there exists a separation of scales such that at each point in the continuum, the MSMA sample, there exist a smaller

length scale at which a sufficient number of martensitic twins and magnetic domains coexist such that average quantities like the magnetization can be defined for each point. The contributions of the variant and magnetic domains are then taken into account phenomenologically in a homogenized sense and are no longer "visible" on the continuum scale. It is still a matter of discussion whether this approach is fully justified for MSMA single crystals.

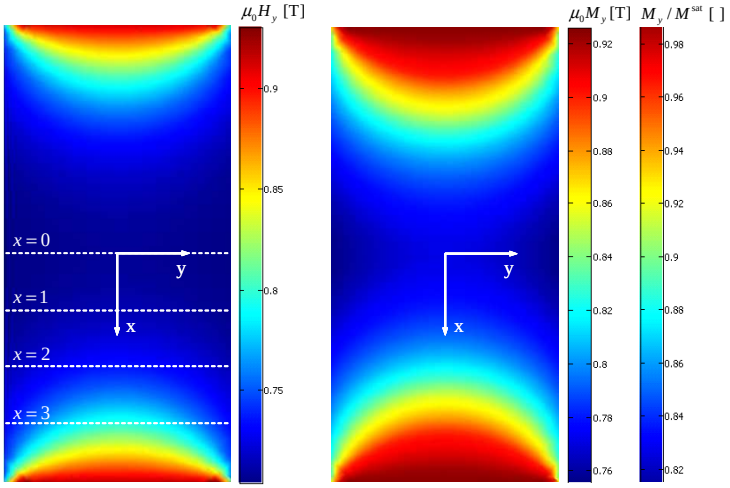

(a) (b)

Fig. 50. (a) Distribution of the magnetic field and (b) magnetization within the specimen at the applied magnetic field of $\mu_0 H_y^a = 1.3$ T.

To take a closer look at the local solution, the variation of the computed magnetic field within the MSMA sample is plotted in Fig. 50 for a specific applied field level. In Fig. 51 the variation of the magnetic field and the magnetization across the specimen are plotted for different locations. Note that at the left ($y = -2$) and right ($y = 2$) sides of the specimen the jump in the magnetic field balances the jump of the magnetization in the transition from free space into the magnetized material. The magnetic induction component $B_y = \mu_0(H_y + M_y)$, which is the normal component

of the magnetic induction on these interfaces, thus stays constant, so that the jump condition specified in (5.2a) is properly satisfied.

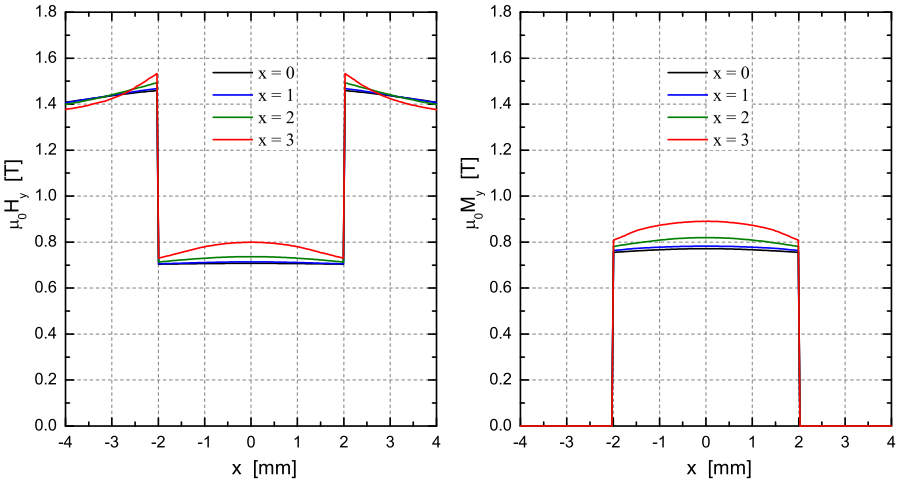

(a) (b)

Fig. 51. (a) Distribution of the y-components of the magnetic field and (b) the magnetization across the specimen and its immediate vicinity at different levels of x, as indicated in Fig. 50, at the applied magnetic induction level of 1.3 T.

C. Influence of the Demagnetization Effect on the Interpretation of Experiments

From the theory of magnetostatics it is well-known, that the magnetic field caused by the magnetization of the material opposes the direction of magnetization. It is therefore called the *demagnetizing or self field*. This *demagnetization effect* can also clearly be observed in the plots of Fig. 51. Furthermore, as a consequence of the interface conditions of Eqs. (5.2), the demagnetization field in a uniformly magnetized ellipsoidal sample is always uniform, while it is non-uniform in a non-ellipsoidal sample. Permanent magnets, by definition, exhibit substantial remnant macroscopic magnetization at zero applied field and, within certain limits, the magnetization of the magnetic sample does not depend on the applied magnetic field [19]. For mag-

netostatic problems involving only permanent magnets the Poisson equation (5.3) is linear and the principle of superposition holds. Thus, if additionally an external magnetic field $\mathbf{H}^a$ is applied, the total magnetic field is then given by

$$\mathbf{H} = \mathbf{H}^a + \mathbf{H}^d \,. \tag{5.6}$$

General integral representations of the solution of the magnetostatic problem defined by (5.3) exist, see e.g. [162, 164]. For uniformly magnetized bodies the magnetization vector can be taken outside the integral expressions for the magnetic field strength [164, 165], such that

$$\mathbf{H}^d(\mathbf{r}) = -\underbrace{\left[\frac{1}{4\pi}\iint\limits_{\partial\Omega^m} \frac{\mathbf{r}-\mathbf{r}'}{|\mathbf{r}-\mathbf{r}'|^3} \otimes \mathbf{n}' \,\mathrm{d}A'\right]}_{=:\mathbf{D}} \mathbf{M} = -\mathbf{D}\mathbf{M} \,. \tag{5.7}$$

Therein $\mathbf{r}$ is the position at which $\mathbf{H}$ is evaluated in $\mathbb{R}^3$ and $\mathbf{r}'$ the location of a point on the surface $\partial\Omega^m$, with unit outward normal $\mathbf{n}'$, of the region Ω^m occupied by the magnetized body. By applying the divergence theorem, an equivalent volume integral representation of (F.2) can be obtained. $\mathbf{D}$ is the *demagnetization tensor*, which only depends on the geometry of the body and can be computed by evaluating the bracketed integral expression in (F.2). For a spatially uniformly magnetized body the demagnetization field can thus be computed by simply multiplying the magnetization with an appropriate demagnetization factor. Such factors have been tabularized for ellipsoids of many different aspect ratios [19, 20, 166]. This procedure is analogous to using Eshelby tensors in elasticity theory to determine the strain field inside ellipsoidal inclusions [167, 168]. The demagnetization tensor has the following properties: i) it is independent of position inside an ellipsoidal body; ii) it is diagonal if its eigenvectors are aligned with the symmetry axes of the body; iii) its trace is 1, if evaluated inside the body. The demagnetization factor for a sphere is therefore 1/3

in any direction. For a prismatic cylinder with square or circular cross-section the axial and transverse demagnetization factors are related by $D^t = 1/2(1 - D^a)$, see [169].

The magnetic field inside a uniformly magnetized sample of non-ellipsoidal shape is always non-uniform. The demagnetization tensor in this case depends on the position inside the sample. It is customary to define average demagnetization tensors for samples of arbitrary shape, sometimes referred to as *magnetometric demagnetization tensors* [169, 170], in the following manner

$$\langle \mathbf{D} \rangle := \frac{1}{\Omega^m} \int\limits_{\Omega^m} \mathbf{D}(\mathbf{r}) \, \mathrm{d}V \, . \tag{5.8}$$

The average demagnetization field can then be written, for uniform magnetization $\mathbf{M}$ as

$$\langle \mathbf{H}^d \rangle = -\langle \mathbf{D} \rangle \mathbf{M} \, . \tag{5.9}$$

Numerical solution schemes have been developed to determine the demagnetization factors for uniformly magnetized bodies of arbitrary shape. They have been computed and documented for many standard geometries, such as prismatic bars with different cross-sectional shapes [165, 169, 170].

By definition the demagnetization factor loses its meaning for bodies with non-uniform magnetization. Thus, the exact demagnetization field inside a non-ellipsoidal body, whose magnetization is induced by an external magnetic field and therefore not uniform unless complete saturation is reached at high fields, can not be computed with the help of demagnetization factors. In this case, which is always encountered in experiments unless ellipsoidal specimen are used, an explicit numerical solution of the magnetostatic boundary value problem has to be obtained. For MSMAs the problem is complicated by the fact that the magnetic properties are nonlinear, hysteretic and

stress level dependent. Furthermore, the shape of the sample changes due to the magnetic field-induced strain. This effect, however, is expected to be small and is neglected within the small strain theory.

On the basis of the magnetostatic analysis presented above, it is now possible to derive an iterative procedure in which the computed load-dependent relation between the applied field and the internal field is utilized to reinterpret the experimental data by accounting for the demagnetization effect. This must be understood as the *inverse problem* of identifying the model parameters such that the simulation results in the applied magnetic field vs. magnetization curve are measured in the experiment for a specific sample geometry.

The first magnetostatic simulation is typically performed using the model parameters obtained from a parameter identification based on the *uncorrected* data. In these magnetostatic simulations, which, except for the assumption of a given constant stress level, are decoupled from the mechanical equations, the material properties are taken into account in terms of a nonlinear magnetization curve. Thus the relation between the internal and applied field computed in one run of the analysis can only serve to find a first correction of the experimental data. Thus the nonlinear magnetization data, which was originally known in terms of the constant applied field, is now known in terms of the average internal magnetic field with the accuracy of the first iteration. Then the model parameters are re-identified based on the corrected data and the analysis is repeated with the output of first iteration as next input. The simulation result can once again be used to correct the magnetization curve. By following this procedure, the relation between the applied field and the internal field is computed more accurately in each iteration step. For our example, the original and corrected magnetization curves resulting from this iterative procedure are depicted in

Fig. 52 for the considered specimen with 2:1 length to width ratio. For conciseness, only the correction of the average magnetization $\langle M_y \rangle$-component is presented here (Fig. 52).

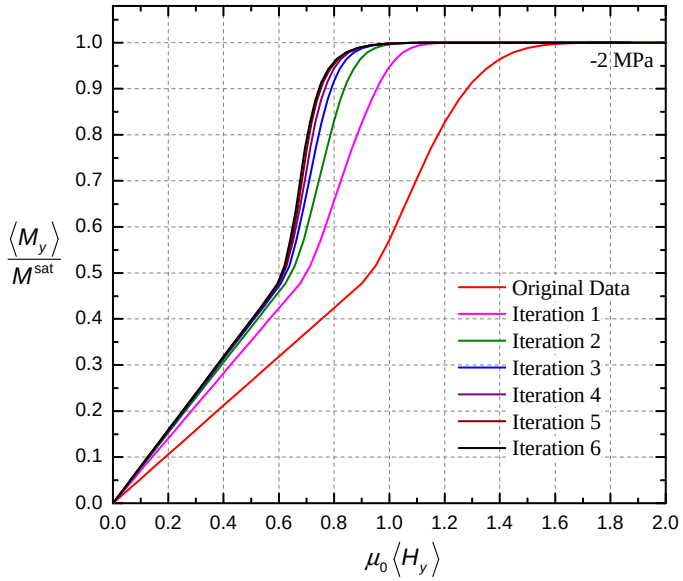

Fig. 52. Magnetization data iteratively corrected for demagnetization. Specimen aspect ratio 2:1.

The corrected procedure may also be interpreted as keeping the same data for the magnetization axes, while rescaling the magnetic field axis by means of the relation between the average internal and applied field at each iteration. One observes the relatively fast convergence of the solution. After six iterations the difference to the solution of the previous iteration is small enough to conclude that the solution has converged. The magnetization curve of iteration six can thus be considered the "true" magnetization response, which is independent of the specimen geometry. The original data on the other hand is the magnetization behavior that would be measured in an experiment using a prismatic sample of this aspect ratio. In an experiment that uses a sample of the same material, but different aspect ratio a different curve would be

measured.

A parametric study has been performed to investigate the sample shape dependence of the demagnetization effect for the prismatic specimen with nonlinear magnetic properties. In Fig. 53 the corrected magnetization data has been plotted for four different aspect ratios of the prismatic specimen. The corresponding corrections of the magnetic field-induced strain data have been plotted in Fig. 54. It is clearly observed that the influence of the specimen aspect ratio on the difference between the apparent material behavior and the true constitutive response is very significant and must therefore be addressed when using data for model calibration. Once the MFIS data has been corrected for demagnetization, the model parameters can be calibrated correctly.

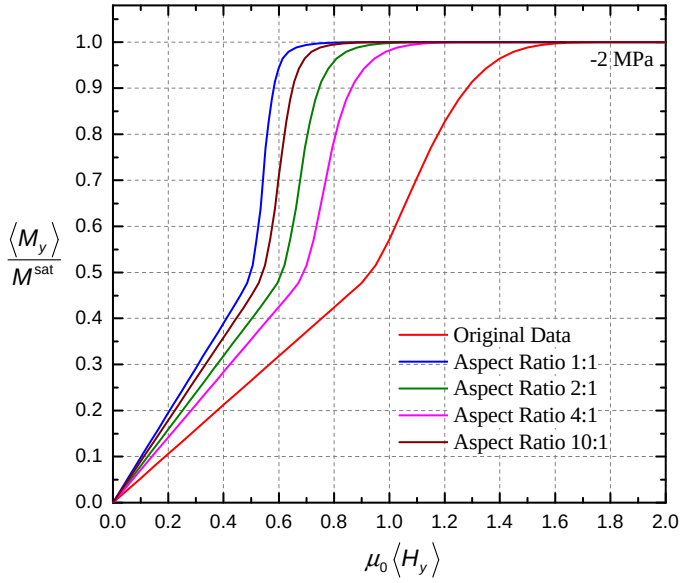

Fig. 53. Influence of specimen aspect ratios on the correction of the magnetization data.

The specific results presented here are based on solutions of 2-D boundary value problems and can thus only be used for a qualitative assessment. The procedure is the same for 3-D problems, which, however, are computationally much more involved.

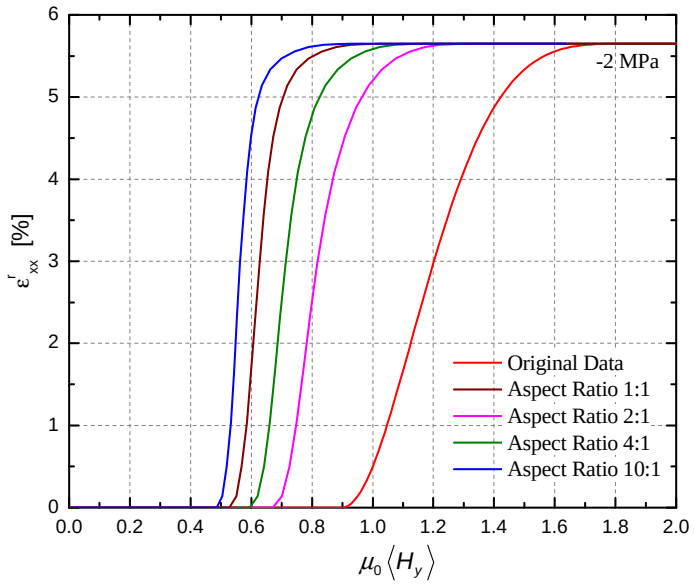

Fig. 54. Influence of specimen aspect ratios on the correction of the magnetic field-induced strain data.

One of the stated goals of this analysis is to compare the differences in the demagnetization correction by the demagnetization factor method and the finite element analysis. The first method is based on the relation

$$\langle H_y\rangle = H_y^a + \langle H_y^d\rangle = H_y^a - \langle D_{yy}\rangle M_y \ , \tag{5.10}$$

which follows from Eqs. (5.8), (5.6) and (5.9). This procedure of course assumes that the magnetization in the sample is uniform. Shield acknowledges in [30] that the demagnetization factor method can therefore only lead to approximations of the demagnetization effect in the prismatic samples typically used in MSMA testing. Nonetheless, this method is often used due to its simplicity or lack of alternatives. However, it is not clear beforehand what kind of error one might expect from making this approximation. With the developed simulation capabilities this error can now be quantified.

Since a literature value was not available for this particular geometry, the factor of $\langle D_{yy} \rangle = 0.65$ was computed using a two-dimensional magnetostatic finite element simulation for a permanent magnet sample, i.e. with spatially uniform and field-independent magnetization $M_y = \langle M_y \rangle$, of rectangular geometry with a 2:1 aspect ratio placed in a free space domain. This technique has proven to yield very accurate demagnetization factors for other geometries for which literature data was available [70, 169]. The different correction methods are compared in Fig. 55.

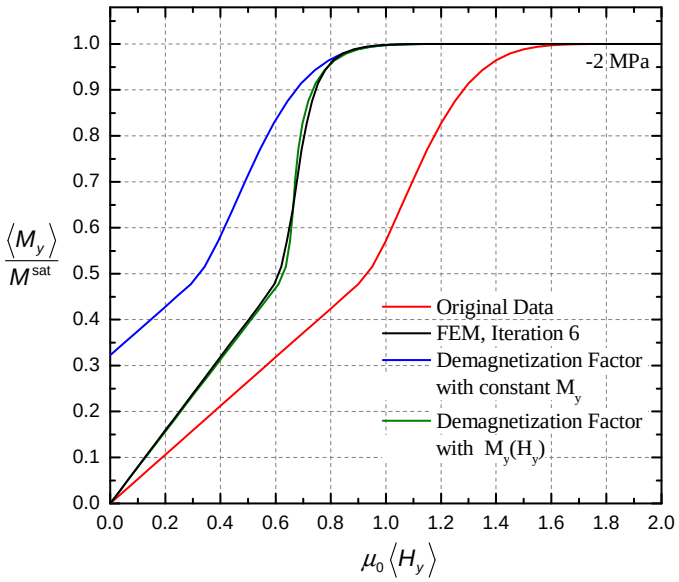

Fig. 55. Comparison of the corrections using the demagnetization factor method and nonlinear FE-analysis. Specimen aspect ratio 2:1.

These observations suggest that by using the demagnetization factor method, which is based on the assumption of uniform magnetization in the specimen, one obtains essentially the same result as performing the FE-analysis of the nonlinear magnetostatic problem with non-uniform magnetization, if average field variables are considered. This conclusion can be misleading, however, since it only holds for average quantities. But as evident from Fig. 50 and Fig. 51, there exists a significant

variation in the local magnetization. To further quantify this variation, Fig. 56 displays local values of the magnetic field at several points in the specimen as a function of the applied field. For problems in which the knowledge of the local magnetic field and magnetization is important, one can not avoid solving the magnetostatic problem explicitly. This is certainly the case for magneto-mechanical boundary value problems involving more complicated, technologically-relevant geometries, e.g. MSMA components in actuators applications.

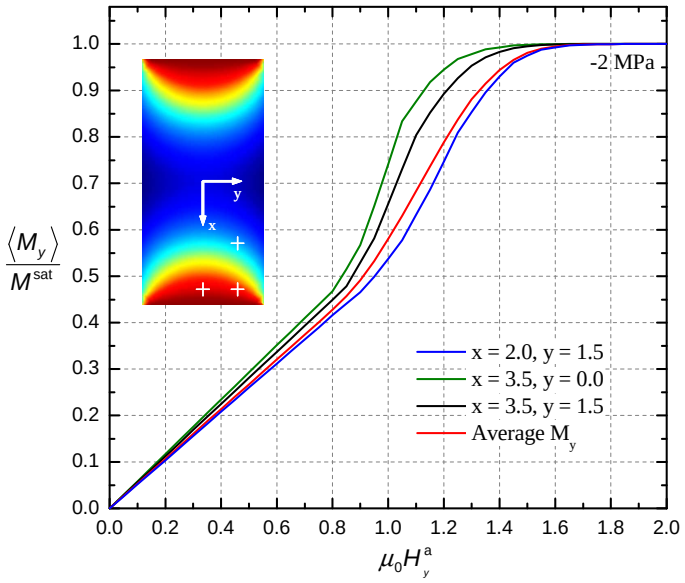

Fig. 56. Position dependence of the magnetization response within the rectangular specimen.

D. Post-Processing Computation of Maxwell Stress Distributions

The second major focus of this paper is to employ the FE-analysis in the investigation of possible stress inhomogeneities in the MSMA sample due to magnetic body forces and body couples. A first estimate of the influence of this effect can be obtained by computing the *Maxwell stress* distribution in a post-processing manner using the

relation [123]

$$\boldsymbol{\sigma}^M = \mu_0 \mathbf{H} \otimes \mathbf{H} + \ \mu_0 \mathbf{H} \otimes \mathbf{M} - \frac{1}{2}\mu_0 (\mathbf{H} \cdot \mathbf{H}) \mathbf{I} \,, \tag{5.11}$$

The Maxwell stress tensor, by definition, accounts for the magnetic body forces and couples in the following manner

$$\nabla \cdot \boldsymbol{\sigma}^M = \rho \mathbf{f}^m = \mu_0 (\nabla \mathbf{H}) \mathbf{M} \,, \tag{5.12}$$

$$\mathrm{skw}\,(\boldsymbol{\sigma}^M) = -\rho \mathbf{L}^m = -\mathrm{skw}\,(\mu_0 \mathbf{M} \otimes \mathbf{H}) \,. \tag{5.13}$$

The body couple vector $\rho \mathbf{l}^m$ is the dual vector of $\rho \mathbf{L}^m$ such that $\mathbf{L}^m \mathbf{a} = \mathbf{l}^m \times \mathbf{a}$ for any

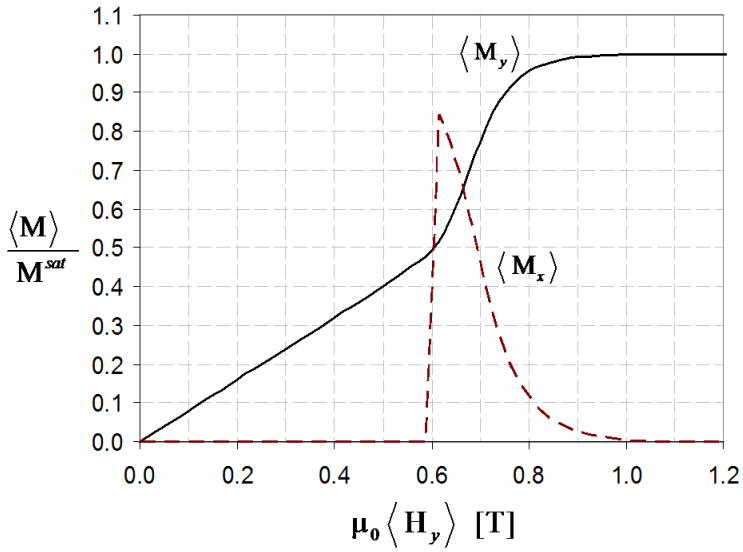

Fig. 57. The x and y-components of the corrected magnetization curves used in the Fe-analysis.

vector $\mathbf{a}$. We investigate the distributions of the magnetic body force, body couple and Maxwell stress based on the numerical solution of the magnetostatic problem at the exemplary applied magnetic induction value of $\mu_0 \langle H_y \rangle = 1\,\mathrm{T}$. We chose this load

level because, as evident from Fig. 57, it is close to the end of the reorientation region, where the intensity of the magnetic field is high.

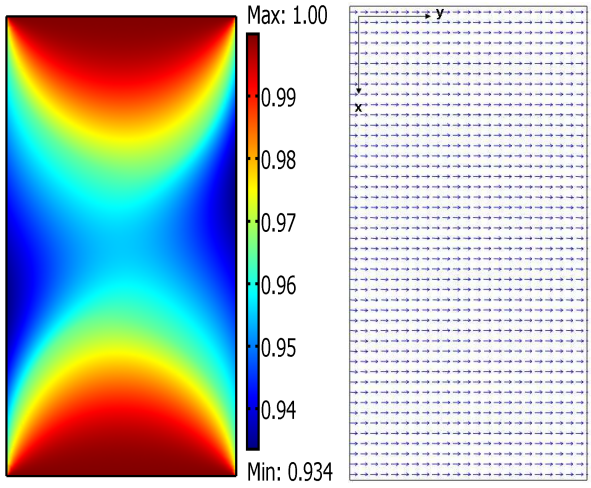

(a) (b)

Fig. 58. (a) Field-induced martensitic volume fraction and (b) normalized magnetization vector distribution at $\mu_0\langle H_y\rangle = 1$ T.

A contour plot of the field-favored variant volume fraction ξ is depicted in Fig. 58(a). The legend shows that ξ ranges from 0.93 to 1.0, such that at this load level the reorientation process is either finished or near completion at every point in the sample. Correspondingly, the normalized magnetization vectors of Fig. 58(b) are aligned with the applied field direction.

The four planar components of the non-symmetric Maxwell stress at the considered load level are shown in Figs. 59 and 61. Highly non-uniform distributions of the Maxwell stress components are observed, which through 5.11 are directly correlated with the spatially inhomogeneous magnetic field and magnetization field. Specific values of the Maxwell stress components are listed in Table XXX for the representative locations P_0 to P_8 indicated in Fig.60.

Note that the σ^M_{xx} component is purely compressive in nature. Furthermore,

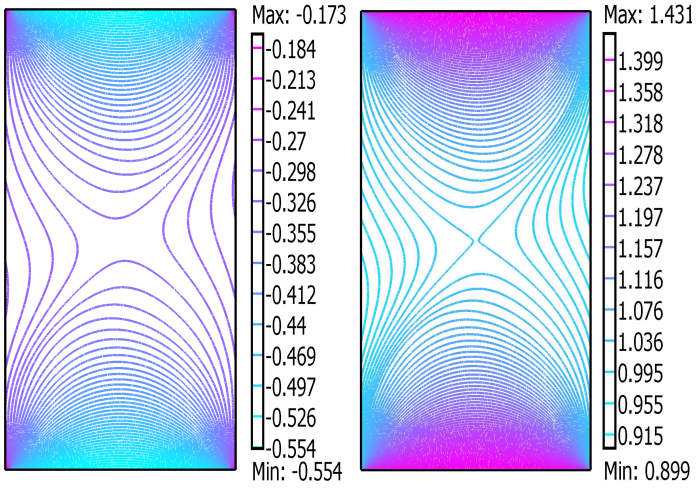

(a) (b)

Fig. 59. (a) σ^M_{xx} and (b) σ^M_{yy}-component distribution of the Maxwell stress (MPa) at $\mu_0\langle H_y\rangle = 1$ T.

magnitudes of nearly 21% of the applied traction of -2 MPa are observed. This implies that this component could potentially influence the formation of the stress-favored variant significantly. The σ^M_{yy}-component on the other hand is tensile, which, however, would enhance the tendency to hinder the forward reorientation process.

According to (5.13b), the σ^M_{xy} and σ^M_{yx} components displayed in Fig. 61 are directly correlated with the magnetic body couple. The computed body couple component values are given in Table XXXI for the selected points. If we consider point P_2, for example, the value of the magnetic moment is $0.039\,\mathrm{Nmm/mm^3}$ and it acts clockwise. The shear stress components at this point are $\sigma^M_{xy} = -0.163$ MPa and $\sigma^M_{yx} = -0.085$ MPa, see Table XXX, and they contribute to balance the magnetic body couple.

Fig. 62(a) shows the non-uniform variation of the magnetic body couple at $\mu_0\langle H_y\rangle = 1$ T. The magnitude of the body couple is observed to have higher values near the corners of the sample as compared to its center. This may be explained

	P_0	P_1	P_2	P_3	P_4	P_5	P_6	P_7	P_8
σ_{xx}^M	-0.336	-0.444	-0.416	-0.329	-0.416	-0.444	-0.416	-0.329	-0.416
σ_{yy}^M	1.011	1.227	1.178	0.996	1.178	1.227	1.178	0.996	1.178
σ_{xy}^M	-0.036	0.004	-0.163	-0.032	0.173	0.005	-0.163	-0.032	0.173
σ_{yx}^M	0.000	0.003	-0.085	0.001	0.090	0.002	-0.085	0.001	0.090

Table XXX. Maxwell stresses (MPa) at $\mu_0\langle H_y\rangle = 1$ T.

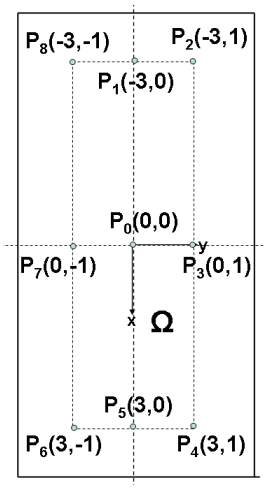

Fig. 60. Location of nine representative points at which the numerical solution is explored in detail. Here Ω represents material domain

by the fact that the body couple vector is computed from the cross product between the magnetic field and magnetization vectors, such that high values result close to the corners, where the magnetic field intensifies and larger relative angles between these vectors occur. This is also illustrated in Fig. 62(b). Here, the two sets of arrows at each point represent magnetization vectors (light arrows) and magnetic field vectors (dark arrows), respectively. It should be noted, that the magnetic field vector changes orientation from the corner region C_1 to C_2, see Fig. 62(a). Due to the point-

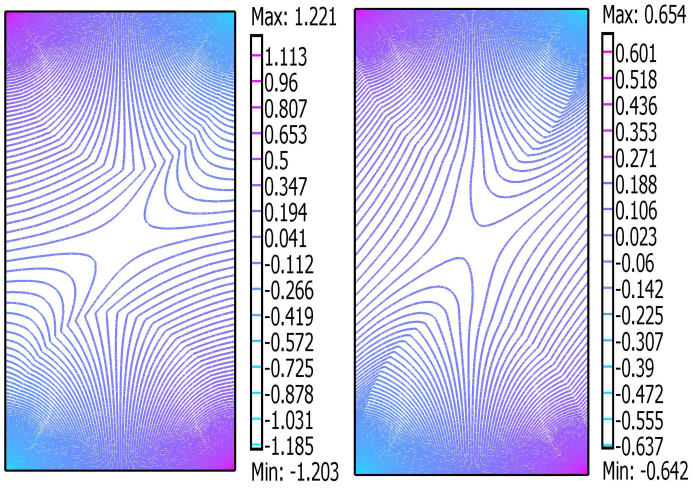

(a) (b)

Fig. 61. (a) σ_{xy}^{M} and (b) σ_{yx}^{M}-component distribution of Maxwell stress (MPa) at $\mu_0\langle H_y\rangle = 1$ T.

	P_0	P_1	P_2	P_3	P_4	P_5	P_6	P_7	P_8
ρL^m	0.018	-0.001	0.039	0.021	-0.041	-0.001	0.039	0.02	0.041

Table XXXI. Out of plane body couple vector (Nmm/mm^3) at $\mu_0\langle H_y\rangle = 1$ T. The positive sign means anti-clockwise and the negative negative sign means clockwise direction.

symmetric nature of the numerical solution, an opposite trend of the sign change is observed between regions C_3 to C_4. The shear stress components show a similar trend in their spatial distributions.

The intensity of the body force on the other hand depends on the gradient of the magnetic field. Spatial distributions of the body force components are plotted in Fig. 63 and corresponding numerical values for points P_0 to P_8 are given in Table XXXII. Since the gradient of magnetic field is high near the sample corners, the body force are large in these regions. Their magnitude decreases near the center of

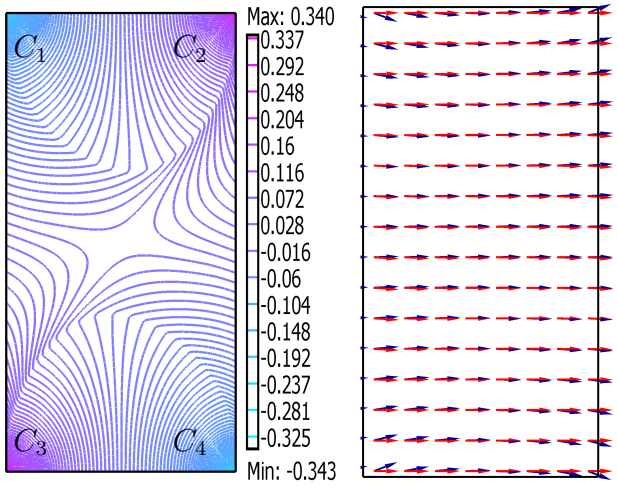

(a) (b)

Fig. 62. (a) Magnetic body couple at $\mu_0\langle H_y\rangle = 1$ T and (b) orientation of magnetization and magnetic field vectors.

the specimen, where the magnetic field distribution is relatively uniform.

	P_0	P_1	P_2	P_3	P_4	P_5	P_6	P_7	P_8
ρf_x^m	-0.001	-0.080	-0.077	0.005	0.078	0.080	0.077	-0.005	-0.080
ρf_y^m	0.000	0.000	-0.046	-0.012	-0.045	0.000	0.046	0.012	0.045

Table XXXII. Body force values (N/mm^3) at $\mu_0\langle H_y\rangle = 1$ T.

E. Finite Element Analysis of the Magneto-Mechanically-Coupled Field Equations for MSMA

The results in the previous section show that the intensity of the Maxwell stress components is significant compared to the applied tractions. This observation motivates us to solve a *coupled magneto-mechanical problem* to investigate the influence of the magnetic body forces and body couples on the Cauchy stress in an equilibrium

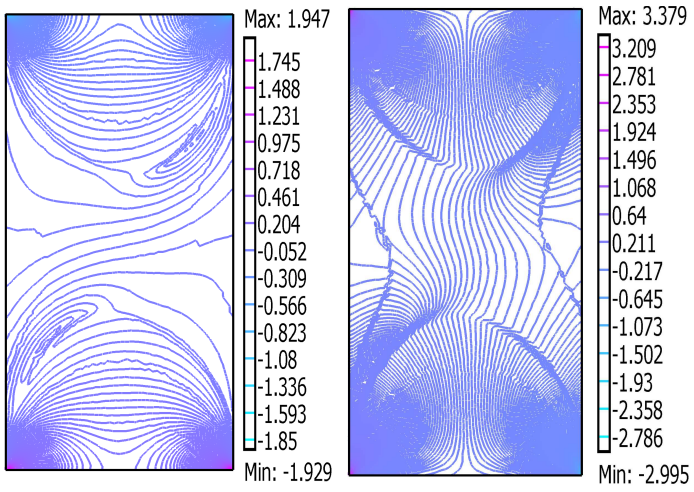

(a) (b)

Fig. 63. (a) ρf_x^m and (b) ρf_x^m component distributions (N/mm^3) at $\mu_0\langle H_y\rangle = 1$ T.

configuration. The magnetic boundary conditions are the same as described for the magnetostatic problem. The mechanical boundary conditions of the problem are illustrated in Fig. 64, where t_x and t_y denote the mechanical traction on the boundaries along the x- and the y-directions, respectively. The compressive traction along the x-direction is imposed by constraining the vertical displacement U of the $\partial\Omega_3$ surface and by applying a mechanical load $P = 2$ MPa on the $\partial\Omega_1$ surface. We fixed the point R to eliminate rigid body motion in the finite element analysis.

In addition to the field equations of the magnetostatic problem described in Section A, the magneto-mechanical problem is described by the conservation of linear momentum and the conservation of angular momentum for the magnetic continuum [123, 124]

$$\nabla\cdot\boldsymbol{\sigma} + \rho\mathbf{f} + \rho\mathbf{f}^m = \mathbf{0} \qquad \text{in } \Omega\,, \tag{5.14a}$$

$$\operatorname{skw}\boldsymbol{\sigma} = \rho\mathbf{L}^m \quad \text{in } \Omega\,. \tag{5.14b}$$

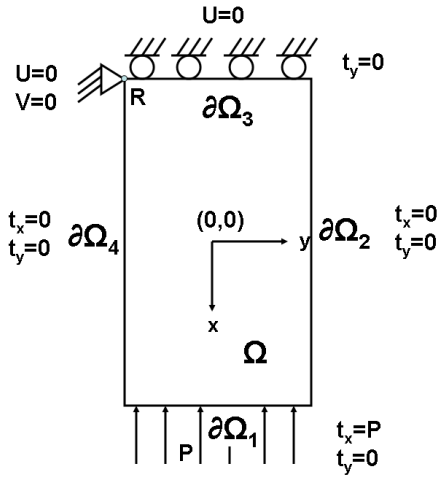

Fig. 64. Imposed mechanical boundary conditions. Ω is the material domain and $\partial\Omega$ its boundary.

The expressions for the Maxwell stress tensor, the magnetic body force and the magnetic body couple were given in Eqs. (5.11), (5.12) and (5.13). By defining the *total stress tensor* as $\boldsymbol{\sigma}^t := \boldsymbol{\sigma} + \boldsymbol{\sigma}^M$, the mechanical equilibrium equations may also be re-written in the more convenient form

$$\nabla \cdot \boldsymbol{\sigma}^t + \rho \mathbf{f} = \mathbf{0} \ , \quad \text{and} \quad \operatorname{skw} \boldsymbol{\sigma}^t = \mathbf{0} \ , \quad \text{in} \, \Omega \ . \tag{5.15}$$

A detailed derivation of the *magneto-mechanical boundary conditions* is given in the appendix.

The presence of the magnetic body couple causes the Cauchy stress tensor to be non-symmetric. The Cauchy stress may be decomposed in the following manner, see e.g. [123, 124],

$$\boldsymbol{\sigma} = \boldsymbol{\sigma}^{MT} - \mu_0 (\mathbf{H} \otimes \mathbf{M}) \ , \tag{5.16}$$

where $\boldsymbol{\sigma}^{MT}$ is a symmetric tensor that can be interpreted as the *mechanical part* of the Cauchy stress tensor. We then modify the proposed Gibbs free energy function

(4.1) by assuming a dependence on $\boldsymbol{\sigma}^{MT}$, rather then the non-symmetric Cauchy stress $\boldsymbol{\sigma}$. The modified expression is given by

$$\begin{aligned} G(\boldsymbol{\sigma}^{MT}, \boldsymbol{H}, \xi, \alpha, \theta_i, \boldsymbol{\varepsilon}^r) = &- \frac{1}{2\rho}\boldsymbol{\sigma}^{MT} : \mathcal{S}\boldsymbol{\sigma}^{MT} - \frac{1}{\rho}\boldsymbol{\sigma}^{MT} : \boldsymbol{\varepsilon}^r - \frac{\mu_0}{\rho}\boldsymbol{M}\cdot\boldsymbol{H} \\ &+ \frac{1}{\rho}f(\xi,\alpha) + G^{an}(\xi,\alpha,\theta) + G_0(T_0) \ . \end{aligned} \tag{5.17}$$

The constitutive equation for the total infinitesimal strain tensor then follows as

$$\boldsymbol{\varepsilon} = -\rho\frac{\partial G}{\partial \boldsymbol{\sigma}^{MT}} = \mathcal{S}\boldsymbol{\sigma}^{MT} + \boldsymbol{\varepsilon}^r \ , \tag{5.18}$$

or the inverse relation

$$\boldsymbol{\sigma}^{MT} = \mathbf{C} : \boldsymbol{\varepsilon}^{\mathbf{e}} = \mathbf{C} : (\boldsymbol{\varepsilon} - \boldsymbol{\varepsilon}^{\mathbf{r}}) \ . \tag{5.19}$$

The newly introduced variables are the elasticity tensor $\mathbf{C}$ and the reorientation tensor $\boldsymbol{\Lambda}$. The latter determines the direction in which the reorientation strain develops according to $\boldsymbol{\varepsilon}^r = \boldsymbol{\Lambda}\xi$ and its specific form for the considered two-dimensional problem is given in Table XXXIII. It should be noted that the constitutive relation for the magnetization remains unchanged.

Using the decomposition of the Cauchy stress (5.16) in (5.14a), the conservation of linear momentum for the magnetic continuum under static conditions and negligible non-magnetic body forces may be written as

$$\nabla\cdot(\boldsymbol{\sigma}^{MT} - \mu_0\mathbf{H}\otimes\mathbf{M}) + \rho\mathbf{f}^m = \mathbf{0} \ . \tag{5.20}$$

This expression can be simplified as follows

$$\begin{aligned} \nabla\cdot\boldsymbol{\sigma}^{MT} + [\rho\mathbf{f}^m - \nabla\cdot(\mu_0\mathbf{H}\otimes\mathbf{M})] &= \mathbf{0} \ , \\ \nabla\cdot\boldsymbol{\sigma}^{MT} + [\mu_0(\nabla\mathbf{H})\mathbf{M} - (\mu_0\mathbf{H}(\nabla\cdot\mathbf{M}) + \mu_0(\nabla\mathbf{H})\mathbf{M})] &= \mathbf{0} \ , \\ \nabla\cdot\boldsymbol{\sigma}^{MT} + [-\mu_0\mathbf{H}(\nabla\cdot\mathbf{M})] &= \mathbf{0} \ . \end{aligned} \tag{5.21}$$

Table XXXIII summarizes the coupled problem consisting of the magneto-mechanical field equations, the constitutive relations and boundary conditions. In addition to the material parameters used in the nonlinear magnetostatic analysis, isotropic mechanical properties of the martensitic phase are assumed for simplicity, with a Young's modulus of 2.0 GPa and a Poisson's ratio of 0.3 (cf. [7], [66]).

It should be emphasized that the problem solved in the finite element analysis as defined in Table XXXIII is only *partially coupled*, since the stress dependence of the magnetic response, although captured in the general formulation of the constitutive model, has been neglected. This is usually valid since all tests are preformed at a constant stress level. In the considered case the coupling thus only exists through the presence of magnetic body forces and couples in the mechanical equilibrium equations. Numerical solutions of the coupled problem in terms of the distributions of the magnetic field variables are therefore *identical* to those of the uncoupled magnetostatic problem presented in the previous section. Nonetheless, this approach is expected to yield much more realistic solutions for the Maxwell stress distributions, because they now satisfy mechanical equilibrium. Furthermore, the spatial variation of the Cauchy stress field under the influence of magnetic body forces and body couples can now be computed, which was the main objective of the numerical analysis.

The computed Cauchy stress field components are shown in the iso-line plots of Fig. 65 for the applied magnetic induction level of $\mu_0\langle H_y\rangle = 1\,\mathrm{T}$. It is observed that the Cauchy stress distribution is, as expected, also strongly non-uniform in the specimen. Detailed numerical data of these components at the nine representative points P_0 to P_8 are given in the Table XXXV.

Note that the deviation of the axial Cauchy stress σ_{xx} from the typically assumed homogeneous stress of $-2.0\,\mathrm{MPa}$ is substantial. The local relative difference of these values is listed in Table XXXIV. The results show that the change in magnitude can

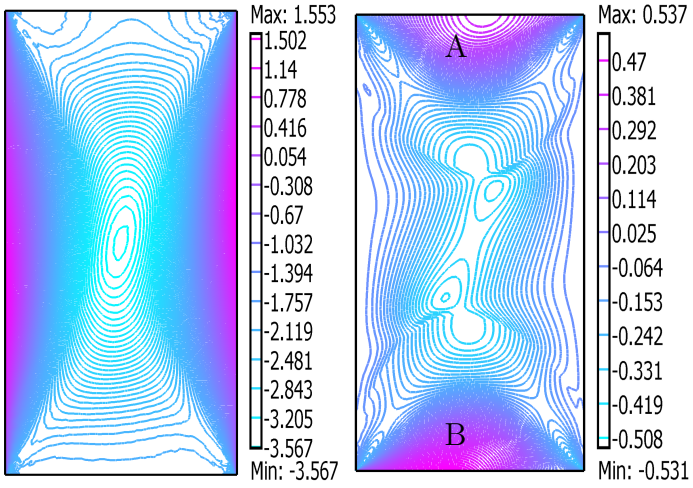

(a) (b)

Fig. 65. (a) σ_{xx} and (b) σ_{yy}-component distribution of the Cauchy stress tensor (MPa) at an applied magnetic induction level of $\mu_0\langle H_y\rangle = 1\,\mathrm{T}$.

be up to 80 %. The maximum compressive stress value of -3.58 MPa occurs at the center of the specimen. The value of the stress gradually increases from the center towards the left and right edges, where the sign changes from negative to positive. Note also that the horizontal component σ_{yy} is *non-zero* and attains values of almost -0.53 MPa as observed in Fig. 65(b). It is compressive in most of the sample, except regions A and B indicated in Fig. 65(b), where it exhibits positive values. Except for the concentrations near the corners, the magnitude of the σ_{yy} component is high around the center, where it reaches the compressive stress of largest magnitude with -0.39 MPa, and then decreases towards the edges.

It is interesting to realize that if magnetic body forces and couples are taken into account, the traction boundary conditions are also influenced by the magnetic field variables. The traction $\mathbf{t}^a$ is related to the Cauchy's formula by $\boldsymbol{\sigma}\mathbf{n} = \mathbf{t}^a$. When Maxwell stress is considered along with the Cauchy stress, an additional magneto-traction is generated. The combined traction can be calculated [113] from the jump

condition $[\![\boldsymbol{\sigma} + \boldsymbol{\sigma}^M]\!]\mathbf{n} = \mathbf{0}$. Since the *mechanical part* $\boldsymbol{\sigma}^{MT}$ of the Cauchy stress is linked with the total strain through the constitutive equation (5.19), we switched our reference stress $\boldsymbol{\sigma}$ to the symmetric mechanical stress $\boldsymbol{\sigma}^{MT}$ to solve the coupled problem. Due to this switching, the traction boundary condition modified by $\tilde{\mathbf{t}} = \boldsymbol{\sigma}^{MT}\mathbf{n}$, which is related to $\mathbf{t}^a$ through the expression (G.13). We can write

$$\tilde{\mathbf{t}}_{\partial\Omega_1} = (-2 + \mu_0 M_x H_x + \frac{\mu_0}{2} M_x^2)\mathbf{e}_x + \mu_0 M_x H_y \mathbf{e}_y \ , \tag{5.22a}$$

$$\tilde{\mathbf{t}}_{\partial\Omega_2} = \mu_0 M_y H_x \mathbf{e}_x + (\mu_0 M_y H_y + \frac{\mu_0}{2} M_y^2)\mathbf{e}_y \ , \tag{5.22b}$$

$$\tilde{\mathbf{t}}_{\partial\Omega_3} = -\mu_0 M_x H_y \mathbf{e}_y \ , \tag{5.22c}$$

$$\tilde{\mathbf{t}}_{\partial\Omega_4} = -\mu_0 M_y H_x \mathbf{e}_x + (-M_y H_y - \frac{\mu_0}{2} M_y^2)\mathbf{e}_y \ . \tag{5.22d}$$

It should be noted that the x-component of the traction in (5.22c) on $\partial\Omega_3$ is not imposed since the displacement boundary condition is given. At $\mu_0\langle H_y\rangle = 1$ T the variant reorientation process is almost complete and the M_x component is almost zero, as we explained in the previous section. So, the traction on the boundary segments $\partial\Omega_1$ and $\partial\Omega_3$ are $\tilde{t}_{x,\partial\Omega_1} \approx -2$ MPa and $\tilde{t}_{y,\partial\Omega_3} \approx 0$ MPa, respectively. The variation of the x-component of $\tilde{\mathbf{t}}$ on $\partial\Omega_2$ and $\partial\Omega_4$ is plotted in Fig. 66(a). It ranges from -0.6 MPa to 0.6 MPa and the two curves coincide at each end point due to point-symmetric behavior of H_x. The variation of the y-component $\tilde{\mathbf{t}}$ on the segments $\partial\Omega_2$ and $\partial\Omega_4$ is displayed in Fig. 66(b). In this case its magnitude exceeds 1.0 MPa.

Maxwell Equations:

$\Delta\boldsymbol{\Phi}^m = -\mu_0 \nabla \times \mathbf{M}$.

Conservation of Linear and Angular Momentum:

$\nabla \cdot \boldsymbol{\sigma}^{MT} - \mu_0 \mathbf{H}(\nabla \cdot \mathbf{M}) = \mathbf{0}$, $\quad \text{skw}(\boldsymbol{\sigma}^{MT}) = \mathbf{0}$.

Constitutive Equations:

$M_y = M_y(H_y),\ M_x = M_x(H_y)$ (Response of Fig. (57))

$\boldsymbol{\sigma}^{MT} = \mathbf{C} : (\boldsymbol{\varepsilon} - \boldsymbol{\varepsilon}^{\mathbf{r}}) \in \text{Sym}$

with $\boldsymbol{\varepsilon} = \frac{1}{2}(\nabla \mathbf{u} + \nabla \mathbf{u}^T)$, $\boldsymbol{\varepsilon}^r = \boldsymbol{\Lambda}\xi$ and

$$\boldsymbol{\Lambda} = \varepsilon^{r,max} \begin{bmatrix} 1 & 0 & 0 \\ 0 & -1 & 0 \\ 0 & 0 & 0 \end{bmatrix} .$$

Boundary Conditions:

$[\![\boldsymbol{B}]\!] \cdot \boldsymbol{n} = 0, \quad [\![\boldsymbol{H}]\!] \times \boldsymbol{n} = \mathbf{0}$,

$[\![\boldsymbol{\sigma} + \boldsymbol{\sigma}^M]\!] \cdot \mathbf{n} = \mathbf{0}$ or

$\Longrightarrow \boldsymbol{\sigma}^{MT}\mathbf{n} = \mathbf{t^a} + \frac{\mu_0}{2}(\mathbf{M}\cdot\mathbf{n})^2\mathbf{n} + \mu_0(\mathbf{H} \otimes \mathbf{M})\mathbf{n}$.

Table XXXIII. Summary of the field equations, constitutive equations and boundary conditions.

	P_0	P_1	P_2	P_3	P_4	P_5	P_6	P_7	P_8
σ_{xx}	79.0	15.5	12.5	15.0	7.5	16.0	12.5	16.0	8.5

Table XXXIV. Percentage difference in the computed local Cauchy stresses and a homogeneous stress level of -2.0 MPa at an applied induction of 1 T.

	P_0	P_1	P_2	P_3	P_4	P_5	P_6	P_7	P_8
σ_{xx}	-3.58	-2.31	-2.25	-2.30	-2.15	-2.32	-2.25	-2.32	-2.17
σ_{yy}	-0.39	-0.08	-0.10	-0.22	-0.11	-0.07	-0.11	-0.22	-0.11

Table XXXV. Cauchy stress values (MPa) at an applied induction level of 1 T.

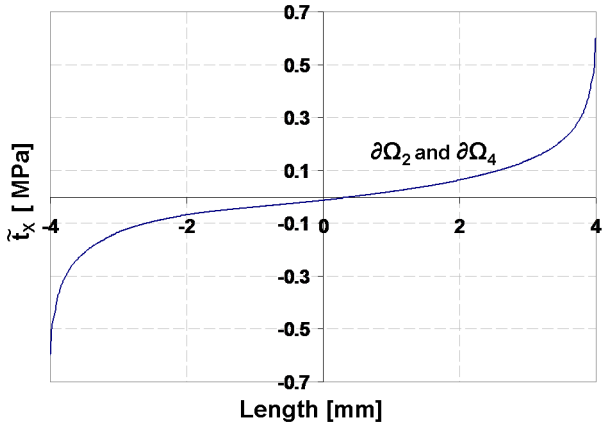

(a)

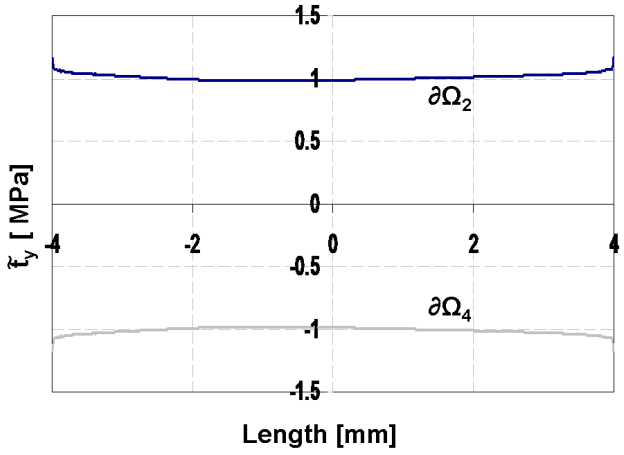

(b)

Fig. 66. Variation of the mechanical traction components on $\partial\Omega_2$ and $\partial\Omega_4$ at $\mu_0\langle H_y\rangle = 1$ T (a) x-components and (b) y-components.

CHAPTER VI

STABILITY ANALYSIS OF MSMA*

One of the major challenges for understanding the magnetostatic response of the MSMAs is the experimental measurement of the magnetic field inside the material. The measurements of the magnetic field are strongly influenced by the shape and size of the specimens [30]. During the reorientation process, the nonuniformity caused by the shape effect combined with the strong nonlinear constitutive response in magnetization leads to localization of the numerical solution. The magnetic field during reorientation changes drastically from the center of the specimen to the boundaries where the mechanical load is applied [171] and band like zones appear. The band zones gradually disappear at the end of the reorientation process at high levels of applied magnetic field. Motivated by the above observations, in the present work we study theoretically the character of the magnetostatic system of equations. The equations of the magnetostatic problem are derived in a non-dimensional form. The obtained results from the boundary value problem are analyzed in the third section by performing stability analysis and a parametric study. In the final two sections we discuss the obtained results and we present the major conclusions of this work

A. Non-Dimensional Magnetostatic Equations

Based on the previous discussion, four material parameters, M^{sat}, ρK_1, $H_y^{s(1,2)}$ and $H_y^{f(1,2)}$, are required to calibrate the constitutive equations. These are the saturation magnetization, the magnetic anisotropy constant, and the critical material parameters

*Portions of this chapter were reproduced with permission from SAGE publication for the published work by K. Haldar, G. Chatzigeorgiou, D.C Lagoudas. "Stability Analysis of Magnetostatic Boundary Value Problems for Magnetic SMAs", Journal of Intelligent Material Systems and Structures, Vol. 21, 2010, pp.1103-1116.

which denote forward reorientation start and forward reorientation finish respectively. Non-dimensionalization of the equations reduces the number of necessary parameters to 3, and allows an easier parametric study of the problem. For the non-dimensional representation of the magnetostatic problem in the 2-D special case, we introduce the non-dimensional spatial coordinates $\widehat{x} = x/L$ and $\widehat{y} = y/W$ where L and W are the characteristic lengths along the x and y axis respectively. The aspect ratio of the geometry is defined by

$$\ell = L/W. \tag{6.1}$$

The non-dimensional form of the 2-D Maxwell equations, using (5.1), are given by

$$\frac{\partial \widehat{B}_x}{\partial \widehat{x}} + \ell \frac{\partial \widehat{B}_y}{\partial \widehat{y}} = 0, \tag{6.2}$$

$$\ell \frac{\partial \widehat{H}_x}{\partial \widehat{y}} - \frac{\partial \widehat{H}_y}{\partial \widehat{x}} = 0, \tag{6.3}$$

while the constitutive relation $\mathbf{B} = \mu_0(\mathbf{H} + \mathbf{M})$ becomes

$$\widehat{B}_x = \frac{1}{\widehat{k}}\widehat{H}_x + \widehat{M}_x, \quad \widehat{B}_y = \frac{1}{\widehat{k}}\widehat{H}_y + \widehat{M}_y, \tag{6.4}$$

where

$$\begin{gathered} \widehat{B}_x = \frac{B_x}{\mu_0 M^{sat}}, \quad \widehat{B}_y = \frac{B_y}{\mu_0 M^{sat}}, \quad \widehat{H}_x = \frac{\widehat{k} H_x}{M^{sat}}, \quad \widehat{H}_y = \frac{\widehat{k} H_y}{M^{sat}}, \\ \widehat{M}_x = \frac{M_x}{M^{sat}}, \quad \widehat{M}_y = \frac{M_y}{M^{sat}}, \quad \widehat{k} = \frac{\mu_0 (M^{sat})^2}{2\rho K_1}. \end{gathered} \tag{6.5}$$

Taking advantage of the specific form of (5.1), the magnetostatic problem is often reformulated by deriving the magnetic field strength from a scalar potential or the flux density from a vector potential $\boldsymbol{A}$. In the latter case $\boldsymbol{B} = \nabla \times \boldsymbol{A}$ identically satisfies the first of (5.1). In non-dimensional form, we are defining $\widehat{\nabla} = L\nabla = \frac{\partial}{\partial \widehat{x}} + \ell \frac{\partial}{\partial \widehat{y}}$ and $\widehat{\boldsymbol{A}} = \boldsymbol{A}/L\mu_0 M^{sat}$ such that $\widehat{\boldsymbol{B}} = \widehat{\nabla} \times \widehat{\boldsymbol{A}}$. The vector potential $\widehat{\boldsymbol{A}} = \widehat{\boldsymbol{A}}(\widehat{x}, \widehat{y})$, in the component form can be written as $\widehat{\boldsymbol{A}} = \{\widehat{A}_x(\widehat{x}, \widehat{y}), \widehat{A}_y(\widehat{x}, \widehat{y}), \widehat{A}_z(\widehat{x}, \widehat{y})\}$. Using the

identity $\widehat{\nabla}\times(\widehat{\nabla}\times\widehat{\boldsymbol{A}})=\widehat{\nabla}(\widehat{\nabla}\cdot\widehat{\boldsymbol{A}})-\widehat{\Delta}\widehat{\boldsymbol{A}}$, the Coulomb gauge $\widehat{\nabla}\cdot\widehat{\boldsymbol{A}}=0$ and equation (5.1b), we get

$$\widehat{\nabla}\times(\widehat{\nabla}\times\widehat{\boldsymbol{A}}-\widehat{\boldsymbol{M}})=\boldsymbol{0}\quad\text{or}\quad\widehat{\Delta}\widehat{\boldsymbol{A}}=-\widehat{\nabla}\times\widehat{\boldsymbol{M}},\tag{6.6}$$

which is the vector-valued Poisson equation for the magnetic potential $\widehat{\boldsymbol{A}}$. Here we also used the non-dimensional constitutive equation (6.4). Under the condition (4.4), the vector valued potential equation (6.6) reduces to

$$\widehat{\triangle}\widehat{A}_x=0,\tag{6.7}$$

$$\widehat{\triangle}\widehat{A}_y=0,\tag{6.8}$$

$$\widehat{\triangle}\widehat{A}_z=-(\frac{\partial\widehat{M}_y}{\partial\widehat{x}}-\ell\frac{\partial\widehat{M}_y}{\partial\widehat{y}}).\tag{6.9}$$

Using $\widehat{\phi}=\widehat{A}_z$, the spatial derivatives of $\widehat{M}_x$ and $\widehat{M}_y$ with respect to $\widehat{y}$ and $\widehat{x}$ respectively can be written in the following form.

$$\begin{aligned}\frac{\partial\widehat{M}_x}{\partial\widehat{y}}&=\frac{d\widehat{M}_x}{d\widehat{H}_y}\frac{\partial\widehat{H}_y}{\partial\widehat{y}}=\frac{d\widehat{M}_x}{d\widehat{H}_y}(\frac{\partial\widehat{B}_y}{\partial\widehat{y}}/\frac{d\widehat{B}_y}{d\widehat{H}_y})=-\frac{d\widehat{M}_x}{d\widehat{H}_y}(\frac{\partial^2\widehat{\phi}}{\partial\widehat{x}\partial\widehat{y}}/\frac{d\widehat{B}_y}{d\widehat{H}_y}),\\ \frac{\partial\widehat{M}_y}{\partial\widehat{x}}&=\frac{d\widehat{M}_y}{d\widehat{H}_y}\frac{\partial\widehat{H}_y}{\partial\widehat{x}}=\frac{d\widehat{M}_y}{d\widehat{H}_y}(\frac{\partial\widehat{B}_y}{\partial\widehat{x}}/\frac{d\widehat{B}_y}{d\widehat{H}_y})=-\frac{d\widehat{M}_y}{d\widehat{H}_y}(\frac{\partial^2\widehat{\phi}}{\partial\widehat{x}^2}/\frac{d\widehat{B}_y}{d\widehat{H}_y}).\end{aligned}\tag{6.10}$$

In the constitutive relation (6.4), $\widehat{M}_y$ is a function only of $\widehat{H}_y$. Differentiating (6.4b) with respect to $\widehat{H}_y$ we get

$$\frac{d\widehat{B}_y}{d\widehat{H}_y}=\frac{1}{\widehat{k}}+\frac{d\widehat{M}_y}{d\widehat{H}_y}.\tag{6.11}$$

Substituting equation (6.10) in (6.9) and using (6.11), we get

$$\frac{\partial^2\widehat{\phi}}{\partial\widehat{x}^2}+\ell\widehat{k}\frac{d\widehat{M}_x}{d\widehat{H}_y}\frac{\partial^2\widehat{\phi}}{\partial\widehat{x}\partial\widehat{y}}+\ell^2\left(1+\widehat{k}\frac{d\widehat{M}_y}{d\widehat{H}_y}\right)\frac{\partial^2\widehat{\phi}}{\partial\widehat{y}^2}=0.\tag{6.12}$$

For the expressions $\frac{d\widehat{M}_x}{d\widehat{H}_y}$ and $\frac{d\widehat{M}_y}{d\widehat{H}_y}$ one needs to use the constitutive relations of the previous section. In non-dimensional form we have

1. **before reorientation**

$$\widehat{M}_x = 0, \quad \widehat{M}_y = \widehat{H}_y, \quad (\widehat{H}_y \leq \widehat{H}_y^{s(1,2)}), \tag{6.13}$$

2. **during reorientation**

$$\widehat{M}_x = (1-\xi)\sqrt{1-\widehat{H}_y^2}, \quad \widehat{M}_y = \xi + (1-\xi)\widehat{H}_y, \quad (\widehat{H}_y^{s(1,2)} \leq \widehat{H}_y \leq \widehat{H}_y^{f(1,2)}), \tag{6.14}$$

respectively with the condition $|\widehat{H}_y| \leq 1$ and

3. **after reorientation**

$$\widehat{M}_x = 1, \quad \widehat{M}_y = 0, \quad (\widehat{H}_y \geq \widehat{H}_y^{f(1,2)}). \tag{6.15}$$

Here, ξ is continuous and differentiable with respect to $\widehat{H}_y$. The expression of ξ with the non-dimensional variables is derived from (4.12) and one can rewrite ξ by,

$$\xi = \frac{1}{2} cos\left[\widehat{F}_1\left(\frac{1}{2}\widehat{H}_y^2 - \widehat{H}_y\right) + \widehat{F}_2 + \pi\right] + \frac{1}{2}, \quad \widehat{H}_y^{s(1,2)} \leq \widehat{H}_y \leq \widehat{H}_y^{f(1,2)}. \tag{6.16}$$

The non-dimensional magnetic field values $\widehat{H}_y^{s(1,2)}$ and $\widehat{H}_y^{f(1,2)}$ are the critical non-dimensional material parameters which denote forward reorientation start and forward reorientation finish respectively. The terms $\widehat{F}_1$ and $\widehat{F}_2$ are given by

$$\widehat{F}_1 = \frac{2\pi}{(\widehat{H}_y^{s(1,2)} - \widehat{H}_y^{f(1,2)})(\widehat{H}_y^{s(1,2)} + \widehat{H}_y^{f(1,2)} - 2)}, \tag{6.17}$$

$$\widehat{F}_2 = \frac{\pi \widehat{H}_y^{s(1,2)}(2 - \widehat{H}_y^{s(1,2)})}{(\widehat{H}_y^{s(1,2)} - \widehat{H}_y^{f(1,2)})(\widehat{H}_y^{s(1,2)} + \widehat{H}_y^{f(1,2)} - 2)}. \tag{6.18}$$

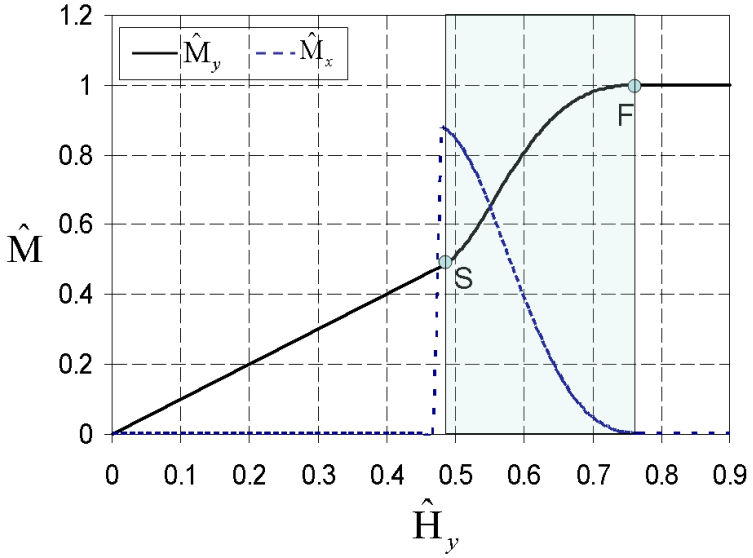

Fig. 67. Non-dimensional magnetic constitutive response of $\widehat{M}_x$ and $\widehat{M}_y$ (Equations (6.13), (6.14) and (6.15)) with respect to non-dimensional magnetic field $\widehat{H}_y$. S and F represent the starting and the finishing points of the reorientation process.

A typical magnetization response, after calibration is presented in Figure 67. In this study, motivated by Ni_2MnGa material data, we choose $\widehat{H}_y^{s(1,2)} = 0.480$ and $\widehat{H}_y^{f(1,2)} = 0.768$. The non-dimensional form of the magnetostatic problem requires three material parameters, $\widehat{k}$, $\widehat{H}_y^{s(1,2)}$ and $\widehat{H}_y^{f(1,2)}$.

B. Finite element results of the magnetostatic problem

As demonstrated in the Figure 48, we have two regions. We denote the MSMA sample by domain Ω_m and the surrounding free space by Ω_{fs}. In the whole domain, (6.9) is

defined in the following way

$$\widehat{\triangle}\widehat{\phi} = 0, \quad \widehat{\phi} \in \Omega_{fs}, \tag{6.19}$$

$$\frac{\partial^2\widehat{\phi}}{\partial\widehat{x}^2} + \ell\widehat{k}\frac{d\widehat{M}_x}{d\widehat{H}_y}\frac{\partial^2\widehat{\phi}}{\partial\widehat{x}\partial\widehat{y}} + \ell^2\left(1 + \widehat{k}\frac{d\widehat{M}_y}{d\widehat{H}_y}\right)\frac{\partial^2\widehat{\phi}}{\partial\widehat{y}^2} = 0, \quad \widehat{\phi} \in \Omega_m. \tag{6.20}$$

For the boundary conditions, spatially constant magnetic flux is applied on all sides of the boundary $\partial\Omega_{fs}$, or, more precisely, the potential

$$\widehat{A}_x = \widehat{A}_y = 0; \quad \widehat{A}_z = -\frac{1}{\widehat{k}}\widehat{H}_y^a\widehat{x}, \tag{6.21}$$

is applied. The Laplace equations $\widehat{\triangle}\widehat{A}_x = 0$ and $\widehat{\triangle}\widehat{A}_y = 0$ with the above boundary conditions give $\widehat{A}_x(\widehat{x},\widehat{y}) = \widehat{A}_y(\widehat{x},\widehat{y}) = 0$.

Here we solve a specific example with a MSMA specimen with 2:1 (ℓ=2) length to width ratio, $\widehat{k} = 0.745$, $\widehat{H}_y^{s(1,2)} = 0.480$ and $\widehat{H}_y^{f(1,2)} = 0.768$. The magnetization constitutive response for this specific geometry is considered to be the relation between material domain average of the magnetic field and magnetization vector. We will use the symbol '<>' to denote the material domain average. In the following figures the length and width of the specimens are presented with their actual dimensions.

First we select a point P_1 in the average $< \widehat{M} > - < \widehat{H}_y >$ response at $< \widehat{H}_y >= 0.248$ (Figure 68(a)), which lies in the linearly varying region 0-S. This point is well below the critical magnetic field to start the reorientation process and no reorientation occurs. The distribution of $\widehat{H}_y$ for this boundary value problem at the particular point P_1 is presented in (Figure 68(b)). The contour plot of magnetic field $\widehat{H}_y$ shows nonuniform distribution inside the specimen. It should be noted that the maximum value of $\widehat{H}_y$ is 0.288 (Figure 68(b)) where the critical value to onset the variant reorientation mechanism is 0.480. This means that new variant does not nucleate. Figure 69(a) shows the fact that the volume fraction of field induced

martensitic variant, variant-2, is zero through out the specimen.

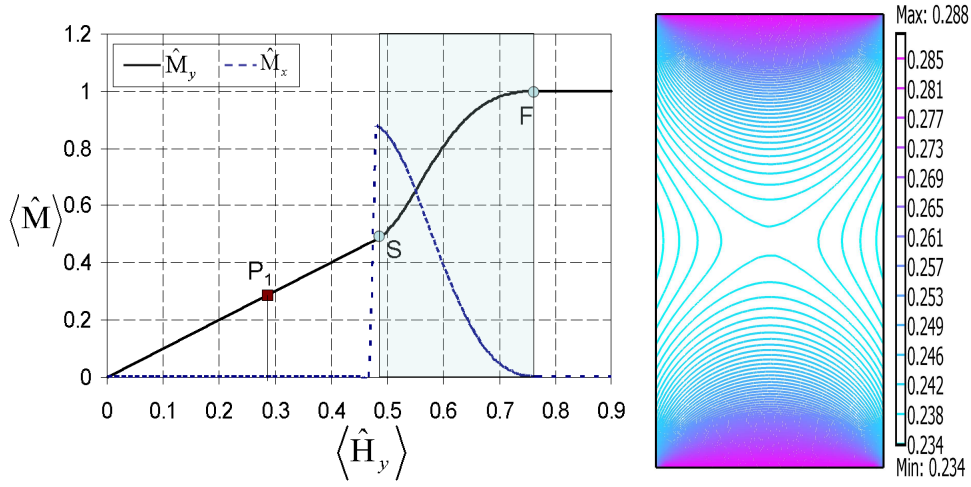

(a) (b)

Fig. 68. (a) A point P_1 which lies in the region before reorientation and (b) non-dimensional magnetic field $\widehat{H}_y$ at $< \widehat{H}_y >= 0.248$.

In Figure 69(b) we present the normalized vector plot of the magnetization vector inside the specimen and we try to track the orientation of the magnetization. In the region of no reorientation, the macroscopic magnetization vectors have non-zero component only in the y-direction as indicated in Figure 69(b).

Next, we consider a point P_2 of the average constitutive response at $< \widehat{H}_y >= 0.506$ (Figure 70(a)), in which reorientation occurs almost everywhere inside the specimen. The contour plot of the magnetic field $\widehat{H}_y$ (Figure 70(b)) demonstrates the strong nonuniform distribution of $\widehat{H}_y$ inside the specimen. In this case the new martensitic variant, which has a nonlinear relation with the magnetic field $\widehat{H}_y$ (6.16), starts to appear (Figure 71(a)). The range of magnitude of $\widehat{H}_y$ varies from 0.301 to 0.687 (Figure 70(b)) which indicates that inside the specimen we have three cases. In the first case we have very small regions where $\widehat{H}_y$ is below the starting critical value (0.480) and no reorientation occurs. In the second case we have some regions

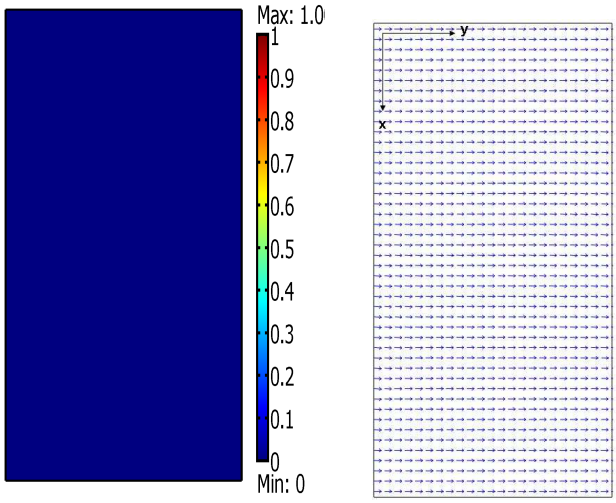

(a) (b)

Fig. 69. Distribution of (a) volume fraction of variant-2 and (b) orientation of magnetization vector at $< \widehat{H}_y >= 0.248$.

where the new variant-2 is present, but with small value of ξ, and in the the third case we observe regions where the magnetic field value is so high that it is close to the reorientation finish critical value (0.768). This observation is more clear in Figure 71(a) which represents the distribution of variant-2 volume fraction. We observe that at the regions of the top-left and bottom-right corners, the volume fraction almost reaches 1 while in the intermediate region, the volume fraction varies from 0-0.3.

In Figure 70(b) and Figure 71(a) an interesting observation is that two band like zones appear, which separate the specimen in three regions A, B, C (Figure 70(b)). The value of magnetic field or martensitic volume fraction changes abruptly across those narrow zones. For example, if we consider the region B between this narrow zones, the value of ξ is roughly 0.3. This value suddenly jumps to roughly 0.9 in regions A and C. The magnetization vector exhibits similar behavior. The direction of magnetization vectors (Figure 71(b)) also changes very sharply in the regions FG

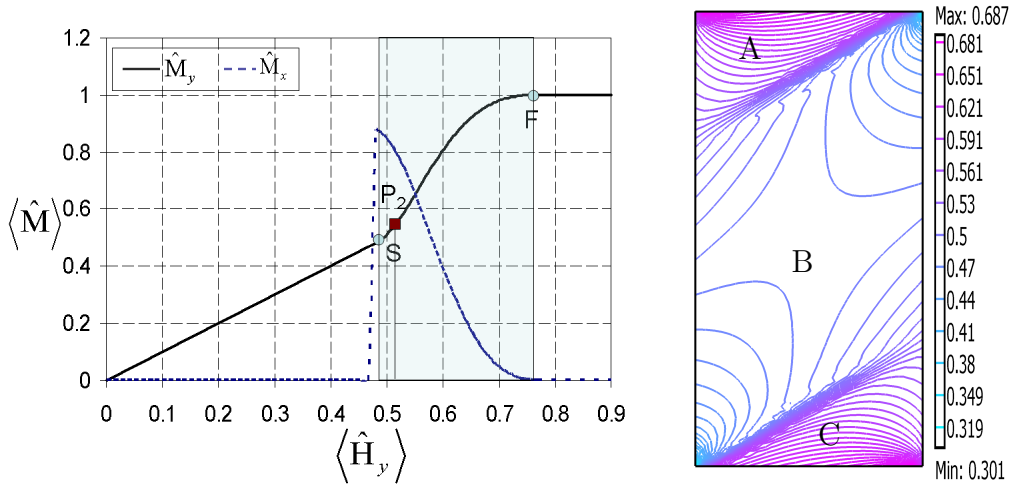

(a) (b)

Fig. 70. A point P_2 which lies in the region of reorientation and (b) non-dimensional magnetic field $\widehat{H}_y$ at $< \widehat{H}_y >= 0.506$.

and GJ. The change in direction of magnetization vectors is almost uniform in the rest of the specimen.

The point P_3 in Figure 72(a) in the average magnetization-magnetic field response also lies in the reorientation region $S-F$ but with a higher magnetic field at $< \widehat{H}_y >= 0.551$. We still observe the band like zones in the $\widehat{H}_y$ distribution (Figure 73(a)) and a sharp change in direction (Figure 71(b)) of the magnetization vectors in the regions FG and GJ. In this case, the banded zones have moved closer to each other.

Finally, we consider the point P_4 at $< \widehat{H}_y >= 0.795$ (Figure 74(a)), in which reorientation process finishes. Figure 74(b) shows that the minimum and maximum value of the nonuniformly distributed magnetic field $\widehat{H}_y$ are 0.730 and 0.964 respectively. The minimum value is very close to the critical value to finish the reorientation process (0.768). Due to this reason, we observe that the specimen is almost fully reoriented and the value of martensitic volume fraction is close to 1 everywhere inside the specimen (Figure 75(a)). Moreover, the magnetization vectors (Figure 75(b))

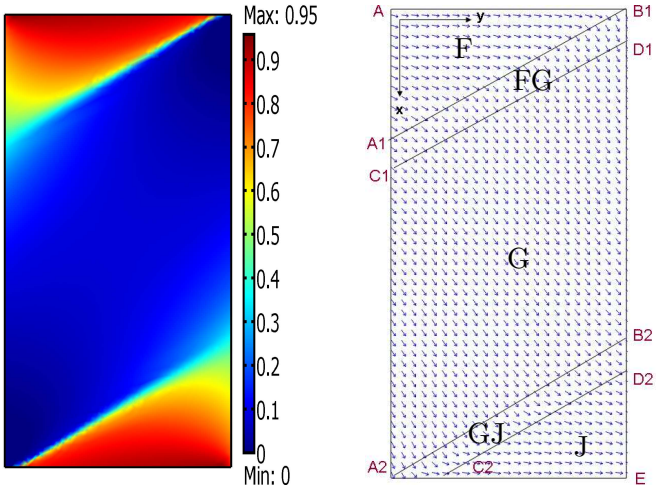

(a) (b)

Fig. 71. Distribution of (a) volume fraction of variant-2 and (b) orientation of magnetization vector at $< \widehat{H}_y >= 0.506$.

are aligned in the y axis, the direction of the easy axis of the variant-2, due to high applied magnetic field. In this case, the band like zones disappear in the distribution of $\widehat{H}_y$, martensitic volume fraction and magnetization vector.

C. Stability analysis and parametric study of forward reorientation

The numerical analysis reveals that a peculiar phenomenon occurs during the reorientation process. Two band like zones FG and GJ appear (Figure 71(b)). The appearance of band like zones can be explained by the loss of stability that occurs during reorientation. In this section we proceed to a stability analysis by investigating the magnetostatic system that we are solving. Combining equations (6.2) and (6.4), we can write,

$$\frac{\partial \widehat{H}_x}{\partial \widehat{x}} + \widehat{k}\frac{d\widehat{M}_x}{d\widehat{H}_y}\frac{\partial \widehat{H}_y}{\partial \widehat{x}} + \ell\left(1 + \widehat{k}\frac{d\widehat{M}_y}{d\widehat{H}_y}\right)\frac{\partial \widehat{H}_y}{\partial \widehat{y}} = 0. \tag{6.22}$$

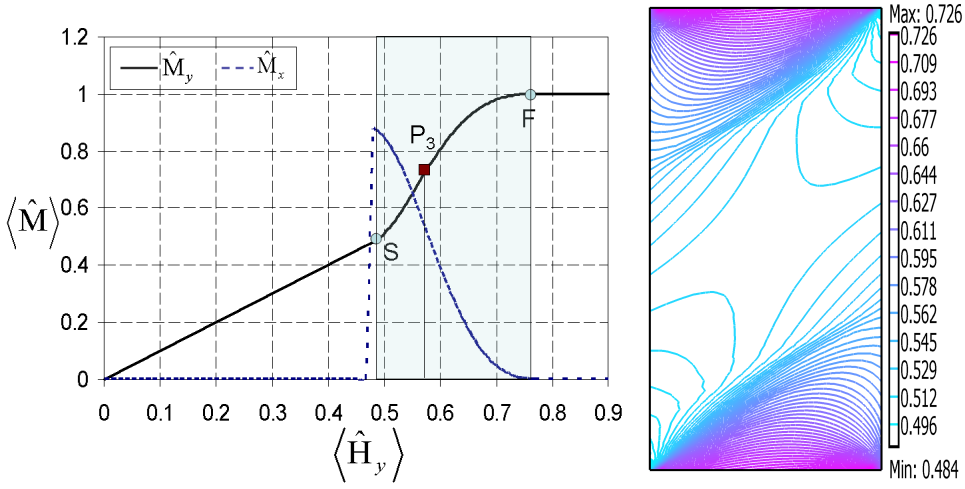

(a) (b)

Fig. 72. A point P_3 which lies in the region of reorientation and (b) non-dimensional magnetic field $\widehat{H}_y$ at $< \widehat{H}_y >= 0.551$.

Equations (6.3) and (6.22) form a system of quasi-linear partial differential equations of first order with respect to $\widehat{H}_x$ and $\widehat{H}_y$. The slopes $\frac{d\widehat{M}_x}{d\widehat{H}_y}$ and $\frac{d\widehat{M}_y}{d\widehat{H}_y}$ are obtained from the constitutive response. The compact form of this system, after some simple computations, is written

$$\frac{\partial \widehat{\boldsymbol{H}}}{\partial \widehat{x}} + \widehat{\boldsymbol{C}} \frac{\partial \widehat{\boldsymbol{H}}}{\partial \widehat{y}} = \boldsymbol{0}, \tag{6.23}$$

with

$$\widehat{\boldsymbol{H}} = \begin{bmatrix} \widehat{H}_x \\ \widehat{H}_y \end{bmatrix}, \quad \widehat{\boldsymbol{C}} = \ell \begin{bmatrix} \widehat{k} \dfrac{d\widehat{M}_x}{d\widehat{H}_y} & 1 + \widehat{k} \dfrac{d\widehat{M}_y}{d\widehat{H}_y} \\ -1 & 0 \end{bmatrix}. \tag{6.24}$$

Equation (6.23) is a system of two 1^{st} order PDEs. It should be noted that for the stability analysis, we are focusing on the 1^{st} order system, though we solved one second order PDE for the numerical analysis. The result of the stability analysis is the same for both cases. The second order PDE equation involves the magnetic

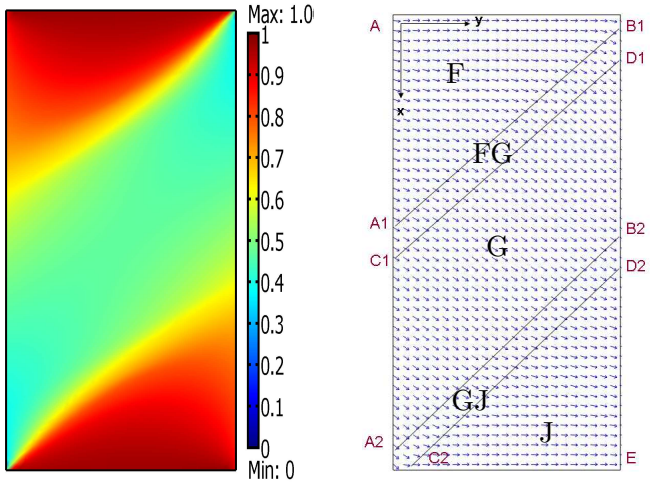

(a) (b)

Fig. 73. Distribution of (a) volume fraction of variant-2 and (b) orientation of magnetization vector at $< \widehat{H}_y >= 0.551$.

potential ϕ, which does not have a direct interpretation of the physical quantities like magnetic field, magnetic induction etc. But, when we reduce the system in the system of 1^{st} order PDEs, the variables become magnetic field components which are physical quantities.

The system can be elliptic, parabolic or hyperbolic (unstable) if $\widehat{\boldsymbol{C}}$ has two complex eigenvalues, one real eigenvalue, or two real and distinct eigenvalues respectively. If $\boldsymbol{I}$ is the identity matrix, then the equation

$$\det\left(\widehat{\boldsymbol{C}} - \lambda \boldsymbol{I}\right) = 0, \tag{6.25}$$

leads to

$$\lambda^2 - \ell\widehat{k}\frac{d\widehat{M}_x}{d\widehat{H}_y}\lambda + \ell^2\left(1 + \widehat{k}\frac{d\widehat{M}_y}{d\widehat{H}_y}\right) = 0. \tag{6.26}$$

The roots λ_1, λ_2 of (6.26) are real, only if

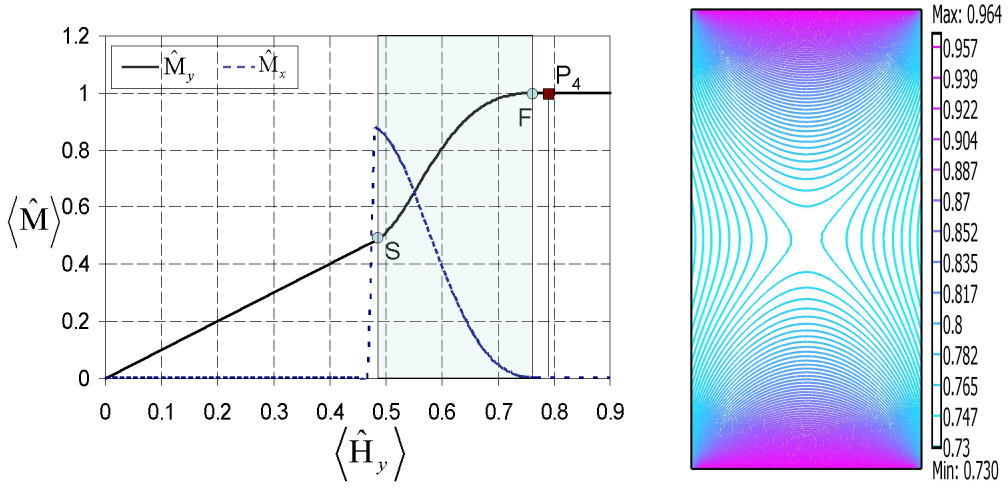

(a) (b)

Fig. 74. A point P_4 which lies in the region after reorientation and (b) non-dimensional magnetic field $\widehat{H}_y$ at $< \widehat{H}_y >= 0.795$.

$$D(\widehat{k}, \widehat{H}_y) = \widehat{k}^2 \left(\frac{d\widehat{M}_x}{d\widehat{H}_y} \right)^2 - 4 \left(1 + \widehat{k} \frac{d\widehat{M}_y}{d\widehat{H}_y} \right) \geq 0, \tag{6.27}$$

From the previous equation it is evident that the type of the system (elliptic, parabolic or hyperbolic) depends exclusively on the value of the magnetic field component $\widehat{H}_y$. It should be noted that the value of D does not depend on the aspect ratio.

Normal ferromagnetic material like α-Fe with BCC crystalline structure, if we consider idealized single crystal structure with 180^0 domain wall, does not exhibit instability under the same magnetic loading condition as described for the MSMA sample. In this case, the mechanism of magnetization is mainly based on the rotation of the magnetization vectors when magnetic field is applied along the hard axis. It should be recalled that we fixed the direction of the hard axis along the y-axis. In general, the magnetization response becomes an increasing function of the applied

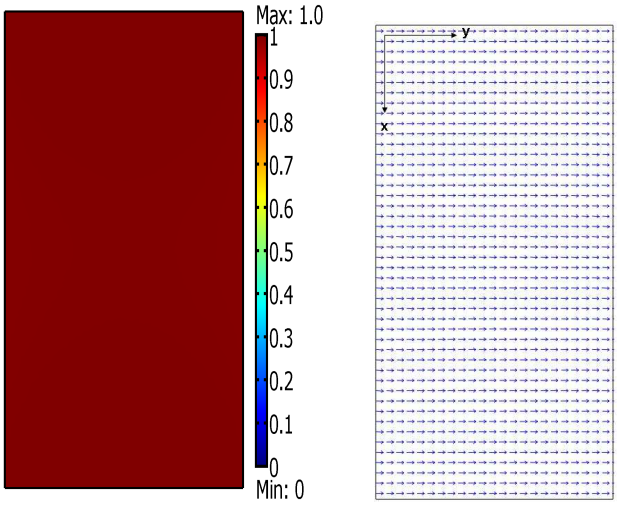

(a) (b)

Fig. 75. Distribution of (a) volume fraction of variant-2 and (b) orientation of magnetization vector at $< \widehat{H}_y >= 0.795$.

magnetic field and we will always get a non-negative slope i.e. $\frac{d\widehat{M}_y}{d\widehat{H}_y} \geq 0$. At the same time, since there is no driving force to move the domain walls, the magnetization response along the x direction is always zero. This means $\frac{d\widehat{M}_x}{d\widehat{H}_y} = 0$ and the ferromagnetic system remains always elliptic (6.27). For a ferromagnetic MSMA material, however, the case is different. The magnetic field is applied along the hard axis of the initial stress-favored variant of the MSMA specimen. Beyond a certain critical value of the applied field, a new variant nucleates due to the variant reorientation mechanism. The coexistence of two variants generates 90^0 domain walls. The new field-favored variant has its easy axis along the direction of the applied field. The critical magnetic field is high enough to eliminate the presence of 180^0 domain wall in each variant. Moreover, due to the 90^0 domain wall, stress-favored variant contributes a net magnetization along the direction perpendicular to the applied field i.e. in the x-direction. Under this condition loss of ellipticity can occur. According to the

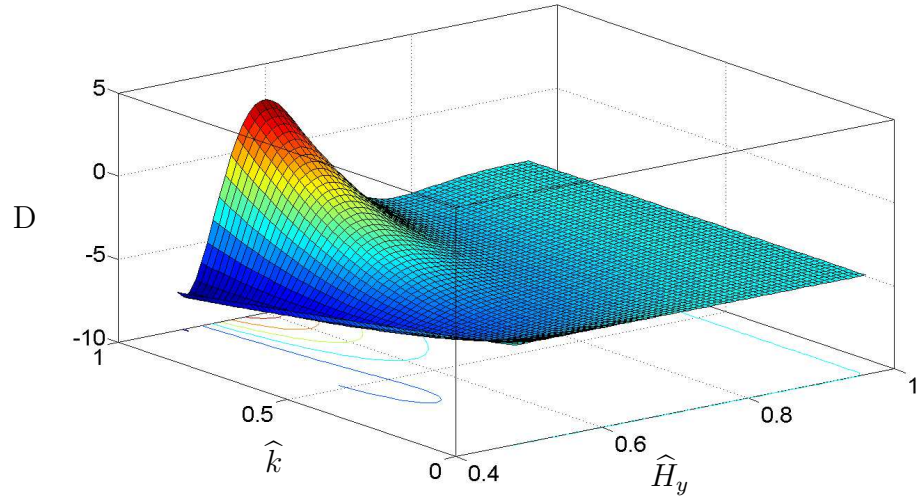

(a)

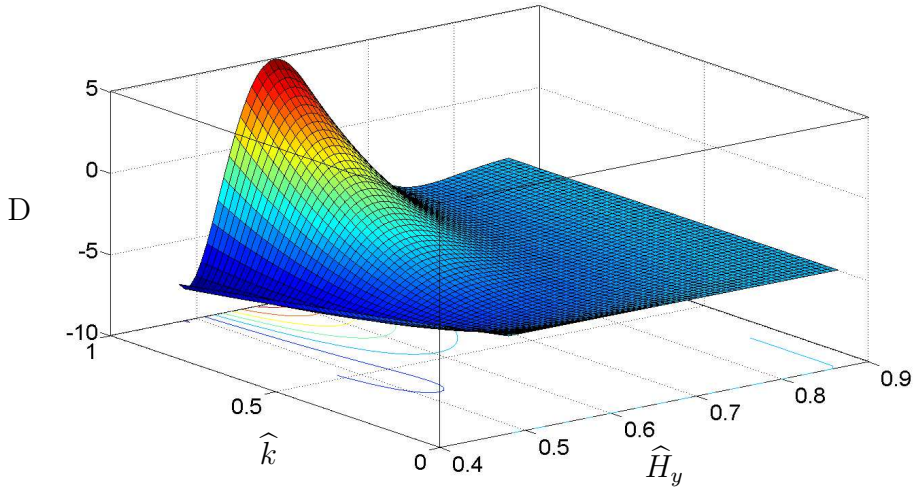

(b)

Fig. 76. Discriminant $D(\widehat{k}, \widehat{H}_y)$ at (a)$\widehat{H}_y^{f(1,2)} = 0.960$ and (b) $\widehat{H}_y^{f(1,2)} = 0.864$.

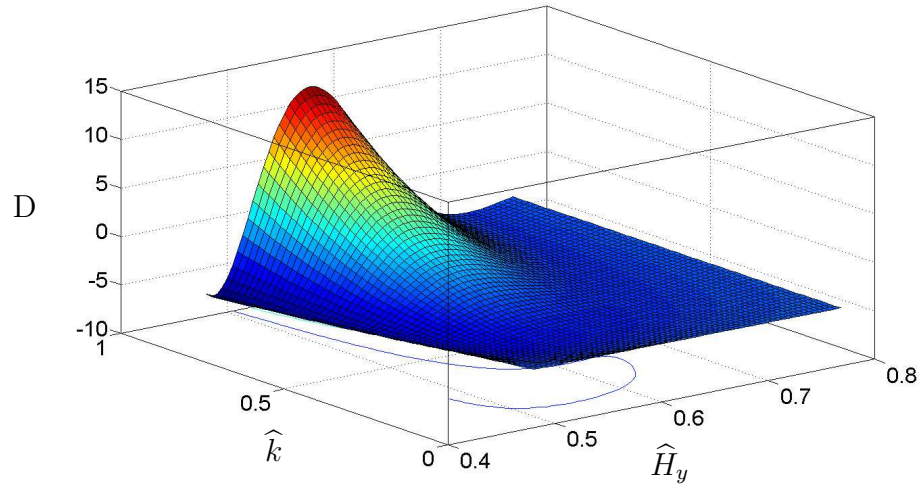

(a)

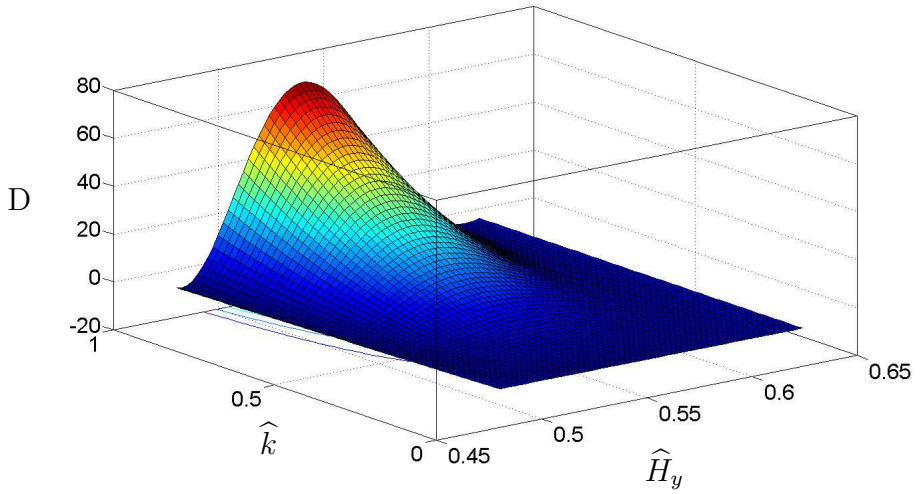

(b)

Fig. 77. Discriminant $D(\widehat{k}, \widehat{H}_y)$ at (a)$\widehat{H}_y^{f(1,2)} = 0.768$ and (b) $\widehat{H}_y^{f(1,2)} = 0.624$.

best of the authors' knowledge, no experimental results have been reported on the appearance of localization zones in any MSMA for magnetostatic loading conditions. The stability analysis performed in this paper is based on the previously developed model which has the capability to predict the nonlinear magnetization response of a MSMA. The predicted magnetization response is in good agreement with experimental results, reported in [47]. Based on this experimentally validated model, loss of stability can occur in the MSMA response under magnetostatic loading.

When the system becomes hyperbolic, there exist two families of characteristics. The differential equations which describe them are given by the solution of the quadratic equation (6.26),

$$\lambda = \frac{d\widehat{y}}{d\widehat{x}} = \frac{\ell}{2}\left(\widehat{k}\frac{d\widehat{M}_x}{d\widehat{H}_y} \pm \sqrt{\widehat{k}^2\left(\frac{d\widehat{M}_x}{d\widehat{H}_y}\right)^2 - 4\left(1+\widehat{k}\frac{d\widehat{M}_y}{d\widehat{H}_y}\right)}\right), \tag{6.28}$$

where,

$$\frac{d\widehat{M}_x}{d\widehat{H}_y} = -\frac{\widehat{H}_y(1-\xi)}{\sqrt{1-\widehat{H}_y^2}} - \frac{d\xi}{d\widehat{H}_y}\sqrt{1-\widehat{H}_y^2}, \quad \frac{d\widehat{M}_y}{d\widehat{H}_y} = (1-\xi) + \frac{d\xi}{d\widehat{H}_y}(1-\widehat{H}_y). \tag{6.29}$$

The above analysis is illustrated clearly with the help of a parametric study. The four parameters $H_y^{s(1,2)}$, $H_y^{f(1,2)}$, M^{sat}, ρK_1 that describe the constitutive material response, are reduced in the non-dimensional model to three, $\widehat{H}_y^{s(1,2)}$, $\widehat{H}_y^{f(1,2)}$ and $\widehat{k}$. We will vary $\widehat{H}_y$ from reorientation start $\widehat{H}_y^{s(1,2)}$ to reorientation finish $\widehat{H}_y^{f(1,2)}$ and $\widehat{k}$ from 0 to 1 to examine the sign of $D(\widehat{k}, \widehat{H}_y)$. We fix $\widehat{H}_y^{s(1,2)}$ at 0.480 and consider the value of $\widehat{H}_y^{f(1,2)}$ at 0.960, 0.864, 0.768 and 0.480. The fixed value $\widehat{H}_y^{s(1,2)}$=0.480 and $\widehat{H}_y^{f(1,2)}$=0.768 correspond to the real material values as described in the earlier section. Figure 76(a) represents the distribution of D where we have reorientation finish magnetic field ($\widehat{H}_y^{f(1,2)}$=0.960) higher than the real experimental value (0.768). For a fixed value of $\widehat{k}$, the value of D gradually increases with the increasing magnetic

field to a maximum value and then gradually decreases towards the end of reorientation process. This is due to the fact that the $\widehat{M}_x$-$\widehat{H}_y$ constitutive response decreases monotonically due to formation of new field-favored variant and the slope $\frac{d\widehat{M}_x}{d\widehat{H}_y}$ tends to zero. Similar trend is observed in Figure 76(b), where $\widehat{H}_y^{f(1,2)}$=0.864. The key observation is the maximum value of D increases and $D \geq 0$ for larger range of $\widehat{k}$ and for magnetic field values that are closer to the reorientation start and finish. The next case with $\widehat{H}_y^{f(1,2)}$=0.768 is presented in Figure 77(a), where higher value of D is observed and $D \geq 0$ expands in higher values of $\widehat{k}$ and in larger range between the magnetic field reorientation bounds. Finally, by decreasing the value of $\widehat{H}_y^{f(1,2)}$ to 0.624, we observe a very high value of D nearly 70 and D becomes non-negative in most of the reorientation region (Figure 77(b)). This study shows that by keeping $\widehat{H}_y^{s(1,2)}$ fixed, the instability ($D(\widehat{k}, \widehat{H}_y) \geq 0$) during reorientation becomes easier with the decrease of $\widehat{H}_y^{f(1,2)}/\widehat{H}_y^{s(1,2)}$ ratio. We can interpret the decreasing of the ratio as the faster energy release and steeper slopes of the nonlinear magnetization responses during the reorientation process. Faster dissipation means that the microstructure is changing rapidly and becomes unstable to accommodate the twin martensitic variants. The steeper nonlinear magnetization response also indicates that with a small change in magnetic field, the magnetization changes significantly and the twin structures need to be change quickly for the rapid change of the magnetization, causing unstable behavior to the material.

It is worth mentioning that the presented stability analysis results are valid for the 2-D model discussed previously. For a 3-D single crystal MSMA model the stability analysis needs to account for the anisotropic material behavior.

The appearance of the band like zones (Figure 71(a)) in the FEM analysis during reorientation is due to loss of ellipticity. The discriminant D that dictates the loss of ellipticity is given by (6.27). The plot of D at $< \widehat{H}_y >= 0.506$ is presented in Figure

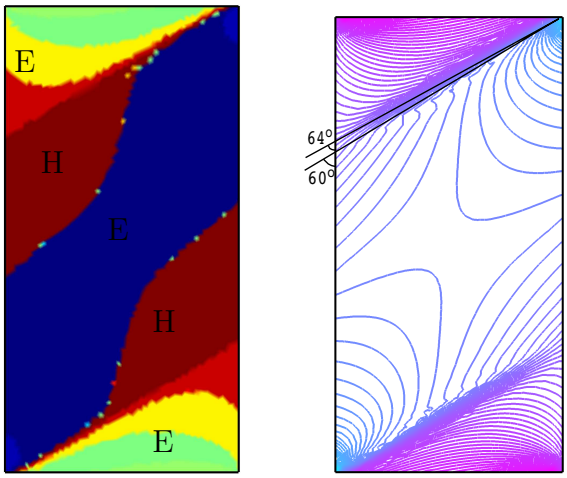

(a) (b)

Fig. 78. (a) Discriminant D at $< \widehat{H}_y >= 0.506$ and (b) jump in the magnetic field across characteristics.

78(a). The Figure shows that for $< \widehat{H}_y >= 0.506$ there are two distinct regions H where $D \geq 0$ and loss of ellipticity occurs. The stable elliptic regions (E in Figure 78(a)) with $D < 0$, which are separated by the unstable hyperbolic regions, have a completely different behavior in terms of the field variables, like the magnetic field $\widehat{H}_y$ (Figure 78(b)), the magnetization vector (Figure 71(b)) and the martensitic variant volume fraction (Figure 71(a)). This shows the drastic effect of the unstable zones appearance in the specimen response. In the absence of these hyperbolic regions, for instance before or after the reorientation process, the field variables have gradual transition in the specimen (Figures 68(b) or 74(b) respectively). In the hyperbolic zones the magnetization vector has a sudden change in direction (Figure 71(b)), especially at the areas closer to the corners.

The values of the characteristic angles in the unstable regions in the non-dimensional spatial description are given by the equation (6.28) and they vary spatially. In the present study the two characteristic angles of all the critical points are almost the

same (-60^0 and -64^0 in the actual specimen dimensions). The magnetic field shows a drastic change across characteristics that start from the top right and bottom left corners (Figure 78(b)). We need to mention that these angles refer to the actual dimensions, since in the non-dimensional spatial description, the angles that occur do not represent the real state of the specimen. It is also important to note that the characteristic angles that are computed are based on the microstructural description given in Figure 40. If the microstructural description changes, then the orientation of the characteristics will also change.

In the present study we assume that, at each material point, the magnetization vector varies only with respect to the magnetic field and does not depend on the stress level. Under this assumption, same localization zone patterns could be observed even in a fully coupled magnetomechanical BVP, where the stress varies pointwise. If the magnetization vector is a function of both the magnetic field and the stress, equation (6.22) changes and different localization patterns are expected to occur in the fully coupled case.

To understand the stability behavior more clearly, we consider some thought experiments which are demonstrated in the following examples. We consider an elliptic specimen since the interior magnetic field is always uniform. This result at $< \widehat{H}_y >= 0.348$ is demonstrated in Fig.79(a). At this field the system is hyperbolic and the whole specimen is assigned a single value of D. We do not observe any band like regions because the specimen is defect free and no disturbances are created anywhere. Next we introduce a small elliptic hole at the center of the geometry (Fig.79(b)). The hole creates singularity in the magnetic field and the disturbance is observed to propagate along the characteristic. When the magnetic field is $< \widehat{H}_y >= 0.51$, the magnetostatic system becomes elliptic. The magnetic field remains uniform when no defect is introduced (Fig.80(a)). After introducing the el-

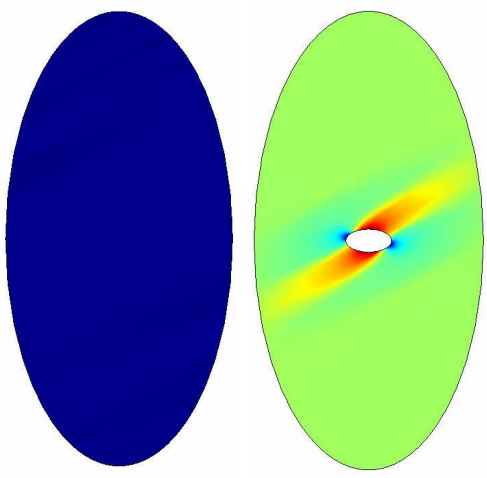

(a) (b)

Fig. 79. Distribution of magnetic field H_y at $< \widehat{H}_y >= 0.348$(hyperbolic) (a) without any defect and (b) with an elliptic hole.

liptic hole, we observe field concentration inside around the hole. But the disturbances thus created do not propagate. Since the system becomes elliptic, the concentrations remain localized around the hole (Fig.80(b)).

In the next example, we provide disturbance from the outside without introducing any defect in the body. In the thought experiment (Fig.81) we place three circular iron bars around the elliptic specimen. These bars induce concentrated magnetic field on the elliptic surface. So, in the hyperbolic condition (Fig.81(a)) the propagation of the disturbances, created by the iron rods, is observed, while the disturbances remain localized when the system is elliptic (Fig.81(b)).

D. Coupled magneto-mechanical system

The coupled system of equations are given below

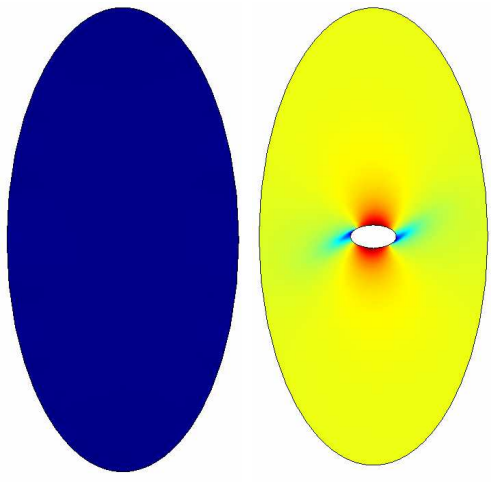

(a) (b)

Fig. 80. Distribution of magnetic field H_y at $< \widehat{H}_y >= 0.51$(elliptic) (a) without any defect and (b) with an elliptic hole.

$$\nabla \cdot \mathbf{B} = 0 \tag{6.30a}$$

$$\mathbf{B} = \mu_0(\mathbf{M} + \mathbf{H}) \tag{6.30b}$$

$$\nabla \times \mathbf{H} = \mathbf{0} \tag{6.30c}$$

$$\nabla \cdot \boldsymbol{\sigma}^E - \mu_0(\nabla \cdot \mathbf{M})\mathbf{H} = \mathbf{0} \tag{6.30d}$$

$$\text{skw}(\boldsymbol{\sigma}^E) = 0 \tag{6.30e}$$

$$\boldsymbol{\sigma}^E = \mathbb{C}(\boldsymbol{\varepsilon} - \boldsymbol{\varepsilon}^r) \tag{6.30f}$$

$$\dot{\boldsymbol{\varepsilon}}^r = \boldsymbol{\Lambda}\dot{\xi} \tag{6.30g}$$

$$\Phi(\boldsymbol{\sigma}^E, \mathbf{H}, \xi) = 0 \tag{6.30h}$$

$$\boldsymbol{\varepsilon} = \frac{1}{2}(\nabla\mathbf{u} + (\nabla\mathbf{u})^T) \tag{6.30i}$$

We denote a tensor potential $\Psi = \nabla\mathbf{u}$ for which $\boldsymbol{\varepsilon} = \frac{1}{2}(\Psi + \Psi^T)$ and we get an

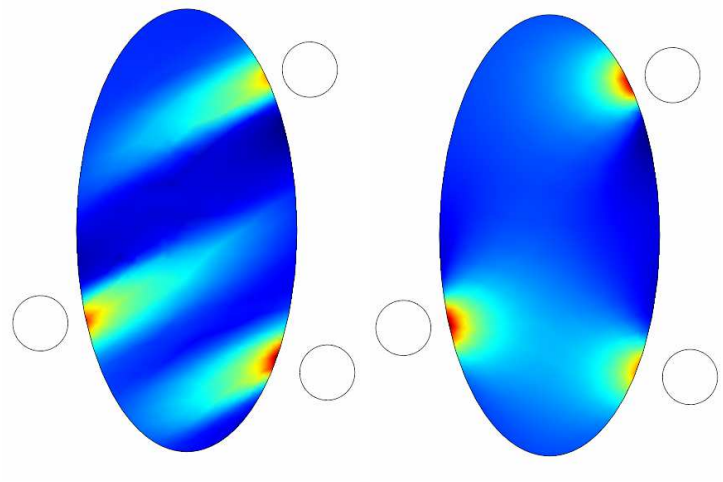

(a) (b)

Fig. 81. Ellipse with circular iron bars near the surface. Distribution of magnetic field H_y at (a) $< \widehat{H}_y >= 0.348$(hyperbolic) and at (b) $< \widehat{H}_y >= 0.51$(elliptic).

additional condition

$$\nabla \times \Psi = \mathbf{0}. \tag{6.31}$$

The tensor potential with the identity (6.31) reduces the mechanical system of equations into a first order system of equations. Now, from the consistency condition (Eq. (6.30h)) we can write

$$\begin{aligned} &\dot{\Phi}(\boldsymbol{\sigma}^E, \mathbf{H}, \xi) = 0 \\ \Rightarrow\ &\Phi_{,\boldsymbol{\sigma}^E} : \dot{\boldsymbol{\sigma}}^E + \Phi_{,\mathbf{H}} \cdot \dot{\mathbf{H}} + \Phi_{,\xi}\, \dot{\xi} = 0 \end{aligned} \tag{6.32}$$

Eq. (6.30f) can be written in the rate form as

$$\dot{\boldsymbol{\sigma}}^E = \mathbb{C}(\dot{\boldsymbol{\varepsilon}} - \dot{\boldsymbol{\varepsilon}}^{\mathbf{r}}) = \mathbb{C}(\dot{\boldsymbol{\varepsilon}} - \boldsymbol{\Lambda}\dot{\xi}) \tag{6.33}$$

and with the help of this relation we replace $\dot{\boldsymbol{\sigma}}^E$ in Eq. (6.32)

$$\begin{aligned} \Phi_{,\boldsymbol{\sigma}^E} : \mathbb{C}(\dot{\boldsymbol{\varepsilon}} - \boldsymbol{\Lambda}\dot{\xi}) + \Phi_{,\mathbf{H}} \cdot \dot{\mathbf{H}} + \Phi_{,\xi}\, \dot{\xi} = 0 \\ \Rightarrow \dot{\xi} = \frac{\Phi_{,\boldsymbol{\sigma}^E} : \mathbb{C}\dot{\boldsymbol{\varepsilon}} + \Phi_{,\mathbf{H}} \cdot \dot{\mathbf{H}}}{\Phi_{,\boldsymbol{\sigma}^E} : \mathbb{C}\boldsymbol{\Lambda} - \Phi_{,\xi}} \end{aligned} \tag{6.34}$$

Now substituting back (6.34) in (6.33) we get

$$\begin{aligned} \dot{\boldsymbol{\sigma}}^E &= \mathbb{C}\left[\dot{\boldsymbol{\varepsilon}} - \boldsymbol{\Lambda}\frac{\Phi_{,\boldsymbol{\sigma}^E} : \mathbb{C}\dot{\boldsymbol{\varepsilon}} + \Phi_{,\mathbf{H}} \cdot \dot{\mathbf{H}}}{\Phi_{,\boldsymbol{\sigma}^E} : \mathbb{C}\boldsymbol{\Lambda} - \Phi_{,\xi}}\right] \\ &= \left[\mathbb{C} - \frac{\mathbb{C}\boldsymbol{\Lambda} \otimes \mathbb{C}\Phi_{,\boldsymbol{\sigma}^E}}{\Phi_{,\boldsymbol{\sigma}^E} : \mathbb{C}\boldsymbol{\Lambda} - \Phi_{,\xi}}\right] : \dot{\boldsymbol{\varepsilon}} - \left[\frac{\mathbb{C}\boldsymbol{\Lambda} \otimes \Phi_{,\mathbf{H}}}{\Phi_{,\boldsymbol{\sigma}^E} : \mathbb{C}\boldsymbol{\Lambda} - \Phi_{,\xi}}\right] \cdot \dot{\mathbf{H}} \\ &= \mathbb{L} : \dot{\boldsymbol{\varepsilon}} - \mathbb{K} \cdot \dot{\mathbf{H}} \end{aligned} \tag{6.35}$$

Here $\mathbb{L}$ is the forth order tangent stiffness tensor and $\mathbb{K}$ is the third order magnetic stiffness tensor. We can further write (6.35)

$$\begin{aligned} \nabla\boldsymbol{\sigma}^E\dot{\mathbf{x}} &= \mathbb{L} : \nabla\boldsymbol{\varepsilon}\dot{\mathbf{x}} - \mathbb{K} \cdot \nabla\mathbf{H}\dot{\mathbf{x}} \\ \Rightarrow \nabla\boldsymbol{\sigma}^E &= \mathbb{L} : \nabla\boldsymbol{\varepsilon} - \mathbb{K} \cdot \nabla\mathbf{H} \end{aligned} \tag{6.36}$$

In indicial notation we can write,

$$\sigma^E_{ij,p} = \mathbb{L}_{ijkl}\varepsilon_{kl,p} - \mathbb{K}_{ijl}H_{l,p}\,. \tag{6.37}$$

E. Stability analysis of the coupled 2D system

We will perform the stability analysis of the 2D coupled system. The detail deduction of the 2D system of equations is given below. We first calculate the tangent stiffness

tensors $\mathbb{L}$ and $\mathbb{K}$ in 2-D. We use Voigt notation and write

$$\mathbb{C} = \begin{bmatrix} \lambda + 2\mu & \lambda & 0 \\ \lambda & \lambda + 2\mu & 0 \\ 0 & 0 & 2\mu \end{bmatrix} \tag{6.38}$$

The transformation tensor $\mathbf{\Lambda} = E^{cur}(\mathbf{e}_x \otimes \mathbf{e}_x - \mathbf{e}_y \otimes \mathbf{e}_y)$ can be written as

$$\mathbf{\Lambda} = E^{cur} \begin{bmatrix} 1 \\ -1 \\ 0 \end{bmatrix}$$

So,

$$\mathbb{C}\mathbf{\Lambda} = \begin{bmatrix} \lambda + 2\mu & \lambda & 0 \\ \lambda & \lambda + 2\mu & 0 \\ 0 & 0 & 2\mu \end{bmatrix} E^{cur} \begin{bmatrix} 1 \\ -1 \\ 0 \end{bmatrix} = 2\mu E^{cur} \begin{bmatrix} 1 \\ -1 \\ 0 \end{bmatrix}$$

Since we considered that Φ only depends on σ^E_{xx}, we can write

$$\Phi_{,\boldsymbol{\sigma}^E} = \Phi_{,\sigma^E_{xx}} \begin{bmatrix} 1 \\ 0 \\ 0 \end{bmatrix}$$

and

$$\mathbb{C}\Phi_{,\boldsymbol{\sigma}^E} = \begin{bmatrix} \lambda + 2\mu & \lambda & 0 \\ \lambda & \lambda + 2\mu & 0 \\ 0 & 0 & 2\mu \end{bmatrix} \Phi_{,\sigma^E_{xx}} \begin{bmatrix} 1 \\ 0 \\ 0 \end{bmatrix} = \Phi_{,\sigma^E_{xx}} \begin{bmatrix} \lambda + 2\mu \\ \lambda \\ 0 \end{bmatrix}$$

Therefore,

$$\mathbb{C}\mathbf{\Lambda} \otimes \mathbb{C}\Phi_{,\boldsymbol{\sigma}^E} = 2\mu E^{cur} \Phi_{,\sigma^E_{xx}} \begin{bmatrix} \lambda + 2\mu & \lambda & 0 \\ -(\lambda + 2\mu) & -\lambda & 0 \\ 0 & 0 & 0 \end{bmatrix}.$$

We denote $a = \Phi_{,\boldsymbol{\sigma}^E} : \mathbb{C}\boldsymbol{\Lambda} - \Phi_{,\xi}$, where $\Phi_{,\boldsymbol{\sigma}^E} \cdot \mathbb{C}\boldsymbol{\Lambda} = 2\mu E^{cur}\Phi_{,\sigma^E_{xx}}$ and $\beta_1 = \frac{2\mu E^{cur}\Phi_{,\sigma^E_{xx}}}{a}$.

So

$$\mathbb{L} = \mathbb{C} - \frac{\mathbb{C}\boldsymbol{\Lambda} \otimes \mathbb{C}\Phi_{,\boldsymbol{\sigma}^E}}{a} = \begin{bmatrix} \lambda+2\mu & \lambda & 0 \\ \lambda & \lambda+2\mu & 0 \\ 0 & 0 & 2\mu \end{bmatrix} - \beta_1 \begin{bmatrix} \lambda+2\mu & \lambda & 0 \\ -(\lambda+2\mu) & -\lambda & 0 \\ 0 & 0 & 0 \end{bmatrix}$$

or

$$\mathbb{L} = \begin{bmatrix} (1-\beta_1)(\lambda+2\mu) & (1-\beta_1)\lambda & 0 \\ \lambda+\beta_1(\lambda+2\mu) & \lambda+2\mu+\beta_1\lambda & 0 \\ 0 & 0 & 2\mu \end{bmatrix} \tag{6.39}$$

We considered that Φ only depends on H_y and we write

$$\Phi_{,\mathbf{H}} = \Phi_{,H_y} \begin{bmatrix} 0 \\ 1 \end{bmatrix}.$$

So,

$$\mathbb{C}\boldsymbol{\Lambda} \otimes \Phi_{,\mathbf{H}} = 2\mu E^{cur}\Phi_{,H_y} \begin{bmatrix} 0 & 1 \\ 0 & -1 \\ 0 & 0 \end{bmatrix}$$

and

$$\mathbb{K} = \beta_2 \begin{bmatrix} 0 & 1 \\ 0 & -1 \\ 0 & 0 \end{bmatrix}$$

where $\beta_2 = \frac{2\mu E^{cur}\Phi_{,H_y}}{a}$. We write,

$$\begin{bmatrix} \dot{\sigma}^E_{xx} \\ \dot{\sigma}^E_{yy} \\ \dot{\sigma}^E_{xy} \end{bmatrix} = \begin{bmatrix} (1-\beta_1)(\lambda+2\mu) & (1-\beta_1)\lambda & 0 \\ \lambda+\beta_1(\lambda+2\mu) & \lambda+2\mu+\beta_1\lambda & 0 \\ 0 & 0 & 2\mu \end{bmatrix} \begin{bmatrix} \dot{\varepsilon}_{xx} \\ \dot{\varepsilon}_{yy} \\ \dot{\varepsilon}_{xy} \end{bmatrix} + \beta_2 \begin{bmatrix} 0 & 1 \\ 0 & -1 \\ 0 & 0 \end{bmatrix} \begin{bmatrix} \dot{H}_x \\ \dot{H}_y \end{bmatrix}. \tag{6.40}$$

The rate form of the constitutive equations in 2-D can be written in the following form

$$\sigma^E_{xx,p} = (1-\beta_1)(\lambda+2\mu)\varepsilon_{xx,p} + (1-\beta_1)\lambda\varepsilon_{yy,p} + \beta_2 H_{y,p} \tag{6.41a}$$

$$\sigma^E_{yy,p} = (\lambda+\beta_1(\lambda+2\mu))\varepsilon_{xx,p} + (\lambda+2\mu+\beta_1\lambda)\varepsilon_{yy,p} - \beta_2 H_{y,p} \tag{6.41b}$$

$$\sigma^E_{xy,p} = 2\mu\varepsilon_{xy,p} \tag{6.41c}$$

where p is x or y. In 2-D we have $\Psi_{xx} = u_{x,x}\,, \Psi_{xy} = u_{x,y}\,, \Psi_{yx} = u_{y,x}\,, \Psi_{yy} = u_{y,y}$. Moreover for small strain

$$\varepsilon_{xx} = u_{x,x}\,, \quad \varepsilon_{xy} = \frac{1}{2}(u_{x,y} + u_{y,x}\,), \quad \varepsilon_{yy} = u_{y,y}\,. \tag{6.42}$$

Then we write $\varepsilon_{xx} = \Psi_{xx}, \varepsilon_{yy} = \Psi_{yy}, \varepsilon_{xy} = \frac{1}{2}(\Psi_{xy} + \Psi_{yx})$. From conservation of linear momentum we get

$$\sigma^E_{xx,x} + \sigma^E_{xy,y} + \mu_0(H_{x,x} + H_{y,y}\,)H_x = 0 \tag{6.43}$$

$$\sigma^E_{xy,x} + \sigma^E_{yy,y} + \mu_0(H_{x,x} + H_{y,y}\,)H_y = 0 \tag{6.44}$$

We calculate $\sigma^E_{xx,x}\,, \sigma^E_{xy,y}\,, \sigma^E_{xy,x}$ and $\sigma^E_{yy,y}$ from (6.41a) with $p = x$, from (6.41c) with $p = y$ and $p = x$ and from (6.41b) with $p = y$ respectively. We also write $\varepsilon_{xx,x} = \Psi_{xx,x}\,, \varepsilon_{yy,y} = \Psi_{yy,y}\,, \varepsilon_{xy,x} = \frac{1}{2}(\Psi_{xy,x} + \Psi_{yx,x}\,)$ and $\varepsilon_{xy,y} = \frac{1}{2}(\Psi_{xy,y} + \Psi_{yx,y}\,)$. From (6.41a), (6.41b) and (6.41c) we get

$$\sigma^E_{xx,x} = (1-\beta_1)(\lambda+2\mu)\Psi_{xx,x} + (1-\beta_1)\lambda\Psi_{yy,x} + \beta_2 H_{y,x} \tag{6.45a}$$

$$\sigma^E_{yy,y} = (\lambda+\beta_1(\lambda+2\mu))\Psi_{xx,y} + (\lambda+2\mu+\beta_1\lambda)\Psi_{yy,y} - \beta_2 H_{y,y} \tag{6.45b}$$

$$\sigma^E_{xy,x} = \mu(\Psi_{xy,x} + \Psi_{yx,x}\,) \tag{6.45c}$$

$$\sigma^E_{xy,y} = \mu(\Psi_{xy,y} + \Psi_{yx,y}\,) \tag{6.45d}$$

Substituting back above equations in the conservation of linear momentum (6.43) and (6.44), we get

$$(1-\beta_1)(\lambda+2\mu)\Psi_{xx,x}+(1-\beta_1)\lambda\Psi_{yy,x}+\mu(\Psi_{xy,y}+\Psi_{yx,y})$$
$$+\mu_0 H_x H_{x,x}+\mu_0 H_x H_{y,y}+\beta_2 H_{y,x}=0 \tag{6.46}$$

$$\mu(\Psi_{xy,x}+\Psi_{yx,x})+(\lambda+\beta_1(\lambda+2\mu))\Psi_{xx,y}+(\lambda+2\mu+\beta_1\lambda)\Psi_{yy,y}$$
$$+\mu_0 H_y H_{x,x}+(\mu_0 H_y-\beta_2)H_{y,y}=0 \tag{6.47}$$

Finally, equation (6.31), $\nabla\times\Psi=\epsilon_{ijk}\Psi_{mj,i}\,\mathbf{e}_k\otimes\mathbf{e}_m=\mathbf{0}$, gives two additional equations

$$\Psi_{xx,y}-\Psi_{xy,x}=0 \tag{6.48}$$

$$\Psi_{yx,y}-\Psi_{yy,x}=0 \tag{6.49}$$

The detail derivation is given in the appendix. We now consider magnetostatic system of equations. First we consider

$$\nabla\cdot\mathbf{H}=-\nabla\cdot\mathbf{M}$$
$$\Rightarrow H_{x,x}+H_{y,y}=-(M_{x,x}+M_{y,y}) \tag{6.50}$$

We assume that each of M_x and M_y only σ^E_{xx} and we write

$$M_{x,x}=\frac{\partial M_x}{\partial H_x}H_{x,x}+\frac{\partial M_x}{\partial H_y}H_{y,x}+\frac{\partial M_x}{\partial \sigma^E_{xx}}\sigma^E_{xx,x}$$
$$M_{y,y}=\frac{\partial M_y}{\partial H_x}H_{x,y}+\frac{\partial M_y}{\partial H_y}H_{y,y}+\frac{\partial M_y}{\partial \sigma^E_{xx}}\sigma^E_{xx,y} \tag{6.51}$$

or

$$\begin{aligned} M_{x,x} &= \frac{\partial M_x}{\partial H_x}H_{x,x}+\frac{\partial M_x}{\partial H_y}H_{y,x}+\frac{\partial M_x}{\partial \sigma^E_{xx}}(1-\beta_1)(\lambda+2\mu)\Psi_{xx,x} \\ &+ \frac{\partial M_x}{\partial \sigma^E_{xx}}(1-\beta_1)\lambda\Psi_{yy,x}+\frac{\partial M_x}{\partial \sigma^E_{xx}}\beta_2 H_{y,x} \\ M_{y,y} &= \frac{\partial M_y}{\partial H_x}H_{x,y}+\frac{\partial M_y}{\partial H_y}H_{y,y}+\frac{\partial M_y}{\partial \sigma^E_{xx}}(1-\beta_1)(\lambda+2\mu)\Psi_{xx,y} \\ &+ \frac{\partial M_y}{\partial \sigma^E_{xx}}(1-\beta_1)\lambda\Psi_{yy,y}-\frac{\partial M_y}{\partial \sigma^E_{xx}}\beta_2 H_{y,y} \end{aligned} \tag{6.52}$$

Substituting equations (6.52) in (6.50) we get,

$$\begin{aligned} &(1+\frac{\partial M_x}{\partial H_x})H_{x,x}+(\frac{\partial M_x}{\partial H_y}+\frac{\partial M_x}{\partial \sigma^E_{xx}}\beta_2)H_{y,x}+\frac{\partial M_x}{\partial \sigma^E_{xx}}(1-\beta_1)(\lambda+2\mu)\Psi_{xx,x} \\ &+\frac{\partial M_x}{\partial \sigma^E_{xx}}(1-\beta_1)\lambda\Psi_{yy,x}+\frac{\partial M_y}{\partial H_x}H_{x,y}+(1+\frac{\partial M_y}{\partial H_y}-\frac{\partial M_y}{\partial \sigma^E_{xx}}\beta_2)H_{y,y} \\ &+\frac{\partial M_y}{\partial \sigma^E_{xx}}(1-\beta_1)(\lambda+2\mu)\Psi_{xx,y}+\frac{\partial M_y}{\partial \sigma^E_{xx}}(1-\beta_1)\lambda\Psi_{yy,y}=0 \end{aligned} \tag{6.53}$$

and from (6.30c) we get,

$$H_{x,y}-H_{y,x}=0 \tag{6.54}$$

So, we have 6 coupled first order PDEs (6.53, 6.54, 6.46, 6.47, 6.48, 6.49) with 6 variables. We can present in the following matrix form,

$$\begin{bmatrix} (1+\frac{\partial M_x}{\partial H_x}) & (\frac{\partial M_x}{\partial H_y}+\frac{\partial M_x}{\partial \sigma^E_{xx}}\beta_2) & \frac{\partial M_x}{\partial \sigma^E_{xx}}(1-\beta_1)(\lambda+2\mu) & 0 & 0 & \frac{\partial M_x}{\partial \sigma^E_{xx}}(1-\beta_1)\lambda \\ 0 & -1 & 0 & 0 & 0 & 0 \\ \mu_0 H_x & \beta_2 & (1-\beta_1)(\lambda+2\mu) & 0 & 0 & (1-\beta_1)\lambda \\ \mu_0 H_y & 0 & 0 & \mu & \mu & 0 \\ 0 & 0 & 0 & -1 & 0 & 0 \\ 0 & 0 & 0 & 0 & 0 & -1 \end{bmatrix} \begin{pmatrix} H_x \\ H_y \\ \Psi_{xx} \\ \Psi_{xy} \\ \Psi_{yx} \\ \Psi_{yy} \end{pmatrix}_{,x}$$

+

$$\begin{bmatrix} \frac{\partial M_y}{\partial H_x} & (1+\frac{\partial M_y}{\partial H_y}-\frac{\partial M_y}{\partial \sigma^E_{xx}}\beta_2) & \frac{\partial M_y}{\partial \sigma^E_{xx}}(1-\beta_1)(\lambda+2\mu) & 0 & 0 & \frac{\partial M_y}{\partial \sigma^E_{xx}}(1-\beta_1)\lambda \\ 1 & 0 & 0 & 0 & 0 & 0 \\ 0 & \mu_0 H_x & 0 & \mu & \mu & 0 \\ 0 & (\mu_0 H_y-\beta_2) & (\lambda+\beta_1(\lambda+2\mu)) & 0 & 0 & (\lambda+2\mu+\beta_1\lambda) \\ 0 & 0 & 1 & 0 & 0 & 0 \\ 0 & 0 & 0 & 0 & 1 & 0 \end{bmatrix} \begin{pmatrix} H_x \\ H_y \\ \Psi_{xx} \\ \Psi_{xy} \\ \Psi_{yx} \\ \Psi_{yy} \end{pmatrix}_{,\,y} \tag{6.55}$$

We denote the above system of equations in the following compact form,

$$\mathbf{A}\Theta_x + \mathbf{B}\Theta_y = 0 \tag{6.56}$$

We denote the list of variables by the set $\Theta = \{H_x, H_y, \Psi_{xx}, \Psi_{xy}, \Psi_{yx}, \Psi_{yy}\}$. Now we will study few cases from which we will find out the conditions for stability.

1. Case-I: Magnetostatic stability condition

$$\begin{bmatrix} (1+\frac{\partial M_x}{\partial H_x}) & \frac{\partial M_x}{\partial H_y} \\ 0 & -1 \end{bmatrix} \begin{pmatrix} H_x \\ H_y \end{pmatrix}_{,\,x} + \begin{bmatrix} \frac{\partial M_y}{\partial H_x} & (1+\frac{\partial M_y}{\partial H_y}) \\ 1 & 0 \end{bmatrix} \begin{pmatrix} H_x \\ H_y \end{pmatrix}_{,\,y} \tag{6.57}$$

The system becomes elliptic, parabolic and hyperbolic when the eigenvalues are complex, equal and real of the following characteristic equation

$$\det(\mathbf{B} - \alpha\mathbf{A}) = 0, \tag{6.58}$$

where $\alpha = \frac{dy}{dx}$. The characteristic polynomial of α of the above equation is

$$(1+\frac{\partial M_x}{\partial H_x})\alpha^2 - (\frac{\partial M_x}{\partial H_y}+\frac{\partial M_y}{\partial H_x})\alpha + (1+\frac{\partial M_y}{\partial H_y})) = 0 \tag{6.59}$$

The roots are real only when the discriminent D of the above equation is greater than or equal to zero i.e

$$D = \left(\frac{\partial M_x}{\partial H_y} + \frac{\partial M_y}{\partial H_x}\right)^2 - 4\left(1 + \frac{\partial M_y}{\partial H_y}\right)\left(1 + \frac{\partial M_x}{\partial H_x}\right) \geq 0 \tag{6.60}$$

If we further consider that the magnetization constitutive responses only depends on H_y, then $\frac{\partial M_y}{\partial H_x} = \frac{\partial M_x}{\partial H_x} = 0$ and above condition reduces to

$$D = \left(\frac{\partial M_x}{\partial H_y}\right)^2 - 4\left(1 + \frac{\partial M_y}{\partial H_y}\right) \geq 0 \tag{6.61}$$

2. Case-II: Magneto-mechanical stability condition where magnetization if not coupled with stress

$$\begin{bmatrix} (1+\frac{\partial M_x}{\partial H_x}) & \frac{\partial M_x}{\partial H_y} & 0 & 0 & 0 & 0 \\ 0 & -1 & 0 & 0 & 0 & 0 \\ \mu_0 H_x & \beta_2 & (1-\beta_1)(\lambda+2\mu) & 0 & 0 & (1-\beta_1)\lambda \\ \mu_0 H_y & 0 & 0 & \mu & \mu & 0 \\ 0 & 0 & 0 & -1 & 0 & 0 \\ 0 & 0 & 0 & 0 & 0 & -1 \end{bmatrix} \begin{pmatrix} H_x \\ H_y \\ \Psi_{xx} \\ \Psi_{xy} \\ \Psi_{yx} \\ \Psi_{yy} \end{pmatrix}_{,\,x}$$

+

$$\begin{bmatrix} \frac{\partial M_y}{\partial H_x} & (1+\frac{\partial M_y}{\partial H_y}) & 0 & 0 & 0 & 0 \\ 1 & 0 & 0 & 0 & 0 & 0 \\ 0 & \mu_0 H_x & 0 & \mu & \mu & 0 \\ 0 & (\mu_0 H_y - \beta_2) & (\lambda + \beta_1(\lambda+2\mu)) & 0 & 0 & (\lambda+2\mu+\beta_1\lambda) \\ 0 & 0 & 1 & 0 & 0 & 0 \\ 0 & 0 & 0 & 0 & 1 & 0 \end{bmatrix} \begin{pmatrix} H_x \\ H_y \\ \Psi_{xx} \\ \Psi_{xy} \\ \Psi_{yx} \\ \Psi_{yy} \end{pmatrix}_{,\,y} \tag{6.62}$$

The characteristic equation of $\det(\mathbf{B} - \alpha\mathbf{A}) = 0$ can be expressed in the following form

$$(A_1\alpha^2 + A_2\alpha + A_3)(C_1\alpha^4 + C_2\alpha^2 + C_3) = 0 \tag{6.63}$$

where,

$$\begin{aligned}
A_1 &= (1 + \frac{\partial M_x}{\partial H_x}) \\
A_2 &= -(\frac{\partial M_x}{\partial H_y} + \frac{\partial M_y}{\partial H_x}) \\
A_3 &= (1 + \frac{\partial M_y}{\partial H_y}) \\
C_1 &= -\mu(1 - \beta_1)(\lambda + 2\mu) \\
C_2 &= \mu(2\beta_1(2\lambda + 3\mu) - 2(\lambda + 2\mu)) \\
C_3 &= -\mu(\beta_1\lambda + \lambda + 2\mu)
\end{aligned}$$

The discriminant of the quadratic polynomial of (6.63) is identical with (6.60). This result suggests that the stability conditions for the magnetostatic system influences the stability of the mechanical system. But also we have to investigate the nature of the roots of the bi-quadratic polynomial

$$C_1\alpha^4 + C_2\alpha^2 + C_3 = 0$$

The roots are

$$\alpha = \pm\sqrt{\frac{-C_2 \pm \sqrt{C_2^2 - 4C_1C_3}}{2C_1}} \tag{6.64}$$

The first necessary condition for the real roots is $L = \frac{-C_2 \pm \sqrt{C_2^2 - 4C_1C_3}}{2C_1} \geq 0$. Let us consider $C_1 > 0$ which means $\beta_1 > 1$ and to be $L > 0$, we need $-C_2 + \sqrt{C_2^2 - 4C_1C_3} \geq 0$ or $C_1C_3 \leq 0$ or $C_3 \leq 0$. This means $\beta_1\lambda + \lambda + 2\mu \geq 0$ or $\beta_1 \geq -1 - \frac{2\mu}{\lambda}$. So the

condition is $\beta_1 > 1$. Similarly, if $C_1 < 0$ i.e $\beta_1 < 1$, then proceeding in a same way we can write $C_3 \geq 0$, which gives $\beta_1 \leq -1 - \frac{2\mu}{\lambda}$. So the required condition is $\beta_1 \leq -1 - \frac{2\mu}{\lambda}$. Next necessary condition for real roots is

$$\begin{aligned} D_1 &= C_2^2 - 4C_1C_3 \geq 0 \\ &= \beta_1(\mu+\lambda)(-8\mu + 9\beta_1\mu - 4\lambda + 5\beta_1\lambda) \geq 0 \\ &= \beta_1(-8\mu + 9\beta_1\mu - 4\lambda + 5\beta_1\lambda) \geq 0 \\ &= \beta_1(\beta_1(9\mu+5\lambda) - 4(\lambda+2\mu)) \geq 0 \\ &= \beta_1(\beta_1 - r) \geq 0 \end{aligned}$$

where $r = \frac{4\lambda+8\mu}{9\mu+5\lambda} > 0$. This implies $\beta_1 \in (-\infty, 0] \cup [r, +\infty)$. When $C_1 > 0$, $\beta_1 > 1$ and we need to check if $r > 1$. This condition implies that $4\lambda + 8\mu > 9\mu + 5\lambda$ or $\lambda + \mu < 0$, which is not true. So for the real roots i.e. for the unstable condition

$$\beta_1 \in \begin{cases} (1, +\infty), & C_1 > 0\,. \\ (-\infty, -1 - \frac{2\mu}{\lambda}), & C_1 < 0\,. \end{cases} \tag{6.65}$$

At the end of this analysis we consider that the transformation surface Φ depends only on the applied stress level i.e we consider $\Phi_{,\sigma^E_{xx}} = 0$, which implies $\beta_1 = 0$. For this condition the characteristic polynomial (6.63) reduces

$$\left[(1 + \frac{\partial M_x}{\partial H_x})\alpha^2 - (\frac{\partial M_x}{\partial H_y} + \frac{\partial M_y}{\partial H_x})\alpha + (1 + \frac{\partial M_y}{\partial H_y})\right]\left[\mu(1+\alpha^2)^2(\lambda+2\mu)\right] = 0 \tag{6.66}$$

Since $\mu(1+\alpha^2)^2(\lambda+2\mu) = 0$ means $\alpha = \pm\sqrt{\pm i}$ where $i = \sqrt{-1}$, the stability condition is same as (6.59).

Finally, when we consider the stress dependence of the magnetization vector, we get an sextic characteristic polynomial. The factorization of such a polynomial becomes extremely complex and we will not consider the stability conditions for the

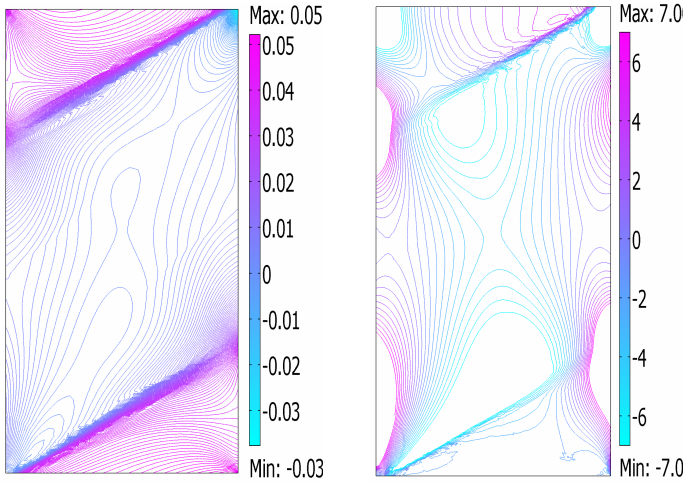

(a) (b)

Fig. 82. Distribution of (a) e_{xx} and (b) σ_{xx} at $< \widehat{H}_y >= 0.348$(hyperbolic).

present study.

CHAPTER VII

SUMMARY AND CONCLUSIONS

A generalized modeling approach for magnetic shape memory alloys is introduced in this work. A finite deformation based nonlinear analysis is performed and magneto-mechanical constitutive equations are derived from a proposed Gibbs energy function in a thermodynamically consistent way. The integrity basis for the Gibbs free energy is derived by considering material symmetry. The evolution equations of the internal variables are restricted by group symmetry operations. Finite symmetry is considered for single crystal MSMA. For polycrystalline MSMAs, continuous symmetry is considered and anisotropy is taken into account by introducing structural tensors in the Gibbs free energy and evolution equations. Selected results are presented for field induced variant reorientation and phase transformation as special cases of the general theory. Considering symmetry restrictions in the modeling not only provides insight to construct an energy potential and evolution equations of the internal variables but also systematically captures cross-coupling between multiple fields.

In this work, a thermodynamic based phenomenological model of field induced phase transformation for a single crystal NiMnCoIn material system is presented. A Gibbs free energy is proposed and the integrity basis is determined based on the external-internal state variables. The magneto-thermo-mechanical constitutive equations are derived in a thermodynamically consistent way. Hysteretic behaviors of such dissipative material is taking into account through the evolution equations of the internal variables. A unique experimental approach for a single crystal specimen is described. The model is then reduced to 1-D and calibrated from experiments. Different thermodynamic planes are used to calibrate different material parameters. The model predictions of magnetization-field, magneto-mechanical and magneto-thermal

responses are validated with the experiments. Different material responses are then presented by using the model and a 3-D (magneto-thermo-mechanical) transformation surface is predicted. Finally, thermo-magneto-mechanical responses are demonstrated by simultaneously varying temperature and magnetic field.

A magnetostatic and magneto-mechanically-coupled finite element analysis involving nonlinear magnetic shape memory behavior is presented. Based on this analysis two important effects that substantially influence the constitutive modeling of MSMAs have been addressed. First, it is shown that magnetostatic computations could be used to properly account for the shape-dependent demagnetization effect which complicates the model parameter identification from experimental data. It is pointed out that this must be understood as the *inverse problem* of finding the model parameters such that the simulation results in the applied magnetic field vs. magnetization curve measured in the experiment for a specific sample geometry. An iterative procedure is established for which in each iteration step the magnetostatic boundary value problem is solved to obtain the relation between the applied and internal magnetic fields needed to correct the data.

The second main effort was concerned with the investigation of the significance of magnetic body forces and body couples and whether or not these can be neglected in the modeling of MSMAs. In a first estimate of this influence, highly non-uniform distributions of the magnetic body force and couple and consequently the Maxwell stress field were computed from the nonlinear magnetostatic finite element analysis in a post-processing manner. In a second step, an extended analysis based on the numerical solution of the magneto-mechanically-coupled problem then revealed that the magnetic body force and body couple cause an inhomogeneous Cauchy stress field, whose components are comparable to the typically applied stresses. This suggests that, considering current blocking stress levels, the influence of body forces should

not be neglected.

An interesting feature of the studied magnetostatic boundary value problem is the appearance of banded zones in the spacial distribution of the magnetic field variables when the magnetization constitutive response becomes highly nonlinear. In the performed finite element analysis, the appearance of band like regions are observed and are explained by the loss of ellipticity of the magnetostatic system of equations. The analytic approach of stability analysis shows that the magnetostatic problem becomes unstable during the martensitic variant reorientation mechanism. A parametric stability analysis reveals the conditions under which loss of ellipticity occurs and quantifies the influence of the non-dimensional material parameters in the stability of the material.

REFERENCES

[1] B. Kiefer, H. E. Karaca, D. C. Lagoudas, and I. Karaman, "Characterization and modeling of the magnetic field-induced strain and work output in Ni_2MnGa shape memory alloys," *Journal of Magnetism and Magnetic Materials*, vol. 312, pp. 164–175, November 2007.

[2] H. E. Karaca, I. Karaman, B. Basaran, , Y. Ren, Y. I. Chumlyakov, and H. J. Maier, "Magnetic field-induced phase transformation in NiMnCoIn magnetic shape memory alloys-a new actuation mechanism with large work output," *Advanced Functional Materials*, vol. 19, pp. 1–16, 2009.

[3] B. Kiefer and D. C. Lagoudas, "Magnetic field-induced martensitic variant reorientation in magnetic shape memory alloys," *Philosophical Magazine Special Issue: Recent Advances in Theoretical Mechanics*, vol. 85, no. 33-35, pp. 4289–4329, 2005.

[4] V. Birman, "Review of mechanics of shape memory alloy structures," *Applied Mechanics Reviews*, vol. 50, no. 11, part I, pp. 629–645, 1997.

[5] K. Otsuka and C. M. Wayman, Eds., *Shape Memory Materials*, Cambridge University Press, Cambridge, UK, 1998.

[6] I. Chopra, "Review of state of art of smart structures and integrated systems," *AIAA Journal*, vol. 40, no. 11, pp. 2145–2187, 2002.

[7] S. J. Murray, M. Marioni, S. M. Allen, and R. C. O'Handley, "6% magnetic-field-induced strain by twin-boundary motion in ferromagnetic Ni-Mn-Ga," *Applied Physics Letters*, vol. 77, no. 6, pp. 886–888, 2000.

[8] L. E. Faidley, M. J. Dapino, G. N. Washington, and T. A. Lograsso, "Reversible strain in Ni-MnGa with collinear field and stress," *in: Proceedings of SPIE, Smart Structures and Materials: Active Materials: Behavior and Mechanics, San Diego, CA, 6–10 March 2005.*, vol. Vol. 5761, pp. 501–512, 2005.

[9] L. Hirsinger, N. Creton, and C. Lexcellent, "Stress-induced phase transformation in Ni-Mn-Ga alloys: Experiments and modelling," *Material Science & Engineering A*, vol. 378, pp. 365–369, 2004.

[10] V. A. Chernenko, V. V. Kokorin, O. M. Babii, and I. K. Zasimchuk, "Phase diagrams in the Ni-Mn-Ga system under compression," *Intermetallics*, vol. 6, no. 1, pp. 29–34, 1998.

[11] J. Pons, V. A. Chernenko, E. Cesari, and V. A. L'vov, "Stress-strain-temperature behaviour for martensitic transformation in Ni-Mn-Ga single crystals compressed along $< 001 >$ and $< 110 >$ axes," *Journal de Physique IV France*, vol. 112, pp. 939–942, 2003.

[12] V. V. Martynov and V. V. Kokorin, "The crystal structure of thermally- and stress-induced martensites in Ni_2MnGa single crystals," *Journal de Physique III France*, vol. 2, pp. 739–749, 1992.

[13] H. E. Karaca, I. Karaman, D. C Lagoudas, H. J. Maier, and Y. I. Chumlyakov, "Recoverable stress-induced martensitic transformation in a ferromagnetic CoNiAl alloy," *Scripta Materialia*, vol. 49, pp. 831–836, 2003.

[14] R. C. O'Handley, S. M. Allen, D. I. Paul, C. P. Henry, M. Marioni, D. Bono, C. Jenkins, A. Banful, and R. Wager, "Keynote address: Magnetic field-induced strain in single crystal Ni-Mn-Ga," *in: Proceedings of SPIE, Symposium on Smart Structures and Materials*, vol. 5053, pp. 200–206, 2003.

[15] K. Ullakko, J. K. Huang, C. Kantner, R. C. O'Handley, and V. V. Kokorin, "Large magnetic-field-induced strains in Ni_2MnGa single crystals," *Applied Physics Letters*, vol. 69, no. 13, pp. 1966–1968, 1996.

[16] R. A. Kellogg, A. B. Flatau, A. E. Clark, M. Wun-Fogle, and T. A. Lograsso, "Temperature and stress dependencies of the magnetic and magnetostrictive properties of $Fe_{0.81}Ga_{0.19}$," *Journal of Applied Physics*, vol. 91, no. 10, pp. 7821–7823, 2002.

[17] J. Tellinen, I. Suorsa, I. Jääskeläinen, Aaltio, and K. Ullakko, "Basic properties of magnetic shape memory actuators," *in: Proceedings of the 8th International Conference ACTUATOR 2002, Bremen, Germany, 10-12 June 2002*, pp. 566–569, 2002.

[18] A. Bhattacharyya, D. C. Lagoudas, Y. Wang, and V. K. Kinra, "On the role of thermoelectric heat transfer in the design of SMA actuators: Theoretical modeling and experiment," *Smart Materials and Structures*, vol. 4, pp. 252–263, 1995.

[19] B. D. Cullity, *Introduction to Magnetic Materials*, Addison-Wesley, Reading, MA, 1972.

[20] R. C. O'Handley, *Modern Magnetic Materials*, John Wiley & Sons, New York, 2000.

[21] C. Kittel, *Introduction to Solid State Physics*, John Wiley & Sons, New York, 7th edition, 1996.

[22] M. Pasquale, "Mechanical sensors and actuators," *Sensors and Actuators A*, vol. 106, pp. 142–148, 2003.

[23] I. Suorsa, J. Tellinen, K. Ullakko, and E. Pagounis, "Voltage generation induced by mechanical straining in magnetic shape memory materials," *Journal of Applied Physics*, vol. 95, no. 12, pp. 8054–8058, 2004.

[24] P. Müllner, V. A. Chernenko, M. Wollgarten, and Kostorz, "Large cyclic deformations of a Ni-Mn-Ga shape memory alloy induced by magnetic fields," *Journal of Applied Physics*, vol. 92, no. 11, pp. 6708–6713, 2002.

[25] P. J. Webster, K. R. A. Ziebeck, S. L. Town, and M. S. Peak, "Magnetic order and phase transformation in Ni_2MnGa," *Philosophical Magazine B*, vol. 49, no. 3, pp. 295–310, 1984.

[26] I. K. Zasimchuk, V. V. Kokorin, V. V. Martynov, A. V. Tkachenko, and V. A. Chernenko, "Crystal structure of martensite in Heusler alloy Ni_2MnGa," *Physics of Metals and Metallography*, vol. 69, no. 6, pp. 104–108, 1990.

[27] A. Sozinov, A. A. Likhachev, N. Lanska, O. Söderberg, K. Ullakko, and V. K. Lindroos, "Effect of crystal structure on magnetic-field-induced strain in Ni-Mn-Ga," *in: Proceedings of SPIE, Symposium on Smart Structures and Materials*, vol. 5053, pp. 586–594, 2003.

[28] J. Cui, T. W. Shield, and R. D. James, "Phase transformation and magnetic anisotropy of an iron-palladium ferromagnetic shape-memory alloy," *Acta Materialia*, vol. 52, pp. 35–47, 2004.

[29] R. D. James and M. Wuttig, "Magnetostriction of martensite," *Philosophical Magazine A*, vol. 77, no. 5, pp. 1273–1299, 1998.

[30] T. W. Shield, "Magnetomechanical testing machine for ferromagnetic shape-

memory alloys," *Review of Scientific Instruments*, vol. 74, no. 9, pp. 4077–4088, 2003.

[31] T. Yamamoto, M. Taya, Y. Sutou, Y. Liang, T. Wada, and L. Sorensen, "Magnetic field-induced reversible variant rearrangement in Fe-Pd single crystals," *Acta Materialia*, vol. 52, no. 17, pp. 5083–5091, 2004.

[32] S. J. Murray, R. Hayashi, M. Marioni, S. M. Allen, and R. C. O'Handley, "Magnetic and mechanical properties of FeNiCoTi and NiMnGa magnetic shape memory alloys," *Proceedings of SPIE*, vol. 3675, pp. 204–211, 1999.

[33] A. Fujita, K. Fukamichi, F. Gejima, R. Kainuma, and K. Ishida, "Magnetic properties and large magnetic-field-induced strains in off-stoichiometric Ni-Mn-Al heusler alloys," *Applied Physics Letters*, vol. 77, no. 19, pp. 3054–3056, 2000.

[34] T. Kakeshita, T. Takeuchi, T. Fukuda, M. Tsujiguchi, T. Saburi, R. Oshima, and S. Muto, "Giant magnetostriction in an ordered Fe_3Pt single crystal exhibiting a martensitic transformation," *Applied Physics Letters*, vol. 77, no. 10, pp. 1502–1504, 2000.

[35] M. Wuttig, L. Liu, K. Tsuchiya, and R. D. James, "Occurrence of ferromagnetic shape memory alloys (invited)," *Journal of Applied Physics*, vol. 87, no. 9, pp. 4707–4711, 2000.

[36] M. Wuttig, J. Li, and C. Craciunescu, "A new ferromagnetic shape memory alloys system," *Scripta Materialia*, vol. 44, pp. 2393–2397, 2001.

[37] H. Morito, A. Fujita, R. Kainuma, K. Ishida, and K. Oikawa, "Magnetocrys-

talline anisotropy in single-crystal Co-Ni-Al ferromagnetic shape-memory alloy," *Applied Physics Letters*, vol. 81, no. 9, pp. 1657–1659, 2002.

[38] T. Sakamoto, T. Fukuda, T. Kakeshita, T. Takeuchi, and K. Kishio, "Magnetic field-induced strain in iron-based ferromagnetic shape memory alloys," *Journal of Applied Physics*, vol. 93, no. 10, pp. 8647–8649, 2003.

[39] A. A. Cherechukin, I. E. Dikshtein, D. I. Ermakov, A. V. Glebov, V. V. Koledov, D. A. Kosolapov, V. G. Shavrov, A. A. Tulaikova, E. P. Krasnoperov, and T. Takagi, "Shape memory effect due to magnetic field-induced thermoelastic martensitic transformation in polycrystalline Ni-Mn-Fe-Ga alloy," *Physics Letters A*, vol. 291, pp. 175–183, 2001.

[40] S. Jeong, K. Inoue, S. Inoue, K. Koterazawa, M. Taya, and K. Inoue, "Effect of magnetic field on martensite transformation in a polycrystalline Ni_2MnGa," *Material Science & Engineering A*, vol. 359, pp. 253–260, 2003.

[41] S. J. Murray, M. Farinelli, C. Kantner, J. K. Huang, A. M. Allen, and R. C. O'Handley, "Field-induced strain under load in Ni-Mn-Ga magnetic shape memory materials," *Journal of Applied Physics*, vol. 83, no. 11, pp. 7297–7299, 1998.

[42] K. Ullakko, Y. Ezer, A. Sozinov, G. Kimmel, P. Yakovenko, and V. K. Lindroos, "Magnetic-field-induced strains in polycrystalline Ni-Mn-Ga at room temperature," *Scripta Materialia*, vol. 44, pp. 475–480, 2001.

[43] T. Wada, Y. Liang, H. Kato, T. Tagawa, M. Taya, and T. Mori, "Structural change and straining in Fe-Pd polycrystals by magnetic field," *Material Science & Engineering A*, vol. 361, pp. 75–82, 2003.

[44] M. A. Marioni, R. C. O'Handley, and S. A. Allen, "Analytical model for field-induced strain in ferromagnetic shape-memory alloy polycrystals," *Journal of Applied Physics*, vol. 91, no. 10, pp. 7807–7809, 2002.

[45] T. Kakeshita, T. Takeuchi, T. Fukuda, T. Saburi, R. Oshima, S. Muto, and K. Kishio, "Magnetic field-induced martensitic transformation and giant magnetostriction in Fe-Ni-Co-Ti and ordered Fe_3Pt shape memory alloys," *Materials Transactions, JIM*, vol. 41, no. 8, pp. 882–887, 2000.

[46] I. Karaman, H. E. Karaca, B. Basaran, D. C. Lagoudas, Y. I. Chumlyakov, and H. J. Maier, "Stress-assisted reversible magnetic field-induced phase transformation in Ni_2MnGa magnetic shape memory alloys," *Scripta Materialia*, vol. 55, no. 4, pp. 403–406, 2006.

[47] O. Heczko, L. Straka, and K. Ullakko, "Relation between structure, magnetization process and magnetic shape memory effect of various martensites occuring in Ni-Mn-Ga alloys," *Journal de Physique IV France*, vol. 112, pp. 959–962, 2003.

[48] A. A. Likhachev, A. Sozinov, and K. Ullakko, "Different modeling concepts of magnetic shape memory and their comparison with some experimental results obtained in Ni-Mn-Ga," *Material Science & Engineering A*, vol. 378, pp. 513–518, 2004.

[49] H. E. Karaca, I. Karaman, B. Basaran, D. C Lagoudas, Y. I Chumlyakov, and H. J Maier, "On the stress-assisted magnetic-field-induced phase transformation in Ni_2MnGa ferromagnetic shape memory alloys," *Acta Materialia*, vol. 55, pp. 4253–4269, 2007.

[50] R. Kainuma, Y. Imano, W. Ito, Y. Sutou, H. Morito, S. Okamoto, O. Kitakami, K. Oikawa, A. Fujita1, T. Kanomata, and K. Ishida, "Magnetic-field-induced shape recovery by reverse phase transformation," *Nature*, vol. 439, pp. 957–960, 2006.

[51] Y. D Wang, E.W. Huang, Y. Ren, Z.H. Nie, G. Wang, Y.D. Liu, J.N. Deng, H. Choo, P.K. Liaw, D.E. Brown, and L. Zuo, "In situ high-energy x-ray studies of magnetic-field-induced phase transition in a ferromagnetic shape memory NiCoMnIn alloy," *Acta Materialia*, vol. 56, pp. 913–923, 2008.

[52] A. N. Vasil'ev, A. D. Bozhko, V. V. Khovailo, I. E. Dikshtein, V. G. Shavrov, V. D. Buchelnikov, M. Matsumoto, S. Suzuki, T. Takagi, and J. Tani, "Structural and magnetic phase transitions in shape-memory alloys $Ni_{2+x}Mn_{1-x}Ga$," *Physical Review B*, vol. 59, no. 2, pp. 1113–1119, 1999.

[53] F. Albertini, L. Pareti, A. Paoluzi, L. Morellon, P. A. Algarabel, M. R. Ibarra, and L. Righi, "Composition and temperature dependence of the magnetocrystalline anisotropy in $Ni_{2+x}Mn_{1+y}Ga_{1+z}$ (x+y+z = 0) Heusler alloys," *Applied Physics Letters*, vol. 81, no. 21, pp. 4032–4034, 2002.

[54] F. Albertini, F. Canepa, S. Cirafici, E. A. Franceschi, M. Napoletano, A. Paoluzi, L. Pareti, and M. Solzi, "Composition dependence of magnetic and magnetothermal properties of Ni-Mn-Ga shape memory alloys," *Journal of Magnetism and Magnetic Materials*, vol. 272–276, no. Part 3, pp. 2111–2112, 2004.

[55] O. Heczko and L. Straka, "Compositional dependence of structure, magnetization and magnetic anisotropy in Ni-Mn-Ga magnetic shape memory alloys,"

Journal of Magnetism and Magnetic Materials, vol. 272–276, no. Part 3, pp. 2045–2046, 2004.

[56] H. E. Karaca, "Magnetic field-induced phase transformation and variant reorientation in Ni_2MnGa and NiMnCoIn magnetic shape memory alloys," Ph.D. dissertation, Texas A&M University, August 2007.

[57] S. J. Murray, M. Marioni, A. M. Kukla, J. Robinson, R. C. O'Handley, and S. M. Allen, "Large field induced strain in single crystalline Ni-Mn-Ga ferromagnetic shape memory alloy," *Journal of Applied Physics*, vol. 87, no. 9, pp. 5774–5776, 2000.

[58] S. J. Murray, "Magneto-mechanical properties and applications of Ni-MnGa ferromagnetic shape memory alloy," Ph.D. dissertation, Massachusetts Institute of Technology, Cambridge, MA, February 2000.

[59] L. Hirsinger, N. Creton, and C. Lexcellent, "From crystallographic properties to macroscopic detwinning strain and magnetisation of Ni-Mn-Ga magnetic shape memory alloys," *Journal de Physique IV France*, vol. 115, pp. 111–120, 2004.

[60] O. Heczko, N. Lanska, O. Soderberg, and K. Ullakko, "Temperature variation of structure and magnetic properties of Ni-Mn-Ga magnetic shape memory alloys," *Journal of Magnetism and Magnetic Materials*, vol. 242–245, pp. 1446–1449, 2002.

[61] A. A. Likhachev and K. Ullakko, "Quantitative model of large magnetostrain effect in ferromagnetic shape memory alloys," *The European Physical Journal B*, vol. 14, no. 2, pp. 263–267, 2000.

[62] A. Hubert and R. Schäfer, *Magnetic Domains*, Springer-Verlag, New York, 2001.

[63] R. Tickle and R. D. James, "Magnetic and magnetomechanical properties of Ni_2MnGa," *Journal of Magnetism and Magnetic Materials*, vol. 195, no. 3, pp. 627–638, 1999.

[64] A. A. Likhachev and K. Ullakko, "Magnetic-field-controlled twin boundaries motion and giant magneto-mechanical effects in Ni-Mn-Ga shape memory alloy," *Physics Letters A*, vol. 275, pp. 142–151, 2000.

[65] O. Heczko, "Determination of ordinary magnetostriction in Ni-Mn-Ga magnetic shape memory alloy," *Journal of Magnetism and Magnetic Materials*, vol. 290–291, pp. 846–849, 2005.

[66] H. E. Karaca, I. Karaman, B. Basaran, Y. I. Chumlyakov, and H. J. Maier, "Magnetic field and stress induced martensite reorientation in NiMnGa ferromagnetic shape memory alloy single crystals," *Acta Materialia*, vol. 54, no. 1, pp. 233–245, 2006.

[67] A. DeSimone and R. D. James, "A theory of magnetostriction oriented towards applications," *Journal of Applied Physics*, vol. 81, no. 8, pp. 5706–5708, 1997.

[68] A. DeSimone and R. James, "A constrained theory of magnetoelasticity," *Journal of the Mechanics and Physics of Solids*, vol. 50, pp. 283–320, 2002.

[69] A. DeSimone and R. D. James, "Energetics of magnetoelastic domains in ferromagnetic shape memory alloys," *Journal de Physique*, vol. 112, pp. 969–972, 2003.

[70] R. C. O'Handley, "Model for strain and magnetization in magnetic shape-memory alloys," *Journal of Applied Physics*, vol. 83, no. 6, pp. 3263–3270, 1998.

[71] S. J. Murray, R. C. O'Handley, and S. M. Allen, "Model for discontinuous actuation of ferromagnetic shape memory alloy under stress," *Journal of Applied Physics*, vol. 89, no. 2, pp. 1295–1301, 2001.

[72] L. Hirsinger and C. Lexcellent, "Modelling detwinning of martensite platelets under magnetic and (or) stress actions on NiMnGa alloys," *Journal of Magnetism and Magnetic Materials*, vol. 254–255, pp. 275–277, 2003.

[73] L. Hirsinger and C. Lexcellent, "Internal variable model for magneto-mechanical behaviour of ferromagnetic shape memory alloys Ni-Mn-Ga," *Journal de Physique IV France*, vol. 112, pp. 977–980, 2003.

[74] B. Kiefer and D. C. Lagoudas, "Phenomenological modeling of ferromagnetic shape memory alloys," *Proceedings of SPIE: Smart Structures and Materials*, vol. 5387, pp. 164–176, 2004.

[75] B. Kiefer, "A phenomenological constitutive model for magnetic shape memory alloys," Ph.D. dissertation, Department of Aerospace Engineering, Texas A&M University, College Station, TX, December 2006.

[76] B. Kiefer and D. C. Lagoudas, "Modeling of magnetic smas," in *Introduction to Modeling and Engineering Applications of Shape Memory Alloys*, D. C. Lagoudas, Ed., pp. 325–393. Springer-Verlag, New York, 2008.

[77] B. Kiefer and D. C. Lagoudas, "Modeling the coupled strain and magnetization response of magnetic shape memory alloys under magnetomechanical loading,"

Journal of Intelligent Material Systems and Structures, vol. 20, pp. 143–170, 2009.

[78] B. Kiefer and D.C. Lagoudas, "Application of a magnetic sma constitutive model in the analysis of magnetomechanical boundary value problems," *Proceedings of SPIE: Smart Structures and Materials*, vol. 6170, pp. 330–341, 2006.

[79] D. C. Lagoudas, B. Kiefer, and A. J. Broederdorf, "Accurate interpretation of magnetic shape memory alloy experiments utilizing coupled magnetostatic analysis," *Proceedings of ASME, International Mechanical Engineering Congress and Exposition, Chicago, IL, 5–10 November 2006*, vol. IMECE2006-15296, pp. 311–321, 2006.

[80] K. Haldar, G. Chatzigeorgiou, and D. C. Lagoudas, "Stability analysis of magnetostatic boundary value problems for magnetic smas," *Journal of Intelligent Material Systems and Structures*, vol. 21, pp. 1103–1116, 2010.

[81] H. Tan and M. H. Elahinia, "On the modeling of ferromagnetic shape memory alloy actuators," *Submitted to Elsevier May 2006*, 2006.

[82] N. I. Glavatska, A. A. Rudenko, I. N. Glavatskiy, and V. A. L'vov, "Statistical model of magnetostrain effect in martensite," *Journal of Magnetism and Magnetic Materials*, vol. 265, no. 2, pp. 142–151, 2003.

[83] V. A. Chernenko, V. A. L'vov, P. Müllner, G. Kostorz, and T. Takagi, "Magnetic-field-induced superelasticity of ferromagnetic thermoelastic martensites: Experiments and modeling," *Physical Review B*, vol. 69, pp. 134410–(1–8), 2004.

[84] P. Müllner, V. A. Chernenko, and G. Kostorz, "A microscopic approach to the

magnetic-field-induced deformation of martensite (magnetoplasticity)," *Journal of Magnetism and Magnetic Materials*, vol. 267, pp. 325–334, 2003.

[85] V. D. Buchelnikov and S. I. Bosko, "The kinetics of phase transformations in ferromagnetic shape memory alloys Ni-Mn-Ga," *Journal of Magnetism and Magnetic Materials*, vol. 258–259, pp. 497–499, 2003.

[86] S. Govindjee and G. J. Hall, "A computational model for shape memory alloys," *International Journal of Solids and Structures*, vol. 37, no. 5, pp. 735–760, 2000.

[87] R. C. Smith, S. Seelecke, M. Dapino, and Z. Ounaies, "A unified framework for modeling hysteresis in ferroic materials," *Journal of the Mechanics and Physics of Solids*, vol. 54, pp. 46–85, 2006.

[88] J. Kiang and L. Tong, "Modelling of magneto-mechanical behavior of Ni-Mn-Ga single crystals," *Journal of Magnetism and Magnetic Materials*, vol. 292, pp. 394–412, 2005.

[89] K. Tanaka, "A thermomechanical sketch of shape memory effect: One-dimensional tensile behavior," *Res Mechanica*, vol. 18, pp. 251–263, 1986.

[90] C. Liang and C. A. Rogers, "One-dimensional thermomechanical constitutive relations for shape memory materials," *Journal of Intelligent Material Systems and Structures*, vol. 1, pp. 207–234, 1990.

[91] J. G. Boyd and D. C. Lagoudas, "A thermodynamical constitutive model for shape memory materials. Part I. The monolithic shape memory alloy," *International Journal of Plasticity*, vol. 12, no. 6, pp. 805–842, 1996.

[92] D. C. Lagoudas, Z. Bo, and M. A. Qidwai, "A unified thermodynamic constitutive model for SMA and finite element analysis of active metal matrix

composites," *Mechanics of Composite Materials and Structures*, vol. 3, pp. 153–179, 1996.

[93] J. Lubliner and F. Auricchio, "Generalized plasticity and shape memory alloys," *International Journal of Solids and Structures*, vol. 33, no. 7, pp. 991–1003, 1996.

[94] L. C. Brinson and M. S. Huang, "Simplifications and comparisons of shape memory alloy constitutive models," *Journal of Intelligent Material Systems and Structures*, vol. 7, pp. 108–114, 1996.

[95] A. Bekker and L. C. Brinson, "Temperature-induced phase transformation in a shape memory alloy: Phase diagram based kinetics approach," *Journal of the Mechanics and Physics of Solids*, vol. 45, no. 6, pp. 949–988, 1997.

[96] Z. Bo and D. C. Lagoudas, "Thermomechanical modeling of polycrystalline SMAs under cyclic loading, Part I: Theoretical derivations," *International Journal of Engineering Science*, vol. 37, pp. 1089–1140, 1999.

[97] D. C. Lagoudas and Z. Bo, "Thermomechanical modeling of polycrystalline SMAs under cyclic loading, Part II: Material characterization and experimental results for a stable transformation cycle," *International Journal of Engineering Science*, vol. 37, pp. 1141–1173, 1999.

[98] E. Patoor, D. C. Lagoudas, P. B. Entchev, L. C. Brinson, and X. Gao, "Shape memory alloys , Part I: General properties and modeling of single crystals," *Mechanics of Materials*, vol. 38, no. 5–6, pp. 391–429, 2006.

[99] D. C. Lagoudas, P. B. Entchev, P. Popov, E. Patoor, L. C. Brinson, and X. Gao,

"Shape memory alloys, Part II: Modeling of polycrystals," *Mechanics of Materials*, vol. 38, no. 5–6, pp. 430–462, 2006.

[100] B. D. Coleman and M. E. Gurtin, "Thermodynamics with internal state variables," *The Journal of Chemical Physics*, vol. 47, no. 2, pp. 597–613, July 1967.

[101] B. D. Coleman and W. Noll, "The thermodynamics of elastic materials with heat conduction and viscosity," *Archive for Rational Mechanics and Analysis*, vol. 13, pp. 167–178, 1963.

[102] M. A. Qidwai and D. C. Lagoudas, "Numerical impementation of a shape memory alloy thermomechanical constitutive model using return mapping algorithms," *International Journal for Numerical Methods in Engineering*, vol. 47, pp. 1123–1168, 2000.

[103] S. Leclercq and C. Lexcellent, "A general macroscopic description of the thermomechanical behavior of shape memory alloys," *Journal of the Mechanics and Physics of Solids*, vol. 44, no. 6, pp. 953–980, 1996.

[104] S. G. Shu, D. C. Lagoudas, D. Hughes, and J. T. Wen, "Modeling of a flexible beam actuated by shape memory alloy wires," *Smart Materials and Structures*, vol. 6, pp. 265–277, 1997.

[105] P. Popov and D. C. Lagoudas, "A 3-d constitutive model for shape memory alloys incorporating pseudoelasticity and detwinning of self-accommodated martensite," *International Journal of Plasticity, in print*, vol. X, pp. xxx, 2006.

[106] P. A. Popov, "Constitutive modelling of shape memory alloys and upscaling

of deformable porous media," Ph.D. dissertation, Texas A&M University, Department of Aerospace Engineering, College Station, TX, May 2005.

[107] A. Dorfmann and R. W. Ogden., "Nonlinear magnetoelastic deformation," *The Quarterly Journal of Mechanics and Applied Mathematics*, vol. 57(4), pp. 599–622, 2004.

[108] A. Dorfmann and R. W. Ogden., "Nonlinear magnetoelastic deformations of elastomers," *Acta Mechanica*, vol. 167, pp. 13–28, 2005.

[109] A. Dorfmann and R. W. Ogden., "Nonlinear electroelasticity," *Acta Mechanica*, vol. 174, pp. 167–183, 2005.

[110] R. M. McMeeking and C. M. Landis., "Electrostatic forces and stored energy for deformable dielectric material," *Journal of Applied Mechanics*, vol. 72, pp. 581–590, 2005.

[111] R. M. McMeeking, C. M. Landis, and S. M. A. Jimenez., "A principle of virtual work for combined electrostatic and mechanical loading of materials," *International Journal of Nonlinear Mechanics*, vol. 42, pp. 831–838, 2007.

[112] A. DeSimone and P. Podio-Guidugli, "On the continuum theory of deformable ferromagnetic solids," *Archive for Rational Mechanics and Analysis*, vol. 136, pp. 201–233, 1996.

[113] David J. Steigmann., "Equilibrium theory for magnetic elastomers and magnetoelastic membranes," *Non-Linear Mechanics*, vol. 39, pp. 1193–1216, 2004.

[114] D. J. Steigmann, "On the formulation of balance laws for electromagnetic continua," *Mathematics and Mechanics of Solids*, vol. 14, pp. 390–402, 2009.

[115] S. V. Kankanala and N. Triantafyllidis, "On finitely strained magnetorheological elastomers," *Journal of the Mechanics and Physics of Solids*, vol. 52, pp. 2869–2908, 2004.

[116] J. L. Ericksen, "A modified theory of magnetic effects in elastic materials," *Mathematics and Mechanics of Solids*, vol. 11, pp. 23–47, 2006.

[117] R. Bustamante, A. Dorfmann, and R. W. Ogden, "On variational formulations in nonlinear magnetoelastostatics," *Mathematics and Mechanics of Solids*, vol. 13, pp. 725–745, 2008.

[118] C. Miehe, D. Rosato, and B. Kiefer, "Variational principles in dissipative electro-magneto-mechanics: A framework for the macro-modeling of functional materials," *International Journal for Numerical Methods in Engineering*, vol. 84, no. 10, pp. 1225–1276, 2011.

[119] C. Miehe, B. Kiefer, and D. Rosato, "An incremental variational formulation of dissipative magnetostriction at the macroscopic continuum level," *International Journal of Solids and Structures*, vol. 48, no. 13, pp. 1846–1866, 2011.

[120] W. F. Brown, Jr., *Magnetoelastic Interactions*, vol. 9 of *Tracts in Natural Philosophy*, Springer-Verlag, New York, 1966.

[121] S. Bobbio, *Electrodynamics of Materials*, Academic Press, San Diego, 2000.

[122] R. Toupin, "The elastic dielectric," *J. Rational Mech. Anal*, vol. 5, no. 6, pp. 849–915, 1956.

[123] K. Hutter, A. A. F. van de Ven, and Ursescu, *Electromagnetic Field Matter Interactions in Thermoelastic Solids and Viscous Fluids*, Lecture Notes in Physics. Springer-Verlag, New York, 2006.

[124] A. C. Eringen and G. A. Maugin, *Electrodynamics of Continua I — Foundations and Solid Media*, Springer-Verlag, New York, 1990.

[125] P. Jr. Penfield and H. A. Haus, *Electrodynamics of Moving Media*, The MIT Press, Cambridge, Massachusetts, Cambridge, 1967.

[126] R. Toupin, "Stress tensors in elastic dielectrics," *Archive for Rational Mechanics and Analysis*, vol. 5, no. 1, pp. 440–452, 1960.

[127] Boehler J. P., *Applications of Tensor Functions in Solid Mechanics*, Springer-Verlag, 1987.

[128] C. Truesdell and Toupin R. A, *The Classical Field Theories, Handbuch der Physik, edited by S. Flugger*, vol. III/1, Springer, Berlin-Heidelberg-New York, 1960.

[129] I-Shih Liu, *Continuum Mechanics*, Springer-Verlag, Berlin, 2002.

[130] M. E. Gurtin, *An Introduction to Continuum Mechanics*, vol. 158 of *Mathematics in Science and Engineering*, Academic Press, San Diego, 1981.

[131] A. Kovetz., *Electromagnetic Theory*, Oxford University Press, Oxford, 2000.

[132] A.E. Green and P.M. Naghdi, "A general theory of an elasticplastic continuum," *Archive for Rational Mechanics and Analysis*, vol. 18, pp. 251–281, 1965.

[133] J. Casey and P.M. Naghdi, "A remark on the use of the decomposition $\mathbf{F} = \mathbf{F}^e\mathbf{F}^p$ in plasticity," *Journal of Applied Mechanics*, vol. 47, pp. 662–665, 1980.

[134] A. P. Cracknell, *Magnetism in Crystalline Materials*, Pergamon Press, 1975.

[135] E. Kiral and A. C. Eringen, *Constitutive Equations of Nonlinear Electromagnetic- Elastic Crystals*, Springer-Verlag, New York, 1990.

[136] E. Kiral and G. F. Smith, "On the constitutive relations for anisotropic materials–triclinic, monoclinic, rhombic, tetragonal and hexagonal crystal systems," *International Journal of Engineering Science*, vol. 12, pp. 471–490, 1974.

[137] G. F. Smith, *Constitutive Equations for Anisotropic and Isotropic Materials*, vol. 3, Elsevier Science B.V., North-Holland, 1994.

[138] A. J. M. Spencer and R. S. Rivlin, "Isotropic integrity bases for vectors and second-order tensors: Part i," *Archive for Rational Mechanics and Analysis*, vol. 9, no. 1, pp. 45–63, 1961.

[139] A. J. M. Spencer, "Isotropic integrity bases for vectors and second-order tensors: Part ii," *Archive for Rational Mechanics and Analysis*, vol. 18, no. 1, pp. 51–82, 1964.

[140] A. C. Eringen, *Continuum Physics (Mathematics)*, vol. 1, Academic Press, New York and London, 1971.

[141] Q. S Zheng, "Theory of representations of tensor functions-a unified invariant approach to constitutive equations," *Appl. Mech. Review*, vol. 47, pp. 545–587, 1994.

[142] J. M. Zhang and J. Rychlewski, "Structural tensors for anisotropic solids," *Archives of Mechanics*, vol. 42, no. 3, pp. 267–277, 1990.

[143] D. E. Laughlin, M. A. Willard, and M. E. McHenry, "Magnetic ordering: Some structural aspects," *Phase Transformations and Evolution in materials*, pp. 121–137, 2000.

[144] C. J Bradley and A. P. Cracknell, *The Mathematical Theory of Symmetry in Solids*, Oxford University Press, 1972.

[145] R. R. Birss, *Symmetry and Magnetism*, North-Holland Publishing Company-Amsterdam, 1964.

[146] P. J. Brown, A. P. Gandy, K. Ishida, W. Ito, R. Kainuma, T. Kanomata, K. U. Neumann, K. Oikawa, B. Ouladdiaf, A Sheikh, and K. R. A. Ziebeck, "Magnetic and structural properties of the magnetic shape memory compound $Ni_2Mn_{1.48}Sb_{0.52}$," *Journal of Physics: Condensed Matter*, pp. 1–9, 2010.

[147] J. C. Toledano and P. Toledano, *The Landau Thory of Phase Transitions*, World Scientific, 1987.

[148] T. Kakeshita, H. Shirai, K. Shimizu, K. Sugiyama, K. Hazumi, and M. Date, "Magnetic field-induced transformation from paramagnetic austenitic to ferromagnetic martensite in an fe-3.9mn-5.0c(at%) alloy," *Transactions of the Japan Institute of Metals*, vol. 28, no. 11, pp. 891–897, 1987.

[149] K. Haldar, B. Kiefer, and D. C. Lagoudas, "FE-analysis of the demagnetization effect and stress inhomogeneities in msma samples," *Philosophical Magazine*, vol. 91(32), pp. 4126–4257, 2011.

[150] J. C. Simo and T. J. R. Hughes, *Computational Inelasticity*, vol. 7 of *Interdisciplinary Applied Mathematics*, Springer-Verlag, New York, 1998.

[151] R. Tickle, "Ferromagnetic shape memory materials," Ph.D. dissertation, University of Minnesota, Minneapolis, MN, May 2000.

[152] M. I. Kaganov and V. M. Tsukernik, *The Nature of Magnetism*, MIR, 1985.

[153] S. Chikazumi and S. H. Charp, *Physics of Magnetism*, John Wiley & Sons, 1964.

[154] J. A. Monroe, I. Karaman, B. Basaran, W. Ito, R. Y. Umetsu, R. Kainuma, K. Koyama, and Y. I. Chumlyakov, "Direct measurement of large reversible magnetic field-induced strain in Ni-Co-Mn-In metamagnetic shape memory alloys," *Submitted to Acta Materialia*, 2012.

[155] D. Lagoudas, D. Hartl, Y. Chemisky, L. Machado, and P Popov, "Constitutive model for the numerical analysis of phase transformation in polycrystalline shape memory alloys," *International Journal of Plasticity*, vol. DOI:10.1016/j.ijplas.2011.10.009, 2011.

[156] K. C. Atli, I. Karaman, R. D. Noebe, A. Garg, Y. I. Chumlyakov, and I.V. Kireeva, "Improvement in the shape memory response of $Ti_{50.5}Ni_{24.5}Pd_{25}$ high-temperature shape memory alloy with scandium microalloying," *Metallurgical and Materials Transactions A*, vol. 41, no. 10, pp. 2485–2497, 2010.

[157] A. A. Likhachev, A. Sozinov, and K. Ullakko, "Optimizing work output in Ni-Mn-Ga and other ferromagnetic shape memory alloys other ferromagnetic shape-memory alloys," *in: Proceedings of SPIE, Symposium on Smart Structures and Materials*, vol. 4699, pp. 553–563, 2002.

[158] Y. Ge, O. Heczko, O. Söderberg, and V. K. Lindroos, "Various magnetic domain structures in Ni-Mn-Ga martensite exhibiting magnetic shape memory effect," *Journal of Applied Physics*, vol. 96, no. 4, pp. 2159–2163, 2004.

[159] M. R. Sullivan and H. D. Chopra, "Temperature- and field-dependent evolution of micromagnetic structure in ferromagnetic shape-memory-alloys," *Physical Review B*, vol. 70, pp. 094427–(1–8), 2004.

[160] M. R. Sullivan, A. A. Shah, and H. D. Chopra, "Pathways of structural and

magnetic transition in ferromagnetic shape-memory alloys," *Physical Review B*, vol. 70, pp. 094428–(1–8), 2004.

[161] R. C. O'Handley, S. J. Murray, M. Marioni, H. Nembach, and S. M. Allen, "Phenomenology of giant magnetic-field-induced strain in ferromagnetic shape-memory materials (invited)," *Journal of Applied Physics*, vol. 87, no. 9, pp. 4712–4717, 2000.

[162] J. D. Jackson, *Classical Electrodynamics*, John Wiley & Sons, New York, 2nd edition, 1975.

[163] H. H. Woodson and J. R. Melcher, *Electromechanical Dynamics, Part I: Discrete Systems*, Krieger Publishing Company, Malabar, FL, Reprint of 1968 edition, 1990.

[164] H. N. Bertram, *Theory of Magnetic Recording*, Cambridge University Press, Cambridge, UK, 1994.

[165] E. Schlömann, "A sum rule concerning the inhomogeneous demagnetizing field in nonellipsoidal samples," *Journal of Applied Physics*, vol. 33, no. 9, pp. 2825–2826, 1962.

[166] R. M. Bozorth, *Ferromagnetism*, IEEE Press, reissue of 1951 edition, 1993.

[167] J. D. Eshelby, "The determination of the elastic field of an ellipsoidal inclusion, and related problems," *Proceedings of the Royal Society of London. Series A, Mathematical and Physical Sciences*, vol. 241, no. 1226, pp. 376–396, 1957.

[168] T. Mura, *Micromechanics of Defects in Solids*, Mechanics of Elastic and Inelastic Solids. Kluwer Academic Publisher, Dordrecht, The Netherlands, 2nd revised edition, 1987.

[169] R. Moskowitz and E. Della Torre, "Theoretical aspects of demagnetization tensors," *IEEE Transactions on Magnetics*, vol. 2, no. 4, pp. 739–744, 1966.

[170] H. Fukushima, Y. Nakatani, and N. Hayashi, "Volume average demagnetizing tensor of rectangular prisms," *IEEE Transactions on Magnetics*, vol. 34, no. 1, pp. 193–198, 1998.

[171] D. C. Lagoudas, B. Kiefer, and A. J. Broederdorf, "Accurate interpretation of magnetic shape memory alloy experiments utilizing coupled magnetostatic analysis," *in: Proceedings of ASME, International Mechanical Engineering Congress and Exposition, Chicago, IL, 5–10 November 2006*, vol. IMECE2006-15296, pp. 1–11, 2006.

[172] A. Das, *The Special Theory of Relativity*, Springer-Verlag, 1993.

[173] A. W. Joshi, *Elements of Group Theory for Physicists*, Wiley Eastern Limited, 1975.

[174] M. Mert and E. Kiral, "On the constitutive relations for anisotropic materials–triclinic, monoclinic, rhombic, tetragonal and hexagonal crystal systems," *International Journal of Engineering Science*, vol. 15, pp. 281–294, 1977.

[175] M. Hamermesh, *Group Theory and Its Application to Physical Problems*, Dover Publications, New York, 1962.

[176] J. S. Lomont, *Application of Finite Groups*, Dover Publications, New York, 1959.

[177] R. I. Joseph and E. Schoemann, "Demagnetization field in nonellipsoidal bodies," *Journal of Applied Physics*, vol. 36, no. 5, pp. 1579–1593, 1965.

[178] R. Aharoni, "Demagnetizing factors for rectangular ferromagnetic prisms," *Journal of Applied Physics*, vol. 83, no. 6, pp. 3432–3434, 1998.

APPENDIX A

BRIEF DESCRIPTIONS OF DIFFERENT TRANSFORMATIONS

A1. Euclidean transformation

The Euclidian transformation between two inertial coordinate systems $(\mathbf{x}, t)$ and $(\mathbf{x}^*, t^*)$ are related by,

$$\mathbf{x}^* = \mathbf{Q}(\mathbf{t})\mathbf{x} + \mathbf{c}(\mathbf{t}), \quad \mathbf{t}^* = \mathbf{t} + \mathbf{a}, \tag{A.1}$$

where, $\mathbf{Q}$ is the rotation matrix between the two frames.

A2. Galilean transformation

The Galilean transformation is used to transform between the coordinates of two reference frames which differ only by constant relative motion within the constructs of Newtonian physics. The transformation also states that the fundamental laws of physics are the same in all inertial frames. Any two inertial coordinate systems $(\mathbf{x}, t)$ and $(\bar{\mathbf{x}}, \bar{t})$ are related by Galilean transformation,

$$\bar{\mathbf{x}} = \mathbf{Q}\mathbf{x} + \mathbf{c_1}\mathbf{t} + \mathbf{c_2}, \quad \bar{\mathbf{t}} = \mathbf{t} + \mathbf{a}, \tag{A.2}$$

where, $a, \mathbf{c_1}, \mathbf{c_2}$ and $\mathbf{Q}$ are constants. $\mathbf{Q}$ is the rotation matrix between the two frames.

A3. Lorentz transformation

The Lorentz transformation describes how, according to the theory of special relativity, two observers' varying measurements of space and time can be converted into

each other's frames of reference. It reflects the surprising fact that observers moving at different velocities may measure different distances, elapsed times, and even different orderings of events. The Lorentz transformation supersedes the Galilean transformation of Newtonian physics, which assumes an absolute space and time. Since relativity postulates that the speed of light is the same for all observers, it must preserve the spacetime interval between any two events in Minkowski space. The Lorentz transformation describes only the transformations in which the spacetime event at the origin is left fixed, so they can be considered as a rotation of Minkowski space.

A4. Minkowsky space

Minkowski space or Minkowski spacetime is the mathematical setting in which Einstein's theory of special relativity is most conveniently formulated. In this setting the three ordinary dimensions of space are combined with a single dimension of time to form a four-dimensional manifold for representing a spacetime [172]. In theoretical physics, Minkowski space is often contrasted with Euclidean space. While a Euclidean space has only spacelike dimensions, a Minkowski space also has one timelike dimension. Formally, Minkowski space is a four-dimensional real vector space equipped with a nondegenerate, symmetric bilinear form. The symmetry group of a Euclidean space is the Euclidean group and for a Minkowski space it is the Poincar group.

APPENDIX B

SYMMETRY AND GROUP THEORY

B1. Point group: basic concepts

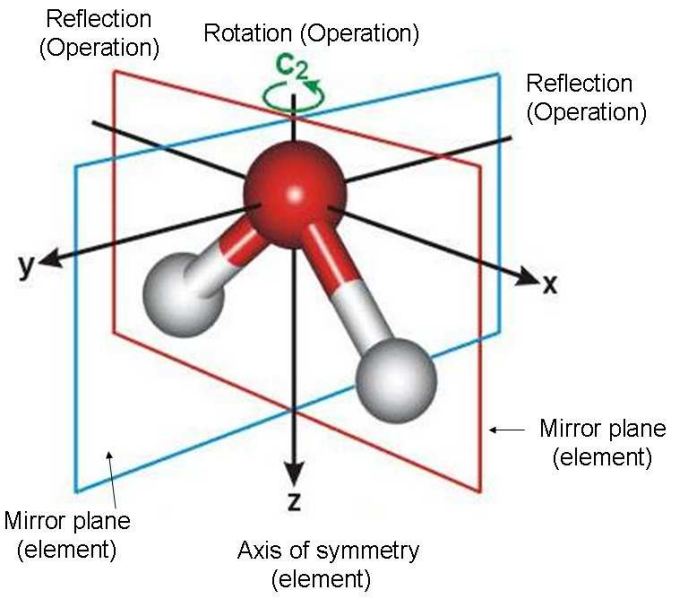

Fig. 83. Symmetry of H_2O molecule, which belongs to a point group.

An object displays *symmetry* if under specific *transformation operation* the object does not change its appearance. A *symmetry operation* S is a coordinate transformation that takes a point (x, y, z) to another point (x', y', z'), without changing the shape and size of an object. This may be denoted by

$$S : (x, y, z) \rightarrow (x', y', z')$$

For example, a *mirror operation* m_α is a symmetry operation that takes a point (x, y, z) to its image (x', y', z') through the reflection with the mirror plane, which

has its normal along the α direction. When α is along the x axis, we can denote

$$m_x : (x, y, z) \to (-x, y, z)$$

Another example is *identity operation* E that takes a point (x, y, z) to itself i.e.

$$E : (x, y, z) \to (x, y, z)$$

A *point group* is a group of such symmetry operations that keep at least one point invariant(in the same place). As a result, point groups can only consist of rotations, mirror reflections and inversions or certain combinations of those. For example, water molecule has one axis of symmetry and two mirror planes of symmetry (Fig. 83). Each symmetry operation has a corresponding *symmetry element*, which is the axis, plane, line or point with respect to the symmetry operation.

1. Point group symmetry in a plane

We first consider objects confined in two dimensions and the points of the object are described by (x, y). There are two operations that leave at least one point invariant.

1. Mirror operations m_x and m_y.

2. Rotation operation

$$C_n : (x, y) \to (\cos\frac{2\pi}{n})x - (\sin\frac{2\pi}{n})y, (\sin\frac{2\pi}{n})x + (\cos\frac{2\pi}{n})y,\ n \in Int.$$

   By rotating multiple times, we end up with the *cyclic group* (also called) C_n.

$$C_n = \{E, C_n, (C_n)^2, (C_n)^3..(C_n)^{n-1}\}.$$

   This is just a group of discrete rotations by $\frac{2\pi}{n}$. This notation has the unfortunate fact of using C_n for both the name of the group and the element of order

n. For a crystal, the allowed rotational groups are

$$C_1, C_2, C_3, C_4, C_6.$$

There are *ten crystallographic plane points group*. They are

Nomenclature	Symmetry operations	Group order
1	E	1
2	E, C_2	2
m	E, m_θ (θ=angle with x axis)	2 2
$2mm$	E, C_2, m_x, m_y	4
3	$E, C_3, (C_3)^2$	3
$3m$	$E, C_3, (C_3)^2, m_{\frac{2\pi}{3}}, m_{\frac{4\pi}{3}}, m_y$	6
4	$E, C_4, (C_4)^2, (C_4)^3$	4
$4mm$	$E, C_4, (C_4)^2, (C_4)^3, m_{\frac{3\pi}{4}}, m_{\frac{\pi}{4}}, m_x, m_y$	8
6	$E, C_6, (C_6)^2, (C_6)^3, (C_6)^4, (C_6)^5$ Note: $(C_6)^2 = C_3, (C_6)^4 = (C_3)^2, (C_6)^3 = C_2$	6
$6mm$	$E, C_6, (C_6)^2, (C_6)^3, (C_6)^4, (C_6)^5, m_{\frac{\pi}{6}}, m_{\frac{2\pi}{6}}, m_{\frac{4\pi}{6}}, m_x, m_y$	12

Table XXXVI. Ten crystallographic plane points group

2. Point group symmetry in three dimensions

There are many standard ways to represent the crystallographic groups. We will follow *Schoenflies* notation and *Hermann-Mauguin* notation, which are described in the following subsection.

a. Points group with pure rotational axis

These point groups each consist of only a single family of symmetry operations-those generated by a single rotation axis. If the rotation axis is of order n, the Schoenflies notation is

$$C_n.$$

The alternative Hermann-Mauguin notation is simply

$$n.$$

There are only five possible n s for the crystallographic point groups.

	Symmetry	Order	Description
$C_1\,(1)$	Triclinic	1	Rotation by 2π about an arbitrary axis (identity).
$C_2\,(2)$	Monoclinic	2	Rotation around 2-fold axis (out of plane axis).
$C_3\,(3)$	Trigonal	3	Rotation around 3-fold axis (out of plane axis). Rotation by $\frac{2\pi}{3}$, $\frac{4\pi}{3}$ and $\frac{6\pi}{3}$ (identity) .
$C_4\,(4)$	Tetragonal	4	Rotation around 4-fold axis (out of plane axis).
$C_6\,(6)$	Hexagonal	6	Rotation around 6-fold axis (out of plane axis).

Table XXXVII. Points group with pure rotational axis

b. Points group with a single rotational axis that lies in a mirror plane: C_{nv} (nm)

In these point groups, a mirror plane is parallel to-and includes-the principal symmetry axis. Since the principal symmetry axis is usually considered to be in a vertical direction, the mirror plane is called a *vertical* mirror plane and is denoted by subscript v. The point group symbol for odd n is

$$nm$$

and for even n is

$$nmm.$$

The second m denotes the set of mirror planes that bisect the principle set.

	Symmetry	Order	Description
$C_{2v}\,(2mm)$	Orthorhombic	4	Two mirror planes perpendicular to each other. The line of intersection generates the 2-fold axis.
$C_{3v}\,(3m)$	Trigonal	6	Combination of Three mirror planes and 3-fold axis
$C_{4v}\,(4mm)$	Tetragonal	8	Four vertical mirror planes and C_4
$C_{6v}\,(6mm)$	Hexagonal	12	Six mirror planes (at interval of $\frac{\pi}{6}$) and C_6

Table XXXVIII. Points group with a single rotational axis that lies in a mirror plane

c. Points group with only rotation-reflection axes: S_n $(\bar{n})$

In these point groups, the basis symmetry operation is the rotation-reflection axis S_n defined by a rotation of $\frac{2\pi}{n}$ followed by a reflection in a plane perpendicular to the principal symmetric axis. The Schoenflies notation is

$$S_n.$$

Instead of choosing the rotation-reflection, it is also possible to choose the rotation-inversion axis, which is defined as a rotation by $\frac{2\pi}{n}$ followed by inversion throgh the origin, by which a point (x, y, z) is transformed to the point $(-x, -y, -z)$. The Hermann-Mauguin notation is

$$\bar{n}.$$

	Symmetry	Order	Description
$S_2, C_i\,(\bar{1})$	Triclinic	2	Inversion through center
$S_4\,(\bar{4})$	Tetragonal	4	4-fold rotation-reflection axis
$S_6, C_{3i}\,(\bar{3})$	Trigonal	2	6-fold rotation-reflection axis

Table XXXIX. Points group with only rotation-reflection axes

d. Points group with a single rotational axis and a mirror plane perpendicular to the axis: C_{nh} (n/m)

These point groups contain a rotation symmetry axis with a mirror plane perpendicular to the axis. Since the rotation axis is usually consider to be vertical, the mirror plane is horizontal and, in the Schoenflies notation, is denoted by h. Thus the symbols of these groups are

$$C_{nh}.$$

The alternative Hermann-Mauguin notation is

$$n/m$$

which indicates a mirror plane perpendicular to the n-fold axis.

e. Simple dihedral point groups: D_n $(n2-)$

In these groups, the principal rotation axis of order n has perpendicular to its n 2-fold axes. These groups are called *dihedral* and have the Schoenflies notation

$$D_n.$$

	Symmetry	Order	Description
$C_{1h}\,(m)$	Monoclinic	2	Identity element and a mirror plane
$C_{2h}\,(2/m)$	Monoclinic	4	2-fold axis and a horizontal mirror plane
$C_{3h}, S_3\,(2/m, \bar{6})$	Hexagonal	6	3-fold axis and horizontal a mirror plane
$C_{4h}\,(4/m)$	Tetragonal	8	4-fold axis and a mirror plane perpendicular to the 4-fold axis
$C_{6h}\,(6/m)$	Hexagonal	12	6-fold axis and a horizontal mirror plane

Table XL. Points group with a single rotational axis and a mirror plane perpendicular to the axis

The alternative Hermann-Mauguin notation has as its principal symbol the integer representing the order of the axis. This is followed by 2 to denote the 2-fold axes. If n is even, a third digit 2 is added to indicate that a second set of 2-fold axes midway between the first is generated by the basic symmetry operation.

	Symmetry	Order	Description
$D_3\,(222)$	Orthorhombic	4	Identity operation and three perpendicular 2-fold axes
$D_3\,(32)$	Trigonal	6	Perpendicular to the 3-fold rotation axes and three 2-fold axes
$D_4\,(422)$	Tetragonal	8	Perpendicular to the 4-fold rotation axes and four 2-fold axes
$D_6\,(622)$	Hexagonal	12	Perpendicular to the 6-fold rotation axes and six 2-fold axes

Table XLI. Simple dihedral point groups

f. Dihedral groups with vertical diagonal mirror planes: D_{nd} $(\bar{n}m)$

These groups are derived from the groups D_n by adding vertical mirror planes that bisect the angles between the 2-fold axes. The subscript d is derived from the fact that such mirror planes are called *diagonal* mirror planes. The Hermann-Mauguin notation for odd n is

$$\bar{n}m$$

and for even n is

$$\overline{2n}m.$$

	Symmetry	Order	Description
$D_{2d}\,(\bar{4}2m)$	Tetragonal	8	Adding two 2-fold axes perpendicular to 4-fold axis of S_4
$D_{3d}\,(\bar{3}m)$	Trigonal	12	Adding inversion to D_3

Table XLII. Dihedral groups with vertical diagonal mirror planes

g. Dihedral groups with horizontal mirror planes: D_{nh} $(n/mm-)$

These groups are obtained from the simple dihedral group D_n by adding mirror planes perpendicular to the principal axis. In an alternate notation, an axis with perpendicular mirror plane is denoted by n/m. The Hermann-Mauguin notation for odd n is

$$n/mm$$

and for even n is

$$n/mmm.$$

	Symmetry	Order	Description
$D_{2h}\,(mmm, 2/mmm)$	Orthorhombic	8	Adding horizontal mirror on D_2
$D_{3h}\,(3/mm, \bar{6}m2)$	Hexagonal	12	Adding 2 mirror plane perpendicular to the 3-fold axis of D_3
$D_{4h}\,(4/mmm)$	Tetragonal	16	Adding a horizontal mirror plane perpendicular to the 4-fold axis of D_4
$D_{6h}\,(6/mmm)$	Hexagonal	24	Adding a mirror plane perpendicular to the 6-fold axis of D_6

Table XLIII. Dihedral groups with horizontal mirror planes

h. Cubic point groups: T, O $(23-)$

The cubic point groups have the characteristic feature of having three perpendicular 2-fold axes with a 3-fold axis equidistant from the three 2-fold axes, that is, along the diagonal of a cube formed by the three 2-fold axes. One of the cubic groups has the symmetry of the regular tetrahedron (denoted by T) and one that of the regular octahedral (denoted by O). The subscripts h and d have the same meaning as described earlier.

	Symmetry	Order	Description
$T\,(23)$	Cubic	12	Adding a 3-fold axes that are equidistant from the three 2-fold axes of 222
$T_d\,(\bar{4}3m)$	Cubic	24	Adding mirror planes that contain the 3-fold and 2-fold axes of T
$O\,(432)$	Cubic	24	
$O_h\,(m3m)$	Cubic	48	
$T_h\,(m\bar{3})$	Cubic	24	

Table XLIV. Cubic point groups

3. The summary of the crystallographic point groups

For crystals, it is more useful to classify the point groups in terms of the *seven crystal systems*. They are given in the table below

Crystal	Group
Triclinic	C_1, C_i
Monoclinic	C_{1h}, C_2, C_{2h}
Orthorhombic	C_{2v}, D_2, D_{2h}
Tetragonal	$C_4, S_4, C_{4h}, D_{2d}, C_{4v}, D_4, D_{4h}$
Trigonal	$C_3, S_6, C_{3v}, D_3, C_{3d}$
Hexagonal	$C_{3h}, C_6, D_{3h}, C_{6h}, C_{6v}, D_6, D_{6h}$
Cubic	T, T_h, T_d, O, O_h

Table XLV. 32 crystallographic point groups

B2. Group theory

Definition of group: A collection of elements, G, will be called a *group* if its elements $A, B, C, ...$ can be combined together (multiplied) in such a way that the rule of combination satisfies the following four axioms:

1. Closer: If $A, B \in G$ then $AB \in G$ and is unique
2. Associative: $A(BC) = (AB)C$
3. Identity: $AE = EA = A$
4. Inverse: $AA^{-1} = A^{-1}A = E$

The number of elements in a group is the *order* of the group. This section is closely followed by [173].

1. Multiplication table

Suppose we have a square cut out in a piece of cardboard as shown in Fig.84 This structure can be represented by the group C_{4v} with the following elements (Fig.85)

$$\{E, C_4, (C_4)^2, (C_4)^3, m_x, m_y, m_{\frac{\pi}{4}}, m_{-\frac{\pi}{4}}\}.$$

The order of the group is 8. Let us consider the following operations

$$C_4 m_x = m_{\frac{\pi}{4}},\ m_{\frac{\pi}{4}}(C_4)^3 = m_y,\ m_{\frac{\pi}{4}} m_{-\frac{\pi}{4}} = (C_4)^2, ...$$

All such products of the group elements can be represented by a table, known as the *group multiplicative table*. In a successive operation such as $ABC...$ the order of operation is *from right to left*. The ordering of the rows and the columns in writing down the multiplication table is immaterial. We have chosen a different ordering

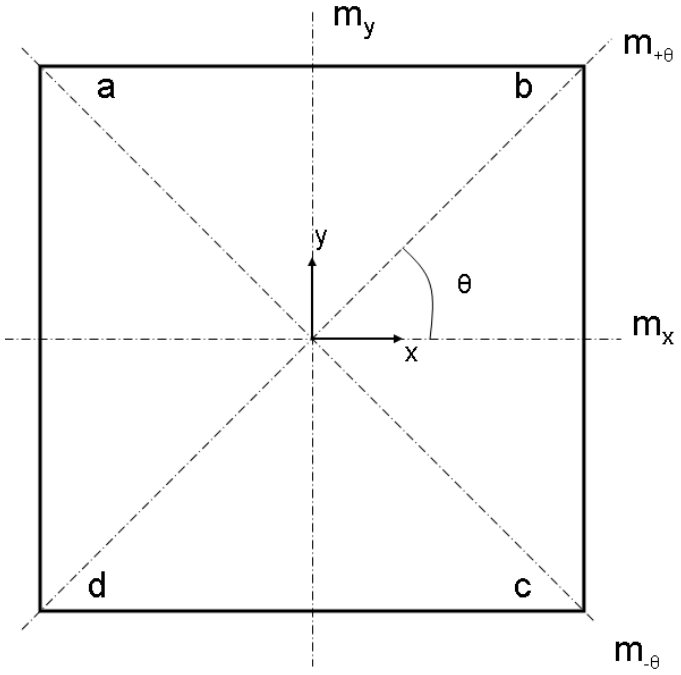

Fig. 84. The axes and planes of symmetry of a square

for the rows and columns such that the principal diagonal contains only the identity element E. This type of arrangement has some advantages in the representation of a group.

2. Conjugate elements and classes

If $A, B, C \in G$ such that $A^{-1}BA = C$ then B and C are knowns as *conjugate elements* and the process is known as *similarity transformation* of B by A. Now it is possible to split the group into sets such that all the elements of a set are conjugate to each other but no two elements belonging to different sets are conjugate to each other. Such sets of elements are called conjugate classes or simply *classes*.

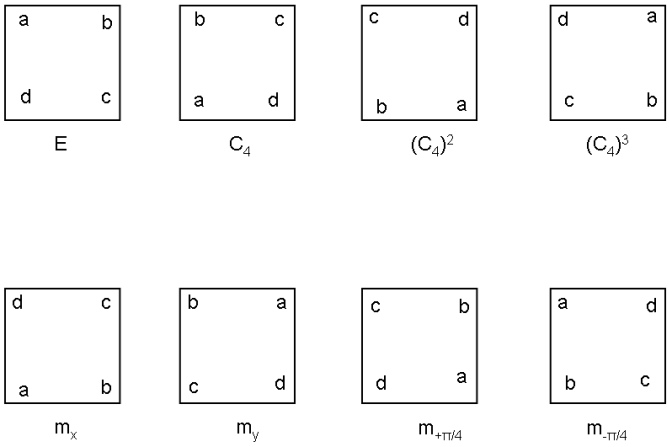

Fig. 85. Symmetry transformation of a square

Example: The classes of the group C_{4v} are

$$(E),\ (C_4,(C_4)^3),\ ((C_4)^2),\ (m_x,m_y),\ (m_{\frac{\pi}{4}},m_{-\frac{\pi}{4}})$$

3. Multiplication of classes

Let us consider two classes

$$\mathscr{C}_i = (A_1, A_2, ..., A_m)$$
$$\mathscr{C}_j = (B_1, B_2, ..., B_n).$$

We denote

$$\begin{aligned}\mathscr{C}_i\mathscr{C}_j &= (A_1B_1, A_1B_2, ..., A_lB_k, ..., A_mB_n)\\ &= (A_\alpha \otimes B_\beta) \qquad \alpha = 1, ..., m \quad \beta = 1, ..., n.\end{aligned}$$

We can express the product of two classes of a group as a sum of complete classes of the group. i.e

$$\mathscr{C}_i\mathscr{C}_j = \sum_k a_{ij,k}\mathscr{C}_k \qquad a_{ij,k} \in Int^+ \text{ or } 0.$$

1st($\rightarrow$)		E	C_4	$(C_4)^2$	$(C_4)^3$	m_x	m_y	$m_{\frac{\pi}{4}}$	$m_{-\frac{\pi}{4}}$
2nd($\downarrow$)	E	E	C_4	$(C_4)^2$	$(C_4)^3$	m_x	m_y	$m_{\frac{\pi}{4}}$	$m_{-\frac{\pi}{4}}$
	$(C_4)^3$	$(C_4)^3$	E	C_4	$(C_4)^2$	$m_{-\frac{\pi}{4}}$	$m_{\frac{\pi}{4}}$	m_x	m_y
	$(C_4)^2$	$(C_4)^2$	$(C_4)^3$	E	C_4	m_x	m_y	$m_{-\frac{\pi}{4}}$	$m_{\frac{\pi}{4}}$
	C_4	C_4	$(C_4)^2$	$(C_4)^3$	E	$m_{\frac{\pi}{4}}$	$m_{-\frac{\pi}{4}}$	m_y	m_x
	m_x	m_x	$m_{-\frac{\pi}{4}}$	m_y	$m_{\frac{\pi}{4}}$	E	$(C_4)^2$	$(C_4)^3$	C_4
	m_y	m_y	$m_{\frac{\pi}{4}}$	m_x	$m_{-\frac{\pi}{4}}$	$(C_4)^2$	E	C_4	$(C_4)^3$
	$m_{\frac{\pi}{4}}$	$m_{\frac{\pi}{4}}$	m_x	$m_{-\frac{\pi}{4}}$	m_y	C_4	$(C_4)^3$	E	$(C_4)^2$
	$m_{-\frac{\pi}{4}}$	$m_{-\frac{\pi}{4}}$	m_y	$m_{\frac{\pi}{4}}$	m_x	$(C_4)^3$	C_4	$(C_4)^2$	E

Table XLVI. The multiplication table for the group C_{4v}

Example: Let us consider

$$\mathscr{C}_1 \Rightarrow (E),\ \mathscr{C}_2 \Rightarrow (C_4, (C_4)^3),\ \mathscr{C}_3 \Rightarrow ((C_4)^2),\ \mathscr{C}_4 \Rightarrow (m_x, m_y),\ \mathscr{C}_5 \Rightarrow (m_{\frac{\pi}{4}}, m_{-\frac{\pi}{4}})$$

So,

$$\begin{aligned} \mathscr{C}_2\mathscr{C}_4 &= 2\mathscr{C}_5 \\ \mathscr{C}_5\mathscr{C}_5 &= 2(\mathscr{C}_1 + \mathscr{C}_4) \\ &..etc.. \end{aligned}$$

This theorem will be used to construct *character table*.

Let $A, B \in \{G_1\}$ and $\phi : G_1 \rightarrow G_2$ such that $\phi(AB) = \phi(A)\phi(B)$.
Homomorphism: If ϕ is a *many-to-one* mapping.

Isomorphism: If ϕ is *one-to-one* mapping.

Automorphism: When $\{G_1\} = \{G_2\}$.

4. Representation of finite group

Let us consider a group with

$$\{G_1\} = \{E, C_4, (C_4)^2, (C_4)^3\}.$$

The multiplication table is given in Table XLVII. Let us consider another group

	E	C_4	$(C_4)^2$	$(C_4)^3$
E	E	C_4	$(C_4)^2$	$(C_4)^3$
$(C_4)^3$	$(C_4)^3$	E	C_4	$(C_4)^2$
$(C_4)^2$	$(C_4)^2$	$(C_4)^3$	E	C_4
C_4	C_4	$(C_4)^2$	$(C_4)^3$	E

Table XLVII. The multiplication table for G_1

$$\{G_2\} = \{1, -1, i, -i\}, \quad (i = \sqrt{-1})$$

and the multiplication table of this group is given in XLVIII. It is possible that $\{G_1\}$

Subgroup (H of G): $H \subset G$ and also a group under some binary composition as in G.

Abelian group: If $A, B \in G$ and $AB = BA$ i.e they commute.

Invariant subgroup: If H is a subgroup of G such that $\forall\, G \in \{G\}$ and $\forall\, H \in \{H\}$, $GHG^{-1} \in \{H\}$, then $\{H\}$ is said to be an *invariant subgroup.*

Direct sum of matrices: Let $[A]_{m\times m}$, $[B]_{n\times n}$ and $[C]_{k\times k}$. Then the direct sum is given by

$$[D]_{m+n+k,m+n+k} = [A]_{m\times m} \oplus [B]_{n\times n} \oplus [C]_{k\times k}$$

Or

$$D = A \oplus B \oplus C = \begin{bmatrix} A & & \\ & B & \\ & & C \end{bmatrix}$$

	1	-1	i	$-i$
1	-1	i	$-i$	
-1	-1	1	i	$-i$
i	i	$-i$	1	-1
$-i$	$-i$	i	-1	1

Table XLVIII. The multiplication table for G_2

and $\{G_2\}$ be *isomorphic* if we make the following correspondence

$$E \leftrightarrow 1,\ C_4 \leftrightarrow i,\ (C_4)^2 \leftrightarrow -1,\ (C_4)^3 \leftrightarrow -i$$

Then they have same multiplication table i.e having same rearrangement. Very often several groups, which arise in different contexts in everyday life and consequently with different physical meanings attached to the elements, are isomorphic to one obstruct group, whose properties can then be analyzed once for all.

Definition Let $G = \{E, A, B, C, ..\}$ be a finite group of order n with E as the identity element. Let $T = \{T(E), T(A), T(B)...\}$ be a collection of *nonsingular square matrices*, all of the same order, having the property

$$T(A)T(B) = T(AB)$$

that is if $AB = C\ \in G$, then

$$T(A)T(B) = T(C).$$

The collection T of matrices is said to be *a representation of group* G. The order of the matrices of T is called dimension of the representation.

General linear group of degree n, denoted by $GL(n)$, is the set of $n \times n$ invertible matrices, together with the operation of ordinary matrix multiplication. This forms a group. The group is so named because the columns of an invertible matrix are linearly independent. Let $GL(n)$ be an n-dimensional vector space on which the operators of a group G acts. If $\{e_1, ..., e_n\}$ be an orthonormal basis in $GL(n)$, then the operation of an element $A \in G$ on a basis vector is given by

$$Ae_i = \sum_{j=1}^{n} T_{ji}(A)e_j \tag{B.1}$$

where $T(A)$ is the matrix representing A with the basis $\{e_i\}$. $GL(n)$ is called the *carrier space of* T.

If all the matrices of T are distinct, there is clearly a one-to-one correspondence between the elements of G and the matrices of T. In this case, the groups G and T are *isomorphic* to each other and called *faithful representation of* G. On the other hand, if the matrices of T are not all distinct, there exists only a *homomorphism* from G to T and such representation is called *unfaithful representation of* G.

Example: Consider the following group,

$$\{G\} = \{E, C_4, (C_4)^2, (C_4)^3\}.$$

Then the following representation

Special linear group, written as $SL(n)$, is the subgroup of $GL(n)$ consisting of matrices with a determinant of 1. The set of unitary transformations $U(n)$ and orthogonal transformations $O(n)$ is a subgroup of $GL(n)$ and are called *unitary group* and *orthogonal group* respectively.

$$\{T\} = \{T(E) = \begin{bmatrix} 1 & 0 \\ 0 & 1 \end{bmatrix},\ T(C_4) = \begin{bmatrix} 0 & 1 \\ -1 & 0 \end{bmatrix},\ T(C_4)^2 = \begin{bmatrix} -1 & 0 \\ 0 & -1 \end{bmatrix}$$
$$T(C_4)^3 = \begin{bmatrix} 0 & -1 \\ 0 & 1 \end{bmatrix}\}$$

is a faithful representation. Similarly

$$\{T\} = \{T(E) = 1, T(C_4) = 1, T(C_4)^2 = 1, T(C_4)^3 = 1\}.$$

is an unfaithful representation.

5. Reducibility of a representation

Let $T = \{T(E), T(A), T(B)...\}$ be a representation of G in the vector space $GL(n)$. We now state that if $GL(n)$ has an invariant subspace $GL(m)$ $(m < n)$ under G, then in a suitable basis the matrices of the representation have the form

$$T(A) = \begin{bmatrix} D^{(1)}(A) & \mathbf{0} \\ X(A) & D^{(2)}(A) \end{bmatrix},$$

where $D^{(1)}(A)$ and $D^{(2)}(A)$ are square matrices of order m and $n - m$ respectively, $X(A)$ is of order $(n - m) \times m$ and $\mathbf{0}$ is a null matrix of order $m \times (n - m)$. It can be shown that any representation T of a finite group, whose matrices may be non-unitary, is equivalent (through similarity transformation) to a representation by unitary matrices. *It is always possible to convert* $T(A)$ *into unitary matrices* $\Gamma(A)$

An *invariant* subspace of a linear mapping $T : V \to V$ from some vector space V to itself is a subspace W of V such that $T(W)$ is contained in W.

A unitary matrix is a square complex matrix U, which satisfies $U^\dagger U = UU^\dagger = I$, where $U^\dagger$ is complex conjugate (also called Hermitian adjoint) of U. For real matrix

through similarity transformation.

a. Irreducible representation

If the representation T considered above is reducible, the representation $\Gamma = \{\Gamma(E), \Gamma(A), \Gamma(B)...\}$ is also reducible. Moreover, since the matrices of Γ are unitary, they must have the form

$$\Gamma(A) = \begin{bmatrix} S^{(1)}(A) & \mathbf{0} \\ \mathbf{0} & S^{(2)}(A) \end{bmatrix},$$

It may be possible that the representations $S^{(1)}$ and $S^{(2)}$ are further reducible. This process can be carried out until we can find no unitary transformation which reduces all the matrices of a representation further. Thus the final form of the matrices of the representation Γ may look like

$$\Gamma(A) = \begin{bmatrix} \Gamma^{(1)}(A) & & & \mathbf{0} \\ & \Gamma^{(2)}(A) & & \\ & & \ddots & \\ \mathbf{0} & & & \Gamma^{(s)}(A) \end{bmatrix},$$

or with all the matrices of Γ having the same reduced structure. When such a complete reduction of a representation is achieved, the component representations $\Gamma^{(1)}(A), \Gamma^{(2)}(A), ..., \Gamma^{(s)}(A)$ are called the *irreducible representations* of the group G and the representation Γ is said to be *fully reduced*, i.e.

$$\Gamma = a_1\Gamma^{(1)}(A) \oplus a_2\Gamma^{(2)}(A) \oplus ... \oplus a_c\Gamma^{(c)}(A) \quad (c \leq s). \tag{B.2}$$

- Number of irreducible representation of a group = number of classes

---

it is simply orthogonal matrix.

- $\sum_{i=1}^{c} l_i^2 = n$(order of the group) and $l_i = \dim \Gamma^{(i)}$

b. Characters of a representation

The matrices of a representation of a group in a given vector space are not unique, for they depend on the choice of the basis vectors. However, all such representations must be related to each other by some similarity transformation and must therefore be equivalent to each other. Since the trace of a matrix is invariant under similarity transformation, the traces of all the matrices of a representation would uniquely characterize a representation.

Let Γ be a representation of a group G. We define the *characters* of the representation Γ as the set of the traces of all the matrices of the representation Γ, i.e,

$$\chi(A) = \operatorname{tr} \Gamma(A)$$

All the elements in a *class* have the same character in a representation. *The character is therefore a function of the classes just as a representations is a function of the group elements.*

c. Orthogonality of characters

It can be shown that

$$\sum_{A \in G} \chi^{(i)}(A) \chi^{(j)*}(A) = n \delta_{ij}.$$

Here $\chi^{(i)}(A)$ is the character of the element A in the representation $\Gamma^{(i)}$, n is the order of the group. If n_k is the number of elements in the class $\mathscr{C}_k$ of the group, then one

can write

$$\sum_{i=1}^{c} \chi_k^{(i)*} \chi_l^{(i)} = \frac{n}{n_k} \delta_{kl}$$

where $\chi_k^{(i)}$ is the character of an element A in the class $\mathscr{C}_k$ in the representation $\Gamma^{(i)}$ etc.

d. Reduction of a reducible representation

It very often happens that we have a representation of a group which is a *reducible one*. Such a representation, say Γ, may be written as a linear combination of the *irreducible representation* as (B.2). We can find the number of times an irreducible representation $\Gamma^{(i)}$ occurs in the reduction Γ. For this we take the trace of both sides of (B.2). If $\chi(A)$, etc., denote the characters of the elements in the representation Γ, then we have

$$\chi(A) = \sum_{i}^{c} a_i \chi^{(i)}(A), \tag{B.3}$$

for all $A \in G$. Now using the orthogonality property i.e, multiplying both sides $\chi^{(j)*}(A)$ and summing over all the elements of G, we get

$$a_i = \frac{1}{n} \sum_{A \in G} \chi^{(i)*}(A) \chi(A).$$

This gives a method for obtaining the coefficients in (B.2). The character of the irreducible representations are called *primitive* or *simple characters*, while the characters of the reducible representations are called compound characters. The compound character can be expressed as a linear combination of the simple characters of a group as (B.3).

6. The example of C_{4v}

We will illustrate now how to find the irreducible representations and the corresponding characters for the group C_{4v}.

a. Character table of C_{4v}

- Find the number of classes for C_{4v}. For this group we have

$$\mathscr{C}_1,\ \mathscr{C}_2,\ \mathscr{C}_3,\ \mathscr{C}_4,\ \mathscr{C}_5.$$

- Number of irreducible representation of a group = number of classes. This means it must have five *irreducible representation*

$$\Gamma^{(1)},\ \Gamma^{(2)},\ \Gamma^{(3)},\ \Gamma^{(4)},\ \Gamma^{(5)},\ .$$

- Since $\sum_{i=1}^{c} l_i^2 = n$(order of the group) and $l_i = \dim \Gamma^{(i)}$, then

$$l_1^2 + l_2^2 + l_3^2 + l_4^2 + l_5^2 = 8$$

  The only possible solution (with integral l_i) is when four of l_i's equal to 1 and the remaining one equals to 2. The order of the l_i's are immaterial. One can choose $l_1 = l_2 = l_3 = l_4 = 1$ and $l_5 = 2$.

- Using the orthogonal relation $\sum_{i=1}^{c} \chi_k^{(i)*} \chi_l^{(i)} = \frac{n}{n_k} \delta_{kl}$ one can construct the character table for C_{4v}

b. Irreducible representation of C_{4v}

After having found the character table, it is easy to find the full irreducible representation. The first four irreducible representations are identical to the corresponding characters. For $\Gamma^{(5)}$ we must choose a suitable set of basis functions. Choosing, for

	$\mathscr{C}_1$	$\mathscr{C}_2$	$\mathscr{C}_3$	$\mathscr{C}_4$	$\mathscr{C}_5$
$\chi^{(1)}$	1	1	1	1	1
$\chi^{(2)}$	1	-1	1	-1	1
$\chi^{(3)}$	1	-1	1	1	-1
$\chi^{(4)}$	1	1	1	-1	-1
$\chi^{(5)}$	2	0	-2	0	0

Table XLIX. The character table for C_{4v}

convenience, the two orthonormal basis vectors $(\hat{i}, \hat{j})$ we can obtain the matrices of $\Gamma^{(5)}$. For example consider the operation of C_4 on the basis vector $(\hat{i}, \hat{j})$ i.e,

$$C_4(\hat{i}, \hat{j}) = (\hat{i}', \hat{j}') = (-\hat{j}, \hat{i}) = (\hat{i}, \hat{j}) \begin{bmatrix} 0 & 1 \\ -1 & 0 \end{bmatrix}$$

Then by definition of representation (Eq.(B.1)), we have

$$\Gamma^{(5)} C_4 = T(C_4) = \begin{bmatrix} 0 & 1 \\ -1 & 0 \end{bmatrix}$$

We can similarly obtain the other matrices of $\Gamma^{(5)}$. The complete table is given below where

	E	C_4	$(C_4)^2$	$(C_4)^3$	m_x	m_y	$m_{\frac{\pi}{4}}$	$m_{-\frac{\pi}{4}}$
$\Gamma^{(1)}$	1	1	1	1	1	1	1	1
$\Gamma^{(2)}$	1	-1	1	-1	-1	-1	1	1
$\Gamma^{(3)}$	1	-1	1	-1	1	1	-1	-1
$\Gamma^{(4)}$	1	1	1	1	-1	-1	-1	-1
$\Gamma^{(5)}$	$T(E)$	$T(C_4)$	$T(C_4)^2$	$T(C_4)^3$	$T(m_x)$	$T(m_y)$	$T(m_{\frac{\pi}{4}})$	$T(m_{-\frac{\pi}{4}})$

Table L. The irreducible representation of C_{4v}

$$T(E) = \begin{bmatrix} 1 & 0 \\ 0 & 1 \end{bmatrix}, \quad T(C_4) = \begin{bmatrix} 0 & 1 \\ -1 & 0 \end{bmatrix} \text{.....etc.}$$

7. The regular representation

We will now consider an example of a reducible representation of C_{4v}. The most natural way of obtaining a representation of a finite group is by inspecting the multiplicative table (Tab. XLVI). Let us now construct square matrices of order 8 for all the elements of C_{4v} in the following ways. The matrix of an element is obtained by replacing the element wherever it occurs in the multiplication table by unity and placing zeros elsewhere. For example, $T(E)$ would be a unit matrix of order 8. Another matrix, say $T(C_4)$, would take the form

$$T(C_4) = \begin{bmatrix} 0 & 1 & 0 & 0 & 0 & 0 & 0 & 0 \\ 0 & 0 & 1 & 0 & 0 & 0 & 0 & 0 \\ 0 & 0 & 0 & 1 & 0 & 0 & 0 & 0 \\ 1 & 0 & 0 & 0 & 0 & 0 & 0 & 0 \\ 0 & 0 & 0 & 0 & 0 & 0 & 0 & 1 \\ 0 & 0 & 0 & 0 & 0 & 0 & 1 & 0 \\ 0 & 0 & 0 & 0 & 1 & 0 & 0 & 0 \\ 0 & 0 & 0 & 0 & 0 & 1 & 0 & 0 \end{bmatrix}. \tag{B.4}$$

The representation generated by such matrices is called *regular representation* of the group. In many problems in physics, we have a set of basis functions generating some representation of a group. However, such a representation may in general be a reducible representation. It can be reduced by a suitable choice of the subsets of basis functions. Suppose that the n basis functions $\{\phi_1, \phi_2, ..., \phi_n\}$ generate a representation

T of the group. The matrix representation is given by

$$A\phi_i = T_{ij}(A)\phi_j.$$

Thus, for example, it can be seen that the eight functions ϕ_1, ϕ_2,...,ϕ_8 of the eight positions 1, 2,...,8 shown in Fig. 86 form a convenient set of basis functions for the regular representation of C_{4v}. The operation of, say C_4, on the basis functions can

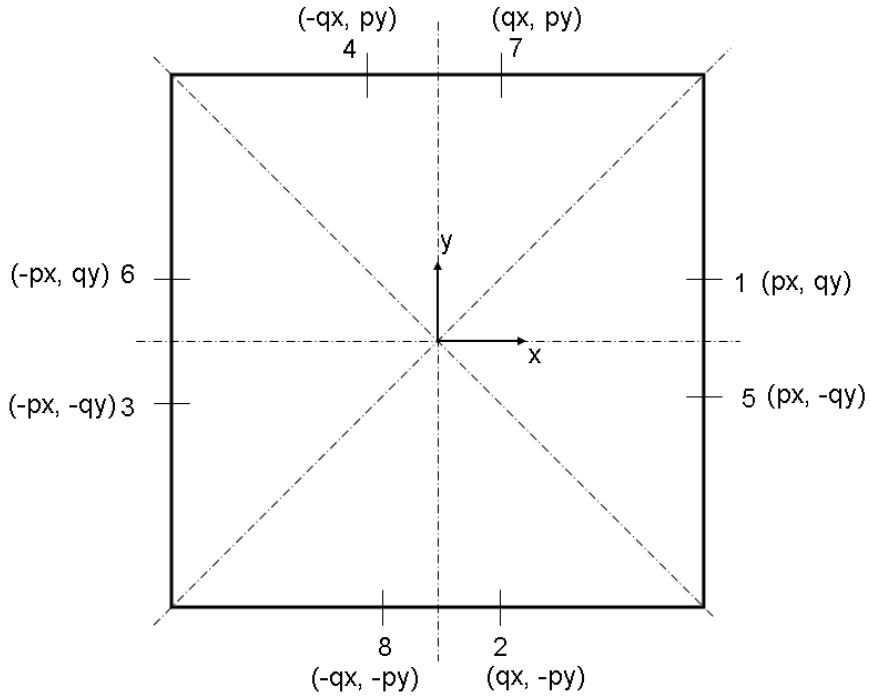

Fig. 86. The eight functions ϕ_i of the positions shown generate the regular representation of C_{4v}

be written in the form

$$\{\phi'\} = T(C_4)\{\phi\},$$

where $T(C_4)$ is given in (B.4).

In order to reduce the representation T, we wish to find a suitable unitary trans-

formation matrix U such that

$$U^{-1}T(A)U = \Gamma(A),$$

for all A in G and $\Gamma(A)$ has the reduced or block-diagonalized form. This suggest that if we choose the new basis function

$$\{\psi\} = U\{\phi\},$$

instead of the basis function $\{\phi\}$, the matrices of the representation would be in the block-diagonalized form. The new basis is *invariant* under the operation of the group elements. This is also known as the *basic quantities* and form a *carrier space* of the irreducible representation. In the expanded form we can write

$$\psi_i = U_{ij}\phi_j. \tag{B.5}$$

For the purpose of finding the coefficients U_{ij}, we write the above equation in a different form as

$$\psi^{\alpha}_{pm} = \sum_{i=1}^{n} U^{i}_{\alpha pm}\phi_i, \tag{B.6}$$

where ψ^{α}_{pm} is the m-th basis function for the irreducible representation Γ^{α} occurring for the p-th time in the reduction of the representation T. If

$$\Gamma = \bigoplus_{\alpha=1}^{c} a_\alpha \Gamma^{(\alpha)}$$

then $1 \leq \alpha \leq c$, $1 \leq p \leq a_\alpha$, $1 \leq m \leq l_\alpha$ (the dimension of $\Gamma^{(\alpha)}$). Equations (B.5) and (B.6) are same. The matrix $[U^{i}_{\alpha pm}]$ is just another label of U_{ij}; a set of values (α, p, m) denotes a column of U and a value of i denotes a row of U. Similarly, ψ^{α}_{pm} is just another name for ψ_i. So, for C_4 we would be looking for U such that

$$U^{-1}T(A)U = \Gamma^{(1)} \oplus \Gamma^{(2)} \oplus \Gamma^{(3)} \oplus \Gamma^{(4)} \oplus 2\Gamma^{(5)}.$$

$$\sum_{\alpha,\,p,\,m} U^{i*}_{\alpha pm} U^{j}_{\alpha pm} = \delta_{ij}$$

$$\sum_{k=1}^{l_\alpha} U^{E}_{\alpha pm} \Gamma^{(\alpha)}_{km} = U^{A}_{\alpha pm}$$

B3. Crystallographic magnetic point group

The classical theory of symmetry was essentially a three dimensional study i.e. a point P can be specified by a vector $\mathbf{r} = (x, y, z)$. We now give each point a fourth coordinate [134] s, which can take only one value between two possible values. The s can be the spin of a particle and the two allowed values correspond to spin-up and spin down. In abstract terms the two allowed values of s can be represented by two colors, such as black and white. If we include the coordinate s and if the values of s for the various atoms in a lattice are randomly distributed, the symmetry of the lattice will be completely destroyed. But if the values of s are distributed in a regular fashion, it is possible for part of the symmetry to survive. For this purpose, we introduce a new operation, which we may call *operation of antisymmetry* $\mathscr{R}$. When this operator acts on classical point group, it is possible to find out a collection of new point groups, which are called *black and white groups* or *magnetic groups* or *Heesch-Shubnikov groups*. If we think of s as being the two allowed values of a magnetic direction, parallel and antiparallel to a particular direction, then $\mathscr{R}$ is the operation which reverses a magnetic moment. Since a reversal of time changes the sign of the current and hence reverses the direction of the magnetic moment vector, the operator $\mathscr{R}$ often known as *time-inversion* operator. We will denote the operation of $\mathscr{R}$ by τ. There are three types of Heesch-Shubnikov point groups which are commonly described as follows

Type I the classical point group (32)

Type II the *grey* point group (32)

Type III the *black and white* or *magnetic* point group (58)

The numbers in brackets give the number of point groups of each type. The total number of Heesch-Shubnikov point groups is therefore 122. In type I groups the operation of antisymmetry τ is not present. These are ordinary or classical point groups $\mathscr{G}$.

The extra coordinate s which we have introduced and which is allowed to take one of two values, is assumed to take both values simultaneously in type II. Any operation of $\mathscr{G}$ leaves s unchanged and τ times any operation of $\mathscr{G}$ changes black into white and white into black, thereby also leaving s unchanged. Therefore, if a spontaneous magnetic moment is developed at any point within the crystal, the presence of τ will develop an equal and opposite moment at the same point. Therefore a grey group cannot describe the symmetry of any crystal in which magnetic ordering exists. Paramagnetic and diamagnetic materials belong to the grey group. Thus the product of τ with any operation of $\mathscr{G}$ is also an element of the type II point group $\mathscr{M}$, which can be written as

$$\mathscr{M} = \mathscr{G} + \tau\mathscr{G}.$$

In type III, the black and white point groups, the half of the elements of the ordinary point group G are multiplied by the antisymmetry operator τ. The other half forms a subgroup $\mathscr{H}$ of $\mathscr{G}$. Type III point group M can be written as

$$\mathscr{M} = \mathscr{H} + \tau(\mathscr{G} - \mathscr{H})$$

Ferromagnetic, antiferromagnetic, ferrimagnetic, weak ferromagnetic materials belong to this group.

Example: Consider the ordinary point group $4mm$. As described earlier, the symmetry operations of a square are denoted by

$$\{E, C_4, (C_4)^2, (C_4)^3, m_x, m_y, m_{\frac{\pi}{4}}, m_{-\frac{\pi}{4}}\}.$$

One way of coloring the square is shown in Fig.87a where four operators $\{E, (C_4)^2, m_x, m_y\}$

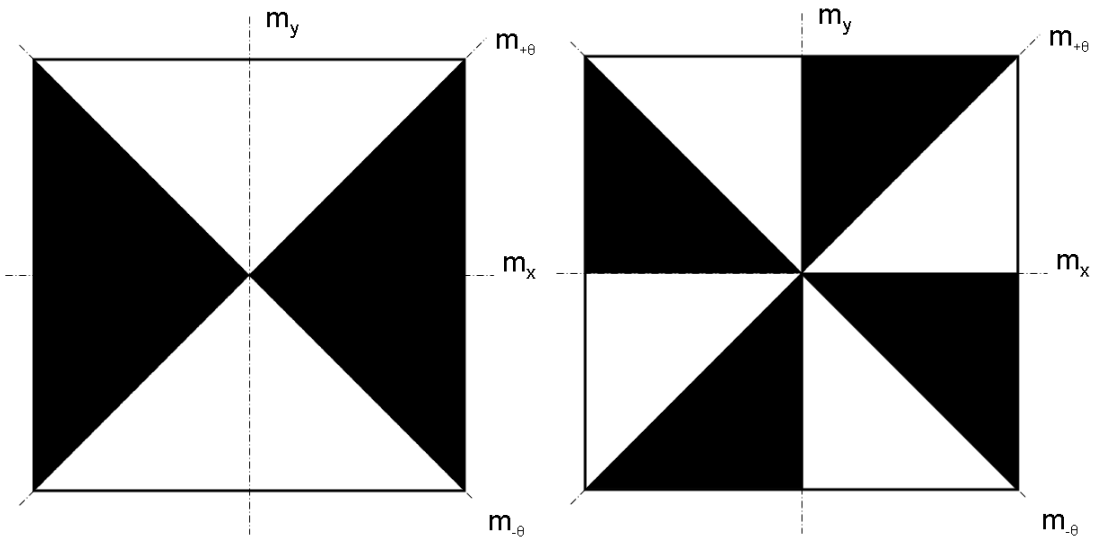

(a) (b)

Fig. 87. Symmetry of (a) $\underline{4}\mathrm{m}\underline{\mathrm{m}}$ (b) $4\underline{\mathrm{mm}}$.

are still symmetry operations and belongs to $\mathscr{H}$. However, the four operations $\tau C_4, \tau(C_4)^3, \tau m_{\frac{\pi}{4}}$ and $\tau m_{-\frac{\pi}{4}}$ are the symmetry operators of the black and white square. For example, τC_4 means rotate the square $+90^o$ and turn black into white and white into black., which reproduce the starting position of the square again. Thus from the ordinary point group $4mm$ we have derived a black and white point group

$$\underline{4}m\underline{m}: \quad E, (C_4)^2, m_x, m_y, \tau C_4, \tau(C_4)^3, \tau m_{\frac{\pi}{4}}, \tau m_{-\frac{\pi}{4}}$$

Another way of coloring the square is shown in Fig. 87b. For this pattern, corresponding black and white group is

$$4\underline{mm}: \quad E, C_4, (C_4)^2, (C_4)^3, \tau m_x, \tau m_y, \tau m_{\frac{\pi}{4}}, \tau m_{-\frac{\pi}{4}}$$

1. Polar and axial tensors

A tensor T obeys the following transformation rule

$$T'_{ijk...n} = Q_{ip}Q_{jq}...Q_{nu}T_{pqr...u}$$

Quantities which are transformed according to this transformation rule are known as *polar tensors* [145]. Such transformation does not change the hand of the axes i.e their reflected images do not change any orientation.

On the other hand, there are numerous physical quantities which obey the transformation law

$$T'_{ijk...n} = -Q_{ip}Q_{jq}...Q_{nu}T_{pqr...u},$$

where the negative sign is taken for transformations which change right-handed coordinate axis into left-handed and vice-versa. Quantities which transform according to the above rule are known as *axial tensors* [145]. A transformation which does change the hand of the axes can always be considered to be a combination of a rotation of the axes and a reversal of their sense (i.e. the inversion $x' = -x$).

The most familiar examples of polar and axial tensors are *polar vectors* and *axial vectors*. We know from basic physics that moving electrical charges generate a magnetic field. In particular, electrons moving around the nucleus of an atom generate tiny electrical currents which give rise to a vector quantity known as the magnetic moment. The direction of the moment vector is determined by the direction of the current; for a counter-clockwise current, the moment vector points up, whereas for a

clockwise current the moment points down. If we consider the electrostatic equivalent, the polarization vector, then the situation is different, since the electrostatic dipole moment is defined as the charge multiplied by the separation between the negative and positive charges. The image of a polar vector parallel to a mirror plane is a new vector with the same direction as the original one. For an axial vector, on the other hand, a counter-clockwise current becomes a clockwise current when viewed in a mirror, so that the mirror image of a magnetic moment vector parallel to a mirror plane is a moment vector parallel to the original one, but pointing in the opposite direction.

2. i and $c-$ tensors

Tensor of any order that are symmetry invariant of time are known as *i-tensors* and tensors whose components change sign with time reversal are known as *c-tensors*. We can thus generalized the transformation rule as follows

$$T'_{ijk...n} = (-1)^p (\det \mathbf{Q}) Q_{ip} Q_{jq} ... Q_{nu} T_{pqr...u},$$

where $p = 1$ for *c-tensors* and $p = 0$ for *i-tensors*. $\det \mathbf{Q} = 1$ for *polar tensors* and $\det \mathbf{Q} = -1$ for *axial tensors*

3. Identification of type of magnetic ordering for a given magnetic group

In order to identify the type of magnetic ordering of a given magnetic group one needs to examine the transformation properties of am atomic magnetic moment $\boldsymbol{\mu}$, which is an axial-c tensor. We will illustrate this through some examples. Let us first consider $4mm$. From Table LI, we can see that the unit cell does not exhibit any magnetism where $4\underline{mm}$ shows a net magnetization along the z axis, which is also known as the *easy axis*

$4mm$	E	C_4	$(C_4)^2$	$(C_4)^3$	m_x	m_y	$m_{\frac{\pi}{4}}$	$m_{-\frac{\pi}{4}}$	Net Moment
μ_x	μ_x	$-\mu_x$	μ_y	$-\mu_y$	μ_x	$-\mu_x$	μ_y	$-\mu_y$	0 (AF)
μ_y	μ_y	$-\mu_y$	$-\mu_x$	μ_x	$-\mu_y$	μ_y	μ_x	$-\mu_x$	0 (AF)
μ_z	μ_z	μ_z	μ_z	μ_z	$-\mu_z$	$-\mu_z$	$-\mu_z$	$-\mu_z$	0 (P)
$4\underline{mm}$	E	C_4	$(C_4)^2$	$(C_4)^3$	τm_x	τm_y	$\tau m_{\frac{\pi}{4}}$	$\tau m_{-\frac{\pi}{4}}$	
μ_x	μ_x	$-\mu_x$	μ_y	$-\mu_y$	$-\mu_x$	μ_x	$-\mu_y$	μ_y	0 (AF)
μ_y	μ_y	$-\mu_y$	$-\mu_x$	μ_x	μ_y	$-\mu_y$	$-\mu_x$	μ_x	0 (AF)
μ_z	μ_z	μ_z	μ_z	μ_z	μ_z	μ_z	μ_z	μ_z	μ_z (F)

Table LI. Transformation properties of magnetic moment under application of symmetry operations. We denote antiferromagnetic by AF, ferromagnetic F and paramagnetic by P.

B4. Decomposition of tensors

The whole linear space of rth order tensor $T_{i_1 i_2 .. i_r}$ is reducible into subspaces consisting of tensors of different symmetry types since symmetry is an invariant property. The reduction can be obtained by applying *Young symmetry operator* to the indices of a tensor [137, 174]. A brief outline of the procedure to symmetrize a tensor is given below. More detailed analysis can be found in [175, 176]. A *partition* $\lambda_1 \lambda_2 .. \lambda_r$ of

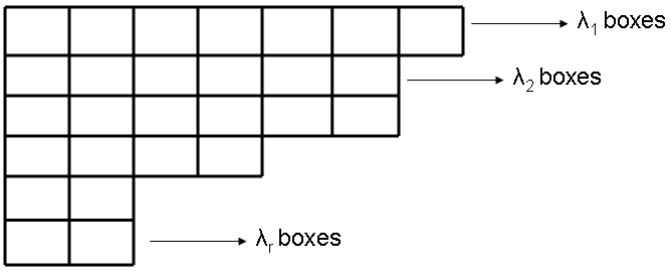

Fig. 88. A frame with n boxes

the positive integer λ is a set of positive integers $\lambda_1 \geq \lambda_2 \geq ... \geq \lambda_r$ such that $\lambda_1 + \lambda_2 + .. + \lambda_r = n$. The *frame* $[\lambda] = [\lambda_1\lambda_2..\lambda_r]$ associated with the partition $\lambda_1\lambda_2..\lambda_r$ consists of a row of λ_1 boxes, a row of λ_2 boxes,... arranged so that their left hand ends are directly beneath one another (Fig. 88). A *tableau* is obtained from a frame $[\lambda]$ by inserting the numbers $1, 2, ...\lambda$ in any manner in to the n square boxes. A *standard tableau* is one in which the integers increases from left to right and from top to bottom. The *Young symmetry operators* $Y_{[\lambda]}$ associated with the standard tableaux obtained from the frame $[\lambda] = [\lambda_1\lambda_2..\lambda_r]$ are given by

$$Y_{[\lambda]} = PQ$$

where

$$P = P_1...P_r, \quad Q = Q_1...Q_c.$$

In the above expression r and c denote the number of rows and columns of the tableau, respectively. The quantities P_m and Q_n are defined by

$$P_m = \sum p_i, \quad Q_n = \sum \delta(q_j)q_j$$

where p_i and q_j are the permutation of the numbers located in the m th row and n th column of the tableau. $\delta(q_j)$ is $+1$ and -1 for an even and odd permutation of q_j, respectively, and the summation is over all possible permutations in a given row and column.

Thus for $\lambda = 4$ we have five possible frames with $[\lambda_1 = 4]$, $[\lambda_1 = 3, \lambda_2 = 1]$, $[\lambda_1 = 2, \lambda_2 = 2]$, $[\lambda_1 = 2, \lambda_2 = 1, \lambda_3 = 1]$ and $[\lambda_1 = 1, \lambda_2 = 1, \lambda_3 = 1, \lambda_4 = 1]$.

Pictorially, we can present them as

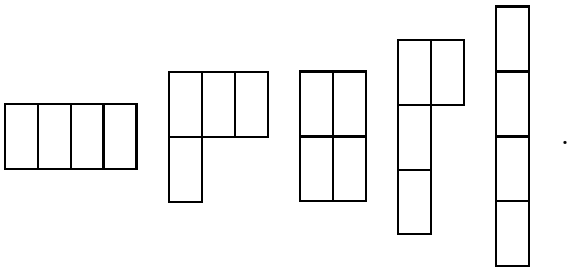

The notation to represents these tables are $[4]$, $[3,1]$, $[2^2]$, $[2,1^2]$ and $[1^4]$ respectively. The standard tableau for $[3,1]$ are given by

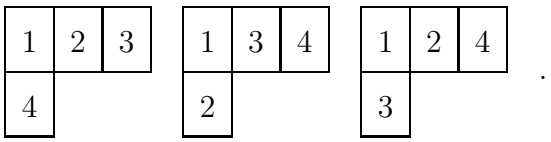

Each frame of the standard tableau has an unique Young operator. Different Young operators can be obtained from the remaining standard tableau [175, 176].

The r th order tensors of basic symmetry type $[\lambda]$ are obtained by applying the Young operators $Y_{[\lambda]}$ to the indices of a general tensor $T_{i_1 i_2 .. i_r}$. To each standard tableau belongs to a frame $[\lambda]$, there corresponds a particular tensor of basic symmetry type $[\lambda]$ which we denote by $T_{[\lambda]}$. The tensors $T_{[\lambda]}$ form the *carrier space* for an *irreducible representation* of $GL(n)$. These irreducible representations of $GL(n)$ are named by the same symbol $[\lambda]$.

1. Decomposition of electromechanical quantities

Following the notation of Kiral-Eringen [135], we consider following categories of tensors (TableLII). The representation of $\mathbf{M}, \mathbf{J}, \mathbf{P}, \mathbf{E}$ in the Table LII are *reducible*. We denote the magnetic point group by $\{\mathscr{M}\}$. For a general case, we say that

$$\{\mathscr{M}\} = \{\mathscr{M}^1, \mathscr{M}^2, ..., \mathscr{M}^n\}$$

Type	Properties	Representation	Examples
M	Axial, c-vector	[1] a,c	Magnetization, magnetic field and magnetic flux
J	Polar, c-vector	[1] p,c	Electric current
P	Polar, i-vectors	[1] p,i	Polarization, electric field and electric displacement
E	Polar, i-tensor, second-order, symmetric	[2] p,i	Stress and strain tensors

Table LII. Properties of electromechanical quantities

If we denote Γ by any one representation of $\mathbf{M}, \mathbf{J}, \mathbf{P}, \mathbf{E}$ then

$$\Gamma = \bigoplus_{i=1}^{r} n_i \Gamma_i$$

where $\Gamma_1, ...\Gamma_r$ are the irreducible representation of $\{\mathscr{M}\}$. To find the coefficients n_i, we will use Eq. (B.4), which is

$$n_i = \frac{1}{n} \sum_{i=1}^{n} \chi_i^*(\mathscr{M}^i)\chi(\mathscr{M}^i).$$

The characters for polar tensors, which are not influenced by time symmetry, are readily obtained in the following ways

$$\begin{aligned}
\chi[1]_{p,i}(\mathscr{M}^i) &= \mathrm{tr}\,(\mathscr{M}^i) \\
\chi[2]_{p,i}(\mathscr{M}^i) &= \frac{1}{2}\left([\mathrm{tr}\,(\mathscr{M}^i)]^2 + \mathrm{tr}\,(\mathscr{M}^{i^2})\right) \\
\chi[1^2]_{p,i}(\mathscr{M}^i) &= \frac{1}{2}\left([\mathrm{tr}\,(\mathscr{M}^i)]^2 - \mathrm{tr}\,(\mathscr{M}^{i^2})\right)
\end{aligned}$$

As described in the Appendix, $\dim [2]_{p,\,i} = 6$ and $\dim [1^2]_{p,\,i} = 3$. The antisymmetric representation thus can be presented by an *axial vector* i.e,

$$\mathbf{A} := [1]_{a,\,i} \Leftrightarrow [1^2]_{p,\,i}$$

and we can write

$$\chi[1]_{a,\,i}(\mathscr{M}^i) \;=\; \frac{1}{2}\left([\mathrm{tr}\,(\mathscr{M}^i)]^2 - \mathrm{tr}\,(\mathscr{M}^{i^2})\right)$$

For the remaining time-asymmetric representation the characters are given by

$$\begin{aligned}\chi[1]_{p,\,c}(\mathscr{M}^i) &= (-1)^p \chi[1]_{p,\,i}(\mathscr{M}^i)\\ \chi[1]_{a,\,c}(\mathscr{M}^i) &= (-1)^p \chi[1]_{a,\,i}(\mathscr{M}^i)\end{aligned}$$

Type	Representation	Decomposition
M	$[1]_{a,\,c}$	$\Gamma^{(3)} \oplus \Gamma^{(5)}$
J	$[1]_{p,\,c}$	$\Gamma^{(4)} \oplus \Gamma^{(5)}$
P	$[1]_{p,\,i}$	$\Gamma^{(1)} \oplus \Gamma^{(5)}$
E	$[2]_{p,i}$	$2\Gamma^{(1)} \oplus \Gamma^{(3)} \oplus \Gamma^{(4)} \oplus \Gamma^{(5)}$

Table LIII. Decomposition of electromechanical quantities of $\underline{4}\mathrm{m}\underline{\mathrm{m}}$ magnetic point group

Example: Let us consider $W = W(\mathbf{M}, \mathbf{P}, \mathbf{J}, \mathbf{E})$, where the arguments $\mathbf{M}, \mathbf{P}, \mathbf{J}, \mathbf{E}$ are as described before. The irreducible representations of $\mathscr{M} = \underline{4}m\underline{m}$ is given in Table LIV and the explicit form of the basic quantities are given in Table LV. Typical

	E	R_2	R_1	D_3	T_3	R_2T_3	R_1T_3	D_3T_3	Basic Quantities
$\Gamma^{(1)}$	1	1	1	1	1	1	1	1	$\phi_1,\ \phi_2....$
$\Gamma^{(2)}$	1	-1	-1	1	-1	1	1	-1	$\psi_1,\ \psi_2....$
$\Gamma^{(3)}$	1	-1	-1	1	1	-1	-1	1	$\nu_1,\ \nu_2....$
$\Gamma^{(4)}$	1	1	1	1	-1	-1	-1	-1	$\tau_1,\ \tau_2....$
$\Gamma^{(5)}$	E	F	$-F$	$-E$	K	L	$-L$	$-K$	$\mathbf{a}_1,\ \mathbf{a}_2....$

Table LIV. Irreducible representation of C_{4v} ($\underline{4}\mathrm{m}\underline{\mathrm{m}}$)

multilinear elements of the integrity bases for $\underline{4}m\underline{m}$ are

Degree 1: $\sum \phi_i$

Degree 2: $\sum \psi_i\psi_j,\ \sum \nu_i\nu_j,\ \sum \tau_i\tau_j,\ \sum \mathbf{a}_i \cdot \mathbf{a}_j$

$\Gamma^{(1)}$			P_3	$E_{11}+E_{22},\ E_{33}$
$\Gamma^{(2)}$				
$\Gamma^{(3)}$	M_3			E_{12}
$\Gamma^{(4)}$		J_3		$E_{11}-E_{22}$
$\Gamma^{(5)}$	$(M_2,\ M_1)$	$(J_1,\ -J_2)$	$(P_1,\ P_2)$	$(E_{31},\ E_{32})$

Table LV. The basic quantities of C_{4v} ($\underline{4}\mathrm{m}\underline{\mathrm{m}}$)

We write

$$\Gamma^{(1)}: \quad \phi_1,\, \phi_2,\, \phi_3 \equiv u_1^{(1)},\, u_2^{(1)},\, u_3^{(1)} = E_{11} + E_{22},\, E_{33},\, P_3$$

$$\Gamma^{(3)}: \quad \nu_1,\, \nu_2 \equiv u_1^{(3)},\, u_2^{(3)} = M_3,\, E_{12}$$

$$\Gamma^{(4)}: \quad \tau_1 \equiv u_1^{(4)} = E_{11} - E_{22}$$

$$\Gamma^{(5)}: \quad \mathbf{a}_1,\, \mathbf{a}_2,\, \mathbf{a}_3 \equiv \begin{bmatrix} u_{11}^{(6)} \\ u_{12}^{(6)} \end{bmatrix},\, \begin{bmatrix} u_{21}^{(6)} \\ u_{22}^{(6)} \end{bmatrix},\, \begin{bmatrix} u_{31}^{(6)} \\ u_{32}^{(6)} \end{bmatrix}$$

$$= \begin{bmatrix} M_2 \\ M_1 \end{bmatrix},\, \begin{bmatrix} E_{31} \\ E_{32} \end{bmatrix},\, \begin{bmatrix} P_1 \\ P_2 \end{bmatrix}$$

We list the element of integrity bases as:

Degree 1: $\phi_1,\, \phi_2,\, \phi_3$

Degree 2: $\nu_1^2,\, \nu_1\nu_2,\, \nu_2^2,\, \tau_1^2,$

$\mathbf{a}_1 \cdot \mathbf{a}_1,\, \mathbf{a}_2 \cdot \mathbf{a}_2,\, \mathbf{a}_3 \cdot \mathbf{a}_3,\, \mathbf{a}_1 \cdot \mathbf{a}_2,\, \mathbf{a}_1 \cdot \mathbf{a}_3,\, \mathbf{a}_2 \cdot \mathbf{a}_3.$

If we further neglect polarization for a magnetic material, the elements of the integrity basis are given by

$$I_1 = E_{11} + E_{22}, \quad I_2 = E_{33}, \quad I_3 = (E_{12})^2, \quad I_4 = (E_{11} - E_{22})^2$$

$$I_5 = E_{31}^2 + E_{32}^2, \quad I_6 = M_3^2, \quad I_7 = M_2^2 + M_1^2, \quad I_8 = M_3 E_{12}$$

$$I_9 = M_2 E_{31} + M_1 E_{32}$$

APPENDIX C

EXPANSION OF POINTING VECTOR

The following expansion is followed from the text of Kovetz [131]. We will start with the following identity for any two vectors $\mathbf{u}, \mathbf{v}$,

$$\begin{aligned} \mathbf{u} \cdot \overset{*}{\mathbf{v}} &= \mathbf{u} \cdot [\dot{\mathbf{v}} + \mathbf{v}\nabla \cdot \dot{\mathbf{x}} - (\nabla \otimes \dot{\mathbf{x}})\mathbf{v}] \\ &= \mathbf{u} \cdot [\dot{\mathbf{v}} + \mathbf{v}\mathbf{I} : \mathbf{L} - \mathbf{L}\mathbf{v}] \\ &= \mathbf{u} \cdot \dot{\mathbf{v}} + [(\mathbf{u} \cdot \mathbf{v})\mathbf{I} - \mathbf{u} \otimes \mathbf{v}] : \mathbf{L} \end{aligned} \tag{C.1}$$

So,

$$\begin{aligned} \nabla \cdot (\widetilde{\mathbf{e}} \times \widetilde{\mathbf{h}}) &= -\widetilde{\mathbf{j}}_f \cdot \widetilde{\mathbf{e}} - \widetilde{\mathbf{h}} \cdot \overset{*}{\mathbf{b}} - \widetilde{\mathbf{e}} \cdot \overset{*}{\mathbf{d}} \\ &= -\widetilde{\mathbf{j}}_f \cdot \widetilde{\mathbf{e}} - \widetilde{\mathbf{h}} \cdot \dot{\mathbf{b}} - \widetilde{\mathbf{e}} \cdot \dot{\mathbf{d}} \\ &- [(\widetilde{\mathbf{h}} \cdot \mathbf{b} + \widetilde{\mathbf{e}} \cdot \mathbf{d})\mathbf{I} - \widetilde{\mathbf{h}} \otimes \mathbf{b} - \widetilde{\mathbf{e}} \otimes \mathbf{d}] : \mathbf{L} \end{aligned} \tag{C.2}$$

Now we will compute each term of (C.2) where

$$\begin{aligned} \widetilde{\mathbf{h}} \cdot \dot{\mathbf{b}} &= (\mathbf{h} - \dot{\mathbf{x}} \times \mathbf{d}) \cdot \dot{\mathbf{b}} \\ &= [(\frac{\mathbf{b}}{\mu_0} - \mathbf{m}) - \dot{\mathbf{x}} \times (\mathbf{p} + \epsilon_0 \mathbf{e})] \cdot \dot{\mathbf{b}} \\ &= [\frac{\mathbf{b}}{\mu_0} - \dot{\mathbf{x}} \times \epsilon_0 \mathbf{e} - (\mathbf{m} + \dot{\mathbf{x}} \times \mathbf{p})] \cdot \dot{\mathbf{b}} \\ &= \frac{\mathbf{b} \cdot \dot{\mathbf{b}}}{\mu_0} - \widetilde{\mathbf{m}} \cdot \dot{\mathbf{b}} - \epsilon_0 \mathbf{e} \times \dot{\mathbf{b}} \cdot \dot{\mathbf{x}} \end{aligned} \tag{C.3}$$

$$\begin{aligned} \widetilde{\mathbf{e}} \cdot \dot{\mathbf{d}} &= (\mathbf{e} + \dot{\mathbf{x}} \times \mathbf{b}) \cdot (\epsilon_0 \dot{\mathbf{e}} + \dot{\mathbf{p}}) \\ &= (\mathbf{e} + \dot{\mathbf{x}} \times \mathbf{b}) \cdot \epsilon_0 \dot{\mathbf{e}} + \widetilde{\mathbf{e}} \cdot \dot{\mathbf{p}} \\ &= \epsilon_0 \mathbf{e} \cdot \dot{\mathbf{e}} + \widetilde{\mathbf{e}} \cdot \dot{\mathbf{p}} - \epsilon_0 \dot{\mathbf{e}} \times \mathbf{b} \cdot \dot{\mathbf{x}} \end{aligned} \tag{C.4}$$

Similarly,

$$\widetilde{\mathbf{h}} \cdot \mathbf{b} = \frac{\mathbf{b} \cdot \mathbf{b}}{\mu_0} - \widetilde{\mathbf{m}} \cdot \mathbf{b} - \epsilon_0 \mathbf{e} \times \mathbf{b} \cdot \dot{\mathbf{x}} \tag{C.5}$$

$$\widetilde{\mathbf{e}} \cdot \mathbf{d} = \epsilon_0 \mathbf{e} \cdot \mathbf{e} + \widetilde{\mathbf{e}} \cdot \mathbf{p} - \epsilon_0 \mathbf{e} \times \mathbf{b} \cdot \dot{\mathbf{x}} \tag{C.6}$$

$$\widetilde{\mathbf{h}} \otimes \mathbf{b} = \frac{\mathbf{b} \otimes \mathbf{b}}{\mu_0} - \widetilde{\mathbf{m}} \otimes \mathbf{b} - \dot{\mathbf{x}} \times \epsilon_0 \mathbf{e} \otimes \mathbf{b} \tag{C.7}$$

$$\widetilde{\mathbf{e}} \otimes \mathbf{d} = \epsilon_0 \mathbf{e} \otimes \mathbf{e} + \widetilde{\mathbf{e}} \otimes \mathbf{p} - \mathbf{b} \times \dot{\mathbf{x}} \otimes \epsilon_0 \mathbf{e} \tag{C.8}$$

Substituting equations (C.3-C.8) in equation (C.2) we get,

$$\begin{aligned} \nabla \cdot (\widetilde{\mathbf{e}} \times \widetilde{\mathbf{h}}) = & -\widetilde{\mathbf{j}}_f \cdot \widetilde{\mathbf{e}} - (\frac{\mathbf{b} \cdot \dot{\mathbf{b}}}{\mu_0} - \widetilde{\mathbf{m}} \cdot \dot{\mathbf{b}} - \epsilon_0 \mathbf{e} \times \dot{\mathbf{b}} \cdot \dot{\mathbf{x}}) - (\epsilon_0 \mathbf{e} \cdot \dot{\mathbf{e}} + \widetilde{\mathbf{e}} \cdot \dot{\mathbf{p}} - \epsilon_0 \dot{\mathbf{e}} \times \mathbf{b} \cdot \dot{\mathbf{x}}) \\ - & [((\frac{\mathbf{b} \cdot \mathbf{b}}{\mu_0} - \widetilde{\mathbf{m}} \cdot \mathbf{b} - \epsilon_0 \mathbf{e} \times \mathbf{b} \cdot \dot{\mathbf{x}}) + (\epsilon_0 \mathbf{e} \cdot \mathbf{e} + \widetilde{\mathbf{e}} \cdot \mathbf{p} - \epsilon_0 \mathbf{e} \times \mathbf{b} \cdot \dot{\mathbf{x}}))\mathbf{I} \\ - & (\frac{\mathbf{b} \otimes \mathbf{b}}{\mu_0} - \widetilde{\mathbf{m}} \otimes \mathbf{b} - \dot{\mathbf{x}} \times \epsilon_0 \mathbf{e} \otimes \mathbf{b}) - (\epsilon_0 \mathbf{e} \otimes \mathbf{e} + \widetilde{\mathbf{e}} \otimes \mathbf{p} - \mathbf{b} \times \dot{\mathbf{x}} \otimes \epsilon_0 \mathbf{e})] : \mathbf{L} \end{aligned} \tag{C.9}$$

After rearranging few terms we get,

$$\begin{aligned} \nabla \cdot (\widetilde{\mathbf{e}} \times \widetilde{\mathbf{h}}) = & -\widetilde{\mathbf{j}}_f \cdot \widetilde{\mathbf{e}} - (\frac{\mathbf{b} \cdot \dot{\mathbf{b}}}{\mu_0} - \widetilde{\mathbf{m}} \cdot \dot{\mathbf{b}} + \epsilon_0 \mathbf{e} \cdot \dot{\mathbf{e}} + \widetilde{\mathbf{e}} \cdot \dot{\mathbf{p}}) + (\epsilon_0 \mathbf{e} \times \dot{\mathbf{b}} \cdot \dot{\mathbf{x}} + \epsilon_0 \dot{\mathbf{e}} \times \mathbf{b} \cdot \dot{\mathbf{x}}) \\ - & [((\frac{\mathbf{b} \cdot \mathbf{b}}{\mu_0} - \widetilde{\mathbf{m}} \cdot \mathbf{b} + \epsilon_0 \mathbf{e} \cdot \mathbf{e} + \widetilde{\mathbf{e}} \cdot \mathbf{p}) - 2\epsilon_0 \mathbf{e} \times \mathbf{b} \cdot \dot{\mathbf{x}}))\mathbf{I} \\ - & ((\frac{\mathbf{b} \otimes \mathbf{b}}{\mu_0} - \widetilde{\mathbf{m}} \otimes \mathbf{b} + \epsilon_0 \mathbf{e} \otimes \mathbf{e} + \widetilde{\mathbf{e}} \otimes \mathbf{p}) - (\dot{\mathbf{x}} \times \epsilon_0 \mathbf{e} \otimes \mathbf{b} + \mathbf{b} \times \dot{\mathbf{x}} \otimes \epsilon_0 \mathbf{e}))] : \mathbf{L} \end{aligned} \tag{C.10}$$

We can further simplify the above expression by using the identity,

$$\mathbf{e} \times \mathbf{b} \otimes \dot{\mathbf{x}} + \dot{\mathbf{x}} \times \mathbf{e} \otimes \mathbf{b} + \mathbf{b} \times \dot{\mathbf{x}} \otimes \mathbf{e} = (\mathbf{e} \times \mathbf{b} \cdot \dot{\mathbf{x}})\mathbf{I} \tag{C.11}$$

This implies

$$\begin{aligned} \nabla \cdot (\widetilde{\mathbf{e}} \times \widetilde{\mathbf{h}}) = & -\widetilde{\mathbf{j}}_f \cdot \widetilde{\mathbf{e}} - (\frac{\mathbf{b} \cdot \dot{\mathbf{b}}}{\mu_0} - \widetilde{\mathbf{m}} \cdot \dot{\mathbf{b}} + \epsilon_0 \mathbf{e} \cdot \dot{\mathbf{e}} + \widetilde{\mathbf{e}} \cdot \dot{\mathbf{p}}) + \frac{d}{dt}(\epsilon_0 \mathbf{e} \times \mathbf{b}) \cdot \dot{\mathbf{x}} \\ - & [((\frac{\mathbf{b} \cdot \mathbf{b}}{\mu_0} - \widetilde{\mathbf{m}} \cdot \mathbf{b} + \epsilon_0 \mathbf{e} \cdot \mathbf{e} + \widetilde{\mathbf{e}} \cdot \mathbf{p}) - \epsilon_0 \mathbf{e} \times \mathbf{b} \cdot \dot{\mathbf{x}}))\mathbf{I} \\ - & ((\frac{\mathbf{b} \otimes \mathbf{b}}{\mu_0} - \widetilde{\mathbf{m}} \otimes \mathbf{b} + \epsilon_0 \mathbf{e} \otimes \mathbf{e} + \widetilde{\mathbf{e}} \otimes \mathbf{p} + \epsilon_0 \mathbf{e} \times \mathbf{b} \otimes \dot{\mathbf{x}})] : \mathbf{L} \end{aligned} \tag{C.12}$$

and by using the identity (2.33), the above equation simplifies to

$$\begin{aligned}
&\nabla \cdot (\widetilde{\mathbf{e}} \times \widetilde{\mathbf{h}}) = -\widetilde{\mathbf{j}}_f \cdot \widetilde{\mathbf{e}} - (\frac{\mathbf{b} \cdot \dot{\mathbf{b}}}{\mu_0} - \widetilde{\mathbf{m}} \cdot \dot{\mathbf{b}} + \epsilon_0 \mathbf{e} \cdot \dot{\mathbf{e}} + \widetilde{\mathbf{e}} \cdot \dot{\mathbf{p}}) + \rho \frac{d}{dt}(\frac{\epsilon_0}{\rho} \mathbf{e} \times \mathbf{b}) \cdot \dot{\mathbf{x}} \\
- \quad &[(\frac{\mathbf{b} \cdot \mathbf{b}}{\mu_0} - \widetilde{\mathbf{m}} \cdot \mathbf{b} + \epsilon_0 \mathbf{e} \cdot \mathbf{e} + \widetilde{\mathbf{e}} \cdot \mathbf{p}) \mathbf{I} \\
- \quad &(\frac{\mathbf{b} \otimes \mathbf{b}}{\mu_0} - \widetilde{\mathbf{m}} \otimes \mathbf{b} + \epsilon_0 \mathbf{e} \otimes \mathbf{e} + \widetilde{\mathbf{e}} \otimes \mathbf{p} + \epsilon_0 \mathbf{e} \times \mathbf{b} \otimes \dot{\mathbf{x}})] : \mathbf{L}
\end{aligned} \tag{C.13}$$

APPENDIX D

TENSOR DIFFERENTIATION

We will consider a scalar valued tensor function $f(\mathbf{A}) : \mathcal{D} \to R$, differentiable in a neighborhood of $\mathbf{A}$, if there exist a tensor $f(\mathbf{A})_{,\mathbf{A}} \in \mathcal{D}$ such that

$$\frac{d}{d\alpha} f(\mathbf{A} + \alpha\mathbf{X})\Big|_{\alpha=0} = f(\mathbf{A})_{,\mathbf{A}} \cdot \mathbf{X}. \tag{D.1}$$

The '$\cdot$' refers to a generalized contraction operation. When, $\mathbf{A}$ is a symmetric second order tensor, the derivative also becomes symmetric and this requrement implies

$$f(\mathbf{A})_{,\mathbf{A}} = \mathrm{Sym}[f(\mathbf{A})_{,\mathbf{A}}]. \tag{D.2}$$

D1. Vector valued function

Let us consider the form of $f(\mathbf{A}) = \mathbf{A} \cdot \mathbf{PA}$ for a given symmetric second order tensor $\mathbf{P}$ and a vector $\mathbf{A}$. The by defination of D.1

$$\begin{aligned} \frac{d}{d\alpha} f(\mathbf{A} + \alpha\mathbf{X})\Big|_{\alpha=0} &= \frac{d}{d\alpha}(\mathbf{A} + \alpha\mathbf{X}) \cdot \mathbf{P}(\mathbf{A} + \alpha\mathbf{X})\Big|_{\alpha=0} \\ &= \frac{d}{d\alpha}(\mathbf{A} \cdot \mathbf{A} + \alpha\mathbf{A} \cdot \mathbf{PX} + \alpha\mathbf{X} \cdot \mathbf{PA} + \alpha^2..)\Big|_{\alpha=0} \\ &= (\mathbf{P}^T\mathbf{A} + \mathbf{PA}) \cdot \mathbf{X}. \end{aligned} \tag{D.3}$$

So, $f(\mathbf{A})_{,\mathbf{A}} = 2\mathbf{PA}$, since $\mathbf{P}$ is symmetric. Similarly, if $g(\mathbf{A}) = \mathbf{A} \cdot \mathbf{Pv}$ for a given symmetric second order tensor $\mathbf{P}$ and a given vector $\mathbf{v}$, then $g(\mathbf{A})_{,\mathbf{A}} = \mathbf{Pv}$.

D2. Tensor valued function

We will consider the derivative of a tensor valued scalar function of the form $f(\mathbf{A}) = \mathrm{tr}(\mathbf{A}^k\mathbf{L})$ $(k = 1, 2..)$ with respect to $\mathbf{A}$. Here $\mathbf{A}$ and $\mathbf{L}$ are second order tensors

Following the definition D.1 we get,

$$\begin{aligned}
\frac{d}{d\alpha}f(\mathbf{A}+\alpha\mathbf{X})\Big|_{\alpha=0} &= \frac{d}{d\alpha}(\mathbf{A}+\alpha\mathbf{X})^k : \mathbf{L}^T\Big|_{\alpha=0} = \frac{d}{d\alpha}(\mathbf{A}+\alpha\mathbf{X})^k\Big|_{\alpha=0} : \mathbf{L}^T \\
&= \frac{d}{d\alpha}[\underbrace{(\mathbf{A}+\alpha\mathbf{X})(\mathbf{A}+\alpha\mathbf{X})..(\mathbf{A}+\alpha\mathbf{X})}_{k\text{times}}]\Big|_{\alpha=0} : \mathbf{L}^T \\
&= \frac{d}{d\alpha}[\mathbf{A}^k + \alpha\sum_{i=0}^{k-1}\mathbf{A}^i\mathbf{X}\mathbf{A}^{k-1-i} + \alpha^2....]\Big|_{\alpha=0} : \mathbf{L}^T \\
&= \sum_{i=0}^{k-1}\mathbf{A}^i\mathbf{X}\mathbf{A}^{k-1-i} : \mathbf{L}^T \\
&= \sum_{i=0}^{k-1}(\mathbf{A}^T)^i\mathbf{L}^T(\mathbf{A}^T)^{k-1-i} : \mathbf{X}. \qquad \text{(D.4)}
\end{aligned}$$

Hence,

$$\text{tr}(\mathbf{A}^k\mathbf{L})_{,\mathbf{A}} = \sum_{i=0}^{k-1}(\mathbf{A}^i\mathbf{L}\mathbf{A}^{k-1-i})^T. \qquad \text{(D.5)}$$

When $\mathbf{A}$ is symmetric, the according to D.2,

$$\text{tr}(\mathbf{A}^k\mathbf{L})_{,\mathbf{A}} = \text{Sym}\sum_{i=0}^{k-1}(\mathbf{A}^i\mathbf{L}\mathbf{A}^{k-1-i})^T = \sum_{i=0}^{k-1}\mathbf{A}^i(\text{Sym}\mathbf{L})\mathbf{A}^{k-1-i} \qquad \text{(D.6)}$$

We will now consider some special cases,

Case-1: When the form of $f(\mathbf{A}) = \mathbf{u}\cdot\mathbf{A}^k\mathbf{P}\mathbf{v}$ and $\mathbf{A}$ is symmetric

Here, $\mathbf{P}$ and $\mathbf{u}, \mathbf{v}$ are arbitrary tensor and vectors respectively. We can write

$$\begin{aligned}
f(\mathbf{A}) &= \mathbf{u}\cdot\mathbf{A}^k\mathbf{P}\mathbf{v} = \mathbf{A}^k\mathbf{P} : (\mathbf{u}\otimes\mathbf{v}) \\
&= \mathbf{A}^k : (\mathbf{u}\otimes\mathbf{v})\mathbf{P}^T = \mathbf{A}^k : (\mathbf{u}\otimes\mathbf{P}\mathbf{v}) \\
&= \text{tr}(\mathbf{A}^k\mathbf{L}). \qquad \text{(D.7)}
\end{aligned}$$

where we denote $\mathbf{L} = \mathbf{u}\otimes\mathbf{P}\mathbf{v}$. So, the scalar function f follows the differentiation rule as given in D.6

Case-2: When k=2,1 and $\mathbf{A}$ is symmetric

$$\begin{aligned} \mathrm{tr}(\mathbf{A}^2\mathbf{L})_{,\mathbf{A}} &= \mathbf{A}(\mathrm{Sym}\mathbf{L}) + (\mathrm{Sym}\mathbf{L})\mathbf{A}, \qquad \text{(D.8)} \\ \mathrm{tr}(\mathbf{A}\mathbf{L})_{,\mathbf{A}} &= \mathrm{Sym}\mathbf{L}. \qquad \text{(D.9)} \end{aligned}$$

Case-3: When $\mathbf{L} = \mathbf{I}$ and $\mathbf{A}$ is symmetric

$$\mathrm{tr}(\mathbf{A}^k)_{,\mathbf{A}} = \sum_{i=0}^{k-1} \mathbf{A}^i \mathbf{A}^{k-1-i} = k\mathbf{A}^{k-1}. \qquad \text{(D.10)}$$

APPENDIX E

CALCULATIONS OF HARDENING PARAMETERS

E1. Field Induced Phase Transformation

Combining the transformation function (3.12) with the driving force (3.51) and enforcing the Kuhn Tucker conditions (3.13), we can write the following conditions.

1. Forward transformation ($\dot{\xi} > 0$):

$\pi^t(\sigma_A, H_s^M, T_c) - Y^t = 0$ and at $\xi = 0$

$$\begin{aligned} & |\sigma_A| E^{cur}(\sigma_A) + \Delta(\frac{1}{2\mathbb{E}})\sigma_A^2 + \mu_0 \Delta M H_s^M + \rho \Delta s_0 T_c - \rho \Delta u_0 \\ - \quad & B - Y^t = 0, \end{aligned} \tag{E.1}$$

$\pi^t(\sigma_M, H_f^M, T_c) - Y^t = 0$ and at $\xi = 1$

$$\begin{aligned} & |\sigma_M| E^{cur}(\sigma_M) + \Delta(\frac{1}{2\mathbb{E}})\sigma_M^2 + \mu_0 \Delta M H_f^M + \rho \Delta s_0 T_c - \rho \Delta u_0 \\ + \quad & \pi A - B - Y^t = 0. \end{aligned} \tag{E.2}$$

2. Reverse transformation ($\dot{\xi} < 0$):

$\pi^t(\sigma_M, H_s^A, T_c) + Y^t = 0$ and at $\xi = 1$

$$\begin{aligned} & |\sigma_M| E^{cur}(\sigma_M) + \Delta(\frac{1}{2\mathbb{E}})\sigma_M^2 + \mu_0 \Delta M H_s^A + \rho \Delta s_0 T_c - \rho \Delta u_0 \\ + \quad & \pi C - D + Y^t = 0, \end{aligned} \tag{E.3}$$

$\pi^t(\sigma_A, H_f^A, T_c) + Y^t = 0$ and at $\xi = 0$

$$
\begin{aligned}
& |\sigma_A| E^{cur}(\sigma_A) + \Delta(\frac{1}{2\mathbb{E}})\sigma_A^2 + \mu_0 \Delta M H_f^A + \rho \Delta s_0 T_c - \rho \Delta u_0 \\
- \quad & D + Y^t = 0, \qquad \text{(E.4)}
\end{aligned}
$$

3. Continuity of hardening function at $\xi = 1$

$$
\begin{aligned}
\int_0^1 f^t\Big|_{\dot{\xi}>0} d\xi &= \int_0^1 f^t\Big|_{\dot{\xi}<0} d\xi \\
\Rightarrow -A[\pi - \frac{\pi}{2}] + B &= -C[\pi - \frac{\pi}{2}] + D \\
\text{(using (3.27)} \quad \text{since} \quad & \int_0^1 \cos^{-1}(2\xi - 1) d\xi = \frac{\pi}{2}) \\
\Rightarrow B - D &= \frac{\pi}{2}(A - C) \qquad \text{(E.5)}
\end{aligned}
$$

So, from the five equations (E.1) to (E.5) we can now solve for five material parameters A, B, C, D and Y^t. (E.1)-(E.2) gives

$$
\begin{aligned}
A \quad = \quad & \frac{1}{\pi}[(|\sigma_A| E^{cur}(\sigma_A) - |\sigma_M| E^{cur}(\sigma_M)) + \Delta(\frac{1}{2\mathbb{E}})(\sigma_A^2 - \sigma_M^2) \\
+ \quad & \mu_0 \Delta M (H_s^M - H_f^M)] \, , \qquad \text{(E.6)}
\end{aligned}
$$

(E.4)-(E.3) gives

$$
\begin{aligned}
C \quad = \quad & \frac{1}{\pi}[(|\sigma_A| E^{cur}(\sigma_A) - |\sigma_M| E^{cur}(\sigma_M)) + \Delta(\frac{1}{2\mathbb{E}})(\sigma_A^2 - \sigma_M^2) \\
+ \quad & \mu_0 \Delta M (H_f^A - H_s^A)] \, , \qquad \text{(E.7)}
\end{aligned}
$$

(E.1)+(E.4)

$$\begin{aligned} B + D &= 2(|\sigma_A| E^{cur}(\sigma_A) + \Delta(\frac{1}{2\mathbb{E}})\sigma_A^2 + \frac{\mu_0}{2}\Delta M(H_s^M + H_f^A) \\ &+ \rho\Delta s_0 T_c) - 2\rho_0\Delta u_0 \\ &= 2(\Theta) - 2\rho_0\Delta u_0 \end{aligned} \tag{E.8}$$

where, Θ denotes the expression under the braces. Solving (E.8) and (E.5) we get,

$$\begin{aligned} B &= \Theta + \frac{\pi}{4}(A - C) - \rho\Delta u_0 \\ D &= \Theta - \frac{\pi}{4}(A - C) - \rho\Delta u_0 \end{aligned}$$

and we denote

$$\widetilde{B} = B + \rho\Delta u_0 = \Theta + \frac{\pi}{4}(A - C) \tag{E.9}$$

$$\widetilde{D} = D + \rho\Delta u_0 = \Theta - \frac{\pi}{4}(A - C) \tag{E.10}$$

Finally by (E.1) we get,

$$\begin{aligned} Y^t &= |\sigma_A| E^{cur}(\sigma_A) + \Delta(\frac{1}{2\mathbb{E}})\sigma_A^2 + \mu_0\Delta M H_s^M + \rho\Delta s_0 T_c \\ &- \widetilde{B}. \end{aligned} \tag{E.11}$$

With the help of transformation function ((3.12)), driving force ((3.51)) and Kuhn Tucker conditions ((3.13)), the evolution of the volume fraction can be calculated in the following way

4. Evolution of ξ, forward transformation ($\dot{\xi} > 0$):

$$\Phi^t\dot{\xi} = 0 \Rightarrow \Phi^t = 0 \Rightarrow \pi^t - Y^t = 0$$

$$|\sigma^E|E^{cur} + \Delta(\frac{1}{2\mathbb{E}})\sigma^{E^2} + \mu_0\Delta M H_x + \rho\Delta s_0 T - \rho\Delta u_0 + A[\pi - \cos^{-1}(2\xi - 1)] - B - Y^t = 0$$

which gives

$$\begin{aligned} \xi &= \frac{1}{2} + \frac{1}{2}\cos[\pi + \frac{1}{A}[|\sigma^E_{xx}|E^{cur} + \Delta(\frac{1}{2\mathbb{E}})(\sigma^E_{xx})^2 + \mu_0\Delta M H_x + \rho\Delta s_0 T - Y^t - \widetilde{B}]] \ . \\ \Rightarrow \xi &= \frac{1}{2} + \frac{1}{2}\cos[f_1|\sigma^E_{xx}|E^{cur} + f_2(\sigma^E_{xx})^2 + f_3 H_x + f_4 T + f_5] \ . \end{aligned} \tag{E.12}$$

where

$$f_1 = \tfrac{1}{A},\ f_2 = \Delta\tfrac{1}{2\mathbb{E}A}\ f_3 = \tfrac{\mu_0\Delta M}{A},\ f_5 = \tfrac{\rho\Delta s_0}{A},\ f_5 = \pi + \tfrac{-Y^t - \widetilde{B}}{A}$$

5. Evolution of ξ, reverse transformation ($\dot{\xi} < 0$):

$$\Phi^t\dot{\xi} = 0 \Rightarrow \Phi^t = 0 \Rightarrow \pi^t + Y^t = 0$$

$$|\sigma^E|E^{cur} + \Delta(\frac{1}{2\mathbb{E}})\sigma^{E^2} + \mu_0\Delta M H_x + \rho\Delta s_0 T - \rho\Delta u_0 + C[\pi - \cos^{-1}(2\xi - 1)] - D + Y^t = 0$$

which gives

$$\begin{aligned} \xi &= \frac{1}{2} + \frac{1}{2}\cos[\pi + \frac{1}{C}[|\sigma^E_{xx}|E^{cur} + \Delta(\frac{1}{2\mathbb{E}})(\sigma^E_{xx})^2 + \mu_0\Delta M H_x + \rho\Delta s_0 T_c + Y^t - \widetilde{D}]] \ . \\ \Rightarrow \xi &= \frac{1}{2} + \frac{1}{2}\cos[r_1|sig^E_{xx}|E^{cur} + r_2(\sigma^E_{xx})^2 + r_3 H_x + r_4 T + r_5] \ . \end{aligned} \tag{E.13}$$

where

$$r_1 = \frac{1}{C},\ r_2 = \Delta\frac{1}{2\mathbb{E}C}\ r_3 = \frac{\mu_0 \Delta M}{C},\ r_4 = \frac{\rho \Delta s_0}{C},\ r_5 = \pi + \frac{Y^t - \widetilde{D}}{C}$$

E2. Variant Reorientation

1. Forward transformation ($\dot{\xi}_4 > 0$):

$\pi^r(\sigma^*, H_s^{M_2}) - Y^r = 0$ and at $\xi_4 = 0$

$$\sigma^* E^{max} + \mu_0 \gamma H_s^{M_2} - \rho_0 u_0^M - B - Y^r = 0, \tag{E.14}$$

$\pi^r(\sigma^*, H_f^{M_2}) - Y^r = 0$ and at $\xi_4 = 1$

$$\sigma^* E^{max} + \gamma H_f^{M_2} - \rho_0 u_0^M + \pi A - B - Y^r = 0. \tag{E.15}$$

2. Reverse transformation ($\dot{\xi}_4 < 0$):

$\pi^r(\sigma^*, H_s^{M_1}) + Y^r = 0$ and at $\xi_4 = 1$

$$\sigma^* E^{max} + \mu_0 \gamma H_s^{M_1} - \rho_0 u_0^M + \pi C - D + Y^r = 0, \tag{E.16}$$

$\pi^r(\sigma^*, H_f^{M_1}) + Y^r = 0$ and at $\xi_4 = 0$

$$\sigma^* E^{max} + \mu_0 \gamma H_f^{M_1} - \rho_0 u_0^M - D + Y^r = 0, \tag{E.17}$$

3. Continuity of Gibbs free energy potential

The cyclic integral of the Gibbs free energy is zero. This implies

$$B - D = \frac{\pi}{2}(A - C) \tag{E.18}$$

So, from the five equations (E.14) to (E.18) we can now solve for five material parameters A, B, C, D and Y^r. (E.14)-(E.15) gives

$$A = \mu_0\gamma(H_s^{M_2} - H_f^{M_2}) \ , \tag{E.19}$$

(E.17)-(E.16) gives

$$C = \mu_0\gamma(H_f^{M_1} - H_s^{M_1}) \ , \tag{E.20}$$

(E.14)+(E.17)

$$\begin{aligned} B + D &= 2(\sigma^* E^{max} + \frac{\mu_0}{2}\gamma(H_s^{M_2} + H_f^{M_1})) - 2\rho_0 u_0 \\ &= 2(\Theta) - 2\rho_0\Delta u_0 \end{aligned} \tag{E.21}$$

where, Θ denotes the expression under the braces. Solving (E.21) and (E.18) we get,

$$\begin{aligned} B &= \Theta + \frac{\pi}{4}(A - C) - \rho_0 u_0 \\ D &= \Theta - \frac{\pi}{4}(A - C) - \rho_0 u_0 \end{aligned}$$

and we denote

$$\widetilde{B} = B + \rho_0\Delta u_0 = \Theta + \frac{\pi}{4}(A - C) \tag{E.22}$$

$$\widetilde{D} = D + \rho_0\Delta u_0 = \Theta - \frac{\pi}{4}(A - C) \tag{E.23}$$

Finally by (E.14) we get,

$$Y^r = \sigma^* E^{max} + \mu_0\gamma H_s^{M_2} - \widetilde{B}. \tag{E.24}$$

The evolution of the volume fraction for the forward reorientation is given below

4. Forward reorientation ($\dot{\xi}_4 > 0$):

$$\Phi^r \dot{\xi}_4 = 0 \Rightarrow \Phi^r = 0 \Rightarrow \pi^r - Y^r = 0$$

$$\sigma_{xx}^E E^{max} + \mu_0 \gamma H_y - \rho \Delta u_0 + A[\pi - \cos^{-1}(2\xi_4 - 1)] - B - Y^r = 0$$

which gives

$$\xi_4 = \frac{1}{2} + \frac{1}{2}\cos[\pi + \frac{1}{A}(\sigma_{xx}^E E^{max} + \mu_0 \gamma H_y - Y^r - \widetilde{B})] \tag{E.25}$$

5. Reverse reorientation ($\dot{\xi}_4 < 0$):

$$\Phi^r \dot{\xi}_4 = 0 \Rightarrow \Phi^r = 0 \Rightarrow \pi^r + Y^r = 0$$

$$\sigma_{xx}^E E^{max} + \mu_0 \gamma H_y - \rho \Delta u_0 + C[\pi - \cos^{-1}(2\xi_4 - 1)] - D + Y^r = 0$$

which gives

$$\xi_4 = \frac{1}{2} + \frac{1}{2}\cos[\pi + \frac{1}{C}(\sigma_{xx}^E E^{max} + \mu_0 \gamma H_y + Y^r - \widetilde{D})] \tag{E.26}$$

APPENDIX F

THE DEMAGNETIZATION EFFECT AND CORRECTION OF EXPERIMENTAL DATA

The magnetostatic field caused by the body's own magnetization is called the *demagnetizing field* $\mathbf{H}_d$ [19]. The demagnetization field in a uniformly magnetized ellipsoidal sample is always uniform, while it is nonuniform in a rectangular body. If an external magnetic field $\mathbf{H}_a$ is applied, the total magnetic field is then given by

$$\mathbf{H} = \mathbf{H}_a + \mathbf{H}_d \, . \tag{F.1}$$

For uniformly magnetized bodies the magnetization vector can be taken outside the integral expressions for the magnetic field strength [164, 165], such that

$$\mathbf{H}_d(\mathbf{r}) = - \underbrace{\left[\frac{1}{4\pi} \iint\limits_{\partial\Omega^{\mathrm{m}}} \frac{\mathbf{r} - \mathbf{r}'}{|\mathbf{r} - \mathbf{r}'|^3} \otimes \mathbf{n}' \, \mathrm{d}A' \right]}_{=:\mathbf{D}} \mathbf{M} = -\mathbf{D}\mathbf{M} \, . \tag{F.2}$$

Therein $\mathbf{r}$ is the position at which $\mathbf{H}$ is evaluated and $\mathbf{r}'$ the location of a point on the surface, with unit outward normal $\mathbf{n}'$, of the region occupied by the magnetized body. $\mathbf{D}$ is the demagnetization tensor, which only depends on the geometry of the body and can be computed by evaluating the bracketed integral expression in (F.2). For a spatially uniform magnetized body the demagnetization field can thus be computed by simply multiplying the magnetization with an appropriate demagnetization factor. Such factors for a rectangular prism have been tabulated for many different aspect ratios [177, 178].

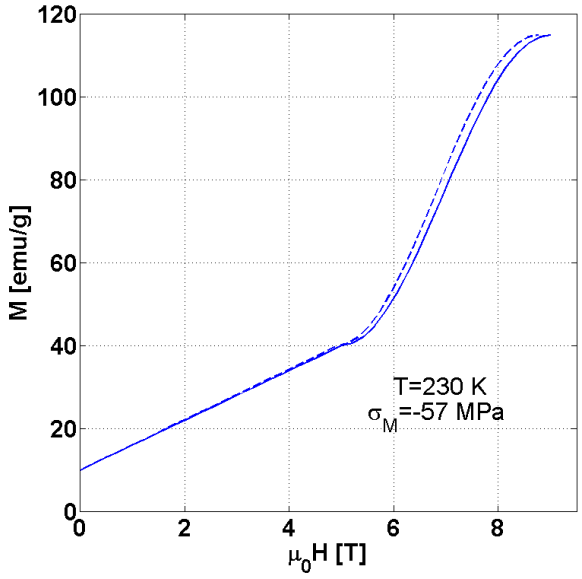

Fig. 89. Shift of magnetization response (dotted line) due to demagnetization effect during reverse transformation at 230 K and σ_M=-57 MPa.

F1. Experimental Data Correction for FIPT

One way to take into account the demagnetization effect is to solve a boundary value problem [149]. However, we can estimate the demagnetization effect at constitutive level by considering the magnetization is uniform. The demagnetization factor for the longitudinal loading condition is given by D_x=0.19832 [178]. We rescale the four critical magnetic values by $H^{crt'} = H^{crt} - D_x M_x \mid_{H^{crt}}$ and the magnetic field by $H_x = H_a - D_x M_x$. The corrected response is shown in Fig.89. It should be observed that, due to low aspect ratio (length of short axis/length of long axis) and high magnitude of the field, the effect of demagnetization is not very strong. Finally, we calculate that the percent change in magnetic field due to demagnetization effect is less than 5%.

F2. Experimental Data Correction for variant reorientation

In the analytical method, the demagnetization factor of the rectangular specimen is approximated by the demagnetization factor of an ellipsoid with the same aspect ratio. The explicit expression of demagnetization factor of a prolate ellipsoid with the semi-major axis(a) and semi-minor axes(c) is given by,

$$D_x = D_a = \frac{\alpha^2}{1-\alpha^2}\left[\frac{1}{\sqrt{1-\alpha^2}}\sinh^{-1}(\frac{\sqrt{1-\alpha^2}}{\alpha}) - 1\right] , \tag{F.3}$$

$$D_y = D_c = \frac{1}{2}(1 - D_a) , \tag{F.4}$$

where $\alpha = c/a$. The above relation is used as the demagnetization factor of the rectangular specimen of dimension $8 \times 4 \times 4\, mm^3$ with a=8 and c=4.

The magnetic properties, which are initially only known in terms of the applied field, were used as if they were the true constitutive response of the material. The magnetization response is obtained by

$$M_y = \xi M^{sat} + (1-\xi)\frac{\mu_0 (M^{sat})^2}{2\rho K_1} H_y \tag{F.5}$$

The demagnetization field is computed from the relation $H_y^d = -D_y M_y$. According to the equation (F.1), total magnetic field is then calculated by $H_y^a - D_y M_y$. This is the first step to relate the applied and internal magnetic field. Similarly, replacing the four critical magnetic properties by $H_{y\,crt}^a - D_y M_y|_{H_{y\,crt}^a}$, we get the correct set of critical values.

This process is iterated unless the final solution converges to the true response. A few iteration steps are required due to nonlinear behavior of the magnetization response. The convergence condition of the global response is obtained by ensuring

the convergence of all four critical magnetic values within a tolerance limit. The algorithm is given in TableLVI. So, starting with the scale of applied magnetic field, the process ends up with the scale of internal magnetic field and true constitutive equation is obtained.

In the following analysis, the system takes four iterations to converge within the tolerance $1E-3$. Following plots give the mode of convergence of the four critical values.

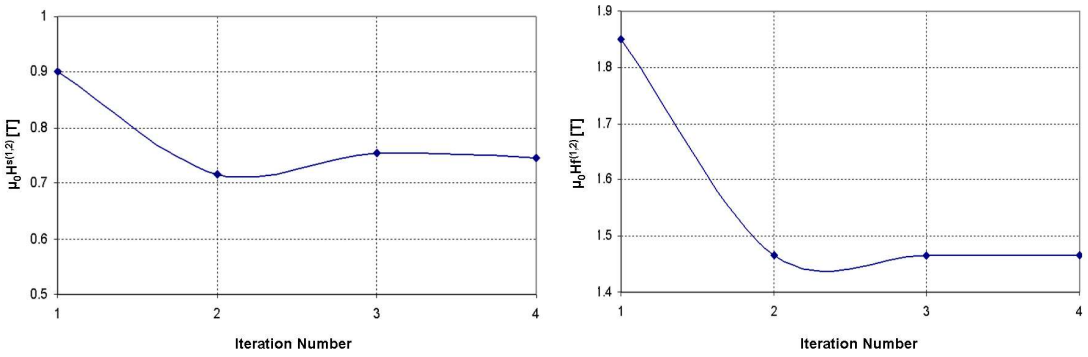

(a) (b)

Fig. 90. Convergence of the critical parameters for the forward reorientation

1^{st} **iteration**

$H_y \simeq H_y^a$

$M_y = \xi M^{sat} + (1-\xi) M^{sat} \frac{\mu_0 (M^{sat})^2}{2\rho K_1} H_y$

$H_y = H_y^a - D_y M_y$

Correction of critical values:

$H_y^{s(1,2)(1)} = H_y^{s(1,2),Experiment} - D_y M_y(H_y^{s(1,2)})$

$H_y^{f(1,2)(1)} = H_y^{f(1,2),Experiment} - D_y M_y(H_y^{f(1,2)})$

$H_y^{s(2,1)(1)} = H_y^{s(2,1),Experiment} - D_y M_y(H_y^{s(2,1)})$

$H_y^{f(2,1)(1)} = H_y^{f(2,1),Experiment} - D_y M_y(H_y^{f(2,1)})$

i^{th} **iteration:**

$H_y^{(i)} = H_y^{a(i)} - D_y M_y^{(i-1)}$

$H_y^{s(1,2)(i)} = H_y^{s(1,2),Experiment} - D_y M_y^{(i-1)}(H_y^{s(1,2)(i-1)})$

$H_y^{f(1,2)(i)} = H_y^{f(1,2),Experiment} - D_y M_y^{(i-1)}(H_y^{f(1,2)(i-1)})$

$H_y^{s(2,1)(i)} = H_y^{s(2,1),Experiment} - D_y M_y^{(i-1)}(H_y^{s(2,1)(i-1)})$

$H_y^{f(2,1)(i)} = H_y^{f(2,1),Experiment} - D_y M_y^{(i-1)}(H_y^{f(2,1)(i-1)})$

Convergence Criteria:

$\|H_y^{Crit(i)} - H_y^{Crit(i-1)}\| \leq TOL$

Table LVI. Iterative algorithm scheme for data correction

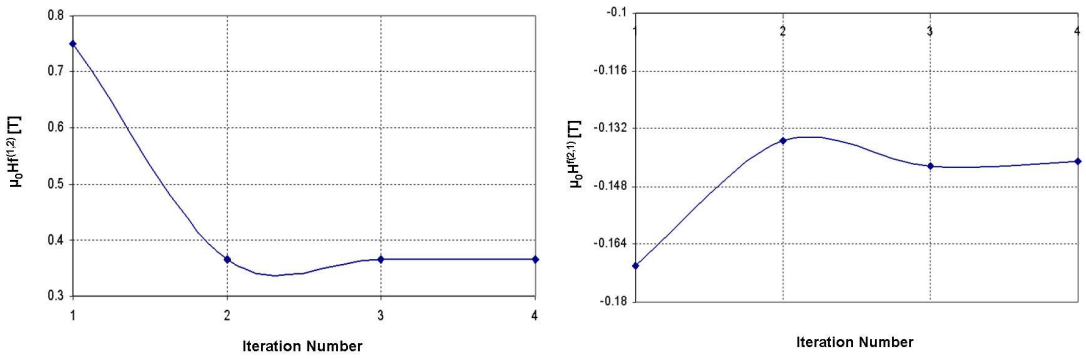

(a) (b)

Fig. 91. Convergence of the critical parameters for the reverse reorientation

The convergence of magnetization and strain response is presented the following plots.

It should be noted that, comparing with the Fig 52, the analytic solution is very close to the numerical one and it converges much faster. Same trend is also observed in the strain response. This approach is thus very effective as well as accurate to obtain the proper constitutive responses, suitable for engineering analysis.

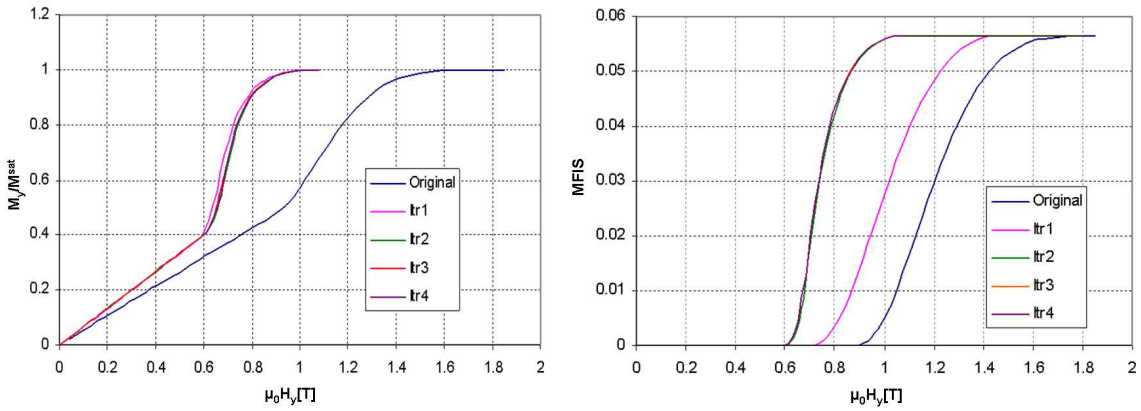

(a) (b)

Fig. 92. Convergence of the magnetization and strain response curve towards the actual response.

APPENDIX G

MAGNETO MECHANICAL BOUNDARY CONDITIONS

We seek to prove that if

$$[\![\boldsymbol{\sigma} + \boldsymbol{\sigma}^M]\!]\mathbf{n} = \mathbf{0}\ , \tag{G.1}$$

then

$$\boldsymbol{\sigma}^{MT}\mathbf{n} = \mathbf{t}^a + \mu_0(\mathbf{H}\otimes\mathbf{M})\mathbf{n} + \frac{\mu_0}{2}(\mathbf{M}\cdot\mathbf{n})^2\mathbf{n}\ , \tag{G.2}$$

where $\boldsymbol{\sigma}\mathbf{n} = \mathbf{t}^a$. Therein, $\mathbf{n}$ is the outward unit normal to the boundary $\partial\Omega$ and $[\![A]\!] := A^+ - A^-$ is the jump operator, where A^+ and A^- represent the values of A on either side of the discontinuity surface. From Ampère's law, we can conclude that $[\![\mathbf{H}^t]\!] = 0$, i.e.(5.2)(b), where the superscript t represents the tangential direction. It then follows $\mathbf{H} = \mathbf{H}^n + \mathbf{H}^t = (\mathbf{H}\cdot\mathbf{n})\mathbf{n} + \mathbf{H}^t$ and

$$[\![\mathbf{H}]\!] = [\![\mathbf{H}^n]\!] + [\![\mathbf{H}^t]\!] = [\![\mathbf{H}^n]\!] = ([\![\mathbf{H}]\!]\cdot\mathbf{n})\mathbf{n}\ . \tag{G.3}$$

Using the constitutive relation $\mathbf{H} = \frac{1}{\mu_0}\mathbf{B} - \mathbf{M}$ in (G.3) and (5.2a) we find

$$\begin{aligned}
[\![\mathbf{H}]\!] &= (\frac{1}{\mu_0}[\![\mathbf{B}]\!]\cdot\mathbf{n} - [\![\mathbf{M}]\!]\cdot\mathbf{n})\mathbf{n} \\
&= -([\![\mathbf{M}]\!]\cdot\mathbf{n})\mathbf{n} \\
&= -[(\mathbf{M}^+ - \mathbf{M}^-)\cdot\mathbf{n}]\mathbf{n} \\
&= (\mathbf{M}\cdot\mathbf{n})\mathbf{n}\ .
\end{aligned} \tag{G.4}$$

Here we have used the fact that $\mathbf{M}^+ = 0$ and $\mathbf{M}^- = \mathbf{M}$. Note that (5.11) can be

rewritten as $\boldsymbol{\sigma}^M = \mathbf{H} \otimes \mathbf{B} - \frac{\mu_0}{2}(\mathbf{H} \cdot \mathbf{H})\mathbf{I}$. It follows that

$$\begin{aligned} \llbracket \boldsymbol{\sigma}^M \rrbracket \mathbf{n} &= \llbracket \mathbf{H} \otimes \mathbf{B} \rrbracket \mathbf{n} - \frac{\mu_0}{2} \llbracket (\mathbf{H} \cdot \mathbf{H})\mathbf{I} \rrbracket \mathbf{n} \\ &= (\mathbf{H}^+ \otimes \mathbf{B}^+ - \mathbf{H}^- \otimes \mathbf{B}^-)\mathbf{n} - \frac{\mu_0}{2}(\mathbf{H}^+ \cdot \mathbf{H}^+ - \mathbf{H}^- \cdot \mathbf{H}^-)\mathbf{n}. \end{aligned} \tag{G.5}$$

The first term in (G.5), using $\llbracket \mathbf{B} \rrbracket \cdot \mathbf{n} = (\mathbf{B}^+ \cdot \mathbf{n}) - (\mathbf{B}^- \cdot \mathbf{n}) = 0$, may be written as

$$\begin{aligned} (\mathbf{H}^+ \otimes \mathbf{B}^+ - \mathbf{H}^- \otimes \mathbf{B}^-)\mathbf{n} &= (\mathbf{B}^+ \cdot \mathbf{n})\mathbf{H}^+ - (\mathbf{B}^- \cdot \mathbf{n})\mathbf{H}^- \\ &= (\mathbf{B}^+ \cdot \mathbf{n})(\mathbf{H}^+ - \mathbf{H}^-) \\ &= (\mathbf{B}^+ \cdot \mathbf{n}) \llbracket \mathbf{H} \rrbracket \end{aligned} \tag{G.6}$$

From (5.2b) it is clear that $\llbracket \mathbf{H}^t \rrbracket = \llbracket \mathbf{n} \times \mathbf{H} \rrbracket = \mathbf{0}$ and consequently $\llbracket \mathbf{H}^t \cdot \mathbf{H}^t \rrbracket = 0$ implies (cf. [113]),

$$|\mathbf{n} \times \mathbf{H}^+|^2 = |\mathbf{n} \times \mathbf{H}^-|^2 \tag{G.7}$$

Using the identity $(\mathbf{a} \times \mathbf{b}) \cdot (\mathbf{c} \times \mathbf{d}) = (\mathbf{a} \cdot \mathbf{c})(\mathbf{b} \cdot \mathbf{d}) - (\mathbf{a} \cdot \mathbf{d})(\mathbf{b} \cdot \mathbf{c})$, we can write

$$(\mathbf{n} \times \mathbf{H}^+) \cdot (\mathbf{n} \times \mathbf{H}^+) = (\mathbf{n} \cdot \mathbf{n})(\mathbf{H}^+ \cdot \mathbf{H}^+) - (\mathbf{H}^+ \cdot \mathbf{n})^2 \ . \tag{G.8}$$

Similarly,

$$(\mathbf{n} \times \mathbf{H}^-) \cdot (\mathbf{n} \times \mathbf{H}^-) = (\mathbf{n} \cdot \mathbf{n})(\mathbf{H}^- \cdot \mathbf{H}^-) - (\mathbf{H}^- \cdot \mathbf{n})^2 \ . \tag{G.9}$$

From Eqs. (G.7), (G.8) and (G.9), we conclude

$$|\mathbf{H}^+|^2 - (\mathbf{H}^+ \cdot \mathbf{n})^2 = |\mathbf{H}^-|^2 - (\mathbf{H}^- \cdot \mathbf{n})^2 \ . \tag{G.10}$$

which means $\llbracket \mathbf{H} \cdot \mathbf{H} \rrbracket = \llbracket (\mathbf{H} \cdot \mathbf{n})^2 \rrbracket$. Now with (G.10) we can write the second term on the right hand side of (G.5) in the following form

$$\begin{aligned} \frac{\mu_0}{2}[\mathbf{H}^+ \cdot \mathbf{H}^+ - \mathbf{H}^- \cdot \mathbf{H}^-]\mathbf{n} &= \frac{\mu_0}{2}[(\mathbf{H}^+ \cdot \mathbf{n})^2 - (\mathbf{H}^- \cdot \mathbf{n})^2]\mathbf{n} \\ &= \frac{\mu_0}{2}[(\mathbf{H}^+ - \mathbf{H}^-) \cdot \mathbf{n}][(\mathbf{H}^+ + \mathbf{H}^-) \cdot \mathbf{n}]\mathbf{n} \ . \end{aligned}$$

Considering that $(\mathbf{H}^+ - \mathbf{H}^-)\cdot\mathbf{n} = [\![\mathbf{H}]\!]\cdot\mathbf{n}$ and $(\mathbf{H}^+ + \mathbf{H}^-)\cdot\mathbf{n} = [(\frac{1}{\mu_0}\mathbf{B}^+ - \mathbf{M}^+) + (\frac{1}{\mu_0}\mathbf{B}^- - \mathbf{M}^-)]\cdot\mathbf{n} = [\frac{1}{\mu_0}\mathbf{B}^+ + \frac{1}{\mu_0}\mathbf{B}^- - \mathbf{M}^-]\cdot\mathbf{n}$, with $\mathbf{B}^+\cdot\mathbf{n} = \mathbf{B}^-\cdot\mathbf{n}$ due to (5.2a) and (G.4), it follows

$$\begin{aligned}
\frac{\mu_0}{2}[\mathbf{H}^+\cdot\mathbf{H}^+ - \mathbf{H}^-\cdot\mathbf{H}^-]\mathbf{n} &= \frac{\mu_0}{2}[\![\mathbf{H}]\!]\cdot\mathbf{n}[\frac{2}{\mu_0}(\mathbf{B}^+ - \mathbf{M})\cdot\mathbf{n}]\mathbf{n} \\
&= (\mathbf{B}^+\cdot\mathbf{n})([\![\mathbf{H}]\!]\cdot\mathbf{n})\mathbf{n} - \frac{\mu_0}{2}(\mathbf{M}\cdot\mathbf{n})([\![\mathbf{H}]\!]\cdot\mathbf{n})\mathbf{n} \\
&= (\mathbf{B}^+\cdot\mathbf{n})[\![\mathbf{H}]\!] - \frac{\mu_0}{2}(\mathbf{M}\cdot\mathbf{n})[\![\mathbf{H}]\!] \\
&= (\mathbf{B}^+\cdot\mathbf{n})[\![\mathbf{H}]\!] - \frac{\mu_0}{2}(\mathbf{M}\cdot\mathbf{n})^2\mathbf{n}\ . \qquad \text{(G.11)}
\end{aligned}$$

Substitution of Eqs. (G.6) and (G.11) into (G.5) yields

$$[\![\boldsymbol{\sigma}^M]\!]\mathbf{n} = \frac{\mu_0}{2}(\mathbf{M}\cdot\mathbf{n})^2\mathbf{n}\ . \qquad \text{(G.12)}$$

In consequence, with (5.16), we obtain

$$\begin{aligned}
[\![\boldsymbol{\sigma} + \boldsymbol{\sigma}^M]\!]\mathbf{n} &= [\![\boldsymbol{\sigma}]\!]\mathbf{n} + [\![\boldsymbol{\sigma}^m]\!]\mathbf{n} \\
&= (\boldsymbol{\sigma}^+ - \boldsymbol{\sigma}^-)\mathbf{n} + [\![\boldsymbol{\sigma}^m]\!]\mathbf{n} \\
&= \mathbf{t}^a - \boldsymbol{\sigma}\mathbf{n} + \frac{\mu_0}{2}(\mathbf{M}\cdot\mathbf{n})^2\mathbf{n} \\
&= \mathbf{t}^a - \boldsymbol{\sigma}^{MT}\mathbf{n} + \mu_0(\mathbf{H}\otimes\mathbf{M})\mathbf{n} + \frac{\mu_0}{2}(\mathbf{M}\cdot\mathbf{n})^2\mathbf{n}\ .
\end{aligned}$$

Finally, (G.1) yields the boundary condition in the following form

$$\boxed{\boldsymbol{\sigma}^{MT}\mathbf{n} = \mathbf{t}^a + \mu_0(\mathbf{H}\otimes\mathbf{M})\mathbf{n} + \tfrac{\mu_0}{2}(\mathbf{M}\cdot\mathbf{n})^2\mathbf{n}} \qquad \text{(G.13)}$$

APPENDIX H

EXPANDED INVARIANT TABLE

The Gibbs free energy contains the set of external variables (experimentally controlled) $\{\mathbf{S}^E, \mathbf{H}, T\}$, the set of internal variables $\{\mathbb{Z}\} = \{\mathbf{E}^I, \mathbf{M}^I, \xi_i, g\}$, the mechanical structural tensor $\mathbf{A_m} = \mathbf{a} \otimes \mathbf{a}$ and the magnetic structural tensor $\mathbf{A_f} = \mathbf{f} \otimes \mathbf{f}$. We denote two anti-symmetric tensors $\mathbf{W}_1$ and $\mathbf{W}_2$ such that $\mathbf{H}$ and $\mathbf{M}^I$ are the respective axial vectors i.e $\mathbf{W}_1\mathbf{z} = \mathbf{H} \times \mathbf{z}$ and $\mathbf{W}_2\mathbf{z} = \mathbf{M^I} \times \mathbf{z}$ for an arbitrary vector $\mathbf{z}$. We are looking for invariants for a scalar valued isotropic functions with four symmetric tensors $\{\mathbf{S}^E, \mathbf{E}^I, \mathbf{A}_m, \mathbf{A}_f\}$ and two anti-symmetric tensors $\{\mathbf{W}_1, \mathbf{W}_2\}$. They are given in tables below.

Argument/s	Tensors whose traces are irreducible invariants (i)		
$\mathbf{W}_1$	$\mathbf{W}_1^2$		
$\mathbf{W}_2$	$\mathbf{W}_2^2$		
$\mathbf{S}^E$	$\mathbf{S}^E$	$\mathbf{S}^{E^2}$	$\mathbf{S}^{E^3}$
$\mathbf{E}^I$	$\mathbf{E}^I$	$\mathbf{E}^{I^2}$	$\mathbf{E}^{I^3}$
$\mathbf{A}_m$	$\mathbf{A}_m$	${\mathbf{A}_m}^2$	${\mathbf{A}_m}^3$
$\mathbf{A}_f$	$\mathbf{A}_f$	${\mathbf{A}_f}^2$	${\mathbf{A}_f}^3$
$\mathbf{W}_1, \mathbf{W}_2$	$\mathbf{W}_1\mathbf{W}_2$		
$\mathbf{W}_1, \mathbf{S}^E$	$\mathbf{W}_1^2\mathbf{S}^E$	$\mathbf{W}_1^2\mathbf{S}^{E^2}$	$\mathbf{W}_1^2\mathbf{S}^E\mathbf{W}_1\mathbf{S}^{E^2}$
$\mathbf{W}_1, \mathbf{E}^I$	$\mathbf{W}_1^2\mathbf{E}^I$	$\mathbf{W}_1^2\mathbf{E}^{I^2}$	$\mathbf{W}_1^2\mathbf{E}^I\mathbf{W}_1\mathbf{E}^{I^2}$
$\mathbf{W}_1, \mathbf{A}_m$	$\mathbf{W}_1^2\mathbf{A}_m$	$\mathbf{W}_1^2{\mathbf{A}_m}^2$	$\mathbf{W}_1^2\mathbf{A}_m\mathbf{W}_1{\mathbf{A}_m}^2$
$\mathbf{W}_1, \mathbf{A}_f$	$\mathbf{W}_1^2\mathbf{A}_f$	$\mathbf{W}_1^2{\mathbf{A}_f}^2$	$\mathbf{W}_1^2\mathbf{A}_f\mathbf{W}_1{\mathbf{A}_f}^2$
$\mathbf{W}_2, \mathbf{S}^E$	$\mathbf{W}_2^2\mathbf{S}^E$	$\mathbf{W}_2^2\mathbf{S}^{E^2}$	$\mathbf{W}_2^2\mathbf{S}^E\mathbf{W}_1\mathbf{S}^{E^2}$
$\mathbf{W}_2, \mathbf{E}^I$	$\mathbf{W}_2^2\mathbf{E}^I$	$\mathbf{W}_2^2\mathbf{E}^{I^2}$	$\mathbf{W}_2^2\mathbf{E}^I\mathbf{W}_1\mathbf{E}^{I^2}$
$\mathbf{W}_2, \mathbf{A}_m$	$\mathbf{W}_2^2\mathbf{A}_m$	$\mathbf{W}_2^2{\mathbf{A}_m}^2$	$\mathbf{W}_2^2\mathbf{A}_m\mathbf{W}_2{\mathbf{A}_m}^2$
$\mathbf{W}_2, \mathbf{A}_f$	$\mathbf{W}_2^2\mathbf{A}_f$	$\mathbf{W}_2^2{\mathbf{A}_f}^2$	$\mathbf{W}_2^2\mathbf{A}_f\mathbf{W}_2{\mathbf{A}_f}^2$
$\mathbf{S}^E, \mathbf{E}^I$	$\mathbf{S}^E\mathbf{E}^I$	$\mathbf{S}^{E^2}\mathbf{E}^{I^*}$	$\mathbf{S}^{E^2}\mathbf{E}^{I^2}$
$\mathbf{S}^E, \mathbf{A}_m$	$\mathbf{S}^E\mathbf{A}_m$	$\mathbf{S}^{E^2}{\mathbf{A}_m}^*$	$\mathbf{S}^{E^2}{\mathbf{A}_m}^2$
$\mathbf{S}^E, \mathbf{A}_f$	$\mathbf{S}^E\mathbf{A}_f$	$\mathbf{S}^{E^2}{\mathbf{A}_f}^*$	$\mathbf{S}^{E^2}{\mathbf{A}_f}^2$
$\mathbf{E}^I, \mathbf{A}_m$	$\mathbf{E}^I\mathbf{A}_m$	$\mathbf{E}^{I^2}{\mathbf{A}_m}^*$	$\mathbf{E}^{I^2}{\mathbf{A}_m}^2$
$\mathbf{E}^I, \mathbf{A}_f$	$\mathbf{E}^I\mathbf{A}_f$	$\mathbf{E}^{I^2}{\mathbf{A}_f}^*$	$\mathbf{E}^{I^2}{\mathbf{A}_f}^2$
$\mathbf{A}_m, \mathbf{A}_f$	$\mathbf{A}_m\mathbf{A}_f$	${\mathbf{A}_m}^2{\mathbf{A}_f}^*$	${\mathbf{A}_m}^2{\mathbf{A}_f}^2$

Table LVII. Isotropic scalar invariants

Argument/s	Tensors whose traces are irreducible invariants (i)		
$\mathbf{W}_1, \mathbf{W}_2, \mathbf{S}^E$	$\mathbf{W}_1\mathbf{W}_2\mathbf{S}^E$	$\mathbf{W}_1\mathbf{W}_2\mathbf{S}^{E^2}$	$\mathbf{W}_1^2\mathbf{W}_2\mathbf{S}^{E^\dagger}$
	$\mathbf{W}_1^2\mathbf{W}_2\mathbf{S}^{E^{2\dagger}}$	$\mathbf{W}_1^2\mathbf{S}^E\mathbf{W}_2\mathbf{S}^{E^{2\dagger}}$	
$\mathbf{W}_1, \mathbf{W}_2, \mathbf{E}^I$	$\mathbf{W}_1\mathbf{W}_2\mathbf{E}^I$	$\mathbf{W}_1\mathbf{W}_2\mathbf{E}^{I^2}$	$\mathbf{W}_1^2\mathbf{W}_2\mathbf{E}^{I^\dagger}$
	$\mathbf{W}_1^2\mathbf{W}_2\mathbf{E}^{I^{2\dagger}}$	$\mathbf{W}_1^2\mathbf{E}^I\mathbf{W}_2\mathbf{E}^{I^{2\dagger}}$	
$\mathbf{W}_1, \mathbf{W}_2, \mathbf{A}_m$	$\mathbf{W}_1\mathbf{W}_2\mathbf{A}_m$	$\mathbf{W}_1\mathbf{W}_2{\mathbf{A}_m}^2$	$\mathbf{W}_1^2\mathbf{W}_2{\mathbf{A}_m}^\dagger$
	$\mathbf{W}_1^2\mathbf{W}_2{\mathbf{A}_m}^{2\dagger}$		$\mathbf{W}_1^2\mathbf{A}_m\mathbf{W}_2{\mathbf{A}_m}^{2\dagger}$
$\mathbf{W}_1, \mathbf{W}_2, \mathbf{A}_f$	$\mathbf{W}_1\mathbf{W}_2\mathbf{A}_f$	$\mathbf{W}_1\mathbf{W}_2{\mathbf{A}_f}^2$	$\mathbf{W}_1^2\mathbf{W}_2{\mathbf{A}_f}^\dagger$
	$\mathbf{W}_1^2\mathbf{W}_2{\mathbf{A}_f}^{2\dagger}$		$\mathbf{W}_1^2\mathbf{A}_f\mathbf{W}_2{\mathbf{A}_f}^{2\dagger}$
$\mathbf{W}_1, \mathbf{S}^E, \mathbf{E}^I$	$\mathbf{W}_1\mathbf{S}^E\mathbf{E}^I$	$\mathbf{W}_1\mathbf{S}^{E^2}\mathbf{E}^{I^*}$	$\mathbf{W}_1\mathbf{S}^{E^2}\mathbf{E}^{I^2}$
	$\mathbf{W}_1\mathbf{S}^{E^2}\mathbf{E}^I\mathbf{S}^{E^*}$	$\mathbf{W}_1\mathbf{S}^{E^2}\mathbf{E}^{I^2}\mathbf{S}^{E^*}$	$\mathbf{W}_1^2\mathbf{S}^E\mathbf{E}^I$
	$\mathbf{W}_1^2\mathbf{S}^{E^2}\mathbf{E}^{I^*}$	$\mathbf{W}_1^2\mathbf{S}^E\mathbf{W}_1\mathbf{E}^I$	$\mathbf{W}_1^2\mathbf{E}^I\mathbf{W}_1\mathbf{S}^{E^{2*}}$
$\mathbf{W}_1, \mathbf{S}^E, \mathbf{A}_m$	$\mathbf{W}_1\mathbf{S}^E\mathbf{A}_m$	$\mathbf{W}_1\mathbf{S}^{E^2}{\mathbf{A}_m}^*$	$\mathbf{W}_1\mathbf{S}^{E^2}{\mathbf{A}_m}^2$
	$\mathbf{W}_1\mathbf{S}^{E^2}\mathbf{A}_m\mathbf{S}^{E^*}$	$\mathbf{W}_1\mathbf{S}^{E^2}{\mathbf{A}_m}^2\mathbf{S}^{E^*}$	$\mathbf{W}_1^2\mathbf{S}^E\mathbf{A}_m$
	$\mathbf{W}_1^2\mathbf{S}^{E^2}{\mathbf{A}_m}^*$	$\mathbf{W}_1^2\mathbf{S}^E\mathbf{W}_1\mathbf{A}_m$	$\mathbf{W}_1^2\mathbf{A}_m\mathbf{W}_1\mathbf{S}^{E^{2*}}$
$\mathbf{W}_1, \mathbf{S}^E, \mathbf{A}_f$	$\mathbf{W}_1\mathbf{S}^E\mathbf{A}_f$	$\mathbf{W}_1\mathbf{S}^{E^2}{\mathbf{A}_f}^*$	$\mathbf{W}_1\mathbf{S}^{E^2}{\mathbf{A}_f}^2$
	$\mathbf{W}_1\mathbf{S}^{E^2}\mathbf{A}_f\mathbf{S}^{E^*}$	$\mathbf{W}_1\mathbf{S}^{E^2}{\mathbf{A}_f}^2\mathbf{S}^{E^*}$	$\mathbf{W}_1^2\mathbf{S}^E\mathbf{A}_f$
	$\mathbf{W}_1^2\mathbf{S}^{E^2}{\mathbf{A}_f}^*$	$\mathbf{W}_1^2\mathbf{S}^E\mathbf{W}_1\mathbf{A}_f$	$\mathbf{W}_1^2\mathbf{A}_f\mathbf{W}_1\mathbf{S}^{E^{2*}}$
$\mathbf{W}_1, \mathbf{E}^I, \mathbf{A}_m$	$\mathbf{W}_1\mathbf{E}^I\mathbf{A}_m$	$\mathbf{W}_1\mathbf{E}^{I^2}{\mathbf{A}_m}^*$	$\mathbf{W}_1\mathbf{E}^{I^2}{\mathbf{A}_m}^2$
	$\mathbf{W}_1\mathbf{E}^{I^2}\mathbf{A}_m\mathbf{E}^{I^*}$	$\mathbf{W}_1\mathbf{E}^{I^2}{\mathbf{A}_m}^2\mathbf{E}^{I^*}$	$\mathbf{W}_1^2\mathbf{E}^I\mathbf{A}_m$
	$\mathbf{W}_1^2\mathbf{E}^{I^2}{\mathbf{A}_m}^*$	$\mathbf{W}_1^2\mathbf{E}^I\mathbf{W}_1\mathbf{A}_m$	$\mathbf{W}_1^2\mathbf{A}_m\mathbf{W}_1\mathbf{E}^{I^{2*}}$

Table LVIII. Isotropic scalar invariants (continued-1)

Argument/s	Tensors whose traces are irreducible invariants (i)		
$\mathbf{W}_1, \mathbf{E}^I, \mathbf{A}_f$	$\mathbf{W}_1\mathbf{E}^I\mathbf{A}_f$	$\mathbf{W}_1\mathbf{E}^{I^2}\mathbf{A}_f{}^*$	$\mathbf{W}_1\mathbf{E}^{I^2}\mathbf{A}_f{}^2$
	$\mathbf{W}_1\mathbf{E}^{I^2}\mathbf{A}_f\mathbf{E}^{I^*}$	$\mathbf{W}_1\mathbf{E}^{I^2}\mathbf{A}_f{}^2\mathbf{E}^{I^*}$	$\mathbf{W}_1^2\mathbf{E}^I\mathbf{A}_f$
	$\mathbf{W}_1^2\mathbf{E}^{I^2}\mathbf{A}_f{}^*$	$\mathbf{W}_1^2\mathbf{E}^I\mathbf{W}_1\mathbf{A}_f$	$\mathbf{W}_1^2\mathbf{A}_f\mathbf{W}_1\mathbf{E}^{I^{2*}}$
$\mathbf{W}_1, \mathbf{A}_m, \mathbf{A}_f$	$\mathbf{W}_1\mathbf{A}_m\mathbf{A}_f$	$\mathbf{W}_1\mathbf{A}_m{}^2\mathbf{A}_f{}^*$	$\mathbf{W}_1\mathbf{A}_m{}^2\mathbf{A}_f{}^2$
	$\mathbf{W}_1\mathbf{A}_m{}^2\mathbf{A}_f\mathbf{A}_m{}^*$	$\mathbf{W}_1\mathbf{A}_m{}^2\mathbf{A}_f{}^2\mathbf{A}_m{}^*$	$\mathbf{W}_1^2\mathbf{A}_m\mathbf{A}_f$
	$\mathbf{W}_1^2\mathbf{A}_m{}^2\mathbf{A}_f{}^*$	$\mathbf{W}_1^2\mathbf{A}_m\mathbf{W}_1\mathbf{A}_f$	$\mathbf{W}_1^2\mathbf{A}_f\mathbf{W}_1\mathbf{A}_m{}^{2*}$
$\mathbf{W}_2, \mathbf{S}^E, \mathbf{E}^I$	$\mathbf{W}_2\mathbf{S}^E\mathbf{E}^I$	$\mathbf{W}_2\mathbf{S}^{E^2}\mathbf{E}^{I^*}$	$\mathbf{W}_2\mathbf{S}^{E^2}\mathbf{E}^{I^2}$
	$\mathbf{W}_2\mathbf{S}^{E^2}\mathbf{E}^I\mathbf{S}^{E^*}$	$\mathbf{W}_2\mathbf{S}^{E^2}\mathbf{E}^{I^2}\mathbf{S}^{E^*}$	$\mathbf{W}_2^2\mathbf{S}^E\mathbf{E}^I$
	$\mathbf{W}_2^2\mathbf{S}^{E^2}\mathbf{E}^{I^*}$	$\mathbf{W}_2^2\mathbf{S}^E\mathbf{W}_2\mathbf{E}^I$	$\mathbf{W}_2^2\mathbf{E}^I\mathbf{W}_2\mathbf{S}^{E^{2*}}$
$\mathbf{W}_2, \mathbf{S}^E, \mathbf{A}_m$	$\mathbf{W}_2\mathbf{S}^E\mathbf{A}_m$	$\mathbf{W}_2\mathbf{S}^{E^2}\mathbf{A}_m{}^*$	$\mathbf{W}_2\mathbf{S}^{E^2}\mathbf{A}_m{}^2$
	$\mathbf{W}_2\mathbf{S}^{E^2}\mathbf{A}_m\mathbf{S}^{E^*}$	$\mathbf{W}_2\mathbf{S}^{E^2}\mathbf{A}_m{}^2\mathbf{S}^{E^*}$	$\mathbf{W}_2^2\mathbf{S}^E\mathbf{A}_m$
	$\mathbf{W}_2^2\mathbf{S}^{E^2}\mathbf{A}_m{}^*$	$\mathbf{W}_2\mathbf{S}^E\mathbf{W}_2^2\mathbf{A}_m$	$\mathbf{W}_2^2\mathbf{A}_m\mathbf{W}_2\mathbf{S}^{E^{2*}}$
$\mathbf{W}_2, \mathbf{S}^E, \mathbf{A}_f$	$\mathbf{W}_2\mathbf{S}^E\mathbf{A}_f$	$\mathbf{W}_2\mathbf{S}^{E^2}\mathbf{A}_f{}^*$	$\mathbf{W}_2\mathbf{S}^{E^2}\mathbf{A}_f{}^2$
	$\mathbf{W}_2\mathbf{S}^{E^2}\mathbf{A}_f\mathbf{S}^{E^*}$	$\mathbf{W}_2\mathbf{S}^{E^2}\mathbf{A}_f{}^2\mathbf{S}^{E^*}$	$\mathbf{W}_2^2\mathbf{S}^E\mathbf{A}_f$
	$\mathbf{W}_2^2\mathbf{S}^{E^2}\mathbf{A}_f{}^*$	$\mathbf{W}_2^2\mathbf{S}^E\mathbf{W}_2\mathbf{A}_f$	$\mathbf{W}_2^2\mathbf{A}_f\mathbf{W}_1\mathbf{S}^{E^{2*}}$
$\mathbf{W}_2, \mathbf{E}^I, \mathbf{A}_m$	$\mathbf{W}_2\mathbf{E}^I\mathbf{A}_m$	$\mathbf{W}_2\mathbf{E}^{I^2}\mathbf{A}_m{}^*$	$\mathbf{W}_2\mathbf{E}^{I^2}\mathbf{A}_m{}^2$
	$\mathbf{W}_2\mathbf{E}^{I^2}\mathbf{A}_m\mathbf{E}^{I^*}$	$\mathbf{W}_2\mathbf{E}^{I^2}\mathbf{A}_m{}^2\mathbf{E}^{I^*}$	$\mathbf{W}_2^2\mathbf{E}^I\mathbf{A}_m$
	$\mathbf{W}_2^2\mathbf{E}^{I^2}\mathbf{A}_m{}^*$	$\mathbf{W}_2^2\mathbf{E}^I\mathbf{W}_2\mathbf{A}_m$	$\mathbf{W}_2^2\mathbf{A}_m\mathbf{W}_2\mathbf{E}^{I^{2*}}$
$\mathbf{W}_2, \mathbf{E}^I, \mathbf{A}_f$	$\mathbf{W}_2\mathbf{E}^I\mathbf{A}_f$	$\mathbf{W}_2\mathbf{E}^{I^2}\mathbf{A}_f{}^*$	$\mathbf{W}_2\mathbf{E}^{I^2}\mathbf{A}_f{}^2$
	$\mathbf{W}_2\mathbf{E}^{I^2}\mathbf{A}_f\mathbf{E}^{I^*}$	$\mathbf{W}_2\mathbf{E}^{I^2}\mathbf{A}_f{}^2\mathbf{E}^{I^*}$	$\mathbf{W}_2^2\mathbf{E}^I\mathbf{A}_f$
	$\mathbf{W}_2^2\mathbf{E}^{I^2}\mathbf{A}_f{}^*$	$\mathbf{W}_2^2\mathbf{E}^I\mathbf{W}_2\mathbf{A}_f$	$\mathbf{W}_2^2\mathbf{A}_f\mathbf{W}_2\mathbf{E}^{I^{2*}}$
$\mathbf{W}_2, \mathbf{A}_m, \mathbf{A}_f$	$\mathbf{W}_2\mathbf{A}_m\mathbf{A}_f$	$\mathbf{W}_2\mathbf{A}_m{}^2\mathbf{A}_f{}^*$	$\mathbf{W}_2^2\mathbf{A}_m{}^2\mathbf{A}_f{}^2$
	$\mathbf{W}_2\mathbf{A}_m{}^2\mathbf{A}_f\mathbf{A}_m{}^*$	$\mathbf{W}_2\mathbf{A}_m{}^2\mathbf{A}_f{}^2\mathbf{A}_m{}^*$	
	$\mathbf{W}_2^2\mathbf{A}_m\mathbf{A}_f$	$\mathbf{W}_2^2\mathbf{A}_m{}^2\mathbf{A}_f{}^*$	
	$\mathbf{W}_2\mathbf{A}_m\mathbf{W}_2\mathbf{A}_f$	321$\mathbf{W}_2^2\mathbf{A}_f\mathbf{W}_2\mathbf{A}_m{}^{2*}$	

Table LIX. Isotropic scalar invariants (continued-2)

Argument/s	Tensors whose traces are irreducible invariants (i)		
$\mathbf{S}^E, \mathbf{E}^I, \mathbf{A}_m$	$\mathbf{S}^E\mathbf{E}^I\mathbf{A}_m$	$\mathbf{S}^{E^2}\mathbf{E}^I{\mathbf{A}_m}^*$	$\mathbf{S}^E\mathbf{E}^{I^2}{\mathbf{A}_m}^{2^*}$
$\mathbf{S}^E, \mathbf{E}^I, \mathbf{A}_f$	$\mathbf{S}^E\mathbf{E}^I\mathbf{A}_f$	$\mathbf{S}^{E^2}\mathbf{E}^I{\mathbf{A}_f}^*$	$\mathbf{S}^E\mathbf{E}^{I^2}{\mathbf{A}_f}^{2^*}$
$\mathbf{S}^E, \mathbf{A}_m, \mathbf{A}_f$	$\mathbf{S}^E\mathbf{A}_f\mathbf{A}_m$	$\mathbf{S}^{E^2}\mathbf{A}_f{\mathbf{A}_m}^*$	$\mathbf{S}^E{\mathbf{A}_f}^2{\mathbf{A}_m}^{2^*}$
$\mathbf{E}^I, \mathbf{A}_m, \mathbf{A}_f$	$\mathbf{E}^I\mathbf{A}_f\mathbf{A}_m$	$\mathbf{E}^{I^2}\mathbf{A}_f{\mathbf{A}_m}^*$	$\mathbf{E}^I{\mathbf{A}_f}^2{\mathbf{A}_m}^{2^*}$
$\mathbf{S}^E, \mathbf{E}^I, \mathbf{W}_1, \mathbf{W}_2$	$\mathbf{W}_1\mathbf{W}_2\mathbf{S}^E\mathbf{E}^{I^*}$	$\mathbf{W}_1\mathbf{W}_2\mathbf{S}^{E^2}\mathbf{E}^{I^{*\dagger}}$	$\mathbf{W}_1\mathbf{W}_2\mathbf{S}^{E^2}\mathbf{E}^{I^2}$
	$\mathbf{W}_1\mathbf{W}_2\mathbf{S}^{E^2}\mathbf{E}^I\mathbf{S}^{E^*}$	$\mathbf{W}_1^2\mathbf{W}_2\mathbf{S}^E\mathbf{E}^{I^\dagger}$	$\mathbf{W}_1^2\mathbf{S}^E\mathbf{W}_2\mathbf{E}^{I^\dagger}$
	$\mathbf{W}_1^2\mathbf{E}^I\mathbf{W}_2\mathbf{S}^{E^{2*\dagger}}$		
$\mathbf{S}^E, \mathbf{A}_m, \mathbf{W}_1, \mathbf{W}_2$	$\mathbf{W}_1\mathbf{W}_2\mathbf{S}^E{\mathbf{A}_m}^*$	$\mathbf{W}_1\mathbf{W}_2\mathbf{S}^{E^2}{\mathbf{A}_m}^{*\dagger}$	$\mathbf{W}_1\mathbf{W}_2\mathbf{S}^{E^2}{\mathbf{A}_m}^2$
	$\mathbf{W}_1\mathbf{W}_2\mathbf{S}^{E^2}\mathbf{A}_m\mathbf{S}^{E^*}$	$\mathbf{W}_1^2\mathbf{W}_2\mathbf{S}^E{\mathbf{A}_m}^\dagger$	$\mathbf{W}_1^2\mathbf{S}^E\mathbf{W}_2{\mathbf{A}_m}^\dagger$
	$\mathbf{W}_1^2\mathbf{A}_m\mathbf{W}_2\mathbf{S}^{E^{2*\dagger}}$		
$\mathbf{S}^E, \mathbf{A}_f, \mathbf{W}_1, \mathbf{W}_2$	$\mathbf{W}_1\mathbf{W}_2\mathbf{S}^E{\mathbf{A}_f}^*$	$\mathbf{W}_1\mathbf{W}_2\mathbf{S}^{E^2}{\mathbf{A}_f}^{*\dagger}$	$\mathbf{W}_1\mathbf{W}_2\mathbf{S}^{E^2}{\mathbf{A}_f}^2$
	$\mathbf{W}_1\mathbf{W}_2\mathbf{S}^{E^2}\mathbf{A}_f\mathbf{S}^{E^*}$	$\mathbf{W}_1^2\mathbf{W}_2\mathbf{S}^E{\mathbf{A}_f}^\dagger$	$\mathbf{W}_1^2\mathbf{S}^E\mathbf{W}_2{\mathbf{A}_f}^\dagger$
	$\mathbf{W}_1^2\mathbf{A}_f\mathbf{W}_2\mathbf{S}^{E^{2*\dagger}}$		
$\mathbf{E}^I, \mathbf{A}_m, \mathbf{W}_1, \mathbf{W}_2$	$\mathbf{W}_1\mathbf{W}_2\mathbf{E}^I{\mathbf{A}_m}^*$	$\mathbf{W}_1\mathbf{W}_2\mathbf{E}^{I^2}{\mathbf{A}_m}^{*\dagger}$	$\mathbf{W}_1\mathbf{W}_2\mathbf{E}^{I^2}{\mathbf{A}_m}^2$
	$\mathbf{W}_1\mathbf{W}_2\mathbf{E}^{I^2}\mathbf{A}_m\mathbf{E}^{I^*}$	$\mathbf{W}_1^2\mathbf{W}_2\mathbf{E}^I{\mathbf{A}_m}^\dagger$	$\mathbf{W}_1^2\mathbf{E}^I\mathbf{W}_2{\mathbf{A}_m}^\dagger$
	$\mathbf{W}_1^2\mathbf{A}_m\mathbf{W}_2\mathbf{E}^{I^{2*\dagger}}$		
$\mathbf{E}^I, \mathbf{A}_f, \mathbf{W}_1, \mathbf{W}_2$	$\mathbf{W}_1\mathbf{W}_2\mathbf{E}^I{\mathbf{A}_f}^*$	$\mathbf{W}_1\mathbf{W}_2\mathbf{E}^{I^2}{\mathbf{A}_f}^{*\dagger}$	$\mathbf{W}_1\mathbf{W}_2\mathbf{E}^{I^2}{\mathbf{A}_f}^2$
	$\mathbf{W}_1\mathbf{W}_2\mathbf{E}^{I^2}\mathbf{A}_f\mathbf{E}^{I^*}$	$\mathbf{W}_1^2\mathbf{W}_2\mathbf{E}^I{\mathbf{A}_f}^\dagger$	$\mathbf{W}_1^2\mathbf{E}^I\mathbf{W}_2{\mathbf{A}_f}^\dagger$
	$\mathbf{W}_1^2\mathbf{A}_f\mathbf{W}_2\mathbf{E}^{I^{2*\dagger}}$		
$\mathbf{A}_f, \mathbf{A}_m, \mathbf{W}_1, \mathbf{W}_2$	$\mathbf{W}_1\mathbf{W}_2\mathbf{A}_f{\mathbf{A}_m}^*$	$\mathbf{W}_1\mathbf{W}_2{\mathbf{A}_f}^2{\mathbf{A}_m}^{*\dagger}$	$\mathbf{W}_1\mathbf{W}_2{\mathbf{A}_f}^2{\mathbf{A}_m}^2$
	$\mathbf{W}_1\mathbf{W}_2{\mathbf{A}_f}^2\mathbf{A}_m{\mathbf{A}_f}^*$	$\mathbf{W}_1^2\mathbf{W}_2\mathbf{A}_f{\mathbf{A}_m}^\dagger$	$\mathbf{W}_1^2\mathbf{A}_f\mathbf{W}_2{\mathbf{A}_m}^\dagger$
	$\mathbf{W}_1^2\mathbf{A}_m\mathbf{W}_2{\mathbf{A}_f}^{2^{*\dagger}}$		

Table LX. Isotropic scalar invariants (continued-3)

Argument/s	Tensors whose traces are irreducible invariants (i)		
$\mathbf{S}^E, \mathbf{E}^I, \mathbf{A}_m, \mathbf{W}_1$	$\mathbf{W}_1\mathbf{S}^E\mathbf{E}^I\mathbf{A}_m$	$\mathbf{W}_1\mathbf{E}^I\mathbf{A}_m\mathbf{S}^E$	$\mathbf{W}_1\mathbf{A}_m\mathbf{S}^E\mathbf{E}^I$
	$\mathbf{W}_1\mathbf{S}^{E^2}\mathbf{E}^I{\mathbf{A}_m}^*$	$\mathbf{W}_1\mathbf{S}^{E^2}\mathbf{A}_m\mathbf{E}^{I^*}$	$\mathbf{W}_1\mathbf{E}^I\mathbf{S}^{E^2}{\mathbf{A}_m}^*$
	$\mathbf{W}_1\mathbf{S}^{E^2}\mathbf{E}^I\mathbf{A}_m\mathbf{S}^{E^*}$	$\mathbf{W}_1\mathbf{E}^{I^2}\mathbf{S}^{E^2}{\mathbf{A}_m}^*$	$\mathbf{W}_1\mathbf{S}^{E^2}\mathbf{E}^{I^2}{\mathbf{A}_m}^*$
	$\mathbf{W}_1^2\mathbf{S}^E\mathbf{E}^I\mathbf{A}_m$	$\mathbf{W}_1^2\mathbf{S}^E\mathbf{A}_m\mathbf{E}^I$	$\mathbf{W}_1^2\mathbf{S}^{E^2}\mathbf{W}_1\mathbf{E}^I{\mathbf{A}_m}^*$
	$\mathbf{W}_1^2\mathbf{S}^E\mathbf{W}_1\mathbf{E}^I\mathbf{A}_m$		
$\mathbf{S}^E, \mathbf{E}^I, \mathbf{A}_f, \mathbf{W}_1,$	$\mathbf{W}_1\mathbf{S}^E\mathbf{E}^I\mathbf{A}_f$	$\mathbf{W}_1\mathbf{E}^I\mathbf{A}_f\mathbf{S}^E$	$\mathbf{W}_1\mathbf{A}_f\mathbf{S}^E\mathbf{E}^I$
	$\mathbf{W}_1\mathbf{S}^{E^2}\mathbf{E}^I{\mathbf{A}_f}^*$	$\mathbf{W}_1\mathbf{S}^{E^2}\mathbf{A}_f\mathbf{E}^{I^*}$	$\mathbf{W}_1\mathbf{E}^I\mathbf{S}^{E^2}{\mathbf{A}_f}^*$
	$\mathbf{W}_1\mathbf{S}^{E^2}\mathbf{E}^I\mathbf{A}_f\mathbf{S}^{E^*}$	$\mathbf{W}_1\mathbf{E}^{I^2}\mathbf{S}^{E^2}{\mathbf{A}_f}^*$	$\mathbf{W}_1\mathbf{S}^{E^2}\mathbf{E}^{I^2}{\mathbf{A}_f}^*$
	$\mathbf{W}_1^2\mathbf{S}^E\mathbf{E}^I\mathbf{A}_f$	$\mathbf{W}_1^2\mathbf{S}^E\mathbf{A}_f\mathbf{E}^I$	$\mathbf{W}_1^2\mathbf{S}^{E^2}\mathbf{W}_1\mathbf{E}^I{\mathbf{A}_f}^*$
	$\mathbf{W}_1^2\mathbf{S}^E\mathbf{W}_1\mathbf{E}^I\mathbf{A}_f$		
$\mathbf{S}^E, \mathbf{E}^I, \mathbf{A}_m, \mathbf{W}_2$	$\mathbf{W}_2\mathbf{S}^E\mathbf{E}^I\mathbf{A}_m$	$\mathbf{W}_2\mathbf{E}^I\mathbf{A}_m\mathbf{S}^E$	$\mathbf{W}_2\mathbf{A}_m\mathbf{S}^E\mathbf{E}^I$
	$\mathbf{W}_2\mathbf{S}^{E^2}\mathbf{E}^I{\mathbf{A}_m}^*$	$\mathbf{W}_2\mathbf{S}^{E^2}\mathbf{A}_m\mathbf{E}^{I^*}$	$\mathbf{W}_2\mathbf{E}^I\mathbf{S}^{E^2}{\mathbf{A}_m}^*$
	$\mathbf{W}_2\mathbf{S}^{E^2}\mathbf{E}^I\mathbf{A}_m\mathbf{S}^{E^*}$	$\mathbf{W}_2\mathbf{E}^{I^2}\mathbf{S}^{E^2}{\mathbf{A}_m}^*$	$\mathbf{W}_2\mathbf{S}^{E^2}\mathbf{E}^{I^2}{\mathbf{A}_m}^*$
	$\mathbf{W}_2^2\mathbf{S}^E\mathbf{E}^I\mathbf{A}_m$	$\mathbf{W}_2^2\mathbf{S}^E\mathbf{A}_m\mathbf{E}^I$	$\mathbf{W}_2^2\mathbf{S}^{E^2}\mathbf{W}_2\mathbf{E}^I{\mathbf{A}_m}^*$
	$\mathbf{W}_2^2\mathbf{S}^E\mathbf{W}_2\mathbf{E}^I\mathbf{A}_m$		
$\mathbf{S}^E, \mathbf{E}^I, \mathbf{A}_f, \mathbf{W}_2$	$\mathbf{W}_2\mathbf{S}^E\mathbf{E}^I\mathbf{A}_f$	$\mathbf{W}_2\mathbf{E}^I\mathbf{A}_f\mathbf{S}^E$	$\mathbf{W}_2\mathbf{A}_f\mathbf{S}^E\mathbf{E}^I$
	$\mathbf{W}_2\mathbf{S}^{E^2}\mathbf{E}^I{\mathbf{A}_f}^*$	$\mathbf{W}_2\mathbf{S}^{E^2}\mathbf{A}_f\mathbf{E}^{I^*}$	$\mathbf{W}_2\mathbf{E}^I\mathbf{S}^{E^2}{\mathbf{A}_f}^*$
	$\mathbf{W}_2\mathbf{S}^{E^2}\mathbf{E}^I\mathbf{A}_f\mathbf{S}^{E^*}$	$\mathbf{W}_2\mathbf{E}^{I^2}\mathbf{S}^{E^2}{\mathbf{A}_f}^*$	$\mathbf{W}_2\mathbf{S}^{E^2}\mathbf{E}^{I^2}{\mathbf{A}_f}^*$
	$\mathbf{W}_2^2\mathbf{S}^E\mathbf{E}^I\mathbf{A}_f$	$\mathbf{W}_2^2\mathbf{S}^E\mathbf{A}_f\mathbf{E}^I$	$\mathbf{W}_2^2\mathbf{S}^{E^2}\mathbf{W}_2\mathbf{E}^I{\mathbf{A}_f}^*$
	$\mathbf{W}_2^2\mathbf{S}^E\mathbf{W}_2\mathbf{E}^I\mathbf{A}_f$		

Table LXI. Isotropic scalar invariants (continued-4)

Argument/s	Tensors whose traces are irreducible invariants (i)		
$\mathbf{S}^E, \mathbf{E}^I, \mathbf{A}_m, \mathbf{A}_f$	$\mathbf{S}^E\mathbf{E}^I\mathbf{A}_m\mathbf{A}_f$	$\mathbf{S}^E\mathbf{E}^I\mathbf{A}_f\mathbf{A}_m$	$\mathbf{S}^{E^2}\mathbf{E}^I\mathbf{A}_m\mathbf{A}_f{}^*$
	$\mathbf{S}^{E^2}\mathbf{E}^I\mathbf{A}_f\mathbf{A}_m{}^*$	$\mathbf{S}^{E^2}\mathbf{E}^{I^2}\mathbf{A}_m\mathbf{A}_f$	$\mathbf{S}^{E^2}\mathbf{A}_f{}^2\mathbf{E}^I\mathbf{A}_m$
	$\mathbf{S}^{E^2}\mathbf{A}_m{}^2\mathbf{E}^I\mathbf{A}_f$	$\mathbf{E}^{I^2}\mathbf{A}_m{}^2\mathbf{S}^E\mathbf{A}_f$	$\mathbf{E}^{I^2}\mathbf{A}_f{}^2\mathbf{S}^E\mathbf{A}_m$
	$\mathbf{A}_m{}^2\mathbf{A}_f{}^2\mathbf{S}^E\mathbf{E}^I$	$\mathbf{S}^{E^2}\mathbf{E}^I\mathbf{S}^E\mathbf{A}_m\mathbf{A}_f{}^*$	
$\mathbf{S}^E, \mathbf{E}^I, \mathbf{A}_m,$	$\mathbf{W}_1\mathbf{W}_2\mathbf{S}^E\mathbf{E}^I\mathbf{A}_m$	$\mathbf{W}_1\mathbf{W}_2\mathbf{S}^E\mathbf{A}_m\mathbf{E}^I$	$\mathbf{W}_1\mathbf{W}_2\mathbf{E}^I\mathbf{S}^E\mathbf{A}_m$
$\mathbf{W}_1, \mathbf{W}_2$	$\mathbf{W}_1\mathbf{W}_2\mathbf{E}^I\mathbf{A}_m\mathbf{S}^E$	$\mathbf{W}_1\mathbf{W}_2\mathbf{A}_m\mathbf{S}^E\mathbf{E}^I$	$\mathbf{W}_1\mathbf{W}_2\mathbf{S}^{E^2}\mathbf{E}^I\mathbf{A}_m{}^*$
	$\mathbf{W}_1\mathbf{W}_2\mathbf{S}^{E^2}\mathbf{A}_m\mathbf{E}^{I*}$	$\mathbf{W}_1\mathbf{W}_2\mathbf{S}^{E^2}\mathbf{E}^I\mathbf{A}_m{}^*$	$\mathbf{W}_1^2\mathbf{S}^E\mathbf{W}_2\mathbf{E}^I\mathbf{A}_m{}^\dagger$
$\mathbf{S}^E, \mathbf{E}^I, \mathbf{A}_f,$	$\mathbf{W}_1\mathbf{W}_2\mathbf{S}^E\mathbf{E}^I\mathbf{A}_f$	$\mathbf{W}_1\mathbf{W}_2\mathbf{S}^E\mathbf{A}_f\mathbf{E}^I$	$\mathbf{W}_1\mathbf{W}_2\mathbf{E}^I\mathbf{S}^E\mathbf{A}_f$
$\mathbf{W}_1, \mathbf{W}_2$	$\mathbf{W}_1\mathbf{W}_2\mathbf{E}^I\mathbf{A}_f\mathbf{S}^E$	$\mathbf{W}_1\mathbf{W}_2\mathbf{A}_f\mathbf{S}^E\mathbf{E}^I$	$\mathbf{W}_1\mathbf{W}_2\mathbf{S}^{E^2}\mathbf{E}^I\mathbf{A}_f{}^*$
	$\mathbf{W}_1\mathbf{W}_2\mathbf{S}^{E^2}\mathbf{A}_f\mathbf{E}^{I*}$	$\mathbf{W}_1\mathbf{W}_2\mathbf{S}^{E^2}\mathbf{E}^I\mathbf{A}_f{}^*$	$\mathbf{W}_1^2\mathbf{S}^E\mathbf{W}_2\mathbf{E}^I\mathbf{A}_f{}^\dagger$
$\mathbf{S}^E, \mathbf{E}^I, \mathbf{A}_m,$	$\mathbf{W}_1\mathbf{S}^E\mathbf{E}^I\mathbf{A}_m\mathbf{A}_f$	$\mathbf{W}_1\mathbf{S}^E\mathbf{E}^I\mathbf{A}_f\mathbf{A}_m$	$\mathbf{W}_1\mathbf{S}^E\mathbf{A}_m\mathbf{A}_f\mathbf{E}^I$
$\mathbf{A}_f, \mathbf{W}_1$	$\mathbf{W}_1\mathbf{E}^I\mathbf{S}^E\mathbf{A}_m\mathbf{A}_f$	$\mathbf{W}_1\mathbf{E}^I\mathbf{S}^E\mathbf{A}_f\mathbf{A}_m$	$\mathbf{W}_1\mathbf{A}_m\mathbf{S}^E\mathbf{E}^I\mathbf{A}_f$
	$\mathbf{W}_1\mathbf{E}^I\mathbf{S}^{E^2}\mathbf{A}_m\mathbf{A}_f{}^*$	$\mathbf{W}_1\mathbf{A}_m\mathbf{S}^{E^2}\mathbf{A}_m\mathbf{E}^{I*}$	$\mathbf{W}_1\mathbf{A}_f\mathbf{S}^{E^2}\mathbf{E}^I\mathbf{A}_m{}^*$
	$\mathbf{W}_1^2\mathbf{S}^E\mathbf{A}_m\mathbf{A}_f\mathbf{E}^I$	$\mathbf{W}_1^2\mathbf{S}^E\mathbf{E}^I\mathbf{A}_m\mathbf{A}_f$	$\mathbf{W}_1^2\mathbf{S}^E\mathbf{E}^I\mathbf{A}_f\mathbf{A}_m$
$\mathbf{S}^E, \mathbf{E}^I, \mathbf{A}_m,$	$\mathbf{W}_2\mathbf{S}^E\mathbf{E}^I\mathbf{A}_m\mathbf{A}_f$	$\mathbf{W}_2\mathbf{S}^E\mathbf{E}^I\mathbf{A}_f\mathbf{A}_m$	$\mathbf{W}_2\mathbf{S}^E\mathbf{A}_m\mathbf{A}_f\mathbf{E}^I$
$\mathbf{A}_f, \mathbf{W}_2$	$\mathbf{W}_2\mathbf{E}^I\mathbf{S}^E\mathbf{A}_m\mathbf{A}_f$	$\mathbf{W}_2\mathbf{E}^I\mathbf{S}^E\mathbf{A}_f\mathbf{A}_m$	$\mathbf{W}_2\mathbf{A}_m\mathbf{S}^E\mathbf{E}^I\mathbf{A}_f$
	$\mathbf{W}_2\mathbf{E}^I\mathbf{S}^{E^2}\mathbf{A}_m\mathbf{A}_f{}^*$	$\mathbf{W}_2\mathbf{A}_m\mathbf{S}^{E^2}\mathbf{A}_n\mathbf{E}^{I*}$	$\mathbf{W}_2\mathbf{A}_f\mathbf{S}^{E^2}\mathbf{E}^I\mathbf{A}_m{}^*$
	$\mathbf{W}_2^2\mathbf{S}^E\mathbf{A}_m\mathbf{A}_f\mathbf{E}^I$	$\mathbf{W}_2^2\mathbf{S}^E\mathbf{E}^I\mathbf{A}_m\mathbf{A}_f$	$\mathbf{W}_2^2\mathbf{S}^E\mathbf{E}^I\mathbf{A}_f\mathbf{A}_m$
$\mathbf{S}^E, \mathbf{E}^I, \mathbf{A}_m,$	$\mathbf{W}_1\mathbf{W}_2\mathbf{S}^E\mathbf{A}_m\mathbf{A}_f\mathbf{E}^I$	$\mathbf{W}_1\mathbf{W}_2\mathbf{S}^E\mathbf{E}^I\mathbf{A}_f\mathbf{A}_m$	
$\mathbf{A}_f, \mathbf{W}_1, \mathbf{W}_2$	$\mathbf{W}_1\mathbf{W}_2\mathbf{S}^E\mathbf{E}^I\mathbf{A}_m\mathbf{A}_f$	$\mathbf{W}_1\mathbf{W}_2\mathbf{E}^I\mathbf{A}_m\mathbf{A}_f\mathbf{S}^E$	
	$\mathbf{W}_1\mathbf{W}_2\mathbf{E}^I\mathbf{S}^E\mathbf{A}_f\mathbf{A}_m$	$\mathbf{W}_1\mathbf{W}_2\mathbf{A}_m\mathbf{E}^I\mathbf{A}_f\mathbf{S}^E$	

Table LXII. Isotropic scalar invariants (continued-5)